Louisiana Transportation Research Center

Final Report 517

Integral Abutment Bridge for Louisiana's Soft and Stiff Soils

by

George Z. Voyiadjis
Steve Cai
Khalid Alshibli

LSU

4101 Gourrier Avenue | Baton Rouge, Louisiana 70808
(225) 767-9131 | (225) 767-9108 fax | www.ltrc.lsu.edu

TECHNICAL REPORT STANDARD PAGE

1. Report No.	2. Government Accession No.	3. Recipient's Catalog No.
FHWA/LA.13/517		

4. Title and Subtitle	5. Report Date
Integral Abutment Bridge for Louisiana's Soft and Stiff Soils	March 2016
	6. Performing Organization Code

7. Author(s)	8. Performing Organization Report No.
George Z. Voyiadjis, Steve Cai , Khalid Alshibli, Danial Faghihi, Bo Kong and Yi Yang	

9. Performing Organization Name and Address	10. Work Unit No.
Department of Civil and Environmental Engineering Louisiana State University Baton Rouge, LA 70803	11. Contract or Grant No. LTRC Project Number: 07-4ST SIO Number: 30000131

12. Sponsoring Agency Name and Address	13. Type of Report and Period Covered
Louisiana Department of Transportation and Development P.O. Box 94245 Baton Rouge, LA 70804-9245	Final Report October 2007- September 2013
	14. Sponsoring Agency Code

15. Supplementary Notes

Conducted in Cooperation with the U.S. Department of Transportation, Federal Highway Administration. Funding has been provided through the IBRD Program

16. Abstract

Integral abutment bridges (IABs) have been designed and constructed in a few US states in the past few decades. The initial purpose of building such bridges was to eliminate the expansion joints and resolve the joint-induced problems. Although IABs have been widely accepted due to their satisfying performances, they have not been largely applied in practice. Some of the reasons can be attributed to the uncertainties of the structural and geotechnical behaviors of such bridges under the temperature variations, shrinkage and creep of materials, traffic loads, etc. Recently, the first two full IABs were constructed on soft and stiff soil conditions in Louisiana by the Louisiana Department of Transportation and Development (DOTD). This report presents the field instrumentation plans and monitoring results for two bridges: Caminada Bay Bridge, constructed on mainly fine sand and silty sand deposit, and Bodcau Bayou Bridge, on a relatively lean and fat clay with low plasticity.

Finite element modeling was also conducted to understand and assess the bridges' performances. Based on the available information of the bridges, with the monitoring results, 3D numerical models were implemented and validated in the study, where the pile-soil and abutment-backfill interaction behaviors were considered. The concerning parameters are varied through a parametric study to further investigate their effects on the bridge thermal performances under the other complicated structural and geotechnical conditions.

17. Key Words	18. Distribution Statement
In situ full scale pile behavior; bridge bent-pile interaction; integral abutment analysis; soft and stiff soils; IAB finite element analysis	Unrestricted

19. Security Classification (of this report)	20. Security Classification (of this page)	21. No. of Pages	22. Price
N/A	N/A	221	N/A

Project Review Committee

Each research project will have an advisory committee appointed by the LTRC Director. The Project Review Committee is responsible for assisting the LTRC Administrator or Manager in the development of acceptable research problem statements, requests for proposals, review of research proposals, oversight of approved research projects, and implementation of findings.

LTRC appreciates the dedication of the following Project Review Committee Members in guiding this research study to fruition.

LTRC Manager

Walid Alaywan, Ph.D., P.E.
Senior Structures Research Engineer

Members

Arthur D'Andrea, P.E.
Gill Gautreau, P.E.
Stephen Menuier, P.E.
Mike Boudreaux, P.E.
Arturo Aguirre, P.E.

Directorate Implementation Sponsor

Janice P. Williams
DOTD Chief Engineer

Integral Abutment Bridge for Louisiana's Soft and Stiff Soils

by

George Z. Voyiadjis (PI)
Steve Cai (Co-PI)
Khalid Alshibli (Co-PI)

Department of Civil and Environmental Engineering
3513-D Patrick F. Taylor Hall
Louisiana State University
Baton Rouge, LA 70803

LTRC Project No. 07-4ST
SIO Number: 3000131

conducted for

Louisiana Department of Transportation and Development
Louisiana Transportation Research Center

March 2016

ABSTRACT

Integral abutment bridges (IABs) have been designed and constructed in a few US states in the past few decades. The initial purpose of building such bridges was to eliminate the expansion joints and resolve the joint-induced problems. Although IABs have been widely accepted due to their satisfying performances, they have not been largely applied in practice. Some of the reasons can be attributed to the uncertainties of the structural and geotechnical behaviors of such bridges under the temperature variations, shrinkage and creep of materials, traffic loads, etc. Recently, the first two full IABs were constructed on soft and stiff soil conditions in Louisiana by the Louisiana Department of Transportation and Development (DOTD). This report presents the field instrumentation plans and monitoring results for two bridges: Caminada Bay Bridge, constructed on mainly fine sand and silty sand deposit, and Bodcau Bayou Bridge, on a relatively lean and fat clay with low plasticity.

Finite element modeling was also conducted to understand and assess the bridges' performances. Based on the available information of the bridges, with the monitoring results, 3D numerical models were implemented and validated in the study, where the pile-soil and abutment-backfill interaction behaviors were considered. The concerning parameters are varied through a parametric study to further investigate their effects on the bridge thermal performances under the other complicated structural and geotechnical conditions

ACKNOWLEDGMENTS

The investigators appreciate the Louisiana Transportation Research Center (LTRC), Louisiana Department of Transportation and Development, and the Federal Highway Administration (FHWA) for funding this project. The authors would like to acknowledge the help, guidance, and administrative direction provided to them by Walid R. Alaywan, Ph.D., senior structural research engineer at LTRC. They would also like to acknowledge the support of the remaining PRC members Arthur D'Andrea, Gill Gautreau, Stephen Menuier, Mike Boudreaux, and Arturo Aguirre.

IMPLEMENTATION STATEMENT

The project was intended to study the field performance of integral abutment bridges in Louisiana, thus developing needed expertise and application procedures for similar bridges in the future. The research results may be presented to state structural and bridge engineers at the Louisiana American Society of Civil Engineers (ASCE) meeting, the Louisiana Transportation Conference, TRB conferences, and in journals. Dissemination of research results will help the future implementation of integral abutment bridges, and feedback from practical engineers will help judge the progress of implementation.

The field measurement results from this study provided engineers with useful information for a successful design of integral abutment bridges. The study highlights the importance of considering the effect of thermal variations on integral abutment bridges, which was shown to be a dominant factor. Unlike creep and shrinkage effects, which can be reduced by delaying establishing continuity to ensure that a large portion of the creep and shrinkage has already taken place, thermal effects cannot be eliminated and should be considered at the design stage along other loading effects.

During the monitoring period, either the measured seasonal temperatures or daily gradients of the slabs are reaching or slightly exceeding the design values specified by the AASHTO LRFD (2007). Therefore, the DOTD specifications for thermal effects should be re-examined.

While the designs of details for these two monitored bridges seem to be effective in accommodating the thermal effect for these specific bridges, more parametric studies using the calibrated model of the current study, considering longer span and longer bridges etc., are needed to develop more broad applications in Louisiana

TABLE OF CONTENTS

LIST OF TABLES

LIST OF FIGURES

INTRODUCTION

According to a recent report, the average ages of bridges have exceeded 40 years and about 30% of the 600,000 bridges in the US are classified as structurally and/or functionally deficient. In Louisiana, roughly 4,591 bridges out of the total 13,426 bridges are classified as substandard. Louisiana ranks 10th in the nation for the highest deficiency bridge rate.

One of the major maintenance problems for Departments of Transportation (DOTs) is caused by bridge joints, where the intruding water induces problems at the beam-ends, bearings, and supporting substructures. Since the 1980s, many states have chosen or started to explore joint-less construction of bridges to eliminate expansion joints at the bridge ends by using either integral or semi-integral abutments, thus minimizing the maintenance problems. However, being an indeterminate structure, a joint-less bridge may experience significant time-dependent stresses from creep, shrinkage, and temperature changes, thus leading to cracking and serviceability problems. In many extreme cases, the abutment walls and/or supporting piles were broken.

Traditionally in bridge structures, movements due to thermal strains, creep, and shrinkage are accommodated by such components as expansion joints, roller supports, and expansion bearings. However, it is known that expansion joints and bearings are expensive to install and require continuous maintenance. These joints are also prime sites for deterioration of the superstructure and substructure due to cyclic movements and deck leakage. A cost-effective alternative becoming increasingly popular among bridge owners is the integral abutment or integral bridge. An integral abutment bridge (IAB) system is constructed without deck joints, particularly at the abutments. Integral abutment bridges have also been referred to as integral, joint-less, rigid-frame, and U-frame bridges. First built in the United States during the 1930s, integral abutment bridges have experienced extensive worldwide use in the 1990s. Integral abutment bridges can be single or multiple spans. Integral abutment bridges offer several advantages over conventional structures and are currently used in more than 30 American states and Canadian provinces and on the European continent. Benefits offered by integral abutment bridges include reduced initial costs, lower long-term maintenance expenses, elimination of problematic expansion joints and bearings, less deterioration, lower impact loads, improved riding quality, simple construction procedures, and structural continuity to resist overloads. The disadvantages of such construction include subjecting the superstructures to large secondary stresses caused by the response of continuous superstructures to thermal and moisture changes and gradients. These cyclic movements and stresses must be addressed at the bridge abutment. FHWA is promoting the usage of integral abutment and joint-less bridges (IAJB) and a large number of IAJBs have been built in many

states. However, due to Louisiana's unique soft soil condition and the complexity of the pile and soil interaction in the integral abutment bridges, no full integral bridge has ever been explored in Louisiana.

OBJECTIVE

In this project, field-instrumentation, monitoring, and analyzing the design and construction of full integral abutment bridges for Louisiana's fine sand and silty sand deposit and clay soil conditions were conducted. Comparison of results will be submitted to DOTD's Bridge Design and Geotechnical Sections in the form of guidelines to incorporate in future designs. The objective of the study addressed the following:

1. Instrumentation and monitoring of piles, embankment/backfill, abutment, and bridge at two sites representing sandy and clayey soil conditions.
2. Behavior of the backfill material and surrounding soil under the cyclic abutment displacement.
3. Pile and soil interaction.
4. Abutment wall and soil interaction.
5. Effects of temperature and longitudinal movement.

The overall performance of the two bridges (with soft soils in Jefferson Parish and with stiff soils in Caddo Parish) were monitored. The Caminada Bay Bridge was assigned in Jefferson Parish for the fine sand and silty sand deposit conditions. For the stiff soil, the Bodcau Bayou Bridge was assigned. The superstructures were analyzed for thermal movement. The concrete piles for the Caminada Bay Bridge and the steel piles for the Bodcau Bayou Bridge, abutment wall, backfill material, and soils under approach slab were instrumented to measure the pile deformation, soil pressure, and the rotation of the abutment wall due to loads transferred from the superstructures and subsurface deformation

SCOPE

IAB systems are gaining wider acceptability in the US and worldwide mainly because of the reduced initial costs, lower long-term maintenance expenses, and improved ride quality. Louisiana's experience has been limited to the construction of semi-integral abutment bridges in stiff soils only. No full integral abutment bridges have been used in Louisiana so far. Success and effectiveness of the IAB system is dependent on proper understanding of the soil-structure interaction and behavior of components as well as the full system. It is particularly important as soft soils in Louisiana are known for their poor strength quality from the engineering point of view.

An extensive network of instruments for piles, backfill, abutment, deck, and approach slabs was installed and the network was used to monitor the performance of the system at each IAB site. A primary consideration of the project was in selecting the instruments necessary for acquiring the vital information while keeping the network rather simple and robust so that it could be used for acquiring data for both short-term and long-term monitoring. It was envisioned that the services of a professional company would be used in achieving the best instrumentation for the IABs.

For the Caminada Bay Bridge, one section of the bridge was monitored. It included two piles, one abutment, backfill, and superstructure on one side of the bridge. For the Bodcau Bayou Bridge, Bent 1, which included four piles, backwall of the bent, two abutments, backfill, the girders, and the deck, was instrumented.

A finite element analysis was conducted for the substructure, which was used in conjunction with the superstructure finite element analysis. Appropriate constitutive models for the soils were used for the analysis of the substructures. Due to the limitation of resources and an agreement between the sponsor and research team, the superstructure and substructure full model analysis was limited to the Caminada Bay Bridge, and corresponding parametric studies were conducted for this bridge.

METHODOLOGY

A literature review was conducted for the IAB. This includes in-service problems, classification and construction, instrumentation/testing, and monitoring of substructure and superstructure of bridges. This was followed by an extensive plan and implementation of the instrumentation and testing plan of the two bridges chosen for this study. A rigorous plan was outlined for the monitoring system for both the substructure and corresponding superstructure of the two bridges chosen for this study.

The finite element analysis was conducted for the substructure, which was used in conjunction with the superstructure finite element analysis of the two bridges. Appropriate constitutive models for the soils are used for the analysis of the substructures. Parametric studies were conducted for the modeling and analysis of the bridges.

Finally, field monitoring was conducted for the two bridges and the accuracy was compared to that of the predictive numerical models. Conclusions and recommendations were drawn from these analyses.

Literature Review

In an integral abutment bridge, the back wall is integral with the superstructure and dimensionally the same as the diaphragms cast to the girders. This design eliminates both the need for joints and sealers and the maintenance associated with their use, generally resulting in a more economical bridge to construct with lower long-term maintenance costs. Elimination of joints also improves ride quality for drivers. However, because of structural continuity, integral construction may introduce secondary stresses into the superstructure. Additional secondary stresses could develop due to thermal changes and gradients, creep and shrinkage of concrete, and settlement. Flexibility and free movement are essential factors in the design of a joint-less bridge. Also noteworthy is the fact that integral abutment bridges experience less overall movement than what is theoretically assumed. Even though the integral abutment bridges have many advantages, their limitations are obvious. Since the superstructure of the bridge is connected monolithically with the abutment, this rigid connection enables the abutment and superstructure to act as a single structure unit. Therefore, the entire system behaves simultaneously to any response, which includes a multitude of interactions within the structure. Therefore, behavior of this type of structures needs to be investigated by testing and analysis to ensure efficient and reliable design.

This brief summary will first attempt to outline the state-of-art and practice of integral abutments while considering important aspects of design, and then describe the method of

analysis that will be used in conjunction with the measurements obtained from the embedded sensors in the integral abutment.

Contraction and expansion are two unavoidable reactions for bridge structures responding to temperature change, creep, and shrinkage. Traditionally, a system of expansion joints, bearings, roller supports, and other structural releases have been provided to accommodate these movements. After years of inspection, the joint systems, however, become detrimental parts for the whole bridge. Joints allow water or deicing chemicals leaking onto the underlying components and cause steel deterioration and concrete spall. After a long period of time, accumulated debris consolidation in the joint impedes bridge movement, which induces overstress and could damage the bridge elements. In addition, the cost of repeated joint replacement and maintenance during the service-life time, together with the expense on the design, purchase, and installation stage, add enormous amounts to the budget *[1], [2], [3]*. In light of these negative aspects, researchers have been trying to eliminate the joints system, and because of that, the joint-less bridge or integral abutment bridge came out as a result. As indicated by Wolde-Tinsae and Greimann, the initial objectives of the development of a joint-less bridge should meet the following requirements: (1) long-term serviceability of the structure, (2) minimal maintenance requirements, (3) economical construction, and (4) improved overall performance of the facility *[3]*. After years of practice, it is widely admitted that the integral bridge without joints performs much better than that with joints *[4], [5]*. According to a survey of 50 states in 2004, there are approximately 13,000 integral abutment bridges in service, and the response of the question about the future plan indicated that over 90% of the states have a policy to construct joint-less bridges whenever possible *[6]*. However, the design and construction of integral abutment bridges are primarily relying on empirical guidelines and no national standards or uniform policy exists. There is little national consensus on allowable limitations, such as the maximum bridge total length, individual span length, skews, and curvature. The nonlinear interactions among soil, backfill, pile, and abutment are unclear. The analytical and numerical model of the integral abutment bridges remains uncertain.

Dicleli studied the behavior of the abutment-backfill system under positive thermal variation in integral abutment bridges built on sand *[7]*. A structural model of a typical integral bridge is built, considering the nonlinear behavior of the piles and soil-bridge interaction effects. Static pushover analyses of the bridge are conducted to study the effect of various geometric, structural, and geotechnical parameters on the performance of the abutment-backfill system under positive thermal variations. The shape and intensity of the backfill pressure are found to be affected by the height of the abutment. Furthermore, the internal forces in the abutments are found to be functions of the thermal-induced longitudinal movement of the

abutment, the properties of the pile, and the density of the sand around the piles. Using the pushover analysis results, design equations are formulated to determine the maximum forces in the abutments and the maximum length of integral abutment bridges based on the strength of the abutments. Integral abutment bridges with piles encased in loose sand and oriented to bend about their weak axis, abutment heights less than 1310 ft. (400 m), and no compacted backfill are recommended to limit the magnitude of the forces on the abutments.

In-service Problems Associated with IABs. The fundamental cause of in-service problems for IABs as they are currently designed is illustrated in Figure 1. As the bridge superstructure goes through its seasonal length changes, it causes the structurally connected abutments to move inward and away from the soil, they retain in the winter and outward and into the retained soil during the summer. The specific mode of abutment movement is primarily rigid-body rotation about the bottoms of the abutments, although there is a component of rigid-body translation (pure horizontal displacement) of the abutments as well. Because rotation is dominant, the magnitude of the range of horizontal displacements is thus greatest at the top of each abutment. At the end of each annual thermal cycle, there is often a net displacement of each abutment inward toward each other and thus away from the retained soil, as shown in Figure 1. The primary reason for this is that the inward winter displacement is typically of sufficient magnitude to cause an active earth pressure "soil wedge" to develop adjacent to each abutment and follow the abutment inward, with the soil slumping downward somewhat in the process. Because of the fundamentally inelastic nature of soil behavior, this inward/downward soil displacement is not fully recovered during the outward summer cycle. There are two significant consequences of the annual thermal cycle of IABs. The first is the relatively large lateral earth pressures that develop on the abutments during the annual summer expansion of the superstructure, and it was recognized at least as far back as the 1960s and these pressures can approach the theoretical passive state, especially along the upper portion of the abutments where horizontal displacements are largest *[8], [9], and [10]*. Passive earth pressures are typically an order of magnitude greater than the at-rest pressures for which a bridge abutment should typically be designed. This tenfold increase in lateral earth pressures far exceeds any normal margin of structural safety built into the design and thus can result in structural distress and even failure of an abutment. Recent research indicates that this long-recognized seasonal increase in lateral earth pressures may be a more significant and potentially problematic issue than initially thought. This is because the summer-seasonal increase in pressures is not necessarily constant but can increase over time. The reason is that not only is one seasonal cycle of inward-outward-inward displacement nonlinear, but each succeeding season is nonlinear with respect to the preceding one. This means each winter the abutment moves inward slightly more than it did the preceding winter and each summer it moves outward slightly less than it did the preceding summer. As a

result, net soil displacement inward toward the abutments and the fact that the bridge superstructure still expands each summer the same amount as the preceding year, the summer lateral earth pressures increase over time as the soil immediately adjacent to each abutment becomes increasingly wedged in. This overall behavior is a geo-phenomenon called ratcheting. The soil mechanics behavior causing ratcheting is quite complex but is well known and thoroughly described in the geotechnical engineering literature. Because ratcheting causes each summer's lateral earth pressures to be somewhat greater in magnitude than those from the preceding year, it means structural failure of the abutments may take years, even decades, to develop, as has been observed in practice for other types of earth-retaining structures where thermally induced ratcheting occurs. Given the relatively long design life of most IABs (typically 100 years or more), ratcheting represents a potentially serious long-term source of problems, primarily structural distress and failure of the abutments.

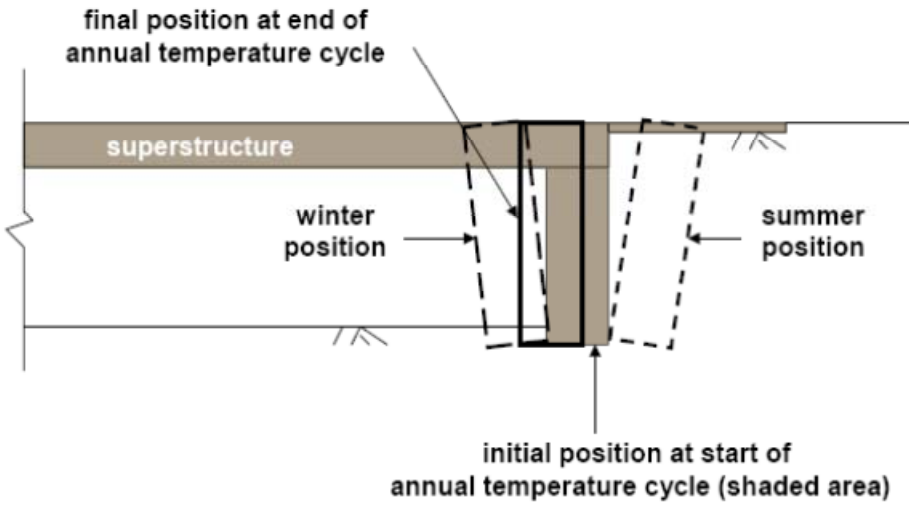

Figure 1
Thermally induced IAB movement

The second significant consequence of the annual thermal cycle of IABs is also related to the net inward displacement of the abutments and has become fully appreciated only in recent years. This is the subsidence pattern that develops adjacent to each abutment and the result of the phenomenon of accumulated, irreversible soil-wedge slumping behind each abutment. The consequences of this subsidence depend on whether or not an approach slab was constructed as part of the bridge. If there is no slab, there will be a difference in road surface elevation occurring over a short distance creating the classical “bump-at-the-end-of-the-bridge” condition. If there is a slab, initially it will span over the void created underneath it by the subsided soil. However, with time and traffic, the slab can fail structurally in flexure.

Subsidence behind IAB abutments has received much more interest in recent years compared to the traditional concern over increased lateral earth pressures. This is because experience indicates subsidence develops and becomes problematic relatively soon (a few years at most) after an IAB is placed in service; whereas, the ratcheting buildup of lateral earth pressures might not create problems for decades as noted above *[11], [12], [13], [14], [15]*. For example, Reid et al. noted that a survey of 140 IABs with approach slabs in South Dakota, found a void under virtually every slab *[13]*. The void depths ranged from 0.5 to 14 in. (13 to 360 mm), and the voids extended as much as 10 ft. (3 m) behind the abutment.

Horvath identified key aspects that are essential to developing improved solutions: expansion and contraction of a bridge superstructure due to seasonal temperature changes is inevitable and unavoidable as it is a natural phenomenon that simply cannot be changed in any significant way *[16]*. This displacement will occur regardless of the specific structural concept used for the bridge design. This means the tendency for differential horizontal displacement between an IAB and the ground surface adjacent to its abutments is unavoidable and must be addressed explicitly.

The ground adjacent to IAB abutments must be made inherently self-stable on a permanent, year-round basis to prevent development of subsidence during the seasonal winter contraction of the IAB. In essence, the ground itself must provide the non-yielding, seasonally constant retention function formerly provided by the abutments of conventional bridge design.

There must be a design detail involving a structural element or material between the self-stable ground and moving IAB abutments to reliably and predictably accommodate the relative movement between them. This detail conceptually replaces the expansion joint/bearing detail of conventional bridge design. Simply leaving a void between ground and abutment, as has been done occasionally in the past, is not considered an acceptable design detail.

The first integral bridge was built early in the 1930s; different terminologies are used for this novel bridge type, such as integral bridge, integral abutment bridge, joint-less bridge, etc. However, from the structural point of view, these different synonyms actually refer to the same bridge structure. When the deck joints and the associated bearings are eliminated by casting superstructure integrally with the substructure, the horizontal movement induced from temperature changes, creep, and shrinkage should be absorbed by other means. Generally, a capped pile stub type abutment with a single row of piles would provide enough flexibility to accommodate the movement. Specifically, as defined, there are three different

kinds of integral abutment bridges *[6]*. Full integral abutment uses a capped pile stub type abutment and the connection between superstructure and foundation cap can be hinged or fixed; a semi-integral abutment bridge has movable bearings between the end diaphragm and foundation; deck extension bridge refers to the one with decks extending over the backwall and placing a joint behind the abutment backwall. As for the connection detail between intermediate piers and the superstructure, they could be any type depending on whether the bridge inherent substructure system is flexible enough to accommodate the superstructure movement *[5]*.

Integral abutment bridges have been classified according to the connections between superstructures and substructures. Even though different terms have been adopted, they all refer to a certain structural meaning. Generally, there are two types of integral abutment bridges: full integral and semi integral. According to Weakley, a full-integral abutment bridge [Figure 2(a)] is a single or multiple span bridge that has its superstructure (including cast-in-place concrete slab over either concrete prestressed girders or steel stringer and a concrete end diaphragm) cast monolithically with the substructure (stub type abutments), connected to a concrete pile cap, found on a single row of piles. The connection and continuity between superstructures and substructures are capable of transferring moments, axial and shear forces *[17]*. A semi-integral abutment bridge [Figure 2(b)] is different, in that the superstructure and abutment are not integrally connected. A movable bearing exists between the integral end diaphragm and the foundation. This kind of bridge is usually considered when the conditions do not meet full-integral abutment requirements. The minimum pile length cannot be obtained, for example, so that it will not be able to provide enough flexibility for piles to accommodate the superstructure thermal movement.

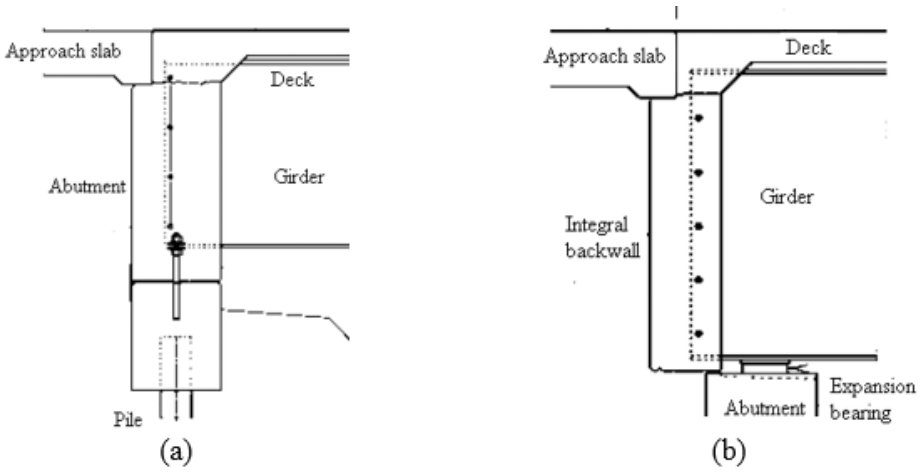

Figure 2
(a) Full integral abutment and (b) semi-integral abutment *[17]*

Length and Skew. According to the survey conducted by Maruri et al., the maximum limits of the length and skews vary greatly from one state to another *[6]*. The reasons for controlling the bridge length are to limit the thermal induced movement, which otherwise would produce secondary stress on the substructure. Besides controlling bridge length limits, it can also restrain the movement at the pile or abutment head.

Burdette et al. stated that the limits of the length could be determined by the maximum lateral displacement, which in turn relates to capacity of structure elements withstanding such deformation without causing damage at service load *[18]*. The Tennessee Department of Transportation (TDOT) adopts the design criteria by a limit of 1.0 in pile horizontal movement.

Christou et al. discussed the aspects of the relationship between superstructures and substructures of this issue of length limit in detail *[19]*. Bridge deck, expanding, and contracting with temperature fluctuation will produce thermal stress to the abutment, foundation pile, and the adjacent soil. To accommodate these lateral deflections, the substructure components are forced to displace and rotate. In the case of increasing bridge length, the magnitude of strains will rise in the substructure. To avoid strains exceeding the substructure limits, a maximum allowable length of integral abutment bridge should be restrained as a result.

Dicleli et al. estimated the length limits for an integral abutment bridge built on clay *[20]*. As it was recommended in his research, design guidelines should limit the maximum length to 690 ft. (210 m) for concrete bridges in cold climates and 850 ft. (260 m) in moderate climates. The corresponding value for the steel bridges is 390 ft. (120 m) and 590 ft. (180 m), respectively.

For the skew limits of integral abutment bridges, differences also exist among the states. Oesterle et al., evaluating the components of passive earth pressure induced by thermal movements, showed that the skewed bridges' response to temperature will move in two directions, longitudinal and transverse *[21]*. As far as he predicted, with a skew angle over 20 degrees, the transverse force component should not be ignored and the integral abutment has to be designed to resist earth pressure in both directions.

Restraint Moments. The primary differences between an integral abutment bridge and a traditional bridge lie in the restraint moments developed in the structure. Arockiasamy et al. attributed restraint moments to time-dependent effects of creep, shrinkage, and thermal variations *[1]*. In this literature, the author tried to present the state-of-art of such restraint moment effects on prestressed integral abutment bridges. Specifically, PCA (Portland

Cement Association) developed a method to account for the influence of creep and shrinkage of concrete on the composite continuous construction. CTL (Construction Technology Laboratories) developed a computer program to calculate the time-dependent restraint moments for prestressed bridges. A modified P-method was put forward for creep and cast-in-place concrete shrinkage estimation.

As for the research of temperature and humidity, such influence factors on short-term creep and shrinkage of the concrete, Russell et al. found that an increase in temperature and a decrease in humidity would negate each other and does not cause bridge length change *[22]*. Some research on thermal effects has also been observed. Seasonal and daily temperature has different effects on bridges. The former one primarily affects the total bridge length change, while the later one produces effects through the depth of the bridge.

Backfill. The inward-outward movement of substructures, especially the abutment, would cause the settlement of the soil behind the back wall. This phenomenon can be explained as: when the abutment moves outwards during the summer season, the adjoining fill would be pushed away from abutment. Therefore, when the abutment contracts in winter, the position originally occupied by the abutment would be void; then the soil naturally subsides, which in turn causes the settlement of soil. Since the subsidence of soil would have negative effects on the abutment and increase earth pressure, several methods have been put forwards and practiced. Changing or adjusting the materials behind the abutment is the main method, using expanded polystyrene (EPS) for example. Weakley adopted EPS material, which can work as a cushion between the back wall and backfill *[17]*. In the field monitoring, the earth pressure was proved to correspondingly be reduced satisfactorily. Hoppe gave an appropriate thickness of the layer of EPS. According to his field studies, a 10-in. layer can perform well and effectively by an elastic inclusion between the back wall and approach fill *[23]*. However, some opposite statements also exist concerning on the use of EPS. Among them, Horvath believed that, as long as the soil subsidence from inward-outward process is not complementary, the soil displacement would occur no matter what type of soil is used or compacted. However, Horvath proposed two different concepts to release the problems. The first one is to utilize mechanically stabilized earth (MSE) mass and a layer of Resilient-EPS-Geofoam. Another one is the combination use of a solid light-weight-fill material and a layer of Resilient-EPS-Geofoam *[24]*.

Approach Slab. The performance and behavior of approach slab were observed as the most unsatisfactory, such as approach settlement, transverse and longitudinal cracking, and bump at the interface between backfill and back wall. The reason still comes from the annual thermal movement. Different solutions and research have been proposed, such as

providing corbels for supporting the approach slab or improving the connections between the back wall and approach slab like using reinforcing projection from the abutment back wall to tie the approach slab. Some other practices put an expansion joint between the approach slab and bridge slab. Figure 3 shows the detail of the approach slab-abutment-deck connection used by the New York State Department of Transportation (NYDOT) *[25]*.

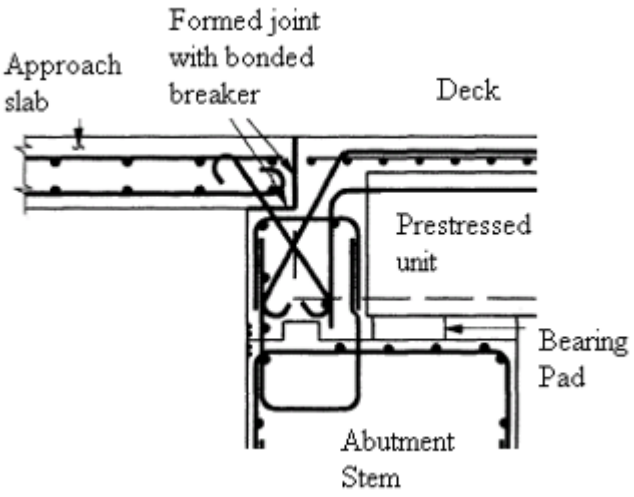

Figure 3
Approach slab connection [25]

Wing Wall/Abutment. For the design and construction of the wing wall and abutment, consideration should be given to the soil-structure interaction. Some research has been conducted to determine the type of earth pressure behind the abutment. The results vary between types of wing walls. In Conboy et al.'s research, full passive earth pressure should be considered for the extension abutment stem compared with active pressure for U-wing walls. As for the more complicated flared wing walls, passive and active earth pressures are respectively acting perpendicular to the centerline of the abutment and the centerline of the bridge. For the paralleled wing wall, full passive earth pressure should be included. In addition, Conboy et al. recommended an extra vertical passive earth pressure checking for the U-wing wall due to abutment rotation *[26]*. As for the abutment stems, they concluded that either full passive earth pressure or a modified horizontal earth pressure coefficient can be modeled as applied forces. In addition to that, the research also studied the lateral earth pressure for different orientations of wing walls. They found that the pressure of U-wall orientation is greater than that of flared and paralleled wing walls. Some states do not allow the use of U-shaped abutment because of its stress complication.

Pile. Finding an appropriate pile is important in the design of an integral abutment bridge since the pile needs to be capable of withstanding annual thermal displacement. As it

was presented by Burdette et al., with steel piles, displacement was limited by cracking in the abutment, while for concrete piles; the piles themselves limited the displacement *[18]*. Several types of piles have been attempted, such as steel bearing piles (H piles and pipe piles), friction piles, spread footings, and drilled shafts for foundation. Choosing an appropriate pile has some rules to comply with. Huckabee showed two aspects, geotechnical and structural. According to his research, the pile should meet the requirements on possessing both the ability to resist Euler's gross and local buckling, and an adequate length to be fixed in the soil and adequate end bearing to transmit vertical load to soil *[27]*.

Until now, no consensus exists in terms of what kinds of pressure should be used to model the applied force on the pile. Passive, active, and a combination of both have been tried in different state DOTs. It is also uncertain which types of load carrying capacity should be designed for, since connection between abutment and pile can be analyzed both for pinned, fixed, or a condition between both. As Husain et al. pointed out, if considering the connection as pinned, free rotation is allowable *[28]*. But for the fixed connection, a plastic hinge would be considered. Conboy et al. improved and modified the traditional empirical formulas, which used axial or a combination of axial and bending forces, by multiplying a new coefficient of inelastic rotational capacity on the standard interaction formulas *[26]*. He found that with the existence of plastic hinge, the pile can continue to translate and rotate even after an elastic period; therefore, the coefficient is added to account for the inelastic rotation capacity. In addition, they presented three design approaches: which are allowable stress design method (ASD), load factor design (LFD), and load and resistance factor design (LFRD).

When the piles are embedded into the abutment, the monolithic nature of the structure would cause pile to translate and rotate with the superstructure when the temperature changes. The rigid pile to abutment connection and fixity at the pile base make the pile perform as fixed-fixed columns. As it concerned Huckabee in alleviating this problem so as not to produce negative impact on substructure, the practice still being used now is to construct the pile on a single row of HP piles, usually one pile on one stringer, and the piles are driven into a predrilled shaft several diameters deep of loose stone *[27]*. As for the exact value of the predrilled depth and backfill material, different researchers have different results. In the survey, Maruri et al. showed that a 10-ft. pre-bored hole filled with bentonite for each pile, and Bonczar et al. indicated the pre-augered holes would be backfilled with sub rounded pea stone *[6] [29]*. Other research recommends a 2-3 ft. embedment of the pile in abutment and an oversized 8 ft. for the pile installation. By the testing study, the revised details can provide a more rotational flexibility so as to reduce the pile stress.

Analytical studies on the behavior of integral abutment bridges have been conducted to verify assumptions and create models for design by comparing with measured data. Furthermore, researchers have always been trying to provide simple and easy but still effective and reasonable models to analyze bridges. Dicleli followed a rational design approach for prestressed-concrete-girder integral abutment bridges. An analysis procedure and simplified analytical models are proposed for the design of integral abutment bridges. The design methodology is developed considering the actual behavior of integral abutment bridges and load distribution among their various components. The methodology recommends the analysis of integral abutment bridges for each construction stage. The earth pressure forces acting on integral bridge abutments are formulated in correlation with the effects of temperature variation. It was concluded that it may be possible to obtain more sound and economical designs for integral abutment bridges using the proposed design method.

The studies and analyses practices can be divided into two main parts: (1) super structure including the bridge deck and approaching slab and (2) sub-structure including piles and cap.

Thermal Analysis. Two basic analysis models have been provided for the thermal effects research. One is a heat-flow model. The other one is thermocouple, which is being widely used in the field study to measure temperature.

Elbadry provided a two-dimensional temperature distribution model with variations of climatic change and cross sectional property *[30]*. As it was observed, the longitudinal stress is the maximum, when solar radiation is maximum and the wind speed is slow.

Potgieter used a one-dimensional model to compute temperature gradients through the depth of bridge superstructures *[31]*. According to the research, solar radiation has effects on the temperature gradients.

Bridge Analysis. Girton provided two models, an axial displacement model and a longitudinal frame model, to investigate thermal induced bridge movement. For the former case, only bridge axial extension was considered regardless of any restraints from deck, girder pile, and backfill. By varying coefficient of thermal expansion value, the total bridge movement ranges were compared with the experimental results. Compared to that, a more complicated two-dimensional frame model was proposed in the second case that includes the effects from pile, deck, and girder stiffness. Together with the equivalent pile length, rigid connection of deck-girder, coupled degree of freedoms at pier-girder, linear temperature distribution, the frame model was compared with the simplified axial model *[32]*.

Thippeswamy discussed effects of primary and secondary load effects on integral abutment bridges by a two-dimension frame model. Specifically, temperature loads, concrete creep, concrete shrinkage, soil pressures, and support settlements were first investigated individually, and then conditions of different combinations from each of these effects were studied *[33]*.

Arsoy investigated effects from soil stiffness on full-integral and semi-integral bridge types on pile stress. In his numerical finite element model, interactions between abutment-approach fill, approach fill-foundation soil, soil-pile, and pile-abutment were included in the computer program SAGE and LPILE. Further, by the finite element model, a parametric study was conducted in terms of effects of approach fill and abutment type. Finally, a simplified method was proposed for piles design *[34]*.

Faraji built 3D Nonlinear Finite-Element Bridge Model using the commercially available computer package GTSTRUDL. In this model, the nonlinear soil behavior was incorporated. For the backfill behind the abutment, the NCHRP design curve was used, and for soil around piles, the design curve recommended from the American Petroleum Institute (API) was included. Further, with this finite element method (FEM), a parametric study was conducted on the soil compaction level *[35]*.

Lehane provided a simplified, elastic model to predict the axial and bending response for the integral bridge to thermal expansion. In this model, an equivalent, linear-stiffness modulus, an equivalent abutment height, and a translational, linear spring were used. By comparing it to a more detailed FEM, this simplified model was shown to be reasonable *[36]*.

Bonczar et al. utilized a 3D model to represent the thermal response of the bridge *[29]*. When constructing a structural analytical model, modeling connections between components are difficult and important. According to Bonczar's model, rigid links were used to simulate deck-abutment and girder-cap connection, and non-linear spring elements to represent the soil structure interaction. In addition, they considered all materials with geometrical non-linear properties, especially a material non-linearity and plastic hinge fiber elements were used at critical piles. Although a 3D model can probably predict more accurate results, Bonczar also tried to validate and provide a 2D model in routine design. The integral abutment bridge was idealized and simplified by beam member, composite properties, pin supports, and fixed supports. After comparing it with the observed data, models can reasonably predict the thermal displacement at the girder centerline. Although the model considered the symmetric response of the two abutments, the difference due to unequal conditions has been observed, which can be explained as unequal backfill or unequal solar

heating at each abutment. The measured pressure near the bottom of the abutment, however, was higher than that calculated from FEM, probably due to the change from density and stiffness of pea stone over years as predicted by the authors.

Despite the FEM model, an alternate model had been evaluated and analyzed by Christou et al. using commercially available FB-Multiplier software *[19]*. Nonlinear response was given to the piles, intermediate piers, and soil behind the abutment walls. According to the conclusion, the performance of the model is efficient. Together with its simplified modeling process and convenience of implementation, it is shown to be a reliable alternative to the more time consuming and sophisticated model.

Analysis of Substructure. The behavior of the piles in the integral abutment bridge was studied using theoretical studies. Various analytical and design methods have been investigated by Steward et al. *[37]*. Table 1 lists existing analytical and design approaches. In 1989, Abendroth, et al. proposed a new method based on a method that was previously published by Greimann and Tinsae *[38] [39]*. The new design method, known as the "Rational Design Method," replaces the actual pile with an equivalent cantilever. The pile embedded in the soil is modeled as an equivalent beam-column without transverse loading between the ends, having a fixed base at a certain depth. However, it is notable that the equivalent cantilever is weak in consideration of the laterally loading. Figure 4 shows an idealization of a fixed cantilever.

Wang and Reese used the COMP624P computer program to model and analyze laterally loaded piles. This incorporation of the analysis and design of laterally loaded piles offers an iterative solution of non-linear differential equation using finite-difference techniques. Currently, the FEM is considered the most powerful method in analyzing the soil-structure interaction in integral abutment bridges. Various finite element models of integral abutment bridge have been developed and studied by many researchers in the past few decades. Both two-dimensional and three-dimensional models had have been developed. Some researchers used commercial software packages while others used their own codes. In these models, the structure and soil are modeled using either continuum elements or special element such as beams and springs *[40]*.

Table 1
Existing analytical and design approaches *[37]*

Grouping	Category	Reference	Method	Output*
Empirical	1	Marche & Lacroix (1972)	Horizontal abutment displacement related to embankment settlement through relative pile flexibility	y_{cap}
	1	Oteo (1977)	Maximum bending moment related to relative pile length, with correction for embankment geometry	M_{max}
	1	Stewart (1992)†	Maximum bending moment and pile head deflection related to the relative soil–pile stiffness and current loading level	M_{max}, y_{cap}
Pressure-based	2A	Begemann & DeLeeuw (1972)	Approximate displacement compatibility between pile and soil used to derive lateral pressure	M_{max}
	1/2A	DeBeer & Wallays (1972)	Simple estimate of lateral pressure acting on piles. Two methods, depending on factor of safety of the embankment against failure	M_{max}
	1/2A	Tschebotarioff (1973)	Simple estimate of lateral pressure acting on piles based on estimates of soil stress	M_{max}
	1/2A	Fedders (1977) Franke (1977)	German design recommendations for limit state conditions	M_{max}
	2A	Springman (1989)	Parabolic-shaped pressure distribution estimated on the basis of approximate relative soil–pile displacement	BMD, DS
	2A/B	Stewart (1992)†	Modifications to Springman's approach for greater accuracy and allowing for non-linear behaviour and geometrical effects	M_{max}, y_{cap}
Displacement-based	3B	Poulos (1973)	Finite difference analysis of a single pile with soil reactions calculated from elastic theory, including interaction: limited parametric solutions presented in chart form (category 2B)	BMD, DS
	3B	Marche (1973), Bourges, Frank & Mieussens (1980)	Finite difference p–y analysis of a single pile	BMD, DS
Finite element	3A	Carter (1982)	Axisymmetric analysis of a single pile with unsymmetric surface load	BMD, DS
	3A/B/C	Springman (1984), Stewart (1992)	Plane-strain analysis of pile groups, with rows of piles represented by equivalent sheet-pile walls	BMD, DS
	3A	Springman (1989)	Fully three-dimensional analysis	BMD, DS

* BMD pile bending moment distribution, DS full deflected pile shape.
† Described in this Paper.

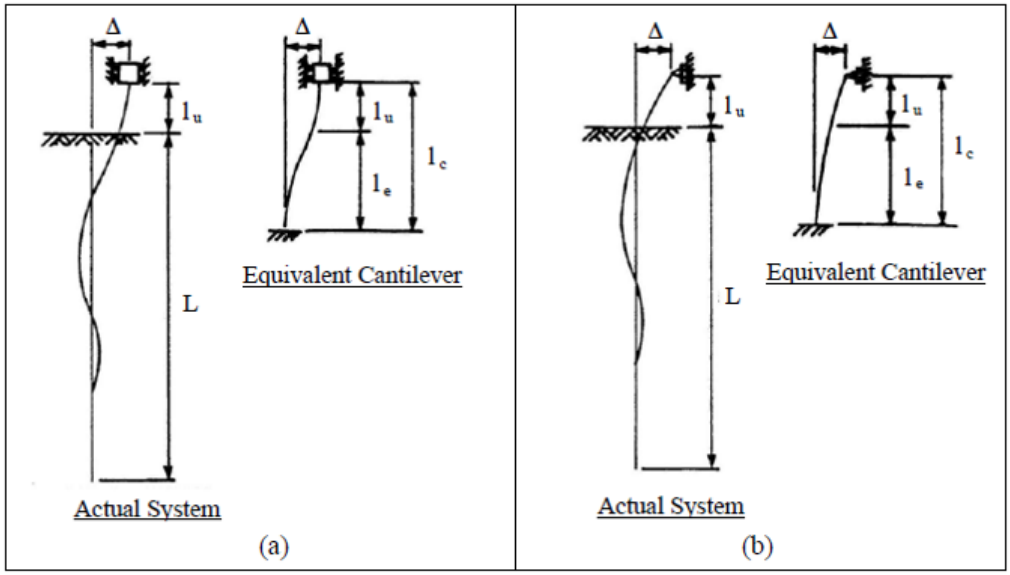

Figure 4
Equivalent cantilevers for: (a) fixed-head condition (b) pinned-head condition *[41]*

Springman and Steward developed plane-strain FEM analyses of pile groups, with rows of piles represented by equivalent sheet-pile walls *[42]* and *[43]*. In 1986, Greimann, et al. compared experimental data with the FEM results *[44]*. Ellis and Springman used the same method while incorporating three-dimensional effects associating with the pile rows and vertical drain*[45]*. Their success was illustrated by comparing plane-strain FE model with the centrifuge data. They stated the soil-structure interaction was more readily analyzed in plane strain by incorporating the vertical drains in the clay layer to conform to the Geotechnical Centrifuge test. Faraji et al. developed a full 3D finite-element model of an integral abutment bridge system that incorporated the nonlinear soil response using the commercially available computer package GTSRUDL *[46]*. They successfully incorporated the nonlinear soil behavior behind the abutment walls and next to the vertical piles into the 3D FE model. Using GTSRUDL, the nonlinear soil behavior was handled using nonlinear springs at the abutment wall and pile nodes. Their results show that the dense granular backfill strongly influenced the overall soil reaction and also had a great impact on the overall structure response of the bridge system. Hara et al. monitored the behavior of piles based on the results of in situ prototype tests, where the piled bridge abutments were constructed on soft soils *[47]*. Then they incorporated Cam-clay model and Biot's theory and proposed a self-coded 2D FEM program to take into account the coupling of elasto-plastic deformation and consolidation of the soft soil. It predicted the behavior of the abutment and piles in the practice level. Steward et al. used the 2D elasto-plastic coupled FEM based on the modified Cam-clay model *[48]*. Results from this method show a strong agreement under some conditions with experimental data obtained from the centrifuge models *[49]*.

Wakai et al. used 3D elastic-plastic coupled with FE analysis based on the Cam-clay model *[50]*. They stated that 3D analysis is necessary to explain such a problem because the mechanism of deformation of the soil possesses 3D characteristics; in their paper, 2D modeling analysis was not recommended because the deformation and the seepage in the subsoil profile in the direction perpendicular to the axial direction of the bridge are completely neglected.

Alternative model is proposed for the analysis of integral abutment bridges using the commercially available FB-Multiplier software package *[19]*. The model allows for nonlinear behavior of the piles and the intermediate piers and also includes nonlinear soil springs to describe the response of the soil behind the abutment walls as well as the response of the soil around the piles. A parametric analysis was conducted on both 2D and 3D non-linear FEM of the Orange-Wendell Bridge *[29]*. Pile elements included non-linear geometric effects and non-linear material properties. Non-linear spring curves representing soil effects were included in the models at pile, pier and abutment locations. The authors used both FEM results and field data to address the pile deformation, moment at the top of abutment piles, properties of abutment and pile backfill materials, effect of pile yielding, and pile design assumptions.

Dicleli and Erhan investigated the behavior of the abutment on the distribution of live-load effects under the effect of soil-structure interaction and substructure properties *[51]*. They used both 2D and 3D FEM of typical integral abutment bridge to study the influence of geotechnical and substructure properties such as foundation soil stiffness, considering and neglecting the effect of backfill, backfill compaction level, considering and neglecting the effect of wing walls, abutment height and thickness, as well as the number, size, and orientation of the piles. Their analyses revealed that the soil- structure interaction had a significant effect on the live load distribution factors (LLDFs) for the abutment, but negligible effects on those for girders and piles. Moreover, the abutment height also has a considerable effect on the LLDFs calculated for the abutment and pile moments.

The response of an integral abutment bridge located in Orange, Massachusetts, was instrumented with 85 gauges for evaluating the thermal seasonal effects on the bridge *[29]*.The soil-abutment interaction at the abutments was monitored to provide an understanding of the bridge and sensitivity to variations in soil properties. The author also constructed a detailed 2D and 3D FE models to evaluate the performance of the bridge using GT-STRUDL. The 3D model was used to represent the thermal response of the bridge and compare it with field data. The 2D model was used to evaluate the consistency of the 3D model response and the measured field data. They concluded that the model predictions

match well the field measurements within the shallow depths of the soil pressure behind the abutment and the difference between the modeling result and the field data of the abutment soil pressure is largely due to the properties of the backfill. Khodair, et al. conducted another research on study the effect of thermal load on the soil-pile system by comparing the 3D, non-linear finite element model with the field data *[52]*. They found that the influence of lateral loads imposed by the superstructure on the piles is confined within a small volume of soil around the piles and the lateral loads are not transferred to the MSE wall.

Interaction of the Abutment-Pile-Soil System. Integral Abutment Bridges are defined as simple or multiple span bridges in which the superstructure is cast monolithically with the substructure. The main issue related to the analysis of this type of bridge is dealing with the abutment-pile-soil interaction.

In 1994, Jewell et al. studied the influence of soil movement generated by the approaching embankment to the behavior of abutment and the pile foundation using the Geotechnical Centrifuge Tests. They concluded that pile behavior was found to be critically dependent on the factor of safety of the embankment. Frosch and his co-workers investigated the abutment and piles *[53]*. They drew the following conclusion:

The abutment response to temperature changes could be estimated as $\Delta L = \alpha(\Delta T)L$, where ΔL is the change in length, α is the coefficient of thermal expansion, ΔT is temperature change, and L is the length of the structure. However, the displacement is expected to be slightly less due to backfill restraint, pile resistance, and approach slab friction.

Piles integrally connected with the abutment bend in double curvature and lateral displacements in the soil correspond directly with temperature changes.

Kerokoski and Laaksonen focused on the influence of the properties of backfills to the behavior of abutments and piles foundation. They incorporated the laboratory tests results of backfill properties into the modeling process and then compared it with the field test data. The results show that the behavior of large steel pipe piles under the integral abutment can be sufficiently predicted by structural calculations. The abutment displacement influences the soil deformations and stresses around the upper part of abutment supporting piles. Also, the measured earth pressures on the bridge abutment were quite high because the backfill was well compacted *[54]*.

Duncan and Arsoy used the FEM to investigate the complex interactions taking place among the abutment, the approach fill, the foundation soil, and the piles supporting integral abutment bridges *[55]*. The results of this study indicate that these interactions have a

beneficial effect on the stresses in the piles supporting the bridges. Because of these interactions, the foundation soil acts as if it was softer, resulting in reduced shear and moment in the piles at a given amount of deflection at the tops of the piles and therefore reduced stresses in the piles. Lehane et al. developed a simplified elastic model for predicting thermal expansion effects by making use of standard frame analysis computer programs *[36]*. Only bridges with high abutments are considered, where sliding resistance effects are not significant. The expression for the equivalent abutment height and the spring stiffness are derived using data obtained from parametric computer studies which modeled the backfill soil as a linear elastic continuum of stiffness. A typical example demonstrates the simplicity of the application of the method using a frame analysis program of the type commonly used by bridge designers. The results are shown to comply well with those from a more elaborate finite element model of the soil and the structure. Ellis and Springman used both the FEM analysis results and the Geotechnical Centrifuge tests results to study the influence of the displacement of embankment to the abutment and soil interaction on the soft soil *[45]*. The results of the FEM match the centrifuge tests very well. They also gave some suggestion about the design approaches concerning the soil-structure interaction especially on the soft soil.

Finite Element Analysis and Modeling of IAB. In performing a finite element (FE) analysis, several material models need to be incorporated in the formulation to describe the different components of the integral abutment.

Approach Slab

The most common problems of integral abutment bridges are related to approach slab *[6], [2], [56]*. Initially, the approach slab is designed as a transition from approach to bridge, providing a smooth ride, preventing water leaking on to the abutment, and redistributing load when they are connected with the abutment. However, from a report by the Iowa Department of Transportation, the approach slabs are prone to settlement and cracking, which is manifested as the “bump at the end of the bridge” *[56]*. After a detailed review of approach slabs, four aspects were illustrated as primary factors which can affect its performance: (1) approach slab dimensions, (2) steel reinforcement, (3) the use of a sleeper slab, and (4) the type of connection between the approach slab and bridge. No consistency in the detailing of approach slabs exists from the survey which can be either connecting approach slab to deck slab with reinforcement, or connecting approach slab to corbel or lips of the abutment with reinforcement *[6], [2]*. In addition to that, a simple configuration by resting it on corbel or lip is also used.

Pile

According to the research, H or HP piles are the types that are most frequently used. However, other types such as cast-in-place, prestressed pipes, and concrete-filled steel-shell piles have are also been tried. Integral abutment piles should be designed with flexibility to accommodate lateral movement without losing its vertical load carrying capacity. The loads that the pile could be subjected to are dead loads, live loads, braking loads, temperature, shrinkage, and creep loads. Different states have different considerations. As is indicated, slightly less than half of the states only consider axial loads compared to the others, which analyze both the axial and lateral effects. For a pile under lateral load, soil-structure interaction is complex since the deflected shape of pile is dependent on the soil response, and the soil response is a nonlinear function of pile deflection. During the analysis, material and geometrical nonlinearities should be involved. The design method has been developed by considering the plastic behavior of pile, and the pile is modeled as an equivalent beam element with a fixed end at a certain length called equivalent embedded length. The pile head can be taken as either pinned or fixed. As for the pile orientation, weak axis bending and strong axis bending all display satisfactory performance. Preboring before pile driven, and backfill with granular material is a construction method to reduce the pile stress adopted by many states varying only the hole size and depth and the backfill soil density.

Soil

There is no consistency in the soil pressure used behind and around abutment. Soil-passive, active, and the combination of both soil pressures have been used among states and the distributions are considered to be uniform, triangular, and Rankine *[6], [2]*. As indicated, two thirds of the respondents did not consider any special procedure for reducing soil pressure on abutment and skew effects on soil pressure. Considering the characteristics for the soil in the soil-structure relation, p-y, f-z,q-z curves are used which respectively define the relationship between horizontal movement and lateral forces, vertical movement and slipping and pile tip settlement.

Abutment / Wingwall

The most desirable abutment is stub type, which, supported by a single row of piles, provides the greatest flexibility *[1]*. Regarding the survey question about the height limit of abutment, most of states have no such limitation though some applied a limitation to full integral abutments *[6]*.

A survey was conducted to study the wingwall type selection for integral abutment bridges *[57]*. The questions asked were about what limits, if any, should be considered for wingwall types, lengths, and support conditions. From investigations on the six different types of

wingwall, including cantilevered and independent supported in-line, U-type and flared wingwalls, results indicated little agreement exists among all the responding states.

Integral Abutment

The performance of the abutment–backfill system under thermal variations in integral abutment bridges built on clay was studied by Dicleli and Albhaisia *[20]*. They established a structural model of a typical integral bridge to analyze the nonlinear behavior of the piles and soil–bridge interaction effects. In their model, static pushover analyses of the bridge were conducted to study the effect of various geometric, structural, and geotechnical parameters on the performance of the abutment–backfill system under uniform positive thermal variations. It was observed that the intensity and distribution of backfill pressure is affected by the height of the abutment. Furthermore, the internal forces in the abutments were found to be functions of the thermal-induced displacements of the bridge deck, properties of the pile, and stiffness of the foundation clay. The stiffness of the clay surrounding the pile was observed to have a remarkable effect on the magnitude of the internal forces in the abutment such that the clay stiffness increases as the bending moment in the abutment increases.

Khodair and Hassiotis developed a three-dimensional, non-linear FE model of an integral abutment bridge to study the effect of thermal loading on the soil/pile system *[52]*. The FE model consists of soil continuum elements. Material non-linearity is accounted for both the piles and the soil. Hassiotis discussed the issue of data gathering and design details of an integral abutment bridge *[58]*. Scotch Road Integral Abutment Bridge at Trenton, New Jersey, was instrumented and the reactions of the bridge and its foundation to annual and daily thermal loading were observed. Most research on the integral abutment bridges is concentrated on the performance of such bridges under thermal effects *[20], [59], [60], [61],* and *[62]*. Recently Erhan and Dicleli developed the live load distribution equations for integral bridge substructures *[51]*. They created numerous 3D and corresponding 2D structural models of typical the integral abutment bridges and analyzed under AASHTO live loads. In their analyses, the effect of various superstructure and substructure properties such as span length, girder spacing, girder stiffness, abutment height, pile size, pile spacing, and foundation soil stiffness were considered.

A study by Karantzikis and Spyrakos demonstrated the importance in accounting for soil–abundant interaction of integral abutment bridges and develops an iterative design procedure of successive linear dynamic response analyses that considers the nonlinear behavior of the abutment caused by backfill soil yielding *[63]*. In this paper, the effect of dynamic soil-structure interaction (SSI) is studied for a new post-tensioned bridge system. Spyrakos and Loannidis examined the seismic response of a bridge with integral abutments based on the

analytical model validated through in situ testing *[64]*. Parametric studies were conducted to evaluate the response of the bridge system for various soil conditions. Their results demonstrated that the backfill has influential effect on the behavior of the bridge system. They also showed that including the construction of hinges at the foundation abutment joints greatly reduces the effect of thermal loads, creep, and shrinkage on the structure while they also reduce the magnitude of the lateral loads on the foundations.

Connection of Pile and Abutment. Dunker and Liulisted the foundation design concepts such as fixed-head pile, pinned-head pile, hinged abutment, fixed-base pile, pre bored hole, sleeved pile, etc. (see Table 2) *[65]*. They also state that the fixed-head H pile is the typical foundation connection between the abutment and pile in most integral-abutment bridges. Comodromos and Pitilakis conducted a parametric 3D non-linear numerical analysis to evaluate the influence of the interaction between a group of piles fixed in a rigid pile cap on both the lateral load capacity and the stiffness of the group *[66]*. Under the horizontal loading, for the particular soil profile and large diameter piles founded in soft clay, it was found the interaction significantly affects the stiffness efficiency factors of the pile group. Especially at the low deformation levels, the interaction is the largest with the central piles taking approximately 50% of the load of the side piles, Ooi et al. used the characteristic load method to estimate lateral deflections and maximum bending moments in fixed-head piles under lateral loads *[67]*. Since the single-fixed head piles can be influenced by the adjacent soil and by the response of other nearby piles, group amplification factors are introduced to amplify the single pile deflection and bending moment to reflect pile to soil and pile-to-pile interaction. The approach provides a good continuity by measuring the other published lateral tests on groups of fixed-head piles *[67]*.

Foundation Type. Dunker and Liu summarized the foundation type for support of integral abutment as the Steel H pile, Precast prestressed-concrete pile, pipe pile, etc. (see Table 3) *[65]*. They also stated that the Steel H pile is the most common pile in integral-abutment bridges. Then the second choice is the precast concrete pile. In fact, considerable research work has been performed recently to evaluate the performance of the Steel H pile and precast prestressed-concrete piles. Huckabee developed and evaluated the plastic design of the Steel HP- piles *[27]*. This design methodology is based on the ductility approach to permit incorporating the yielding in the piles as the bridge cycles through expansion and contraction. So that it can ensure the economical use of the material in the foundation and provide a long service life.

Nonetheless, Abendroth et al. presented the details of the first precast-concrete piled abutment bridge in Iowa *[68]*. They instrumented the bridge with a variety of strain gages,

displacement sensors, and the thermocouples to monitor and evaluate the performance of structure behavior. They concluded that the longitudinal movement of the east abutment was attributed to the rotation of the abutment, and there is also a formation of a crack in the PC piles matching the distinct change in behavior in the pile. Another test was conducted for the Tennessee Department of Transportation by Burdette et al. *[69]*. It took three years to investigate the behavior of integral abutments supported by prestressed concrete piles. In the field data of abutments on the prestressed concrete pile, it indicates precast concrete pile is appropriate for use in the integral bridge. Elchelman stated that the concrete piles are not a good choice to support integral abutment bridge *[70]*.

Joints. One of the most important factors of bridge design that may affect the bridge life is the expansion and contraction of joints. Those joints are usually expensive to purchase, install, and maintain. Therefore, the integral abutment bridge offers an alternative design with no expansion joints in the bridge deck. These types of bridges are mostly one single or multiple span with their superstructure combined integrally with their substructure *[71]*. The simple design, reduced costs, and long service life has made this type of bridge very common in both USA and Canada. Until 1999, more than 9773 bridges had been widely constructed in more than 30 US states and Canadian provinces *[2]*. Horvath conducted a survey about the condition of in-service bridges in 39 US States *[16]*. Table 4 summarizes the results of the survey regarding number, size of the bridge and structure components. Also, it includes the software that was used to design the bridge.

Table 2
Summary of design concepts *[65]*

Concept	Detail	Features	References
Fixed-head pile	Fig. 2	Relatively high moment at pile head, fixity provided by 300 to 600 mm embedment	Wasserman and Walker (1996), Burdette et al. (2000)
Pinned-head pile	Fig. 3	Negligible moment at pile head, usually detailed with padding	Abendroth et al., unpublished manuscript, (2006); Kamel et al. (1996)
Hinged abutment	Fig. 4	Negligible moment at pile head, usually detailed with elastomeric strip and dowels	Arsoy et al. (2004), PCI (2001), Maine DOT (2003)
Fixed-base pile	Fig. 5	Applicable for shallow bedrock, potential for insufficient flexibility and ductility	Dunker and Abu-Hawash (2005), Greimann et al. (1987), Abendroth and Greimann (2005)
Prebored hole	Fig. 6	Increased pile flexibility, reduction of downdrag	Iowa DOT (2006)
Pile sleeve	Fig. 5	Applicable for constructed fill especially adjacent to MSE walls, increased pile flexibility, reduction of downdrag	Dunker and Abu-Hawash (2005), Hassiotis et al. (2005)
Asymmetry		Accommodation for asymmetric site conditions, limited to moderate bridge length	Dunker and Abu-Hawash (2005), Abendroth and Greimann (2005)

Table 3
Summary of foundation types *[65]*

Type	Comments	State policies and examples	References
Steel H pile, weak axis	Potential for yield and low-cycle fatigue, need for relatively compact shape	Iowa, N.Y., and W.Va. policies	Iowa DOT (2006), New York DOT (2002), West Virginia DOT (2004)
Steel H pile, strong axis	Less flexible than weak axis orientation, may be less subject to flange buckling	Tenn., Colo., and Ill. policies	Burdette et al. (2002), Colorado DOT (2002), Illinois DOT (2003)
Prestressed concrete pile	Less flexible than H pile, may require padding	Tenn. policy, Iowa example	Burdette et al. (2004), Abendroth et al., unpublished manuscript, (200
Pipe pile	Less flexible than H pile	Ill., N.Y., and N.J. policies	Illinois DOT (2003), New York DOT (2002), New Jersey DOT (2004)
Timber pile	Less flexible than H pile, may require padding	Iowa policy	Iowa DOT (2006)
Combined pile and drilled shaft	Accommodates sensitive adjacent structures	Iowa example, Colo. examples	Liu et al. (2005)
Drilled shaft	Minimal flexibility	Colo. example	Liu et al. (2005)
Sheet pile	Limited to relatively short bridges	N.Y. examples	Carle and Whitaker (1989)
Spread footing	Minimal flexibility	Tenn. and Me. policies	PCI (2001), Maine DOT (2003)

Table 4
Summary of state and provincial responses *[16]*

State or Province* (1)	Total built (2)	First built (3)	Last built† (4)	Longest Built (m)			Software programs in use (8)
				Steel girder (5)	Precast-concrete girder (6)	Cast-in-place concrete girder (7)	
AK	50	1975	1995	—	41.2	—	L-pile, COM 624
AZ	50	1975	1985	—‡	—‡	—‡	—‡
AR	2	1996	1996	90.9	—	—	In-house software
CA	Thousands	1950	1995	—	—	122.0	BDS
CO	1,643	1905	1996	318.4	339.2	290.4	None
GA	25	1975	1992	91.5	—	125.1	P-frame, continuous beam
IL	350	1983	1996	61.0	91.5	36.6	No special application
IA	Hundreds	1962	1996	82.4	152.5	41.2	None
KS	1,000	1935	1996	136.8	126.4	177.6	None
KY	260	1970	1996	89.1	122.0	31.7	No special application
ME	18	1983	1994	57.3	45.8	29.3	No special application
MD	18	1986	1996	—	15.9	—	None
MA	20	1930	1996	106.8	84.8	43.9	GT STRUDL, L-pile, FEA
MI	6	1990	1996	—	147.9	—	In-house software
MN	No records	1958	1996	53.4	53.4	30.5	Staad 3
NV	Many	1980	1996	77.8	33.6	84.2	Standard girder design software
NH	2	1993	1996	45.8	24.4	—	—
NY	155	1980	1996	93.3	68.3	—	—
ND	600	1960	1996	122.0	122.0	48.8	None
NS	2	1986	1996	—	38.0	—	—
OK	50	1980	1996	—	91.5	—	No special application
OR	Unknown	1940	1996	—	335.5	—	STRUDL, BRIG2D
PA	50	1946	1996	122.0	183.0	—	Software being developed
QC	1	1988	1988	—	78.1	—	ANCAD, Structural analysis 2D
SD	818	1948	1996	112.9	209.2	106.8	No special application
TN	1,000	1965	1996	175.4	358.4	189.1	None
VT	10	1975	1993	24.4	—	—	In-house software
VA	25	1982	1996	97.6	235.5	—	None
WA	1,000	1965	1996	—	183.0	61.0	In-house, SEISAB
WV	60	—	1993	97.6	137.3	33.6	None
WY	1,458	1957	1996	100.0	127.0	99.0	BRASS, Risa, BDS
Over 9,773 built		1905	1996	318.4 maximum 24.4 minimum	358.4 maximum 15.9 minimum	290.4 maximum 29.3 minimum	

Note: 1 m = 0.305 ft.
*NS = Nova Scotia, QC = Quebec. Responses from Delaware, Louisiana, Manitoba, Mississippi, Montana, New Jersey, Newfoundland, and North Carolina indicated they had not built integral bridges.
‡At time of survey, several integral bridges were either under construction or in planning stages.
†Use of integral abutments discontinued.

(Correction in the table footnote: 1m=3.05 ft.)

Burdette et al. performed two sets of field tests on integral abutment bridges to compare the performance of steel H-piles and prestressed concrete piles *[18]*. Six abutments with steel piles and four with concrete piles were tested to describe the overall load-defection behavior of the pile-abutment system including a discussion of factors that limit horizontal displacement of both types of piles. The pile cracking at interface with abutment limits the maximum longitudinal displacement an abutment can withstand for concrete piles. The limiting element in the amount of displacement that an abutment supported by steel piles can tolerate is the behavior of the pile-abutment interface. In the tests of the steel H-pile, the abutment concrete remained essentially pristine for displacements up to 1.0 in., with only minor flaking. As the displacement was increased to 2 in. and beyond, a thin layer of concrete flaked off, with no apparent effect on the load-deflection behavior of the system. Even at displacements of 3 to 4 inches, the pile-abutment interface continued to function adequately. Burdette et al. stated that TDOT current design criterion, which limits displacement of the pile at the ground surface to 1.0 in., is conservative *[18]*. The data indicate that horizontal displacements as large as 1.5 in. and even beyond can be reasonably tolerated.

Other cyclic lateral load tests have been performed on a steel H-pile, a pipe pile and a precast concrete pile simulating 75 years of bridge year by applying over 27,000 displacement cycles *[72]*. From the test data, they concluded Steel H-piles loaded on the weak axis were the best pile type for supporting integral abutment bridges while precast concrete piles were not recommended for integral bridge, since under cyclic lateral loads, tension cracks progressively worsen and significantly decrease vertical load carrying capacity of these piles.

Overview of Bridge Monitoring Practice

Since there are no national guidelines for the design and construction of integral abutment bridges, some assumptions and theories have to be experimented on field studies in order to compare the monitored data with the analytical models. Over the decades, many field studies have been conducted; a brief literature review from 2000 and a detailed description of the recent years are discussed below.

In 1996, the Virginia Department of Transportation (VDOT), with an aim to study the behavior of integral bridge, instrumented and monitored an integral backwall bridge for 2.5 years. Based on the field monitoring data, the bridge behavior was satisfactory; only approach span settlements were found, and the relationships between soil pressure and temperature fluctuation were observed. As in 2005 and 2006, researchers began to put emphasis on the soil-structure interaction, and the method to relieve earth pressure on the

backwall. As a result, research to examine the use of EPS (elasticized expanded polystyrene) was conducted both for skewed and non-skewed integral abutment bridges. The EPS functioned well, and a proposed combination use of EPS and well-compacted granular backfill were put forward. In 2008, another project to study the performance of highly skewed semi-integral abutment bridges was ongoing.

The Minnesota Department of Transportation (MNDOT) conducted a research project on concrete integral bridge behavior from 1996 to 2004. A bridge in Rochester was instrumented to obtain abutment, pile, soil girder, deck, and thermal behavior. The effects of temperature, creep, and shrinkage were discussed. In addition, two live load tests were conducted in 1997 and 1999.

The Massachusetts Highway Department (MHD) monitored an integral abutment bridge for three years around 2005. Their efforts were put on the seasonal and yearly bridge behavior. The measured and designed temperature, abutment movement, and pile behavior were compared.

In Iowa, two skewed PC girder integral abutment bridges were studied for over two years of monitoring from 2005. Through this project, some guidelines were suggested for design, such as design temperature related parameters, and the time-dependent effects such as creep and shrinkage. In 2007, the first integral abutment bridge with concrete piles was studied in IA. By monitoring and analysis, the applications of concrete piles, which were supposed not to be appropriate for integral abutment bridges, were discussed. In 2008, the behavior of the approach slab was studied. Two different approach slabs were considered, a precast concrete one and a cast-in-place concrete one. Taking into the consideration of the reported unsatisfactory performance of approach slab by other literature, these two approach types were studied and compared.

DOTD has more experience in semi-integral abutment bridges, since it began to design this type of bridge in 1989. In their practice, an annular space, constructed between the backwall and roadway embankment, was created to accommodate the movement induced from temperature, creep, and shrinkage. Based on several analyses including conventional structural and geotechnical aspects, this bridge configuration was proved to be satisfactory.

The Pennsylvania Department of Transportation (Penn DOT) monitored four bridges around year of 2006. From this study, the following data were obtained and studied: abutment behavior, earth pressure, pile internal forces, girder stains and approach slab strains. A Penn DOT IA Design spreadsheet was evaluated and proposed.

The New Jersey Department of Transportation (NJDOT) instrumented a Scotch-Road bridge in Trenton around 2006. Thermocouples were used to measure temperatures; strain gauges were installed on the pile, abutment, and girder to obtain data about bending moments and axial stress; and soil pressure cells were utilized for measuring soil pressure on abutment, piles, and mechanically stabilized earth (MSE). Round displacement transducers were connected to four strain gauges for measuring the longitudinal displacement at the relief slab. Finally, the design procedure for integral abutment bridges and a step-by-step design procedure for piles were recommended.

The Indiana Department of Transportation (INDOT) studied the integral abutment pile system in 2004. They conducted two phases of research. The first one was a field study on the behavior of pile in-service, and the second one is an experimental study. For the later one, a nine-low-cycle lateral displacement was applied on the pile to evaluate its capacity. Through both studies, design recommendations were provided.

Field studies on the in-service or constructing integral abutment bridges provide valuable information about the behavior of the structure. Hartt et al. did a literature review about the field study of Integral Abutment Bridges *[73]*. During the past several decades, different research institutes, state DOTs, and universities have conducted many surveys regarding the practice. Here, several results are compared and summarized to describe the current practice on integral abutment bridges *[1], [2], [6]*.

North Dakota. Jorgenson completed a field study on the Cass Country Bridge in North Dakota. Jorgenson focused on the effect of air and deck temperature on the long concrete bridge with integral abutments and piers *[74]*. Experiments of the bridge's movement were made on a monthly basis for one year. The length of the bridge was measured directly with a steel tape corrected for temperature change. Measurements also considered the void space between the backside of the abutment, backfill soil, and the size of the opening in the expansion joint in the approach slab. Slope indicator casings were installed on each corner pile of each abutment and read on a monthly basis. The slopes of the piles were used to measure pile movement as well as bending stress in the pile.

Jorgenson concluded that the change of the length in bridge was due to the thermal expansion, which is a function of the air temperature at dawn on the hottest day, the air temperature at dawn on the coldest day, and the maximum air temperature on the hottest day *[74]*. The change of the length due to these functions complies with the changes in length determined from tape measurements and measurements of the openings in the expansion joints.

Minnesota. Lawver et al. instrumented and monitored an integral abutment bridge near Rochester, Minnesota, from the beginning of construction through several years of service *[75]*. One hundred eighty instruments were installed to measure abutment horizontal movement, abutment rotation, abutment pile strains, earth pressure behind abutments, pier pile strains, prestressed girder strain, concrete deck strains, thermal gradients, steel reinforcement strain, girder displacements, approach panel settlement, frost depth, and weather. The behavior of the bridge components was monitored throughout the construction process and during live load testing, and agreed with anticipated behavior. It was concluded that the instrumentation was working as intended with exception of the earth pressure cells, which were found to respond nonlinearly with temperature variations.

Research on the Integral Abutment Bridges in Iowa. The objectives of research program in Iowa were to evaluate the state-of-art for the design of pre stressed-concrete (PC) and integral abutment bridges; to validate the assumptions that are incorporated in the current-design procedures for these types of bridges when they are subjected to thermal-loading conditions; and, as appropriate, to revise and improve the current-design procedures for this type of a bridge, as that design relates to the thermally-induced displacements of the abutments and the thermally induced forces in the abutments and abutment piles.

Two skewed, PC girder, integral-abutment bridges in Iowa were instrumented over a two-year period to measure structural behavior. Longitudinal and transverse displacements and rotation of the integral abutments, strains in the steel piles and in the PC girders, and temperature distributions were recorded throughout the monitoring period for both bridges. The coefficient of thermal expansion and contraction for the concrete in core specimens that were taken from 20 bridge decks and from several PC girders was experimentally measured at the 100%-dry and 100%-saturated conditions. The longitudinal displacements of the integral abutments correlated well with the recorded change in the bridge temperature. Total longitudinal, pile strains exceeded the minimum specified yield strain of the steel for both bridges. Longitudinal strains in the PC girders were well within acceptable limits. The experimental data were used to calibrate and refine finite-element models of both bridges. Discrepancies were not fully explained for the differences between the predicted and measured thermal expansion of the bridge and vertical rotations of the integral abutments

Girton et al. instrumented and monitored two pile-supported integral abutment bridges in Iowa *[32]*. Field data were collected for two years and were compared to previously developed design equations. Field data included air temperature, bridge temperature, bridge displacements, and pile strains. Additionally, concrete core sample were collected from the

bridges and the coefficient of the thermal expansion was measured in the laboratory. However, they did not complete live load testing of the bridge.

They concluded that the coefficient of thermal expansion for bridges should be experimentally determined or predicted by some other means, as the AASHTO specification values for the coefficient of the thermal expansion were determined in this study to be too high. For skewed bridges, they suggest battering the piles in the lateral direction to limit lateral motion.

Research Integral Abutment Practice in Tennessee. The state of Tennessee has developed their guidelines for integral abutment bridge, which is summarized as follows.

Pile Configuration - Piles driven vertically and in only one row are highly recommended. In this manner, the greatest amount of flexibility is achieved to accommodate cyclic thermal movements. Likewise, in seismic events, the dampening forces are engaged to the largest extent by the embankment backfill rather than by the cap and piling, thereby reducing the damage resulting from large displacements.

Pile Orientation - Orienting the piling for weak-axis bending offers the least resistance and facilitates pile-head bending for fixed head conditions. However, due to the potential for flange buckling of steel H-piles, the total lateral displacement that can be accommodated is more limited than when piling is oriented for strong-axis bending.

Approach Pavements - Due to the difficulties in obtaining proper embankment and backfill compaction around abutments, approach pavements are recommended, especially for new construction. The approach slab must be anchored into the abutment back wall so that it moves in concert with the bridge. Otherwise, cyclic expansions will force the slab to move with the bridge without a mechanism to pull it back when the bridge contracts. As debris fills the resulting opening, repeated cycles will ratchet the slab off its support. The anchorage used to fasten the approach slab should be detailed to act as a hinge so that the slab can rotate downward without distress as the embankment settles.

Backfill Material - Porous, granular backfill, well-graded material is desirable. Uniformly graded material does not compact well and provides less interlocking of particles, thus acting more like marbles.

Drainage - Drain should be placed between the abutment back wall and the embankment backfill and should wrap around the back wall – between the parallel wing walls and the roadway embankment – since any settlement of the approach pavement will create a potential

gap through which surface runoff will flow. A perforated drain pipe, overlying an impervious layer of soil or plastic, should be placed at the base of the vertical stone column and should be sloped to provide drainage away from the abutment area.

Provisions for Expansion - In all cases where the approach roadway or a ramp is constructed of concrete, provisions for an expansion joint must be provided. Where the anticipated total movement at an abutment exceeds ½ in. and the approach roadway is asphalt, an expansion joint should also be considered. The reason for the latter is that larger movements can damage asphalt adjacent to the end of the approach pavement in the expansion cycle. During the contraction phase, a significant gap is created through which water can infiltrate the sub grade. If regular maintenance can be arranged to fill this gap with a suitable joint sealer in cold weather, no joint will be needed.

Construction Sequence - The following sequence is recommended when constructing steel bridges with integral abutments to reduce the effects of thermal movement on fresh concrete and to control moments induced into the supporting pile system:

- Drive the piling and pour the pile cap to the required bridge seat elevation. Pour the pile caps for the wing walls concurrently.
- Set the beams/girders.
- Pour the bridge deck in the desired sequence excluding the abutment back wall/diaphragm and that portion of the bridge deck equal to the back wall/diaphragm width. In this manner, all dead-load slab rotations will occur prior to lock-up, and no dead load moments will be transferred to the supporting piles.
- Pour the back wall/diaphragm and end area of the slab.
- Place the vertical drain system and backfill in 6 in. lifts until the desired sub grade elevation is reached. Place a bond breaker on the abutment surfaces in contact with the approach pavement.
- Pour the approach pavement, starting at the end away from the abutment, and progressing toward the back wall. If it can be so controlled, approach pavements should be poured in the early morning so that the superstructure is expanding and, therefore, not placing the slab in tension.

Burdette and et al. have investigated the behavior of integral abutments *[69]*. Although field monitoring was conducted, no full- scale field-testing was reported. Wieldable strain gages

were affixed apart for the top of the pile. Pressure sensors were also installed at regular intervals in the vicinity of expected points of zero lateral pressure. Rotation of the end of the pile was limited to the range of a typical bridge. Lateral variable differential transformers (LVDTs) were used to monitor lateral movement of the bottom of the abutment and the pile.

Semi-integral Abutment Bridges in Louisiana. DOTD designed and constructed its first prototype semi- integral abutment bridge in 1989. In this design, large longitudinal movements due to expansion and contraction, creep, shrinkage, and settlement are mitigated with an annular space, or gap, constructed between the back wall and the roadway embankment. This annular space is created using a geo synthetic-reinforced embankment constructed underneath the approach slab on the roadway side. To date, DOTD has constructed six prototype semi- integral abutment bridges. These bridges are located in the north, central, and western parts of the state. All six-prototype bridges were replacement projects in areas of the state where soil conditions are relatively good and, therefore, settlement was not a concern. The approach slab in the DOTD prototype design is cast integral with the bridge making it one continuous structure. Construction of a geo synthetic-reinforced embankment would eliminate the lateral pressure transfer to the back wall of the semi- integral bridge. The prototype design addresses the problem of the loss of soil support under the approach slab due to settlement or lateral movement. A gap created between the back wall and the reinforced embankment would eliminate the passive pressure from developing on the back wall due to bridge movement into the backfill. Permitting free back wall movement would also eliminate the potential for abutment rotation. Specifically, in the absence of a gap on the typical integral bridge, large movements would develop because of two factors:

Rotation/movement of the back wall would cause the development of higher lateral pressure that is closer in magnitude to the passive value, which is possibly higher than the design value (active or at rest). Rotation could cause the earth pressure distribution to become non-hydrostatic. Accordingly, the earth pressure resultant would act at a higher location. This results in higher overturning moments that may exceed the design values.

Field inspection of the six prototype semi-integral abutment bridges confirmed that they are all performing well, with a few exceptions. The presence of a gap was confirmed in all bridges. Some hairline cracks were found in several of the bridge decks, specifically at the connection between the approach slab and the back wall. These are expected and should be of no concern. Bridge SP 39-04-31 does not include an open joint at the interface of the approach slab with the roadway. Over the years, the bridge repeatedly expanded and contracted due to thermal variations. As a result, it pushed the adjacent asphalt pavement

away from the approach slab, forming a noticeable mound of asphalt and an open joint. This problem produced a bump that motorists felt when driving over the bridge ends. Periodically, the DOTD district office removed the asphalt mound and filled the joint with asphalt.

This problem was corrected in all subsequent semi- integral abutment bridges. Bridges SP 129-02-1799-1 and 129-02-1338-1 are presently in good condition, but may experience future problems due to the placement of incompressible gravel fill in the annular space between the geo synthetic-reinforced embankment and the back wall according to the design plans. This was confirmed by field inspections. The short spans of these bridges, and the fact that the fill material was probably not fully compacted, have reduced the impact of longitudinal movements. However, more frequent inspections of these two bridges should be made focusing the back walls and the connection of the back wall with the approach slab. In view of the review of existing records, field inspections, conventional structural and geotechnical analyses, and the finite element parametric study, the researchers concluded that the present DOTD design for semi- integral abutment bridges is structurally sound. Based on the results of a cost/benefit analysis, the researchers concluded that the present design is also cost effective. Therefore, the present design could be continued by DOTD in areas with fair to good subsoil conditions. Future designs should consider the effect of settlement and the potential for deep-seated slope stability at sites with thick, soft cohesive and/or highly compressible sub soils, specifically when the grades require relatively high embankments. A continuous gap should be established between the embankment and back wall in all future semi-integral bridge designs or to fill it with a soft compressible material, such as expanded polystyrene (EPS) geofoam. Attention should be given during construction to eliminate or minimize the potential for fallen debris inside the gap. Also, a weak joint should be created in the approach slab at some distance away from the back wall, e.g., 10 ft. (3 m) on a 40 ft. (12 m) long approach slab, to maintain a smooth transition between the bridge and roadway if excessive settlement does develop under the roadway embankment with time.

Integral Abutment bridges in New Jersey. The existing Scotch Road Bridge is a 45m-span composite steel structure supported on conventional abutments. The proposed structure is a 2-span continuous composite steel structure with integral abutments skewed at approximately 15_o. High Performance Steel (HPS) has been specified for the stringers. The Load and Resistance Factor Design (LRFD) method has been used to yield a more efficient structure. The performance of integral abutments could be improved by the development of new compressible elastic materials to be installed between the abutment and the surrounding backfill.

In order to revise the design specifications on integral abutment bridges, the New Jersey Department of Transportation funded a testing program to monitor the Scotch Road Integral Abutment Bridge *[76]*. The bridge was instrumented during construction and was monitored continually for two years. The following types of measuring devices were used: (1) strain gauges along the depth of the piles (as well as inside the abutment), (2) soil pressure cells for measuring the horizontal soil pressure behind the abutment, on the galvanized sleeves surrounding the piles, and at two elevations on the MSE wall, (3) inclinometers for measuring the rotations at the connection between the abutment and the stringers, (4) round displacement transducers connected to four strain gages for measuring the longitudinal displacement at the relief slab, and (5) thermocouples to monitor the temperature of the concrete slab and the steel girders.

Pennsylvania. Civjan et al. installed instrumentation in Bridge 109 on the US 220 section of I-99 at Port Matilda *[77]*. They monitored the behavior of Bridges 109, 203, 211, and 222 which were previously instrumented. Sixty-four vibrating wire based instruments were installed on Bridge 109 between November 2005 and May 2006. These instruments consisted of 5 pressure cells (VW-4820), 5 extensometers (VW-4450), 8 tiltmeters (VW-6350), 6 reinforcing bar strain gages (VK-4911), and 40 strain gages (VSM-4000). Two pressure cells and two extensometers were installed on the south abutment and three pressure cells and three extensometers were installed on the north abutment, and one pressure cell was placed to face the backfill. Twenty-four strain gages were installed on four HP piles with six gages placed at each of two different elevations. The arrangement of three strain gages at two different elevations permits the measurement of both axial load and moment variation. Another 16 strain gages were installed on four precast concrete girders at both the top and bottom flanges. Data obtained from the weather station consisted of ambient temperature, relative humidity, air pressure, solar radiation, wind speed, wind direction, and rainfall.

Indiana. Four bridges in Indiana were instrumented to observe the in-service behavior of integral abutment bridges as well as the behavior of the piles. These bridges ranged in length from 150 to 990 ft., providing a spectrum of behavioral data *[53]*.

To better understand the soil-pile-abutment system, the five-span, continuous prestressed, concrete bulb-tee integral bridge was instrumented. To evaluate the abutment movement, tilt meters and convergence meters were installed on the end bents. The convergence meter was oriented horizontally and operated perpendicular to the abutment. This meter measured the relative displacement between the end and the reference pile to determine the longitudinal abutment movement.

Strain gages were installed on piles along the length of the pile to evaluate the soil-structure interaction. All strain gages except the ones at ground level were installed prior to pile driving to provide the strain profile along the length of the pile enabling investigation of overall pile behavior. The strain gages at ground level were installed after pile driving.

The investigation resulted in the following conclusions:

- The abutment response to temperature changes can be estimated as $\Delta L = \alpha(\Delta T)L$. However, the displacement is expected to be slightly less due to backfill restraint, pile resistance and approach slab friction.

- Piles integrally connected with the abutment bend in double curvature and lateral displacements in the soil correlate directly with temperature changes.

Massachusetts. Bonczar et al. conducted a field study of integral abutment bridge located in Orange, Massachusetts to validate and economize the design of integral abutment bridges *[29]*. The integral abutment bridge described in this study spans over Millers River on Wendell Depot road in Orange, MA. The bridge was monitored using 85 instruments that capture critical parameters of bridge behavior during seasonal thermal fluctuations. There are six different types of gages using in the bridge; they are earth pressure cells, joint meters, tilt meters, temperature gages, strain gages and thermistors. Longitudinal and transverse displacements of the bridge are measured using joint meters on the east and west of each abutment. These instruments measure the displacement of the abutment walls relative to reference piles located on each side of the bridge. Figure 5 shows the abutment construction and instrumentation details.

Earth pressure cells were located behind the abutment walls at different heights to measure the backfill pressure distribution behind the walls. Vibrating wire strain gages were placed on the two exterior HP piles supporting each abutment. These instruments were concentrated in the top portion of the piles and are located at depth to 0.5, 2.5, 6.5 and 8.5 ft. measured from the bottom of the abutments. Temperature gages are located on the underside of the bridge deck at 10 ft. from the face of the abutments. All instruments are connected to CR10X Campbell Scientific data-logging unit through the use of six 16-channel multiplexer cards. The system is programmed to acquire and store data daily every 6 hours starting at 12:30 am from January 2002 to December 2004.

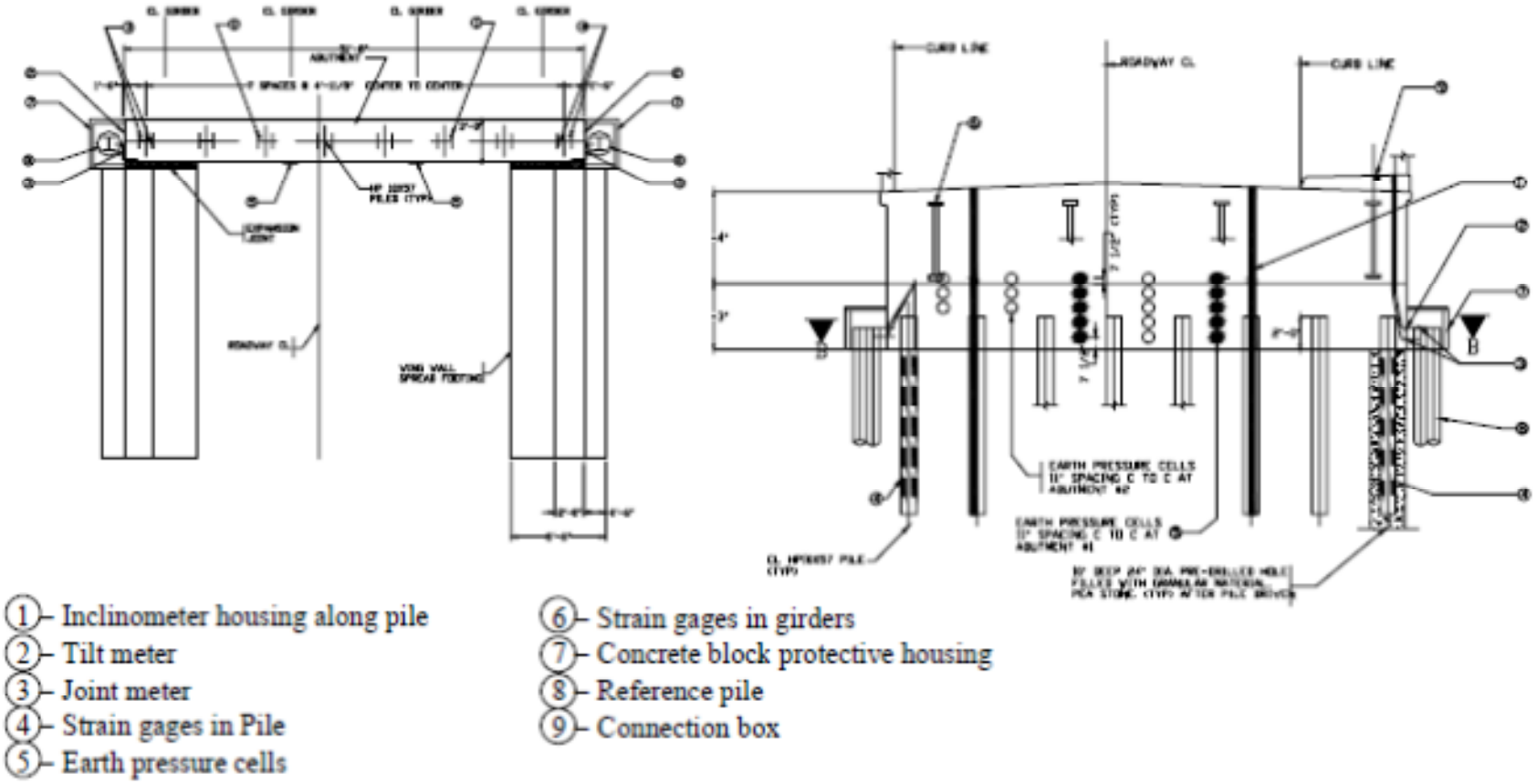

1– Inclinometer housing along pile
2– Tilt meter
3– Joint meter
4– Strain gages in Pile
5– Earth pressure cells
6– Strain gages in girders
7– Concrete block protective housing
8– Reference pile
9– Connection box

Figure 5
The abutment construction and instrumentation details

Overview of the Integral abutment bridges Practice in America: According to a 2004 survey, which included 50 state DOTs, District of Columbia DOT, Puerto Rico Highway and Transportation Authority and the Federal Lands Highway Division, the number of integral abutment bridges has increased significantly since 1995, when the two leading states (Tennessee and Missouri) were reported possessing 2000 and 4000 integral abutment bridges respectively *[6]*. Since 1995, some of the northern states were reported having a large number of integral abutment bridges, such as Illinois, Iowa, Kansas and Washington with each having over 1000 in-service, and Michigan, Minnesota, New Hampshire, North Dakota, South Dakota, Oregon, Wyoming, and Wisconsin each having around 100-500 in-service. However, it is not the case for southern states, like Florida, Alabama and Texas, which barely use integral abutment bridges. In addition, based on the survey, some of the design parameters were summarized and categorized in terms of maximum span, total length, maximum skew, and maximum curvature for prestressed concrete and steel girder bridges, respectively, details of which can be found in Table 5.

Table 5
Range of design criteria used for selection of integral abutments *[6]*

Prestressed	Max Span	Total Length	Max Skew	Max Curvature
Full Integral	60-200	150-1175	15-70	0-10
Semi Integral	90-200	90-3280	20-45	0-10
Deck extension	90-200	200-750	20-45	0-10
Integral Piers	120-200	300-400	15-80	3- No Limit
Steel	Max Span	Total Length	Max Skew	Max Curvature
Full Integral	65-300	150-650	15-70	0-10
Semi Integral	65-200	90-500	30-40	0-10
Deck extension	80-200	200-450	20-45	0-10
Integral Piers	100-300	150-1000	15-No limit	0- No Limit

Specifically, several states have their own design guidelines based on experience and research. Among all the states, Tennessee is the leader in the use of integral abutment bridges. With great experience, Tennessee DOT limits their integral abutment bridge length to 500 ft. for steel superstructure and 800 ft. for concrete one. However, this length has been actually exceeded since a 575 ft. steel bridge and a 1175 ft. concrete bridge are being used in-service now *[18]*.

New York DOT has constructed its longest in-service integral abutment bridges to 350 ft. The first integral abutment bridges can be tracked back to the late 1970s, which is a single

span steel bridge with a 100 ft. length; by 2004, there were 447 integral abutment bridges, 290 concrete superstructures, and 147 steel superstructures. The limits from the current criteria recommended that no limitation on individual length, but 650 ft. limits for total length together with no more than 45 degrees of skews *[25]*.

As for the Indiana DOT, they control the total length within 300 ft., and skew less than 30 degrees. However, they have already tried to design a bridge longer than the criteria, which is 990 ft., 13 skew degrees, individual spans ranging from 87-115 ft. *[53]*.

The criteria of the DOTs of Iowa, Colorado, and Virginia are illustrated as Tables 6 to 8.

Table 6
Bridge length limits for integral abutments in Iowa *[78]*

Beam type and pile shape	length and skew limits	Maximum end span
concrete beam HP 10×57	0-degree skew-575 feet 45-degree skew-425 feet interpolation for intermediate value	120 feet
steel girder HP 10×57	0-degree skew-400 feet 45-degree skew-300 feet interpolation for intermediate value	105 feet

Table 7
Bridge length limits for integral abutments in Colorado *[78]*

Type of Girder	Maximum Structure Length
Steel	640 feet
Concrete	790 feet

Table 8
VDOT length and skew limits for joint-less bridges *[17]*

	Full Integral	Semi-Integral	Deck Extensions
Steel Bridges	300 feet for 0° skew 150 feet for 30° skew	450 feet 30° max skew	450 feet 30° max skew
Concrete Bridges	500 feet for 0° skew 250 feet for 30° skew	750 feet 45° max skew	750 feet 45° max skew
Total Movement at abutment	1.5 in	2.25 in	2.25 in

It is a fact that many states have already constructed or plan to build integral abutment structures. In some states, it is even a requirement to give priority to integral abutment bridges when they consider the bridge structure styles in the preliminary design stage. Several other states otherwise prefer to use other integral types like semi-integral and deck extension bridges based on their successful experience. For example, New Hampshire uses deck extension and New Mexico uses semi-integral abutment bridges.

A survey in 2000 showed a detailed description of integral abutment bridge construction information such as number of bridges built, length of the longest bridges, etc. As it was stated, Tennessee built the longest precast-concrete-girder structure, 1,175 ft. (358.4 m). The longest steel-girder and cast-in-place concrete bridges were both built in Colorado, measuring 1,044 ft. (318.4 m) and 952 ft. (290.4 m), respectively. Table 9 shows results of a survey in 2005.

Table 9
2005 survey for prestressed concrete versus steel girders

	Prestressed concrete girder	**Steel girder**
Total Length	(ft)	(ft)
Full Integral	150-1175	150-650
Semi Integral	90-3280	90-500
Deck Extension	200-750	200-450
Integral Piers	200-750	150-1000
Maximum skew	(o)	(o)
Full Integral	15-70	15-70
Semi Integral	20-45	30-40
Deck Extension	20-45	20-45
Integral Piers	15-80	15-no limit

Backfill Materials. The most common backfill material used by European countries is well-compacted gravel or sand. In the USA, 69% of the responding states require well-compacted granular backfill, while 15% require the backfill to be left loose in an effort to reduce forces on the moving abutment stem. Some European countries require that the backfilling operations be conducted evenly on both sides of the structure, so as to not induce any undue lateral forces on the structure.

Other countries have no requirements at all for backfilling procedure.

None of the countries requires the use of an elastic 'cushioning' material behind the abutments. In the USA, 23% of the respondents use some sort of compressible material behind the abutment stem to lessen the soil pressure on the abutment stem.

When questioned about the design soil pressure behind the abutment stem, there is a little agreement among the European countries. Germany uses full passive pressure. Ireland and England have formulas in their design codes that estimate the soil pressure behind an Integral Abutment bridge as typically being between the classical 'at rest' pressure and full passive pressure. In Sweden, full passive pressure is only used if the movement is more than 0.005 times the abutment stems height. In Finland, the type of soil and the horizontal displacement of the abutment stem into that soil dictate when full passive pressure is applied *(5)*. In the USA *(3)*, 59% of the states surveyed accounted for full passive pressure. The remaining states used either minimum mandated loadings, active or at rest pressures, or no lateral loads were considered.

Approach Slabs. According to the European Survey, approach slabs are not required to be used with FIAB. However, most countries indicated that approach slabs were desirable and the length ranged from 10-25 ft. (3-8 m). Most states in the USA require the use of approach slabs to reduce impact forces on FIAB. Almost half (46%) of those states report that settlement of the approach slab has maintenance problems. Use of a buried approach slab or 'drag plate' makes settlement of the approach slab more easily repairable and may eliminate this concern (Figure 6).

Wing Walls. A wing wall, for the purpose of this survey, is defined as the retaining walls adjacent to the abutment stem to retain the fills behind the abutments and to ensure slope stability of the approach roadway.

New York State requires rigidly cast wing walls to be limited to 13 ft. (4 m). Wing walls longer than this are placed on their own foundation and isolated from the movement of the abutment stem. The European Survey respondents indicated that there are no restrictions on the use of U-wing walls (wing walls that are perpendicular to the abutment stem). Typically, the U-wing walls are cantilevered off the rear of the abutment stem. Although it is not common, some permit the use of piles beneath the U-wing walls. This is similar to typical details used in the USA, where 66% of surveyed states permit the use of U-wing walls but do not permit piles to be placed below them in order to allow the entire abutment to translate and rotate. Having multiple piles in the line of rotation provides a moment coupling force that restrains rotation of the abutment stem and may induce forces into the structure that were not accounted for in the design.

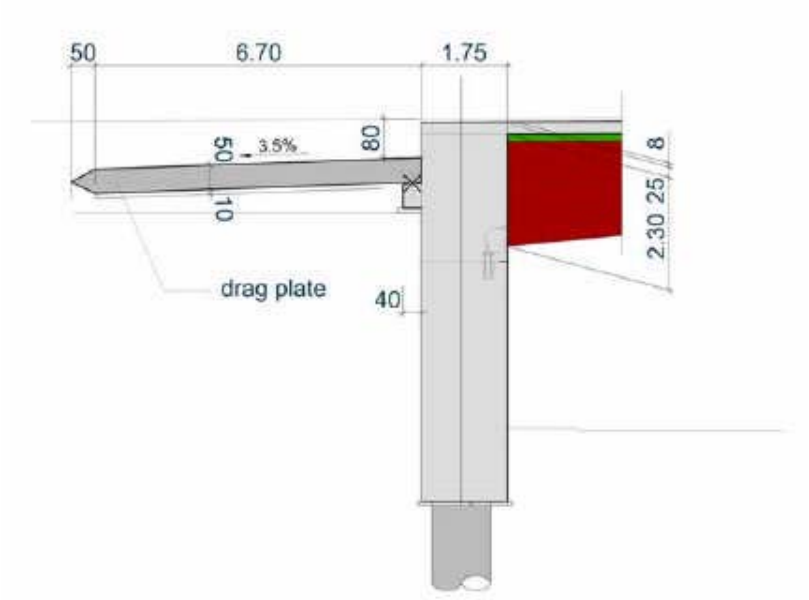

Figure 6
Example of 'drag plate' used in Germany

Table 10 shows a summary of design specification of integral abutment bridges in several European countries.

Table 10
Design specifications of integral abutment bridges in different countries

Criteria	England	Finland	Ireland	Germany	Sweden
Use fully integral abutment bridges	Yes	Yes	Yes	Yes	Yes
Maximum skew angle	30+	30	30+	None	None
Steel pile foundation used	Yes	Yes	Yes	Rarely	Yes
Steel pipe pile filled with reinforced concrete	Rarely	No	Yes	Rarely	Yes
Reinforced concrete pile foundation used	Yes	Rarely	Yes	Yes	No
Pre stressed piles used	Rarely	No	Rarely	No	Yes
Spread footing used	Yes	No	Yes	Yes	Yes
Use active soil pressure, passive soil pressure or other requirement	Other requirement	Depends on span length	Other requirement	Passive	Depends on span length
Approach slabs recommended	No	Yes	No	Yes	Varies
Wing walls permitted to be cast rigid with abutment stem?	Yes	Yes	Yes	Yes	Yes
Use semi integral abutment bridges	Yes	Yes	Yes	No	Yes
Maximum skew angle used	30+	30	30+	-	None
Steel pile foundation used	Yes	Yes	Yes	-	Yes
Steel pipe pile filled with reinforced concrete	Rarely	No	Yes	-	Yes
Reinforced concrete pile foundation used	Yes	Rarely	Yes	-	-
Pre stressed piles used	Rarely	No	Rarely	-	Yes
Spread footings used	Yes	Yes	Yes	-	Yes
Approach slabs recommended	No	Yes	No	-	Varies
Wing walls permitted to be cast rigid with abutment stem	Yes	Yes	Yes	-	Yes

Iowa Highway Research Board and IDOT: Design Procedure Guidelines

The following criteria are utilized in providing integral abutment bridge designs for the state of Iowa:

Hydraulics

Integral abutment bridges provide fixity between the superstructure and substructure, and provide greater protection against translation and uplift than conventional bridges. To address potential impact of a scour effect on proposed Integral abutment bridge sites, the following areas should be reviewed and analyzed where scour potential exists:

Stream Velocity

Any history of erosion or scour at the bridge site should be reviewed and a determination made if the new structure will alleviate any problems (alignment, restricted opening etc.) that may contribute to scour. Where a scour history is determined, the potential positive effects of an Integral abutment bridge should be noted. Scour information may be obtained by researching the IDOT Bridge Scour Evaluation Program and Structural Inventory and Appraisal coding records.

Bank Protection

To provide protection against scour, suitable slope protection construction should be provided. On all integral abutment bridges, geo-textile bedding shall be used against the front face of the abutment, under the slope protection and down the slope a minimum of 2m.

Skew Angle

The maximum skew angle for integral abutment bridge designs shall be thirty (30) degrees. Skew angles greater than this shall preclude the use of integral abutment bridge construction.

Foundation Types

The abutment and pile design shall assume that the girders transfer all moments and vertical and horizontal forces that are produced by the superimposed dead load, live load plus impact, earth pressure, temperature, shrinkage, creep, and seismic loads. The transfer of these forces shall be considered to be achieved after the rigid connection to the abutments is made. The rigid connection shall be detailed to resist all applied loads.

All abutment substructure units shall be supported on a single row of piles. Cast in- place (C.I.P.) or steel H piles may be used for structures with span lengths of 165 ft. (50 m) or less. Only steel H piles should be used for structures with span lengths over 165 ft. (50 m). When

steel H piles are used, the web of the piles shall be perpendicular to the centerline of the beams regardless of the skew. This will facilitate the bending about the weak axis of the pile.

To facilitate expansion, for bridge span lengths of 100 ft. or more, each pile at each substructure unit shall be inserted into a pre-bored hole that extends 100 in. below the bottom of the footing. The cost of provision of pre-boring these holes, casings and cushion sand shall be included in the Unit Price Bid for the pile item.

All details and notes required by the Foundation Design Report shall be placed on the plans. For bridge lengths less than 100 ft., pre-boring is not required.

The designer must determine the practical point at which the embedded pile is determined to be fixed. The following steps may be followed to perform such an analysis.

Calculate the thermal movement demand. For a bridge structure with equal intermediate bent stiffness, the movement demand will be equal. The atmospheric temperature range, coefficient of expansion and the structure's length should be considered.

The plastic moment capacity of the embedded length of the pile (embedded in the concrete cap) must be calculated. As stated earlier, the pile shall be oriented for bending about the strong axis.

The column capacity must then be calculated.

The adequacy of the back wall to resist passive pressure due to expansion must be calculated.

When CIP piles are used, they must be pipe casings conforming to ASTM A252, Grade 2 with a minimum wall thickness of 0.25 in. (6 mm). This shall be noted on the plans.

All piles shall be driven to provide proper penetration into a soil stratum where the required pile action is achieved, or to a minimum penetration of 6 m. This is to avoid a stilt type effect, provide for scour protection and to provide sufficient lateral support to the pile.

A pile bent configuration should be used for the integral abutment substructure detailing. For steel superstructure bridges, a minimum of one pile per girder shall be used.

The piles shall be designed to be flexible under forces and moments acting on the abutment. They shall be designed for vertical and lateral loads and for bending induced by superstructure movement. The fixity between the superstructure and the pile top may be ignored.

The initial choice of pile selection shall be based upon the recommendations that are contained in the Geotechnical Report. The axial loads shall be based upon the reactions from the superstructure design. This shall include the superstructure dead load, live load plus impact and the substructure dead load.

Live load impact shall be included in the design of integral abutment piles. The total length for single span bridges and the end span length for multiple span length bridges should be considered.

Superstructure

Adjacent pre-stressed box beams, pre-stressed concrete girders and structural steel beams may be used for integral abutment designs. They shall be analyzed to determine the stresses in the beams that will result from thermal movements. In pre-stressed box beams, such stresses shall be judged to be critical when the beams act by pulling an abutment with an approach slab. Mild reinforcement shall be added to the ends of pre-stressed box beams to resist such stresses.

Standard Drawings 2.13-1 through 2.13-5 provide conceptional detailing for rigidly connecting the pre-stressed concrete box beams and structural steel type superstructures to the abutments. Steel superstructures may have their girders directly attached to the piles through the use of welded load plates as shown on Standard Drawing number 2.13-1. Other type connections, such as bolting the girder to the abutment, may also be used. Pre-stressed girders may be connected by doweling them to the abutments.

Steel girders may be placed on plain elastomeric pads. The anchor bolts will pass through both the pad and the bottom flange of the girder. Another method is to use a longer bolt so that nuts may be placed above and below the bottom flange. The grade of the girder may be better controlled this way. Slotted holes should be used to allow better flexibility in aligning the girder.

Slotted holes should also be used with the doweling of pre-stressed members to the abutments.

Abutments

In integral abutment bridges, the ends of the superstructure girders are fixed to the integral abutments. Expansion joints are thus eliminated at these supports. When the expansion joints are eliminated, forces that are induced by resistance to thermal movements must be proportioned among all substructure units. This must be considered in the design of integral abutments.

The integral bridge concept is based on the theory that, due to the flexibility of piles, thermal stresses are transferred to the substructure by way of a rigid connection. The concrete abutment contains sufficient bulk to be considered a rigid mass. To facilitate the stress transfer, abutments shall be placed parallel to each other and ideally be of equal height.

The positive moment connection between the girder ends and the abutment provides for full transfer of temperature variation and live load rotational displacement to the abutment piling.

To support the integral abutment, it is customary to use a single row of piles. The piles are driven vertically and none are battered. This arrangement of piles permits the abutment to move in a longitudinal direction under temperature effects.

The most desirable type abutment is the stub type. It will provide greater flexibility and will offer the least resistance to cyclic thermal movements.

Piers

Piers for integral abutment bridges have similar design requirements and share common design procedures with the piers of a more traditional bridge. The primary distinguishing features of the piers for an integral abutment bridge involve their ability to accommodate potentially large superstructure movements and the sharing of lateral and longitudinal forces among the substructure units.

As with integral abutments, the piers must also be designed to accommodate the movements of the superstructure. Thermal movements are usually the major concern, although superstructure movements, due to concrete creep and drying shrinkage, will also be present to some degree. Creep and shrinkage movements may be ignored for pre-stressed concrete girders; however, for longer bridges, these effects must also be considered in the design of the piers.

As part of the overall structural system, integral abutment bridge piers will typically be required to carry a portion of the externally applied longitudinal and transverse loads on the bridge. In addition, thermal movements of the superstructure will induce forces as the piers attempt to restrain those movements.

As the superstructure expands and contracts with seasonal temperature changes and, to a lesser extent, creep and shrinkage, the tops of the piers will be forced to undergo displacements relative to their bases. These displacements will produce curvatures in the columns that can be closely estimated based on the magnitude of the movements, the fixity conditions at the top and bottom of the columns, and the height of the columns.

Once curvatures are estimated, effective column stiffness must be considered to compute internal moments and shears. A set of equivalent external forces, in equilibrium with the computed internal moments and shears, must be computed. This set of equivalent forces is used in subsequent analysis to represent the effects of superstructure movements on the piers.

Forces induced by the distribution of the superstructure movements must be computed. Also, the distribution of externally applied loads to the substructure units must be estimated.

Similar to the design of a traditional pier, piers of integral abutment bridges are designed for load combinations. Often, load combinations involving temperature, creep, and shrinkage control the design of integral abutment bridges, as opposed to combinations containing external loads only. A pier must be capable of undergoing the imposed superstructure movements while simultaneously resisting external forces.

A bearing at a pier of an integral abutment bridge structure should only be fixed when the amount of expected expansion from the bearing to both abutments and adjoining pier is equal. All other cases should use expansion bearings.

The following guidance shall be followed in determining the type of pier selection in integral abutment bridge designs:

Continuity at Piers. The concrete deck slab must be physically continuous, with joints limited to saw cut control joints or construction joints. Distinction must be made between slab continuity and girder continuity at the piers.

If, in accommodating the load transfer, girder continuity is deemed appropriate by the design, the superstructure shall be assumed continuous for live loads and superimposed dead loads only. Girders shall be erected as simple spans and made continuous by the addition of mild steel in the deck slab.

Longer span integral abutment bridges; i.e., those with spans over 100 ft. shall be detailed to provide a deck slab placement sequence if girder continuity is to be provided. Where applicable, casting of concrete diaphragms over the piers should be done concurrently with placement of the slab.

When slab-only continuity is provided over the piers, girders are to be designed as simply supported for all loads.

Types of Piers. To design piers to accommodate potentially large superstructure movements, the following options are available:

- Flexible piers rigidly connected to the superstructure;
- Isolated rigid piers, connected to the superstructure by means of flexible bearings;
- Semi-rigid piers, connected to the superstructure with dowels and neoprene bearing pads;
- Hinged-base piers, connected to the superstructure with dowels and neoprene bearing pads.

Flexible Piers. A single row of piles, with a concrete cap that may be rigidly attached to the superstructure, provides a typical example of a flexible pier. This type of pier is assumed to provide vertical support only. The moments induced in the piles due to superstructure rotation or translations are small and may be ignored.

A bridge constructed with flexible piers relies entirely on the integral abutments for lateral stability and for resisting lateral forces. Passive pressures behind the back walls, friction, and passive pressures on the abutment piles should be mobilized to resist lateral and longitudinal forces.

With this type of pier use, temporary lateral bracing may be required to provide stability during construction. Designers must consider a means to account for passive soil pressures in the vicinity of the back walls.

Isolated Rigid Piers. Rigid piers are defined as piers whose base is considered fixed against rotation and translation, either by large footings bearing on soil or rock, or by pile groups designed to resist moment. The connection to the superstructure is usually detailed in a way that allows free longitudinal movement of the superstructure, but restrains transverse movements. This type of detailing permits the superstructure to undergo thermal movements freely, yet allows the pier to participate in carrying transverse forces.

With this class of pier, the superstructure is supported on relatively tall shimmed neoprene bearing pads. A shear block, isolated from the pier diaphragm with a compressible material such as cork, is cast on the top of the pier cap to guide the movement longitudinally, while restraining transverse movements.

This type of pier represents the traditional solution taken with steel girder bridges at so called expansion piers. It offers the advantage of eliminating the stresses associated with

superstructure thermal movements. It also provides piers that require no temporary shoring for stability during construction.

In utilizing this system, additional consideration must be given to the detailing associated with the taller bearing pads and the detailing associated with the shear key. In addition, because the pier and the superstructure are isolated longitudinally, the designer must ensure that the bearing seats are wide enough to accommodate seismic movements.

Semi-Rigid Piers. These piers are similar to rigid piers. Their bases are considered fixed by either large spread footings or pile groups; however, the connection of the piers to the superstructure differs significantly.

In utilizing pre-stressed concrete girders that bear on elastomeric pads, a diaphragm is placed between the ends of the girders.

Dowels, perhaps combined with a shear key between girders, connect the diaphragm to the pier cap. Compressible materials are frequently introduced along the edges of the diaphragm, and, along with the elastomeric bearing pads, allow the girders to rotate freely under live load.

The dowels force the pier to move with the superstructure as it undergoes thermal expansion and contraction and, to a lesser extent, creep and shrinkage. Accommodation of these movements requires careful analysis during the design of the piers. Normally, the stiffness of the piers is assumed to be reduced due to cracking and creep.

There are several advantages to this type of pier: detailing is simplified, uses of thin elastomeric pads are relatively inexpensive, temporary shoring is not required during construction, all piers participate in resisting seismic forces, and the girders are positively attached to the piers. In addition, with many piers active in resisting longitudinal and transverse forces, the designer need not rely on passive soil pressures at the integral abutments to resist lateral forces.

Design of semi-rigid piers is slightly more complicated because careful assessment of foundation conditions, pier stiffness and estimated movements is required. In some situations, semi-rigid piers are inappropriate. For example, short piers bearing on solid rock may not have adequate flexibility to accommodate movements without distress.

Hinged-Base Piers. This type of pier may be used to avoid the need for an expansion pier in a situation where semi-rigid piers have inadequate flexibility. A “hinge” is cast into the top of the footing to permit flexibility of the column.

Temporary construction shoring may be required, and additional detailing requirements at the top of the footing may increase cost; however, the designer should keep this alternate in mind under special circumstances where the other pier types are not feasible.

The Virginia DOT conducted a study designed to test the feasibility of using elastic inclusion at the integral backwall. The bridge was monitored continuously for 5 years *[23]*. Electronic instrumentation consists of earth pressure cells installed at the backwall, strain gages attached to girder flanges, and linear displacement transducers and tiltmeters placed on the backwall. Earth pressure cells and strain gages are of the vibrating-wire type. All sensors are interfaced with Campbell Scientific CR-10X dataloggers, sampling every hour. All pressure cells are recessed in the backwall, with the sensing surface flush with the backwall surface.

A simple telltale gages was installed to measure the thickness of elastic inclusion in service. This gage consists of a 7.9 x 7.9 x 0.079 in. (200 x 200 x 2 mm) aluminum plate attached to the face of the EPS, with a connecting stainless steel threaded rod of 0.2 in. (5 mm) in diameter, protruding through the opening in the backwall. Periodic measurements of the length of the protruding rod indicate the magnitude of EPS compression. These manual measurements are typically conducted during the hottest and coldest times of the year to reveal the full range of EPS working strains and to detect creep. All ambient air temperatures are recorded under the deck, in the proximity to the backwall.

The elastic inclusion consisting of a layer of elasticized EPS 10 in. thick has performed effectively during the 5 years of field monitoring. The function of the elastic inclusion is to interface a stiff backfill mass with a structure without generating excessive stresses and settlements. The presence of a well-compacted select backfill material at the bridge approach is essential for good results (low maintenance). The use of inferior backfill negates advantages provided by the elastic inclusion.

Design and analysis of integral abutment bridges vary from one state to another. Currently, the American Association of State Highways and Transportation Officials (AASHTO) do not directly address specific methods of analysis and design for integral abutment bridges *[79]*. Many states developed their own methodologies for the design of integral abutment bridges and built their own specifications and regulations due to the local construction circumstances. A survey summary was compiled by the Maruri and Petro *[80]*. The purpose of the survey was to collect the usage of integral abutment, their policy, and their design criteria of different states. Their conclusion indicates that many problems regarding the behavior of the foundation remain unresolved. In the survey report, the design of the foundation for integral abutments needs to account for most attention because the interaction of the abutment, pile,

and soil remains uncertain and most of the research concentrated on the response of the abutment-pile-soil system. Different states also have different choices regarding connection of pile and abutment, foundation type, type of pile, pile design consideration and modeling, etc.

IAB for Louisiana's Soft and Stiff Soils

This section is devoted to the instrumentation of superstructure and substructure of the bridge in order to monitor the performance of the bridge during its life. This section also includes part of finite element modeling using ABAQUS software including the mesh, material models and materials parameters. The numerical modeling part is still under process and the outcomes of the instruments will help to improve it.

The extensive instrumentation planned for this project will allow for the monitoring of short and long-term performance of IAB components and system. Field monitoring consists of placing instruments as shown in Figure7, Figure 8, and Figure 9 on integral abutment bridge. Instruments used for field monitoring include vibrating wire strain gages, vibrating wire tiltmeters, borehole vibrating wire extensometers, vibrating wire pressure cells, and piezometers. An appropriate data logger and data acquisition system was installed. Data was acquired by the research team on a monthly basis for a period of six hours during the period of two years.

A detailed instrumentation plan for Caminada Bay Bridge was developed with the objective of obtaining useful and reliable field data for sufficient time to obtain detailed information about the response of piles, backfill, embankment, abutments, and other components of the IAB system with the goal of understanding the response of IAB system in Louisiana soils. The data obtained from the proposed research was analyzed and results will be presented in a form suitable so that DOTD can use the results for developing specifications for construction of IAB systems in Louisiana. The secondary stresses due to time-dependent effects such as temperature change, creep, and shrinkage are the major concerns for IABs. Therefore, the bridge superstructure was instrumented for temperature changes and strains induced by all time-dependent factors. Instrumentations were placed across the bridge section at mid-span for positive moment effect and at the bridge end for negative moment effects. The sensors were also placed on the abutment and the approach slab span (see Figure 9) since these are the areas of concern as discussed earlier. Therefore, the bridge was monitored not only the superstructure, but also the abutment, backfill, piles, and approach slab as a system. The strain gages on piles are proposed to be 8 ft. apart from each other on piles of approximately 56 ft. length. The additional details of instrumentation of superstructure are shown in Figure 9. Figure 8 shows the plan view of piles that were instrumented. In this way the performance

of the whole structural system (bridge and approach span) is evaluated, which will provide guidance for future applications of similar bridges.

Monitoring of Substructure. The instrumentation plans for two IABs are shown below. Figures 7, 8, and 9 show the instrumentation plan for the IAB at Caminada Bay Bridge. One side of the IAB was proposed to be monitored. It included two piles, one abutment, backfill on one side of the bridge, slab span, and approach slab. This instrumentation plan has been refined according to the design details (see Bent 1, DOTD Design Sheets 104 and 147) of the IAB. DOTD installed a separate pile, which will be specifically used for lateral load test to develop P-Y curve for the pile in soft soil. DOTD data from settlement instrumentation at the soft site will also be available to the LSU team for this research.

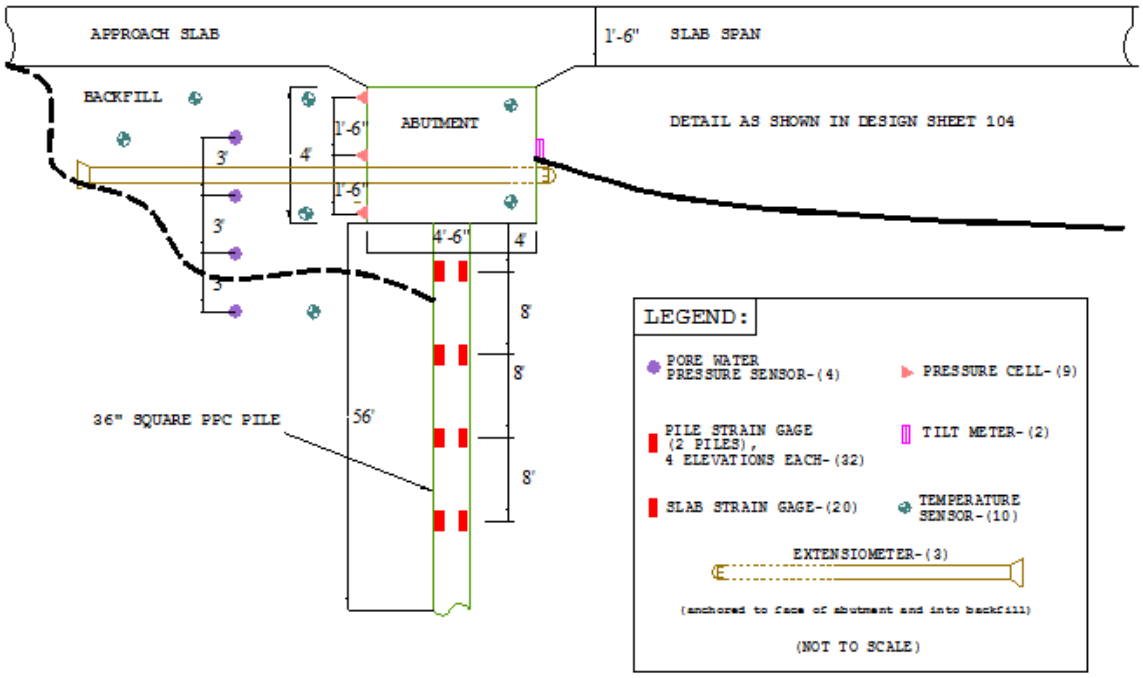

Figure 7
Instrumentation plan for Caminada Bay Bridge –substructure

(Bent 1, DOTD Design Sheets 104 and 147)

The temperature of the bridge was measured through thermocouples at the mid-span and on one or two ends of the bridge, along the depth of the bridge in the bridge deck. The temperature induced strains were measured in beams near the abutment section and mid-span section. Movement of bridges due to temperature changes was also monitored.

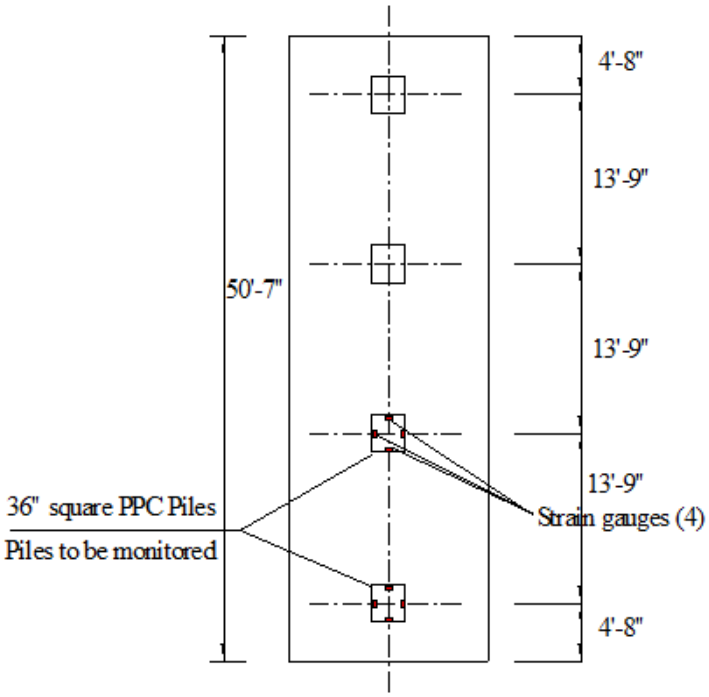

Figure 8
Plan view of piles (Bent 1, DOTD Design Sheet 109)

Bridge Diagnostic Inc. (BDI) provided and installed all sensors. Thirty-two sisterbar strain gages were attached to pre-stressing steel of two piles in the concrete cast yard before casting the piles. After applying the pre-stressing tension to the tendons, the concrete was cast and the piles were shipped to the bridge site. Strain gage integrity was checked before shipping, after arrival and after pile driving. Figure 10 shows a photo of pile driving. The piezometers were installed in two locations in the backfill. Two boreholes were drilled and the piezometers were attached to PVC piles and were lowered in the cased boreholes (Figure 11), gravel was poured around the piezometers, and then the casings were pulled out. Care was taken to protect the cables and route them inside PVC pipes to the data logger.

The pressure cells were mounted at the locations shown in Figure 7 using stainless mounting hardware. In addition, BDI provided a mason for a small pad of mortar that was placed behind each cell during installation to ensure that it is making uniform contact with the concrete surface (Figure 12). The tiltmeter was bolted to the outer face on Bent 1 and

protected with a cover plate before placing a granular fill soil around it (Figure 13). Four strainmeters were buried in the backfill soil; two were attached to Bent 1; whereas, the other two were installed in the backfill soil to measure the soil movement (Figure 14).

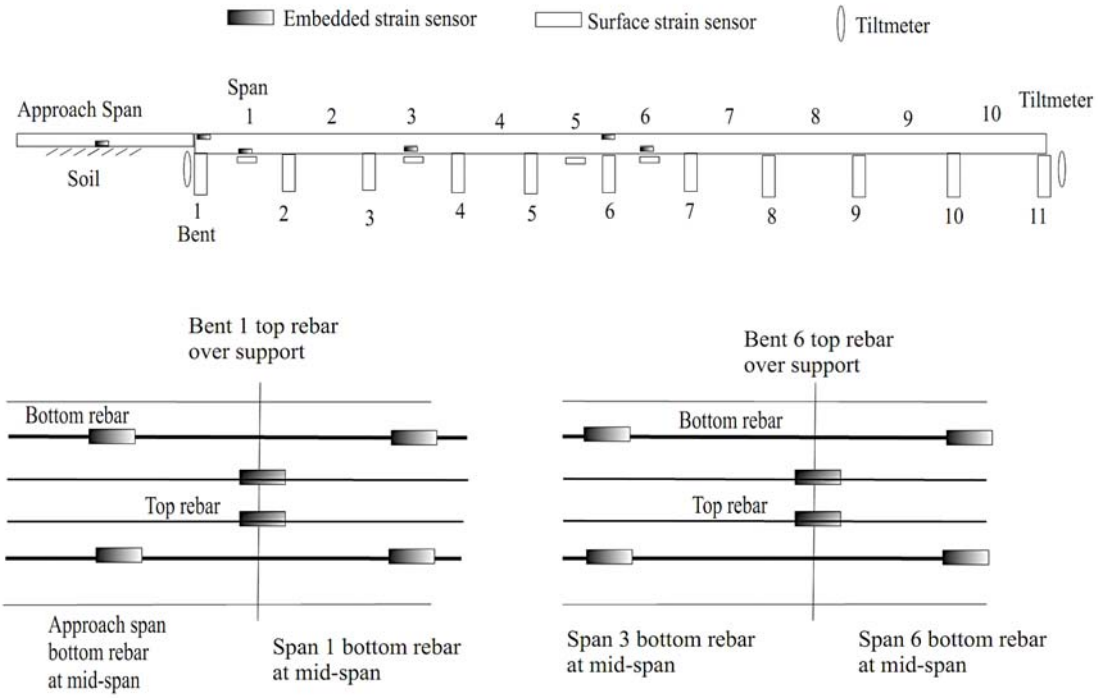

Figure 9
Instrumentation plan for the superstructure at Caminada Bay Bridge

Figure 10
Pile driving at Caminada Bay Bridge

Figure 11
Installation of piezometers

Figure 12
Pressure cells mounted on Bent 1 face

Figure 13
Titlmeter mounted on Bent 1 face

Figure 14
Two strainmeters; one is attached to Bent 1 face while the other is buried in the backfill soil

The following parameters are identified for monitoring of the superstructure:

(a) Strains: two types of strain gages are used for this purpose:

- Embedded strain gages will be installed during the constructions of the cast in-place slabs.
- External Vibrating Wire (VW) strain sensors will be placed at the surfaces of bridge slabs.

(b) Temperature: Temperature effects are the major concerns of integral abutment bridges.

- A continuous monitoring of temperature effects is essential for establishing the performance of integral abutment bridges.

(c) Slopes: The slopes changing of abutments are monitored using tiltmeters.

The original proposal calls for 12 embedded sensors and 8 surface sensors. They are arranged as shown in Figure 9. The two tiltmeters are arranged at Bent 1 (abutment, Figure 13) and Bent 11.

This section is devoted to introducing the procedure of instrumentation applications on the superstructure, specifically the installation of the embedded strain gages on the slabs. The sensors were provided and installed by BDI. The initial discussion of the sensor locations was issued on Nov 3, 2010, the installation of sensors was arranged on Nov 17, 2010, and the corresponding slab concrete pouring was finished on Nov 18, 2010. Everything was

implemented according to the original plan. There were no errors or defects in the aspects of construction and installation and no environmental detrimental on the sensors on the day of construction, so there was no damage to any of the sensors.

The strain gage embedded in the slab is shown in Figure 15. The sensor with the blue color was attached on the green rebar which were tied with the rebar in the slab. Through measuring the strain of the rebar in the green color, the strain of the slab will be deduced. The size effect of the green rebar which may affect the actual slab strain was considered during designs as referred from the BDI engineers. In addition, the strain gage was embedded with the thermometer to measure the real time temperature and that will be conveniently used for further evaluation of thermal behaviors.

Figure 15
Strain gage

The final instrumentation applied on the superstructure had a total of 22 sensors, with 14 embedded sisterbars and 8 surface strain gages, as shown in Figure 16. They are applied on the 18 in. (46 cm) depth decks and used to measure both the positive and negative strains due to the temperature changes. Specifically, the embedded sisterbars were placed at the rebar locations before the pouring of concrete with about 3 in. (7.5 cm) above the slab bottom surfaces on the approach slab, Span 1, Span 3, and Span 5, and about 2 in. (5 cm) below the top surface on Bent 1, Bent 2, and Bent 5. The surface strain gages, otherwise, are mounted under the slab bottom surfaces from Span 3 to Span 6 after the completion of the concrete pouring.

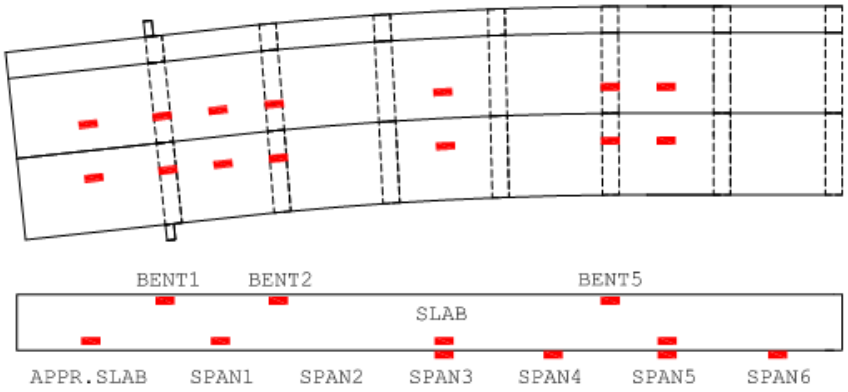

Figure 16
Plan and aide views of instrumentations on the approach slab and the first six slabs

Fourteen strain gages were applied on the first five spans and the approach slab. As shown in Figure 17, strain gages were placed on the slab and approach slab bottom to measure the positive bending strain and on the top of the bents for the negative bending stain. As shown, the bottom strains gages were placed at the approach slab, Span 1, 3 and 5; while the top strain gages were on Bent 1, 2, and 5. Both the top and bottom strain gages are placed at the center of the roadway, not the center of the bridge width.

First, all the locations with sensors were marked by orange paint, as shown in Figure 18. Then, the engineers tied the strain rebar to the slab rebar at the corresponding top or bottom locations. In order to be deformed with the slab rebar and to reflect the real conditions, the sensor rebar was tightly attached to the slab rebar. In this project, both steel and plastic wires were used for binding in case of any slip or separation between the two rebar during concrete pouring and vibration. In addition, all the cables were arranged under the designed path and assembled and ran through a hole out to the temporary location. After all the sensors were installed, the engineers checked all the cables to specify the locations and the corresponding numbers of the sensor. From the device reading, all the sensors were under normal conditions.

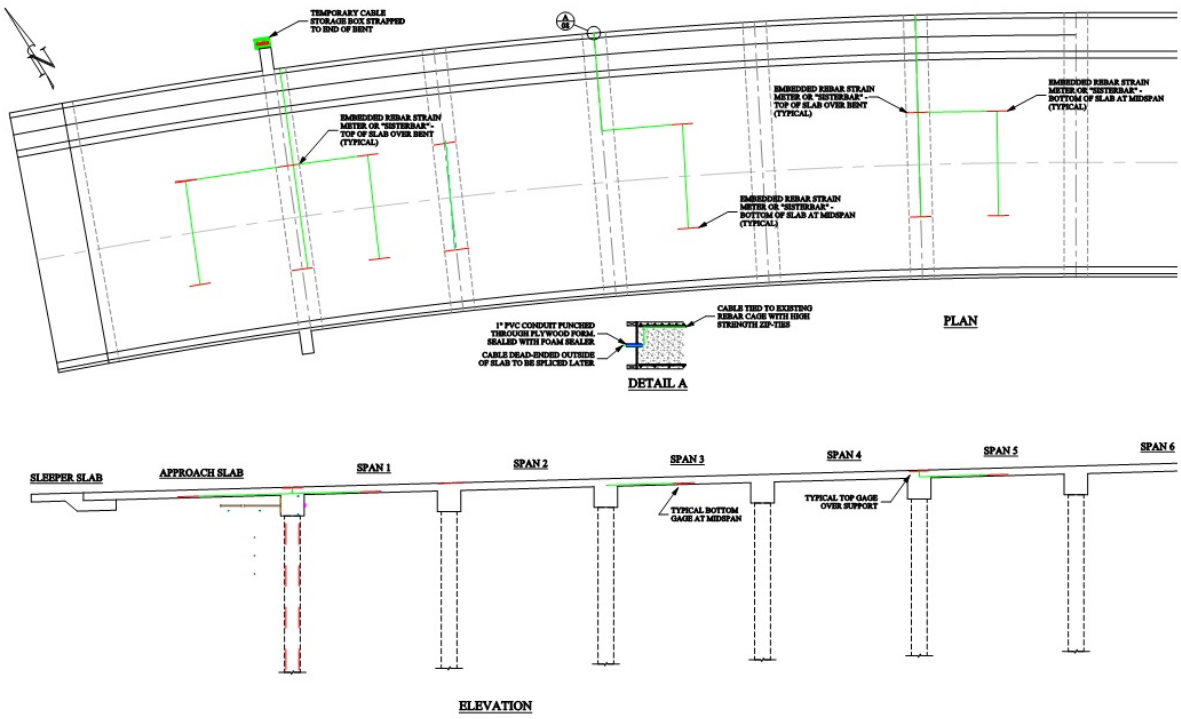

Figure 17
Instrumentation view

Figure 18
Sensor installation

The concrete was placed around 8 am and lasted for six hours, as shown in Figure 19. The engineers were informed to be careful when vibrating concrete around the sensors in case of any damage to the sensors. Although it was done with extreme caution, vibrations could still damage the sensors because, after the concrete, the sensor will be covered and may not be located. Also, there was a possibility for the vibrator to touch the steel rebar attached by the

sensor rebar. However, generally, such vibrations will not damage the sensors as referred from the BDI engineers.

Figure 19
Concrete placement

All the work was completed around 2 pm in the afternoon, as shown in Figure 20. There were no breaks during the work and all the sensors were successfully embedded in the slab. There was no check on the sensor at this step and no data recorded during the concrete pouring.

Figure 20
Final condition

Figure 21 shows the instrumentation plan for the IAB at the stiff soil site (Bodcau Bayou Bridge) and this IAB is expected to be much smaller compared to the IAB at the soft soil site.

The instrumentation plan includes four piles at Bent 1, backfill next to Bent 1, approach slab, and sleeper slab.

The following parameters are identified for monitoring of the sub-structure:

(a) Strains in piles: four piles were instrumented with vibrating wire strain gages to monitor their deflection which will be used to compare the behavior with the FE modeling.

(b) Interaction between Bent 1 and soil: pressure cells and deformation meters acquire the soil pressure and lateral movement of the bent as a result of thermal stresses.

(c) Temperature*:* Temperature effects are the major concern of integral abutment bridges. Continuous monitoring of temperature effects is essential for establishing the performance of integral abutment bridges.

Forty-six vibrating wire strain gages were welded onto the flanges of the HP 14x89 piles supporting End Bent 1 before driving the piles (10 gages on HP1-1 and 12 on each of HP1-3, HP1-4, and HP1-7) (see Figure 22, Figure 23, and Appendix A). All strain gages were protected using steel channels welded around them. Two tiltmeters were mounted on the back face of Bent 1 (Figure 24), four pressure cells were bolted on the same face (Figure 25), and three deformation meters were attached (Figure 26). In addition, two thermistors were buried in the backfill soil.

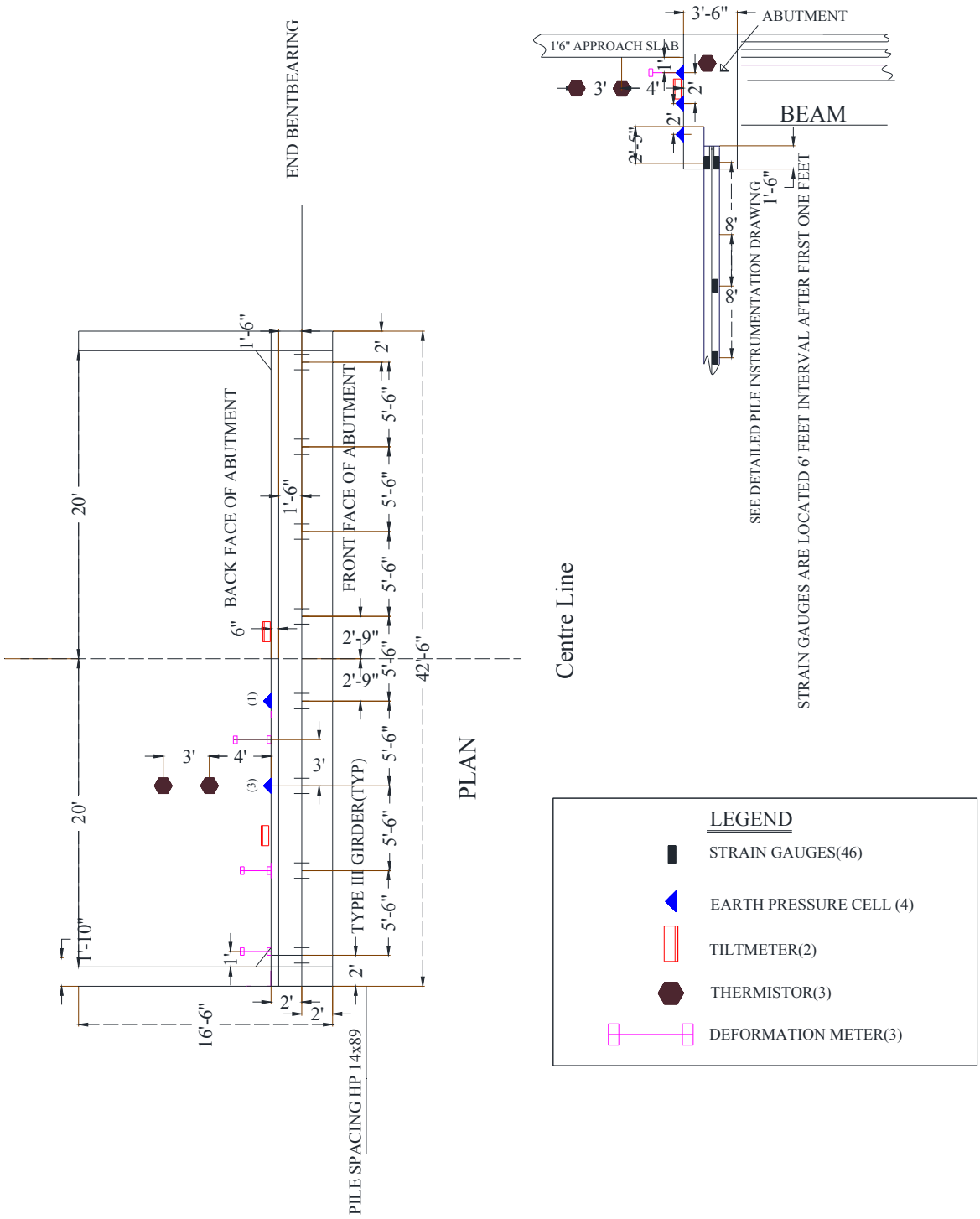

Figure 21
Instrumentation plan for Bodcau Bayou Bridge sub-structure (End Bent 1)

Figure 22
Photo of strain gage welded on the pile flange and cover plates to protect wiring

Figure 23
Pile driving at Bodcau Bayou Bridge site

(a) (b)

Figure 24
Installation of tiltmeters on the back face of Bent 1 of Bodcau Bayou Bridge: (a) one tiltmeters installed (b) two tiltmeters

Figure 25
Installation of four pressure cells on the back face of Bent 1 of Bodcau Bayou Bridge

Figure 26
Installation of deformation meters on the back face of Bent 1 of Bodcau Bayou Bridge

Layout of Instrumentation. The instrumentation applications on the superstructure are conducted by the BDI Company. Specifically, 12 sisterbar strain gages were embedded in the concrete slabs and prestressed and precast concrete (PPC) girders, as shown in Figure 27; and 10 surface strain gages were mounted on the surfaces of the PPC beams, as shown in Figure 28. The information pertained to the sensor locations are referred to the report by BDI instrumentation manual.

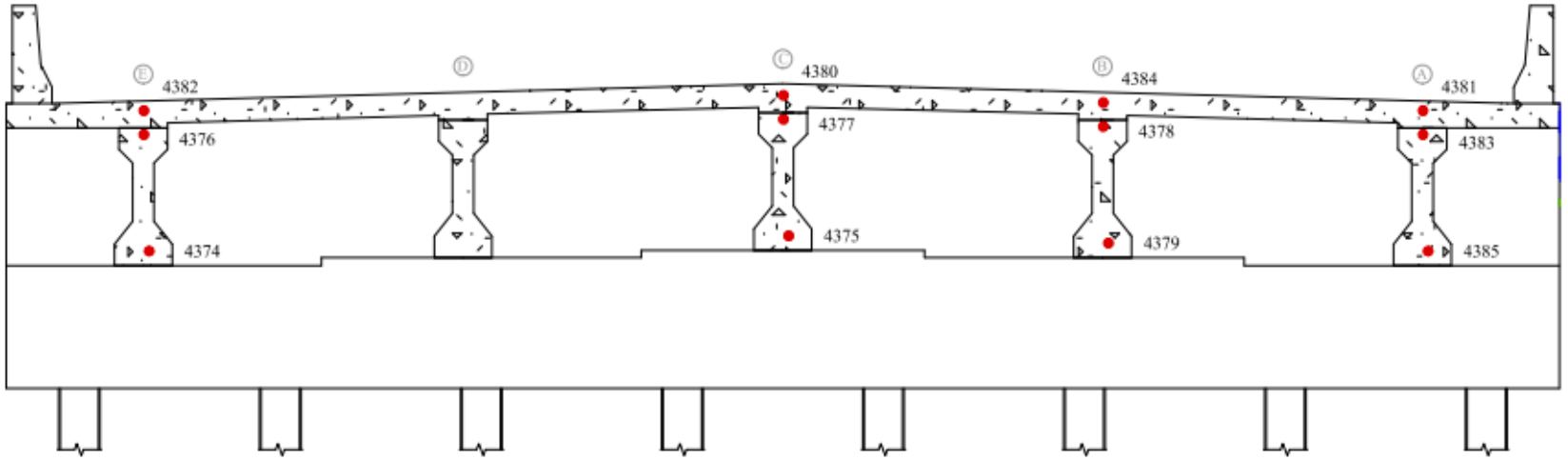

Figure 27
Embedded strain gages applied in the superstructure above Bent 1

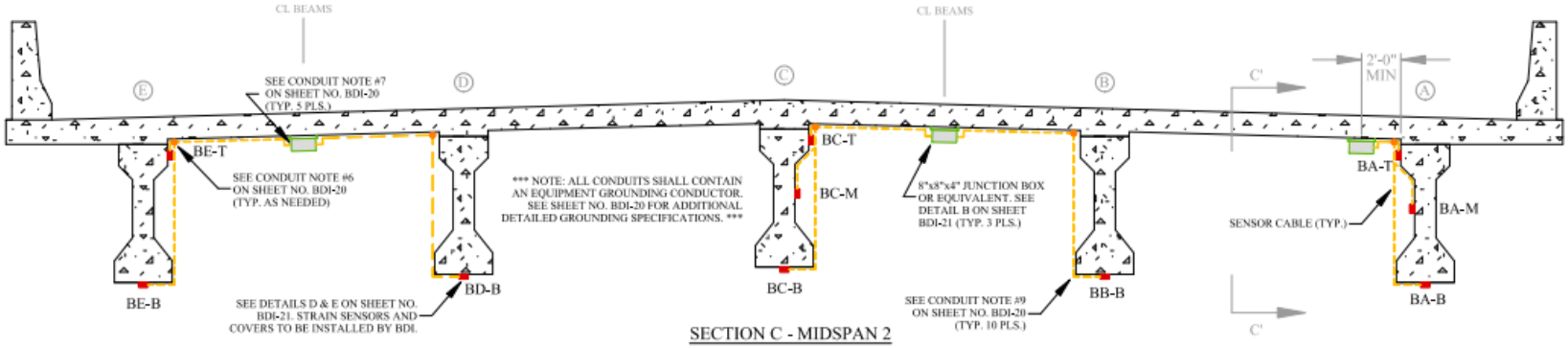

Figure 28
Surface strain gages applied on the superstructure at the mid-span of Span 2, Bodcau Bayou Bridge

Installation of Instrumentation. The sisterbar within the prestressed concrete beams, was applied on March 22, 2011. The initial installation plan was issued, discussed, and arranged by Dan Belleau from the BDI (Bridge Diagnostic, Inc.) on Mar 14, 2011. The whole sensor installation procedure was planned to be completed at the Gulf Coast Pre-Stress located at Pass Christian, MS.

The installation began around 10:00 am, on Mar 22, 2011. The purpose was to apply eight sisterbars at the end of four prestressed beams, each at the top and bottom parts of the beams. Data was recorded to investigate the integral behavior at the connection of beam and abutment. Generally, five installation steps were conducted, as shown in Figure 31, including (1) stresses were applied by the contractors for those rebars to be applied with strain gages; (2) strain gages were prepared by checking the signal and recording the sensor numbers; (3) the location was marked for the strain gages on the rebar; (4) sisterbars were bound on one of the prestressing tendons by both plastic and steel zippers; (5) a cable box was installed. This is a very special but important step. All of the cables were temporarily put in a box. The level of the box should be adjusted in such a way that the top surface of the box will be at the same level of the beam after concrete casting. In addition, the box was protected, covered, and sealed until the casting of concrete. In this way, the box protected the whole cable and sensor systems, which was very fragile and easily damaged; after concrete casing, the top surface of the box can be opened and the cable arranged to be connected to the computer systems. The final steps included: (6) check the sensor signal again to verify their function; and (7) cast the concrete for the PPC beams.

For applications of the surface gages on the prestressed concrete beams, the field trip was arranged on 02/23/2012 to 02/24/2012, during which time the construction of the bridge was completed, as shown in Figure 30. The purpose was to check the surface sensors application and to learn about the data acquisition system installations. Figure 31 shows the strain gages applied on the bottom and side surfaces of the PPC beams. Figure 32 shows the connections constructed for integral abutments at two bridge ends and the simply supported conditions for interior bents in-between. Figure 33 shows the data acquisition system and the solar panel applied on the bridge.

Figure 29
Sisterbar strain gages embedded in the PPC beams

Figure 30
Bodcau Bayou integral abutment bridge

Figure 31
Strain gages applied on the bottom and side surfaces of beams

Figure 32
Connections between end abutments and interior bents

Figure 33
Data acquisition system including solar panel

Finite Element Analysis Integral Abutment Bridge for Louisiana's Soft and Stiff Soils-Substructure

A 3D finite element (FE) model was developed to study the behavior of different parts of the Integral Bridge Abutment under different types of loads and temperature changes. The FE model includes the study of:

1. piles, embankment/backfill, abutment, and deck;
2. behavior of the backfill material and surrounding soil under the cyclic abutment displacement;
3. pile and soil interaction;
4. abutment wall and soil interaction;

5. slab and soil interaction (may not be applicable);
6. settlement of soil and its effect on the slab design; and
7. effect of temperature and longitudinal movement.

The numerical simulation was performed using ABAQUS/Standard software *[81]*. This software provides extensive tools for 3D modeling, powerful constitutive models for soil, and capability of modeling the interaction of two different media. For modeling the superstructure (bridge deck), the mesh and model was developed by Dr. Cai using the ANSYS commercial code. The two codes using ABAQUS and ANSYS will be integrated in the final analysis appropriately.

Based on Louisiana's soft soil, and in order to capture the pile and soil interaction and settlement of the soil, an elasto-plastic model (Modified Drucker-Prager) was used. Although in a bridge the piles and superstructures should not have catastrophic displacement so the state of the material remains in elastic region, elasto-plastic models are used in order to model the deflection of piles, abutment, and slab.

Since the pile displacement determines the displacement of the abutment, pile-soil interaction is one the most important aspect of this study. In order to model the frictional resistance of pile wall and separation process between pile and soil, when soil is in tension, a surface-to-surface contact algorithm in ABAQUS/Standard was used in the interface of pile and surrounding soil *[82*, *83]*.

Caminada Bay Bridge

Figure 34 shows the different parts of the integral abutment. The approach slab (super structure) is considered as a continuous part, which is rigidly connected to the bents. The modeled 36-in. piles and surrounding soil can be seen in this figure. The 36-in. piles are used in this model; however, the lengths of the piles vary at different locations. Based on the experimental results of bore holes No. 1 and 2, the modeled soil is divided to two parts. The upper part of the soil, which mainly consists of sand, is considered as granular soil, and the lower part is considered as fine grain material mostly composed of clay.

Figure 35 shows the super structure and bents with the piles above the soil layers for the first four bents. The first bent is of type SL1 and the three following ones are type SL2. The differences among the bent type SL1 and SL2 mainly arise from the construction details and does not affect the results of current analyses.

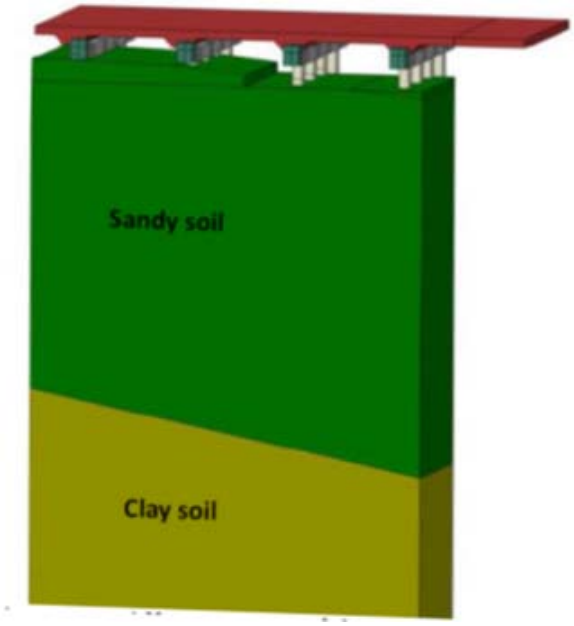

Figure 34
Different parts of the integral abutment

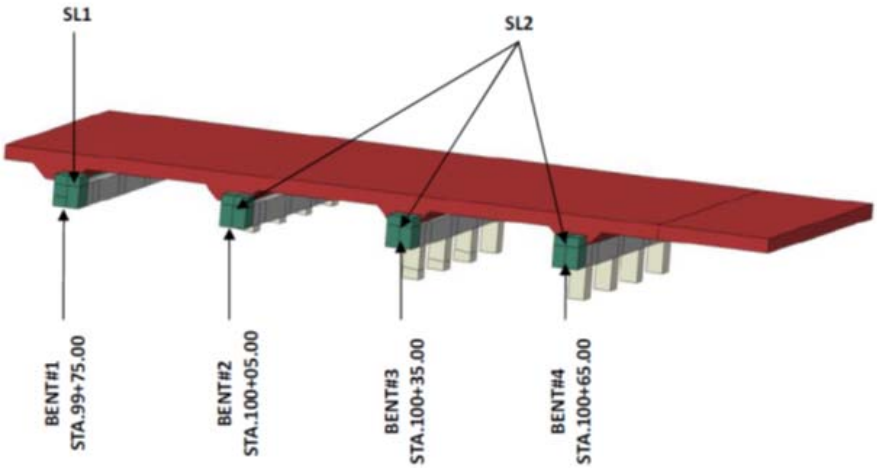

Figure 35
Location and type of bent in the first four piers

The results of the numerical analysis will be compared with the data obtained from the instruments/sensors in order to improve the proposed model and for better prediction of the behavior of the integral abutment. Figure 36 indicates the location of different types of instruments such as pressure cells, pile strain gages and pore water pressure in the pile and bent located at 99+75.00 (SL1) as well as in the soil.

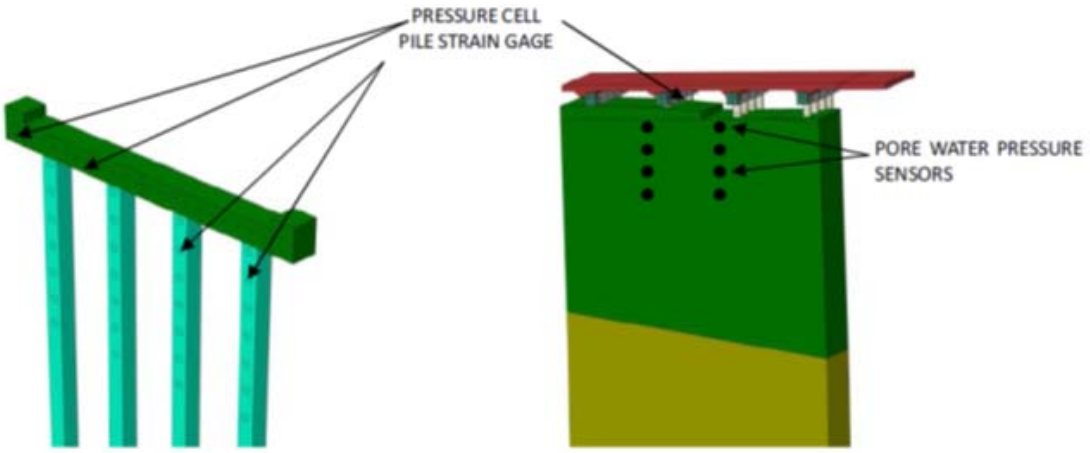

Figure 36
Location of instruments/sensors in the model

Due to the difference in the stiffness between the soil and piles, the deformation of the pile and surrounding soil is different under loading. It should be noted that under axial loads, the pile surface may slide or separate from the soil. The friction and cohesion properties of the soil play a paramount role in this case as shown in Figure 37.

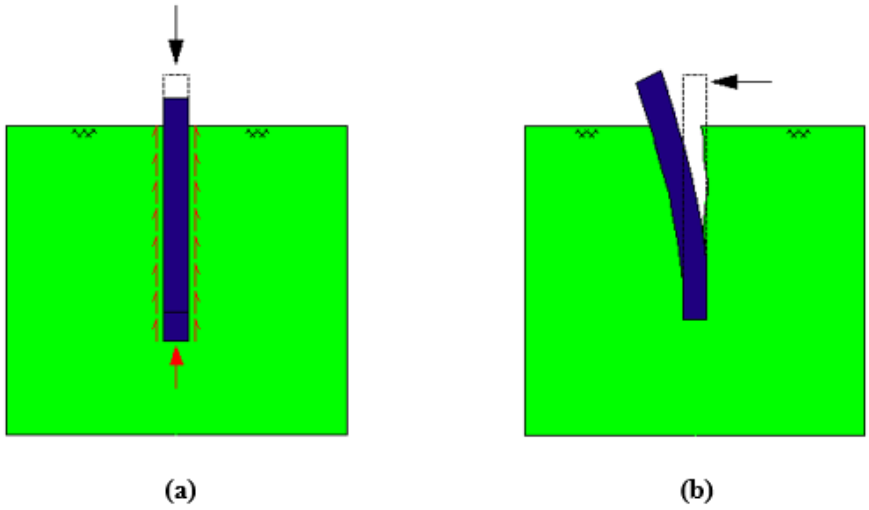

Figure 37
(a) Sliding between pile and soil under axial load; (b) gap between soil and pile under lateral loading

In order to simulate the real behavior of pile and soil under different loadings, contact elements are defined at the interface of the soil and pile in the finite element model. By defining a proper value of the coefficient of friction and cohesion, these elements are capable of simulating the interaction between the soil and pile in axial and lateral loadings. Figure 38

and Figure 39 show the finite element model and mesh of the piles, bent, and soil for the pier located at 99+75.00 (bent type: SL1). Pile-soil interaction can be recognized by the independent mesh of the soil and piles.

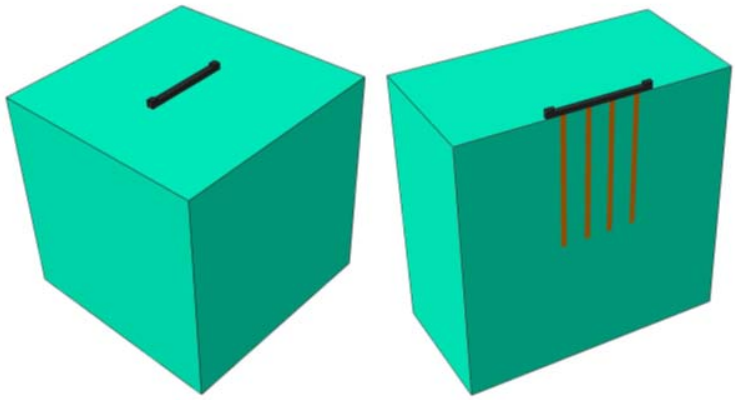

Figure 38
FEM model of bent, piles, and soil for pier located at 99+75.00 (bent type: SL1)

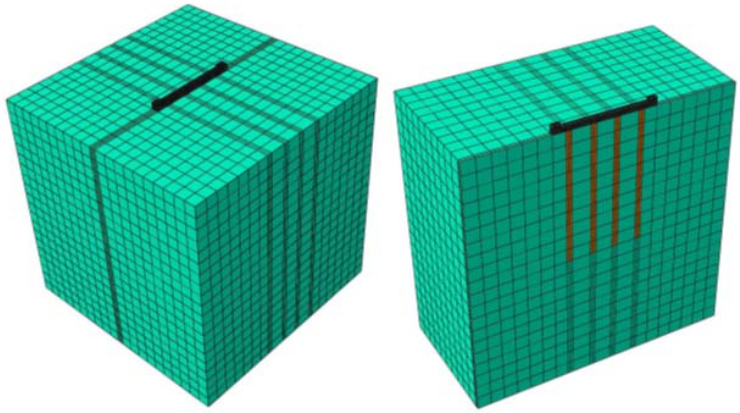

Figure 39
Finite element mesh of the pier located at 99+75.00 (bent type: SL1)

Constitutive Models for Soil, Piles, and Bent

One of the important parts in the numerical simulation is the proper choice of the constitutive models for the materials used in the analysis. The accuracy of the analysis depends on the correct choice of these models. Materials used in the integral abutment are reinforced concrete for the piles, bent, and superstructure, and, as mentioned above, the coarse and fine grain soils. The uncertainty of the soil behavior is more than that of concrete. It is therefore paramount to obtain the proper material model for the soil.

For modeling the behavior of soil, the Modified Drucker-Prager model is taken into account and the Mises type plasticity model with isotropic hardening is used for the bent and pile *[81]*.

Modified Drucker-Prager Model. The Modified Drucker-Prager model is used to model the frictional materials, which are typically granular-like soils and rock, and exhibit pressure-dependent yield (the material becomes stronger as the pressure increases) *[81]*. This model allows a material to harden and soften isotropically, and it is used to model materials in which the compressive yield strength is greater than the tensile yield strength. Generally, Modified Drucker-Prager allows volume change with inelastic behavior: the nonassociated flow rule, defining the inelastic straining, inelastic dilation (volume increase), and inelastic shearing.

The yield criterion of this model is shown in Figure 40 and equation (1) represents this yield surface:

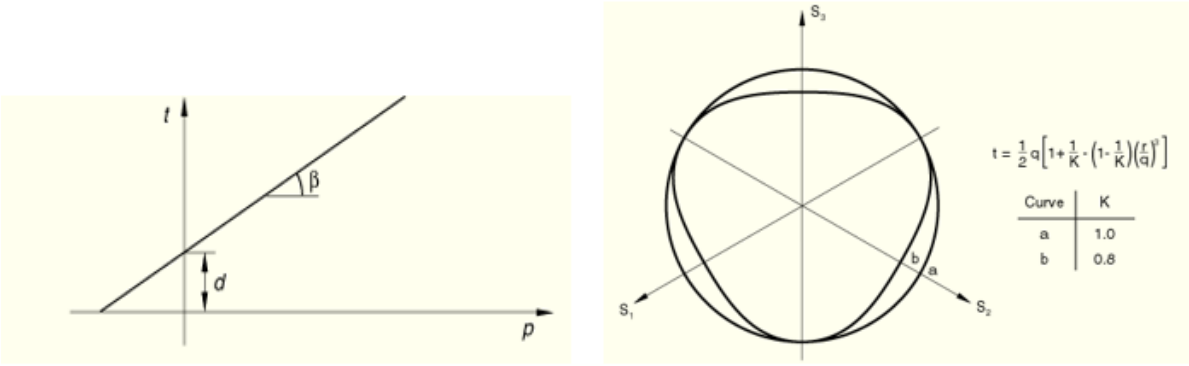

Figure 40
Yield surface of the Modified Drucker-Prager model (Hibbit et al. *[81]*)

$$F = t - \rho \tan\beta - d = 0 \qquad (1)$$

This model can be used for noncircular yield surfaces in the deviatoric plane (Π-plane) for different yield values in tension and compression, associated inelastic flow in the deviatoric plane, and separate dilation and friction angles in addition to the original Drucker-Prager model. As can be seen in this figure, when = 0.8, the behavior of this model will be relatively like Mohr-Coulomb behavior, which is close to the behavior of soil, as well as not have the numerical issues of the Mohr-Coulomb.

Materials Parameter for Soils

The required material parameters of this model such as β (friction angle), d (cohesion), E (modulus of elasticity), and ψ (dilation angle) for different soils are primarily determined based on the experimental tests from the bore holes in the site and engineering judgment. The outcomes of instrumentation in pile tests and bridges will help to verify the obtained parameters and improve them.

Bore holes provide the results of SPT (standard penetration test) for sandy soils and Atterberg limits and q_u (unconfined compression strength) for the clay soil. There are several empirical equations in the textbooks and literature for correlating the results of SPT and soil parameters. For example in obtaining the modulus of elasticity the equations of Kulhawy, Mayne, and Bowles and for friction angle (φ) equations of Terzaghi, Peck, Mesri, Hatanaka and Uchida can be take into account *[84] [85] [86] [87]*. The parameters of existing soils for modeling the integral abutment will be obtained based on these values and engineering judgment. Figure 41 shows the modulus of elasticity and friction angle (φ) for coarse grain soils based on SPT results of bore hole No.1 with different equations obtained from NovoSPT software *[88]*.

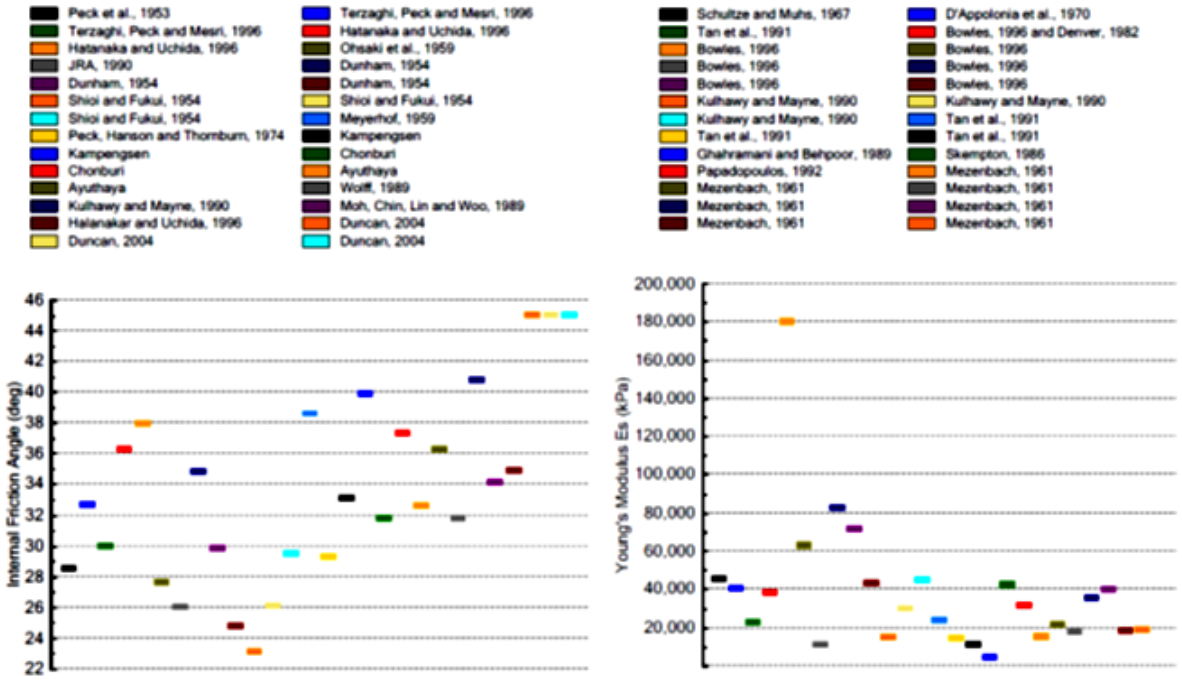

Figure 41
Soil parameters based on SPT results (after NovoSPT*[88]*)

It should be noted that, almost all of the above equations give the shear strength parameter of the soil based on the Mohr-Coulomb model (C and φ). In order to use this parameter in Modified Drucker-Prager models, equation (2) will be used for the 3D analysis *[89]*:

$$\tan\varphi = \frac{6\sin\varphi}{3-\sin\varphi}$$
$$d = \frac{6c\cos\varphi}{3-\sin\varphi} \qquad (2)$$

Finite Element Analysis Results

In this section, the results of analyses of the pile groups and the bents are shown. The locations and the information about the piles length and shapes are shown in Figure 42 and Table 11, respectively. For each bent, first the load capacity of the pile group is obtained based on CPT data of field test which is a reliable approximation of the pile capacity and can be compared with the finite element analyses results, after which the required material parameter of soil for use in numerical analyses are determined. Then, the procedure of numerical simulation using ABAQUS is explained and the load – displacements obtained from the analyses are shown *[81]*.

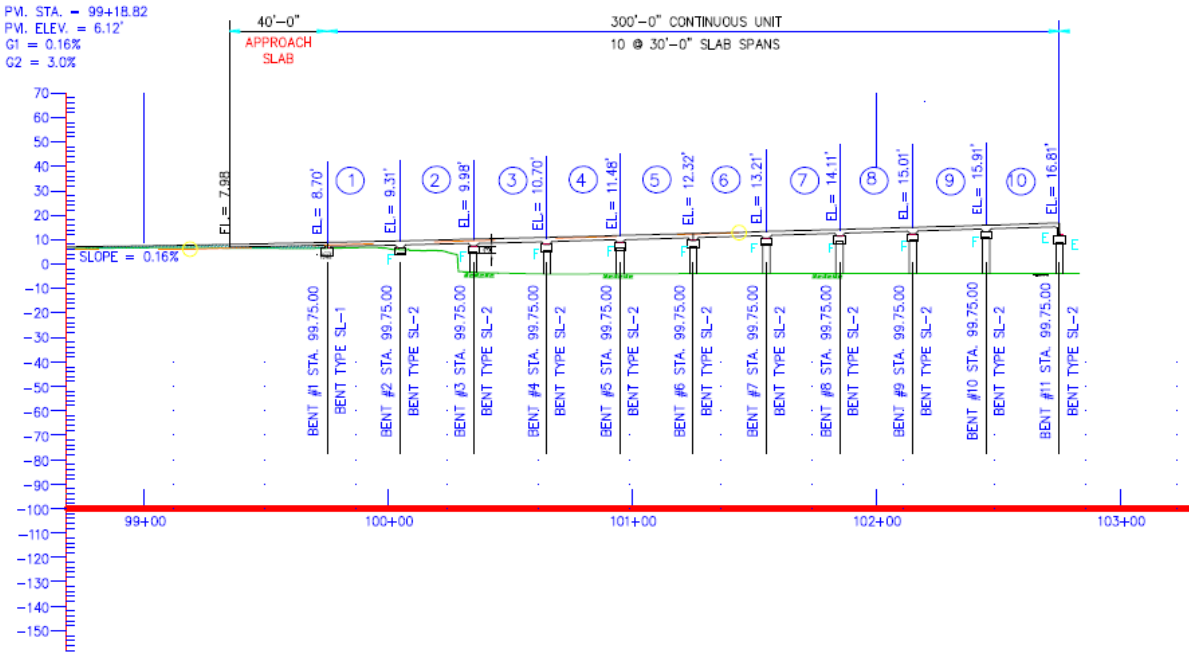

Figure 42
Location of analyzed bents

Table 11
Piles information for each bent

BENT	C/L STA	PILE TYPE	# OF PILES	ORDER LENGTH (ft)
1	*99+75*	36" Sq. Pile	4	82
2	*100+05.00*	36" Sq. Pile	4	82
3	*100+35.00*	36" Sq. Pile	4	82
4	*100+65.00*	36" Sq. Pile	4	82
5	*100+95.00*	36" Sq. Pile	4	85
6	*101+25.00*	36" Sq. Pile	4	85
7	*101+55.00*	36" Sq. Pile	4	85
8	*101+85.00*	36" Sq. Pile	4	85
9	*102+15.00*	36" Sq. Pile	4	88
10	*102+45.00*	36" Sq. Pile	4	88
11	*102+75.00*	36" Sq. Pile	4	95

Analyses of Bent 1 (STA 99+75)

CPT. In order to obtain an estimation of the load capacity of each pile, results of The "Louisiana Pile Design by Cone Penetration Test" (LPD-CPT) was obtained before performing the numerical analysis. The available data of Cone Penetration Test (CPT) at 99+75 was given to the software as well as shape and diameter of the pile and the software provides classifications of the soil in addition to predicted pile capacity in different depths based on LCPC Method, Schmertmann Method, and de Ruiter and Beringen Method [90] [91] [92]. The summary of approaches that the software is using is as follows:

Soil Classification by CPT. Soil classification and identification of soil stratigraphy were achieved by analyzing the CPT data. Clayey soils usually show low cone tip resistance, high sleeve friction and therefore high friction ratio, while sandy soils show high cone tip resistance, low sleeve friction, and low friction ratio. Zhang and Tumay proposed the probabilistic region estimation method for soil classification [93]. This method is similar to the classical soil classification methods based on soil composition. The method identifies three soil types: clayey, silty, and sandy. The probabilistic region estimation determines the probability of each soil constituent (clay, silt, and sand) at certain depth. Zhang and Tumay's method was modified by Abu-Fsarsakh to allow for continuous profiling of soil probabilities with depth and implemented in the program for soil classification *[94]*.

Ultimate Pile Capacity from Cone Penetration Testing. The ultimate axial capacity of the pile (Q_u) is composed of the end-bearing capacity (Q_t) and the shaft friction capacity (Q_s) as given by the following equation:

$$Q_u=Q_t+Q_s=q_t A_t+f\ A_s \tag{3}$$

where, q_t is the unit tip bearing capacity. A_t is the area of the pile tip, f is the unit skin friction, and A_s is the area of the pile shaft. In sand, the end-bearing capacity (Q_t) dominates, while in soft clays the shaft friction capacity (Q_s) dominates. The design load carrying capacity (Q_d) of the pile can be calculated by:

$$Q_d = \frac{Q_u}{F.S.} \tag{4}$$

where, *F.S.* is the factor of safety.

Several methods are available in the literature to predict the axial pile capacity utilizing the CPT data. Three methods were implemented in this program. A brief description of these methods is presented below. For more details, refer to Titi and Abu-Farsakh *[94]*.

Schmertmann Method. Schmertmann proposed the following relationship to predict the unit tip bearing capacity of the pile (q_t) from the cone tip resistance (q_c) *[91]:*

$$q_t = \frac{q_{c1} + q_{c2}}{2} \tag{5}$$

where, q_{c1} is the minimum of the average cone tip resistances of zones ranging from *0.7D* to *4D* below the pile tip (where *D* is the pile diameter) and q_{c2} is the average of minimum cone tip resistances over a distance 8D above the pile tip (Figure 43). Schmertmann suggested an upper limit of 150 TSF (15 MPa) for the unit tip bearing capacity (q_t).

The unit skin friction of the pile (*f*) is given by:

$$f = \alpha_c f_s \tag{6}$$

where, α_c is a reduction factor that varies from 0.2 to 1.25 for clayey soil, and *fs* is the sleeve friction.

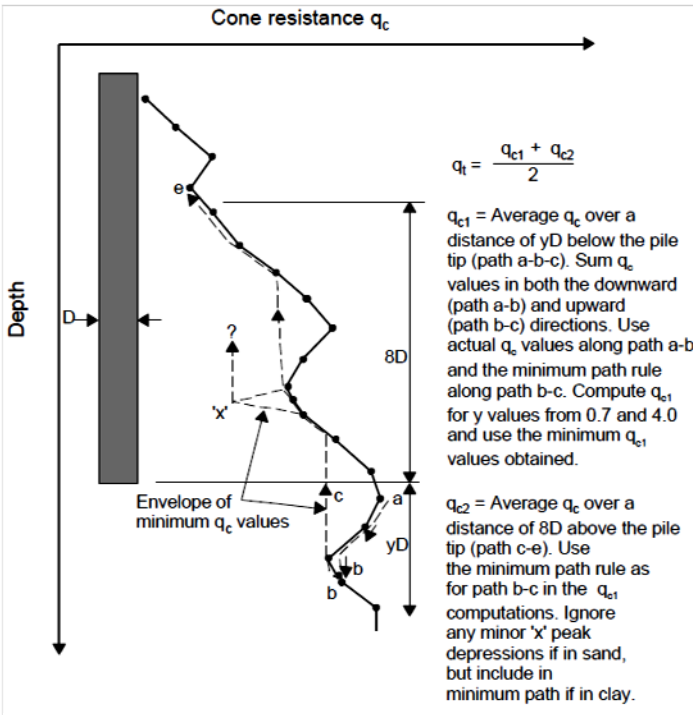

Figure 43
Calculation of the average cone tip resistance in Schmetmann method *[94]*

For piles in sand, the friction capacity (Qs) is obtained by:

$$Q_s = \alpha_s \left(\sum_{y=0}^{8D} \frac{y}{8D} f_s A_s + \sum_{y=8D}^{L} f_s A_s \right) \tag{7}$$

where, α_s is the correction factor for sand, which is a function of pile depth/pile length ratio. Schmertmann suggested a limit of 1.2 TSF (120 kPa) on *f*.

de-Ruiter and Beringen Method. This method is proposed by de-Ruiter and Beringenand is based on the experience gained in the North Sea *[92]*. This method uses different procedures for clay and sand.

In clay, the undrained shear strength (S_u) for each soil layer is first evaluated from the cone tip resistance (q_c). Then, the unit tip bearing capacity and the unit skin friction are computed by applying suitable multiplying factors. The unit tip bearing capacity is given by:

$$q_t = N_c S_u(tip) \tag{8}$$

$$S_u(tip) = \frac{q_c(tip)}{N_k}$$

where, N_c is the bearing capacity factor and $N_c = 9$. N_k is a cone factor that ranges from 15 to 20, depending on the local experience. The parameter $q_c(tip)$ is the average of cone tip resistances around the pile tip computed similar to the Schmertmann method.

The unit skin friction is given by:

$$f = \beta S_u(side) \tag{9}$$

where, β is the adhesion factor, β equals 1 for normally consolidated (NC) clay, and $\beta = 0.5$ for overconsolidated (OC) clay. $S_u(side)$, the undrained shear strength for each soil layer along the pile shaft, is determined by:

$$S_u(side) = \frac{q_c(side)}{N_k} \tag{10}$$

where, $q_c(side)$ is the average cone tip resistance along the soil layer.

In the current study, the cone factor $N_k = 20$ and the adhesion factor $\beta = 0.5$ were adopted in the analysis, since these values gave better-predicted ultimate pile capacity for the investigated piles. In sand, the unit tip bearing capacity of the pile (q_t) is calculated similar to the Schmertmann method.

Bustamante and Gianeselli Method (LCPC/LCP Method). Bustamante and Gianeselli proposed this method for the French Highway Department based on the analysis of 197 pile load tests with a variety of pile types and soil conditions *[90]*. It is also known as the French method and the LCPC/LCP method. In this method, both the unit tip bearing capacity (q_t) and the unit skin friction (f) of the pile are obtained from the cone tip resistance (q_c). The unit tip bearing capacity of the pile (q_t) is predicted using the following equation:

$$q_t = k_b\, q_{eq}\,(tip) \tag{11}$$

where, k_b is an empirical bearing capacity factor that varies from 0.15 to 0.60 depending on the soil type and pile installation procedure (Table 12) and $q_{eq}(tip)$ is the equivalent average cone tip resistance around the pile tip, which is obtained as follows:

1. Calculate the average tip resistance (q_{ca}) at the tip of the pile by averaging q_c values over a zone ranging from 1.5D below the pile tip to 1.5D above the pile tip (D is the pile diameter).

2. Eliminate q_c values in the zone that are higher than $1.3q_{ca}$ and those are lower than $0.7q_{ca}$ as shown in Figure 44.

3. Calculate the equivalent average cone tip resistance ($q_{eq}(tip)$) by averaging the remaining cone tip resistance (q_c) values over the same zone.

Table 12
LCPC bearing capacity factor (k_b) *[94]*

Soil Type	Bored piles	Driven Piles
Clay-Silt	0.375	0.6
Sand-Gravel	0.15	0.375
Chalk	0.2	0.4

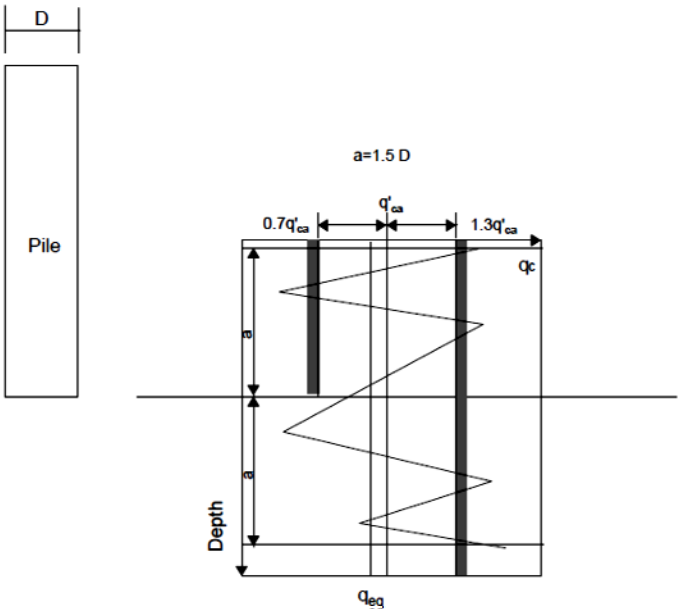

Figure 44
Calculation of the equivalent tip resistance for LCPC method (after [90])

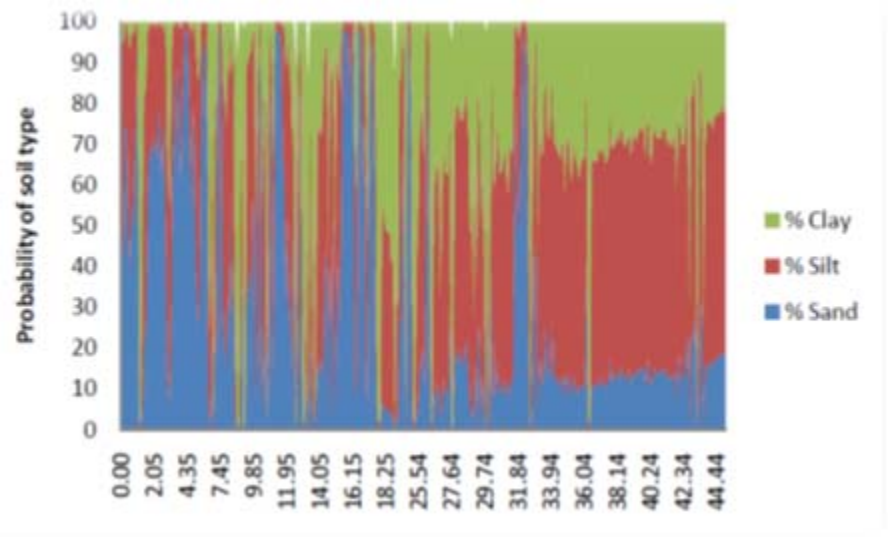

Figure 45
Probability of soil type in different depths of the soil based on CPT data

The pile unit skin friction (*f*) for each soil layer is estimated from the equivalent cone tip resistance [$q_{eq}(side)$] of the soil layer, soil type, pile type, and installation procedure *[94]*.

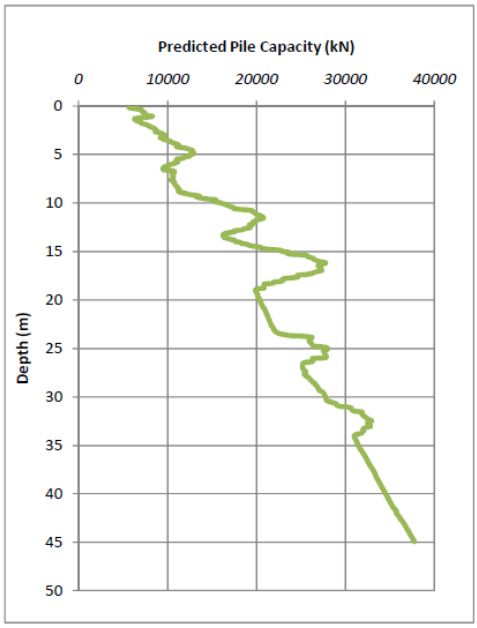

Figure 46
Average pile capacity of four methods based on CPT data

The classification of the soil based on CPT data of Caminada Bay Bridge at STA 99+75 is shown in Figure 45. It is noted from this figure that, except for a few thin layers of clay, the

soil mainly consists of granular material and can be classified as sandy soil, especially near to the soil surface.

The axial capacity of a pile group in sand is usually taken as the sum of individual pile capacities, since in this type of the soil the "block failure" of pile group is not likely to happen. The pile group capacity (= pile load × 4) versus settlement curve obtained from the software is shown in Figure 46. This figure gives a reliable prediction of load capacity of the pile group which can be checked with the finite element results.

Before running the analysis, the researchers needed to obtain the correct material parameters of the soil for the Modified Drucker-Prager constitutive model based on the available data and in-situ measurements must be obtained. As was mentioned before, the Standard Penetration Test (SPT) number is available at STA99+74 which can be used in order to correlate several physical parameters of the soil around Bent 1. Since in granular soil, the standard penetration number is highly dependent on the effective overburden pressure, σ_0', a number of empirical relationships have been proposed to convert the field standard penetration number N_F to a standard effective overburden pressure, $\sigma_0' = 2000\ lb/ft^2\ \left(96\frac{kN}{m^2}\right)$ *[95]*. The general form is:

$$N_{cor} = C_N N_F \tag{12}$$

In this project, the correlation of Skempton was taken into account *[97]*. Table 14 shows the corrected SPT numbers. The corrected values were then used to find the general parameters of the soil using NovoSPT software. The outcomes of NovoSPT for Internal Friction angle and Modulus of Elasticity are shown in Table 14. The decision for the final value for each parameter was made based on these results together with the engineering judgment.

Table 13
Corrected SPT number using Skempton equation *[97]*

Dept(m)	SPT (NF)	$\acute{\sigma} = z\gamma$	CN Skempton (1986)	Ncore
0.03048	11	*0.21336*	2.00	*22*
2.1336	13	*14.9352*	1.74	*23*
3.048	15	*21.336*	1.65	*25*
3.6576	18	*25.6032*	1.59	*29*
4.572	11	*32.004*	1.52	*17*
6.096	13	*42.672*	1.40	*18*
6.7056	6	*46.9392*	1.36	*8*
7.62	9	*53.34*	1.30	*12*
8.2296	21	*57.6072*	1.27	*27*
9.144	22	*64.008*	1.22	*27*
10.0584	17	*70.4088*	1.17	*20*
11.5824	13	*81.0768*	1.10	*14*
13.716	10	*96.012*	1.02	*10*
14.3256	16	*100.2792*	1.00	*16*
15.24	21.3	*106.68*	0.97	*21*
16.4592	44	*115.2144*	0.93	*41*
17.0688	42	*119.4816*	0.91	*38*
17.6784	33	*123.7488*	0.89	*29*
19.2024	35	*134.4168*	0.85	*30*

Using the wet density and moisture content of the soil from the in-situ experiments at the SPT boring hole and assuming a proper value for specific gravity of soil solid of the sandy soil ($G_s = 2.67$), the other required parameters of the soil can be obtained using weight-volume relationships as follow:

$$\gamma_d = \frac{\gamma_{wet}}{1+\omega} \tag{13}$$

$$\gamma_{sat} = \left(1 - \frac{1}{G_s}\right)\gamma_d + \gamma_w \tag{24}$$

$$e = \frac{G_s\gamma_w - \gamma_{sat}}{\gamma_{sat} - \gamma_w} \tag{35}$$

where, γ_d, γ_{wet}, γ_{sat} are the dry, wet, and saturated unit weights of soil, respectively, γ_w is water unit weight, and *e* is the void ratio. Table 14 shows the required soil parameter for analyzing the sub-structure of Bent 1 as well as the definition and the source of obtaining of each parameter.

Table 14
Soil parameters required for Bent 1, Caminada Bay Bridge

Parameter	Value	Definition	source
γ_{wet}	17 (kN/m3)	wet density	available in-situ results
γ_d	13.28 (kN/m3)	dry density	equation (1)
γ_{sat}	18.1 (kN/m3)	saturated density	equation (2)
G_s	2.67	specific gravity of soil solid	assumed for sandy soil
D_r	60.40%	relative density	NovoSPT
e	0.8	void ratio	equation (3)
E	28 (MPa)	Modulus of Elasticity	NovoSPT
v	0.22	Poisson Ratio	NovoSPT
C	0	Cohesion	assumed for sandy soil
φ	30°	Friction Angle	NovoSPT

After determining the required material parameters, the next step is numerical modeling using the ABAQUS software *[81]*.

The substructure finite element mesh of the Bent 1 is shown in Figure 47.

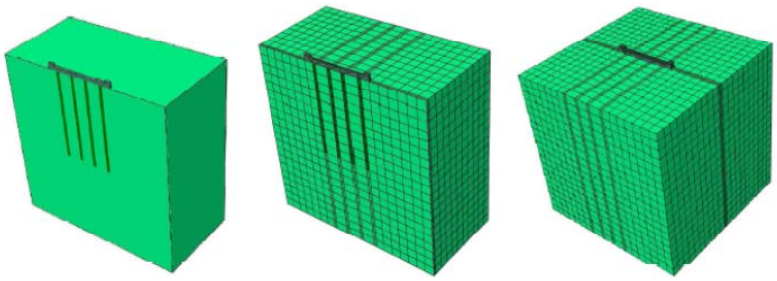

Figure 47
Numerical model and finite element mesh of Bent 1, Caminada Bay Bridge

In this simulation, the piles were assumed to be embedded in perfect contact with the soil before applying pile loads. The interaction between the pile and the soil is simulated using a penalty-type interface between the pile and the soil with a friction factor of 0.3. This type of interface is capable of describing the friction between the pile surface and the soil in contact. Although the amount of friction coefficient seems to be lower than the one suggested in the literature for the sliding friction force of concrete on sandy soil, the value of 0.3 is assumed in order to predict the group pile response with more factor of safety.

The 8-node linear brick, reduced integration, hourglass control elements were used for the soil, bent, and piles. The dimensions of the sandy soil were chosen in a way that the boundary effect on the pile behavior was minimized.

An elastic model was used for the piles and the bent. The stiffness of the bent was assumed to be larger than the pile in order to consider it relatively stiffer in comparison to the other materials.

The analyses were performed in two steps. The so-called geostatic procedure was used as the first step of the analysis and gravity loads were applied during this step. Ideally, the loads and initial stresses (in-situ stress of the soil) should exactly equilibrate and produce zero deformations. ABAQUS will check for equilibrium during the geostatic procedure and iterate, if needed, to obtain a stress state that equilibrates the prescribed boundary conditions and loads (gravity). This stress state, which is a modification of the stress field defined by the initial conditions, would then be used as the initial stress field in a subsequent analysis.

If the stresses given as initial conditions were far from equilibrium under the geostatic loading and there was some nonlinearity in the problem definition, this iteration process may fail (for more information refer to *[81]*).

In order to define the in-situ stresses of the soil, the amounts of vertical stresses at top and bottom of the soil layer obtained from the material density was provided to the software and ABAQUS considers the linear relationship between two values among the layers. Also the researchers need to define the at rest lateral earth pressure, K_0, and ABAQUS uses this value in order to determine the lateral initial stresses. Equation (4) is used to find this value:

$$K_0 = \frac{\nu}{1-\nu} \tag{4}$$

Figure 48 shows the defined initial stresses of the soil and the amount of the stress after the geostatic step. It can be seen that the amount of stresses are almost the same in the two cases so the system is in equilibrium.

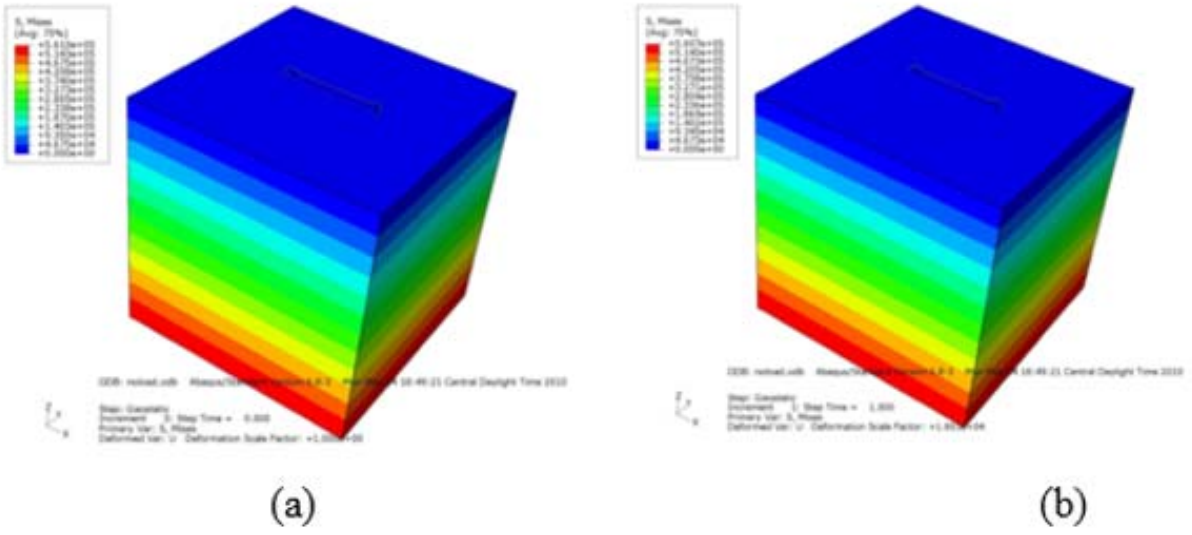

Figure 48
Values of vertical stresses in the soil: (a) defined initial stresses; (b) calculated stress of ABAQUS using geostatic analysis

In the second step, a static, general analysis is invoked and the pile loads and moments are applied at the top surface of the bent in six different directions. In order to capture the load-displacement / moment-rotation response of the pile group, the applied loads / rotations are defined to increase in a linear manner and the average displacement and rotation of the cap are calculated in each case. The results of each type of loading are represented below. It should be noted that the same results can be used for Bent 2 since the pile length and the bent type are the same for two cases.

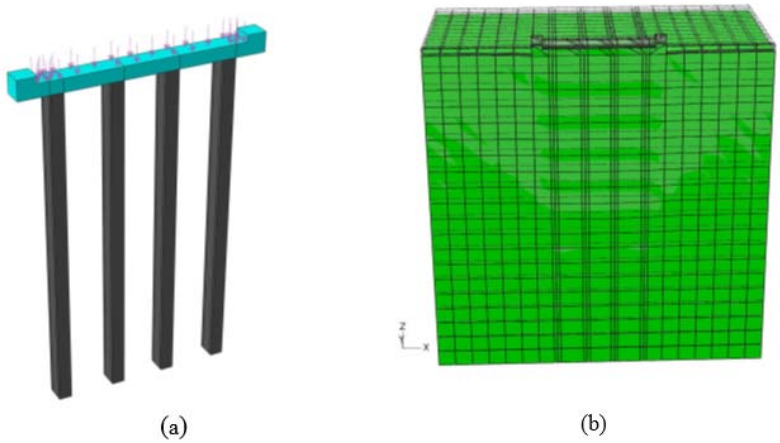

Figure 49
(a) Applied load at the top of the bent; (b) deformed and undeformed mesh for half of the model

Vertical Load

The applied pressure load on the top surface of the bent, deformed, and undeformed mesh at Bent#1 are shown in Figure 49. In this case, since the bottom of the bent is connected to the soil surface and there is an interaction between them, a contact element is used for this area. If a contact property is not defined for this area, the soil will have no resistance in the contact between soil and bent and the bent goes directly to the soil, which does not match the reality.

The pile load versus settlement curve obtained from the finite element analysis is shown in Figure 50. It is noted from the figure that the settlement increases as the load is increased in an approximately linear manner up to about a 4700 kpf (21000 kN) pile load, at which a vertical displacement of about 0.25 in. (0.6 cm) is encountered. Shortly after that, the pile plunges in a fast downward descent, indicating that the load capacity of the pile is reached. The calculated load capacity is within the range of the pile load capacity obtained from the CPT results (Figure 46).

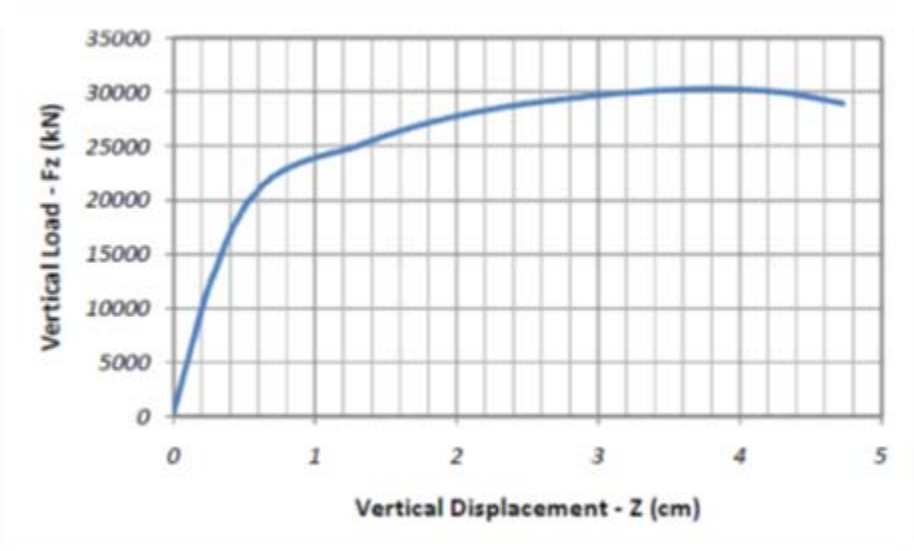

Figure 50
Load- settlement curve of Bent 1

Lateral Loads in X and Y directions

The applied lateral load on the cap and deformed and undeformed meshes of the pile group under lateral load in X direction is shown in Figure 51. Figure 52 indicates the average lateral

deformation of the bent versus pile lateral capacity obtained from the finite element analysis. It is noted from this figure that the horizontal displacement increases as the lateral load is increased up to about a 1050 kpf (4600 kN) pile load, at which a pile group lateral displacement of more than 1.2 in. (3 cm) is encountered. Shortly after that, the bent moves laterally at a greater rate, indicating that the lateral load capacity of the pile in the X direction has been reached.

Figure 51
(a) Lateral load applied to the top of the bent; (b) deformed mesh of the pile group

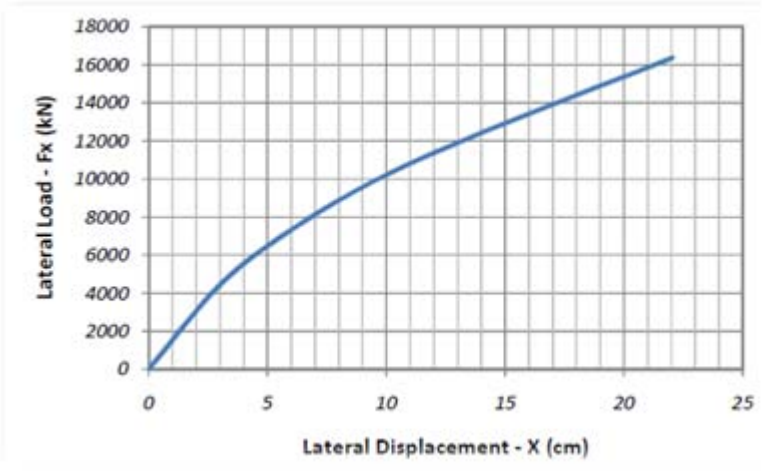

Figure 52
Lateral load- displacement curve in X direction of Bent 1

Figure 53 shows the lateral deflection of one the piles in the X direction versus the pile length for different amounts of lateral load. It can be seen that for lower amounts of the

lateral load, the pile and cap acts like a fixed headed pile but when the load is increased a small value of tilt occurs in the cap.

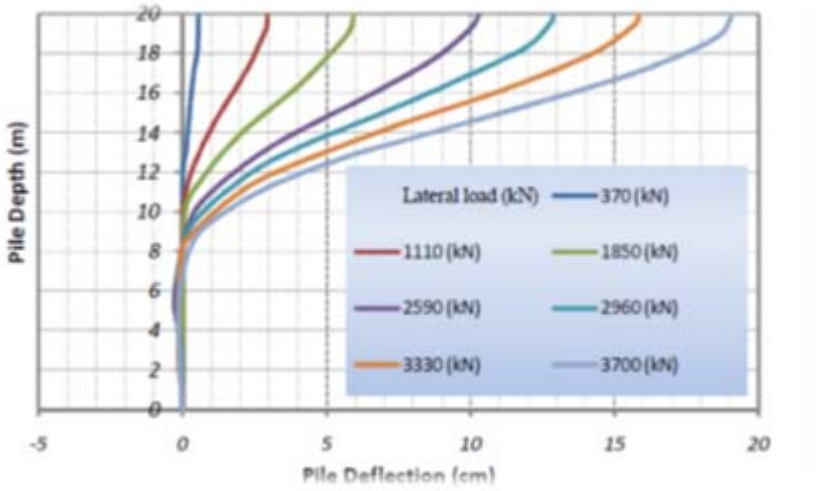

Figure 53
Pile deflection in different lateral loads in the X direction

The applied lateral load on the cap and deformed and undeformed meshes of the pile group under lateral load in the Y direction is shown in Figure 54. Figure 55**Error! Reference source not found.** indicates the average lateral deformation of the bent versus pile lateral capacity obtained from the finite element analysis.

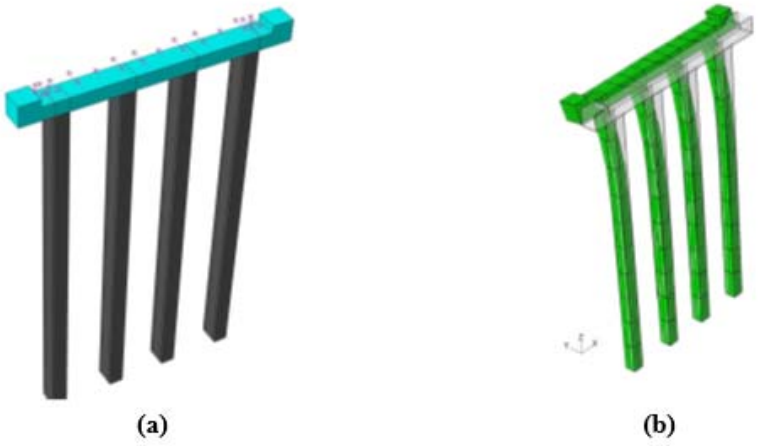

Figure 54
(a) Lateral load applied to the top of the bent; (b) deformed mesh of the pile group

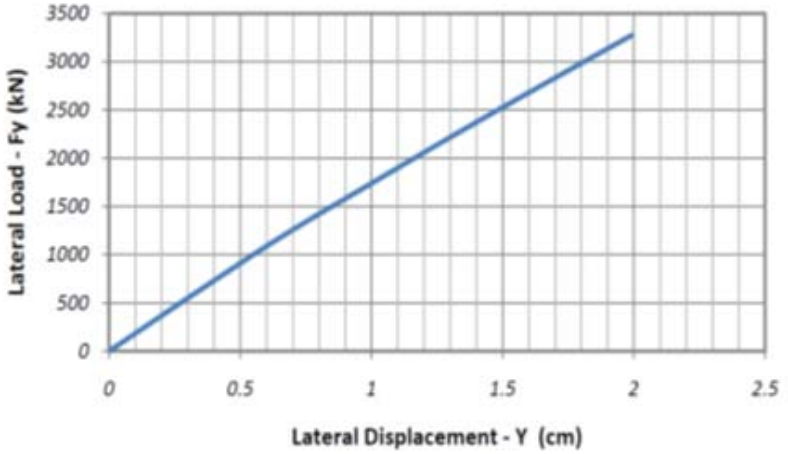

Figure 55
Lateral load- displacement curve in the Y direction of Bent 1

Moment – Rotation Curve in the Y Direction

In order to capture the behavior of the pile group under applied moment around the Y direction, linear distributed loads in the opposite direction are used on the top of the cap as shown in Figure 56 (a). The resultant coupling between the two distributed loads leads to a moment on the cap (Figure 56 (b)). Measuring the settlements of different positions on one half of the cap and averaging the results as shown in Figure 57 leads to find the respective rotation.

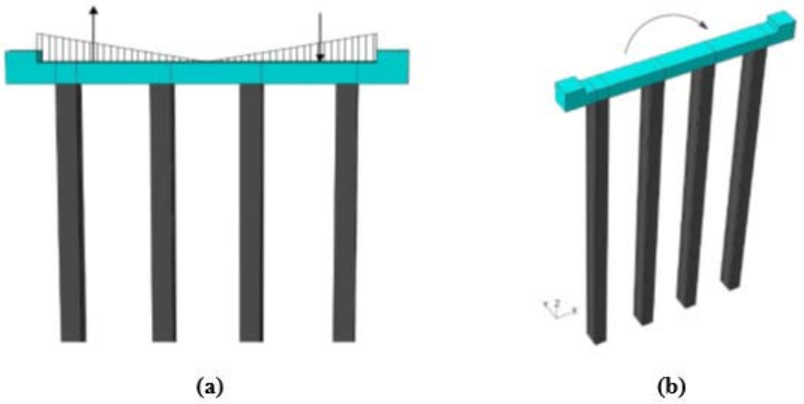

Figure 56
(a) Applied load at the top surface of the bent in order to simulate a moment around the Y direction; (b) resultant moment

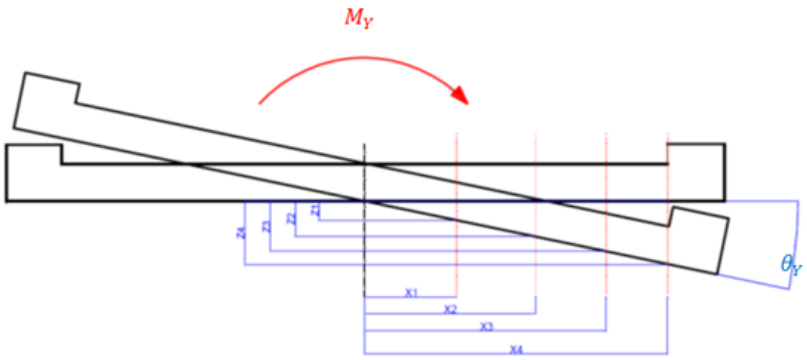

Figure 57
Calculating the rotation of the bent

$$\theta_{Y_i} = \tan^{-1}\left({}^{Z_i}/_{X_i}\right) \; ; \;\; i = 1,2,\dots,n$$

(17)

$$\theta_Y = \frac{\sum_{i=1}^{n} \theta_{Y_i}}{n}$$

The deformed mesh and moment-rotation curve of the substructure are shown in Figure 58 and 59.

Figure 58
Deformed and undeformed meshes of the pile group due to a moment around the Y direction

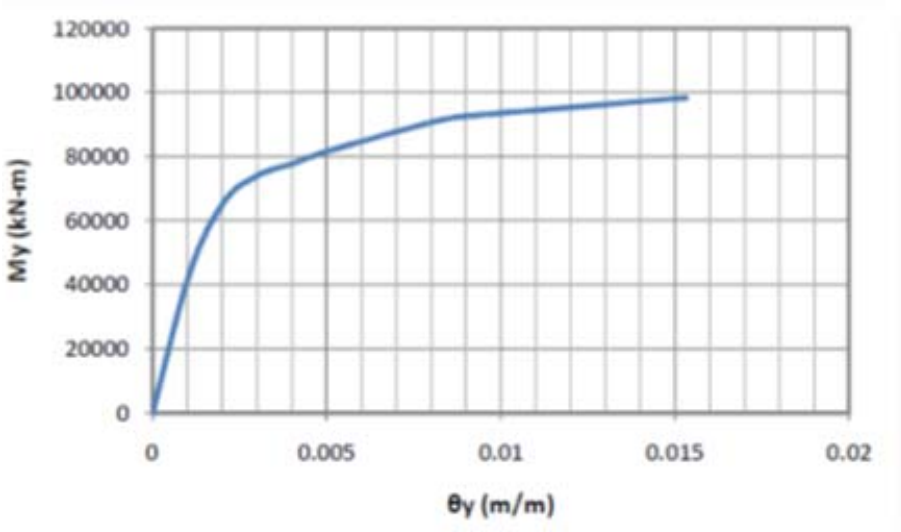

Figure 59
Moment-rotation curve for bent due to moment around the Y direction

Moment – Rotation around the X Direction

The same approach is used to apply the moment around the X direction and the average rotation versus applied moment curve is obtained, as shown in Figures 60 and 61.

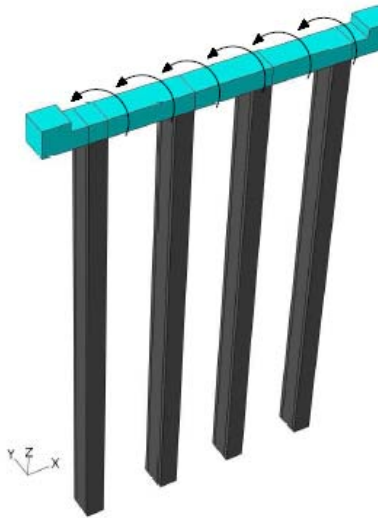

Figure 60
Moment applied to the top of the bent around the X direction

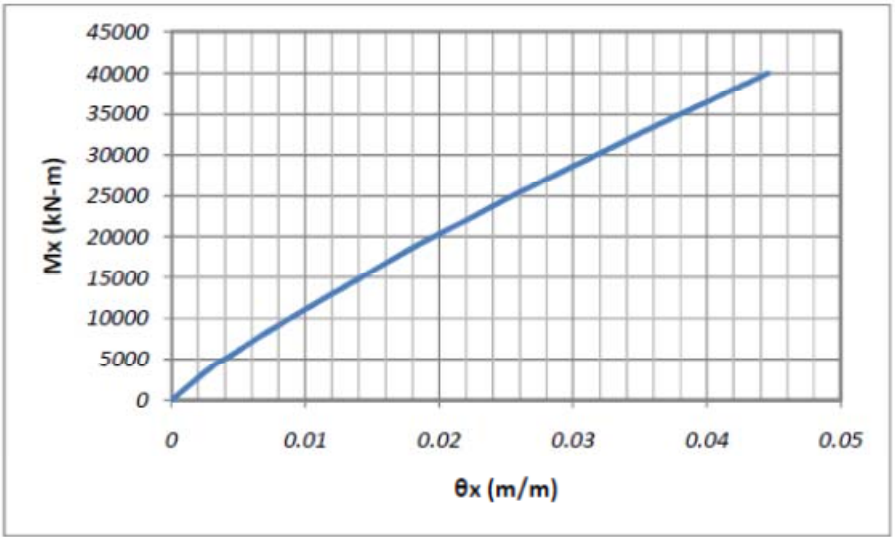

Figure 61
Moment-rotation curve for the bent due to moment around the X axis

Torsion – Rotation around Z Direction

Resultant applied torsion on the cap of the Bent 1 is shown in Figure 62. Figure 63 indicates rotation angle due to different values of torsion.

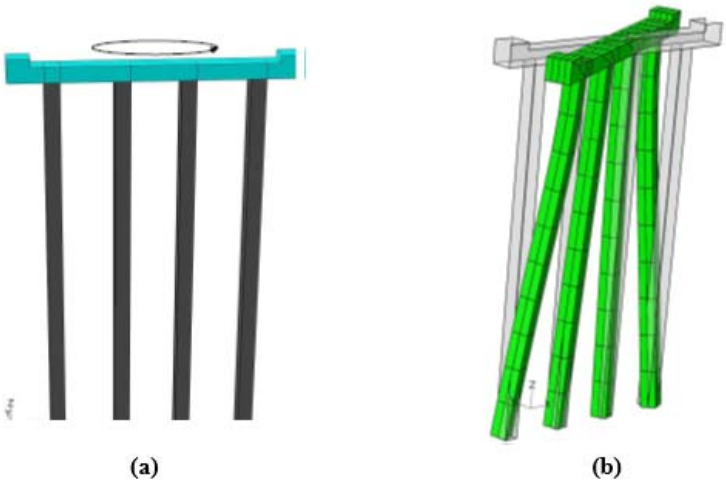

Figure 62
(a) Torsion applied to the top of the bent; (b) deformed mesh of the pile group

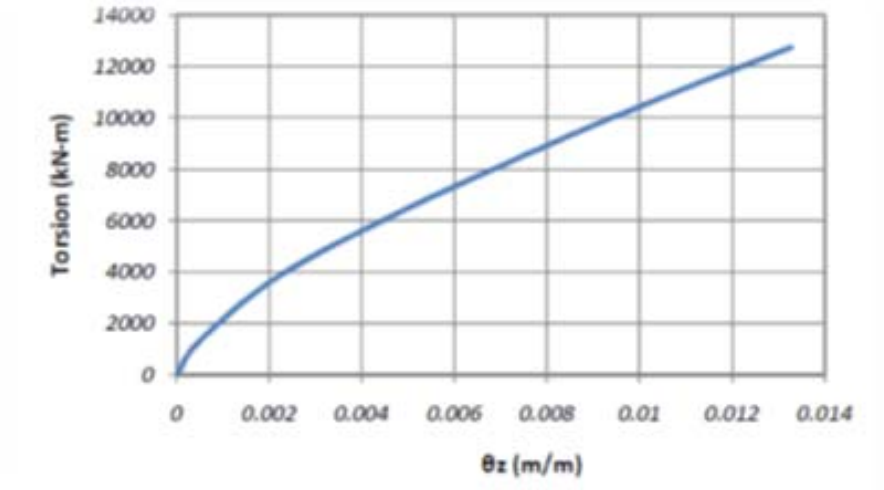

Figure 63
Torsion-rotation curve for the bent

Analyses of Bent 3 (STA 100+35). Numerical model and finite element mesh of the Bent 3 located at 100+35 can be seen in Figure 64 and Figure 6. In this case, the piles are not fully embedded into the soil and there is a 7.5-ft. gap between bent and surface of the soil. Due to this gap, less substructure stiffness is expected in comparison with Bent 1. The results of finite element analyses of this pier, as well as the load displacement curves, are shown subsequently.

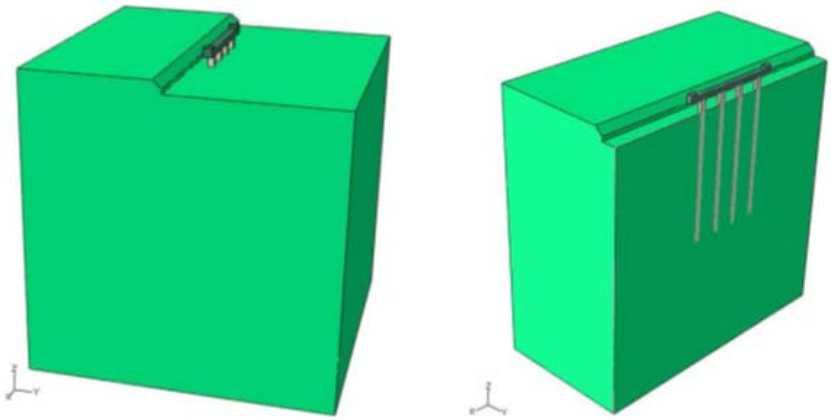

Figure 64
FEM model of bent, piles and soil for pier located at 100+35.00 (bent type: SL2)

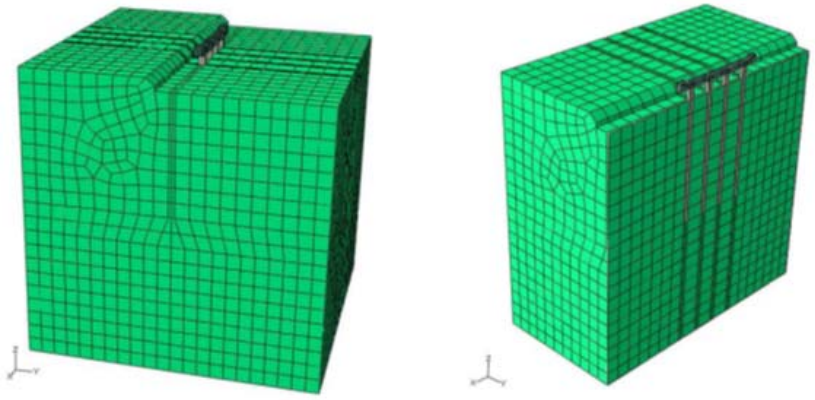

Figure 65
Finite element mesh of the pier located at 100+35.00 (bent type: SL2)

Vertical Load

The applied pressure load on the top surface of the bent and deformed and undeformed mesh at Bent 3 are shown in Figure 66.

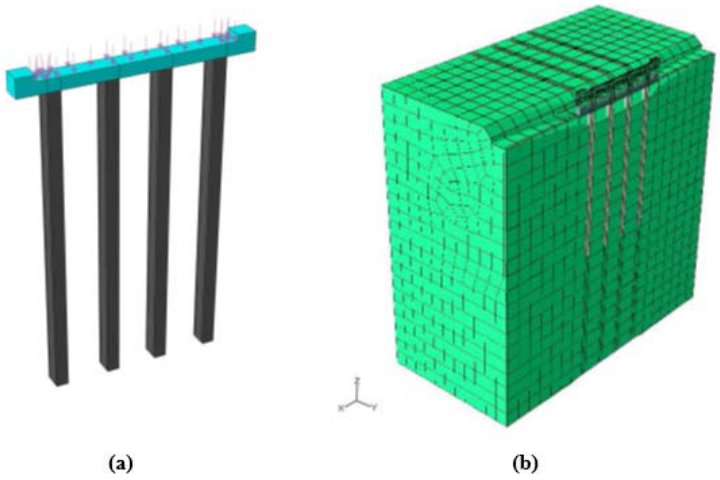

Figure 66
(a) Applied load at the top of the bent; (b) deformed and undeformed mesh for half of the model

The pile load versus settlement curve obtained from the finite element analysis is shown in Figure 67. It is noted from the figure that the settlement increases as the load is increased in an approximately linear manner up to about a 4050 kpf (18000 kN) pile load, at which a vertical displacement of about 0.2 in. (0.54 cm) is encountered. Shortly after that, the pile plunges in a fast downward descent, indicating that the load capacity of the pile is reached.

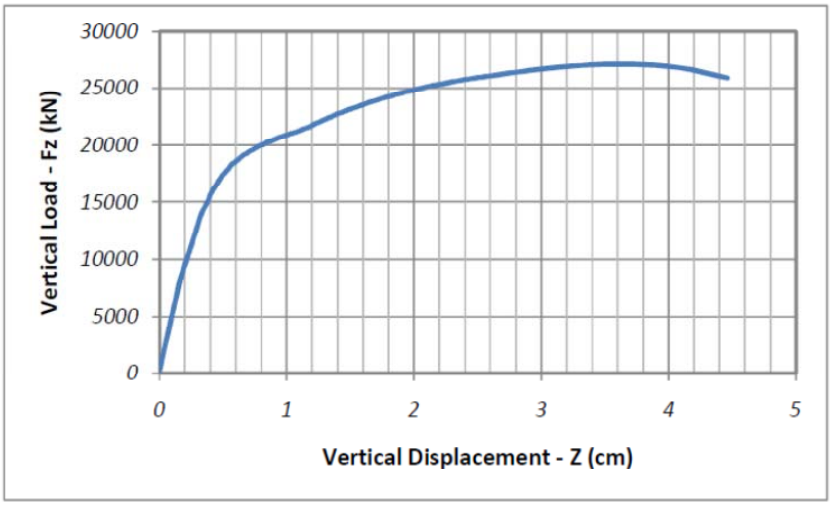

Figure 67
Load- settlement curve of Bent 3

Lateral Loads in X and Y Directions

The applied lateral load on the cap and deformed and undeformed meshes of the pile group under lateral load in X direction is shown in Figure 68. Figure 69 indicates the average lateral deformation of the bent versus pile lateral capacity obtained from the finite element analysis. It is noted from this figure that the horizontal displacement increases as the lateral load is increased up to about a 420 kpf (1880 kN) pile load, at which a pile group lateral displacement of more than 5.15 in. (13.1 cm) is encountered. Shortly after that, the bent moves laterally at a greater rate, indicating that the lateral load capacity of the pile in the X direction has been reached.

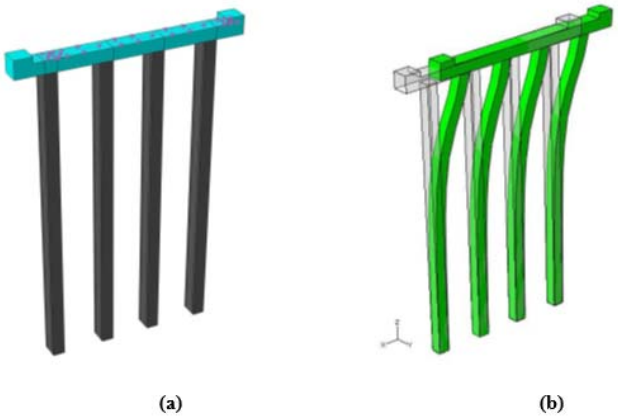

Figure 68
(a) Lateral load applied to the top of the bent; (b) deformed mesh of the pile group

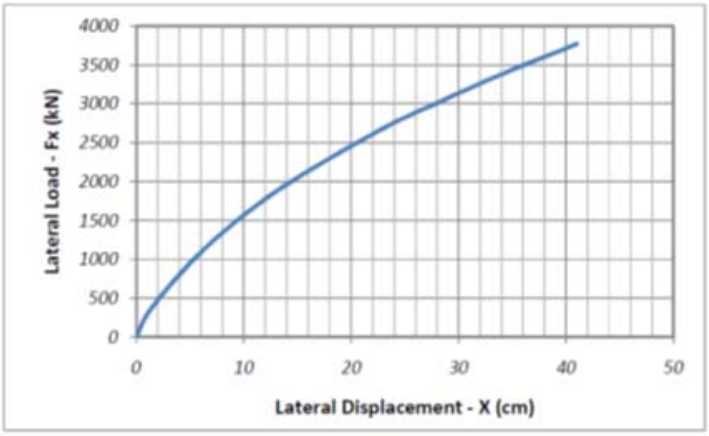

Figure 69
Lateral load- displacement curve in X direction of Bent 3

The applied lateral load on the cap and deformed and undeformed meshes of the pile group under lateral load in the Y direction is shown in Figure 70. Figure 71 indicates the average lateral deformation of the bent versus pile lateral capacity obtained from the finite element analysis. It is noted from this figure that the horizontal displacement increases as the lateral load is increased up to about a 405 kpf (1800 kN) pile load, at which a pile group lateral displacement of more than 0.8 in. (2 cm) is countered. Shortly after that, the bent moves laterally at a greater rate, indicating that the lateral load capacity of the pile in the Y direction has been reached.

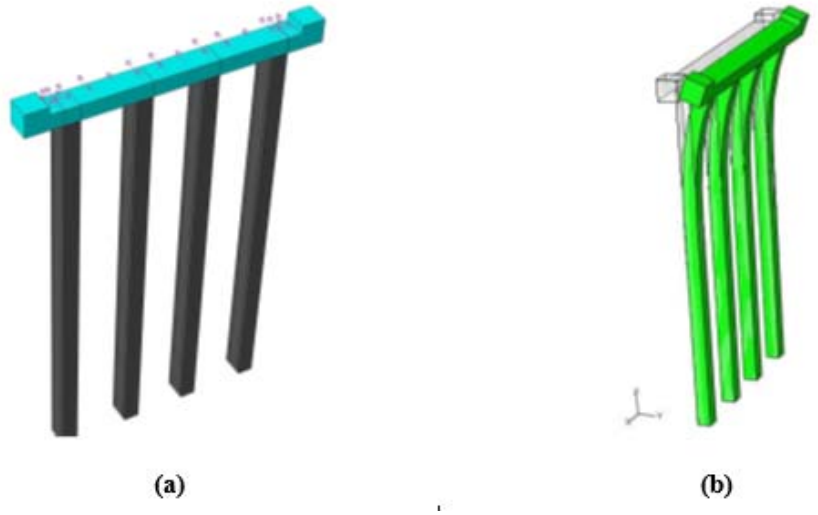

Figure 70
(a) Lateral load applied to the top of the bent; (b) deformed mesh of the pile group

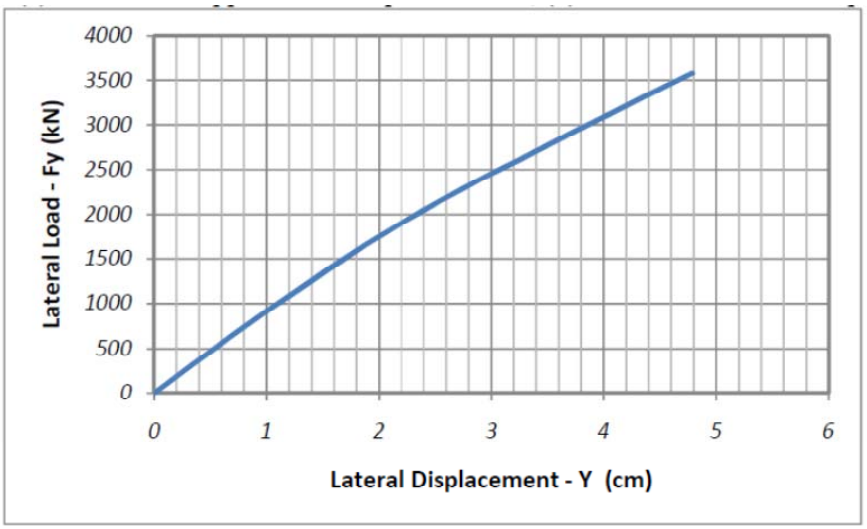

Figure 71
Lateral load- displacement curve in the Y direction of Bent 3

It should be noted that, in this case, the load-displacement curve of the substructure is different for the applied load in +Y and –Y direction due to presence of a 7.5 ft. height backfill. In order to consider more safety factor for the analysis of super structure, the load in +Y is taken into account since in this direction, stiffness of the system is lower.

Moment – Rotation Curve in the Y Direction

In order to capture the behavior of the pile group under applied moment around the Y direction, linear distributed loads in opposite directions are used on the top of the cap, as shown in Figure 72 (a). The resultant coupling between the two distributed loads leads to a moment on the cap (Figure 72 (b)).

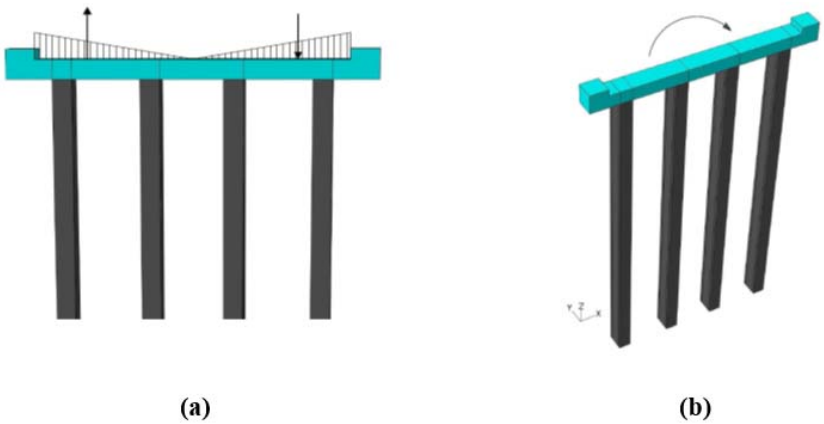

Figure 72
(a) Applied load at the top surface of the bent in order to simulate a moment around the Y direction; (b) resultant moment

The deformed mesh and moment-rotation curve of the substructure are shown in Figures 73 and 74.

Figure 73
Deformed and undeformed meshes of the pile group due to a moment around the Y direction.

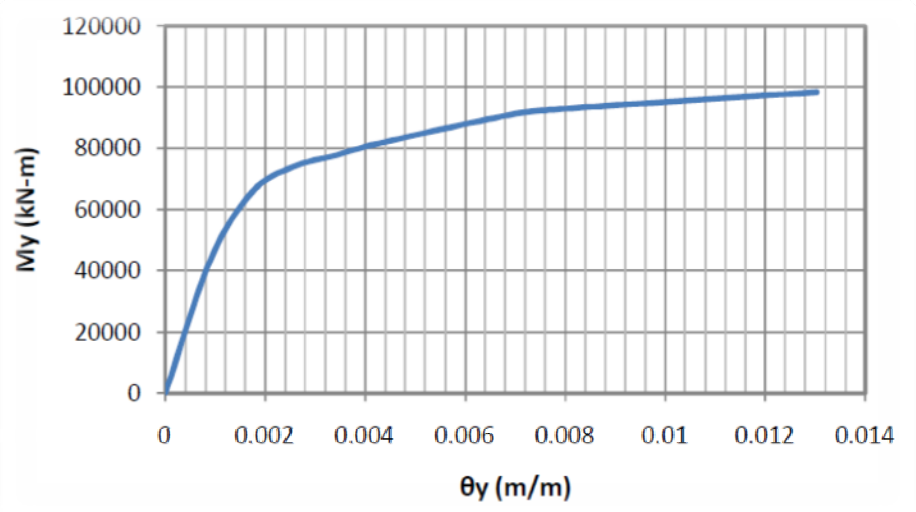

Figure 74
Moment-rotation curve for bent due to moment around the Y direction

Moment – Rotation around the X Direction

The same approach is used to apply the moment around the X direction and the average rotation versus applied moment curve is obtained, as shown in Figures 75 and 76.

Figure 75
Moment applied to the top of the bent around the X direction

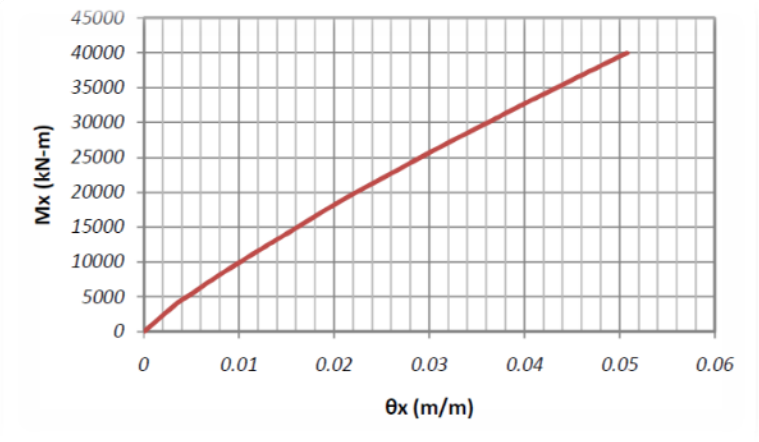

Figure 76
Moment-rotation curve for the bent due to moment around the X axis

Torsion – Rotation around Z Direction

Resultant applied torsion on the cap of the Bent 3 is shown in Figure 77. Figure 78 indicates rotation angle due to different values of torsion.

Figure 77
(a) Torsion applied to the top of the bent; (b) Deformed mesh of the pile group

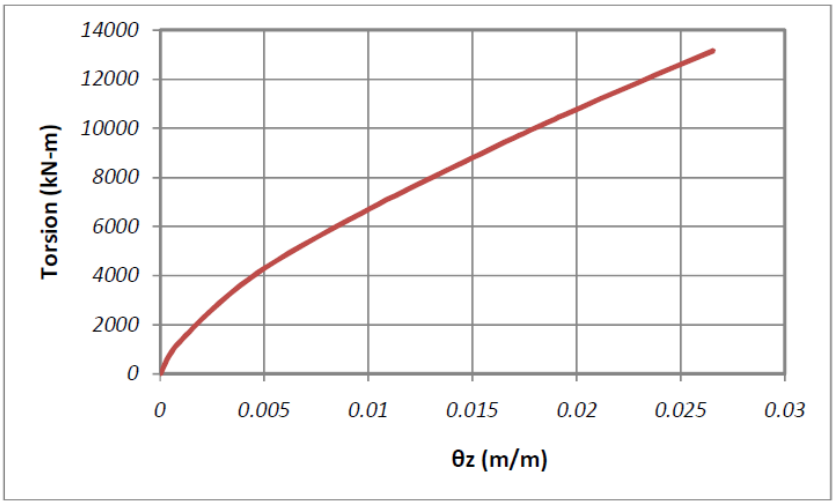

Figure 78
Torsion-rotation curve for the bent

Analyses of Bent 8 (STA 101+85). Numerical model and finite element mesh of Bent 8, located at 101+85, can be seen in Figure 79. In this case, the piles are not surrounded entirely by the soil and there is a 12.4 ft. gap between bent and surface of the soil. The results of this case can be used for Bent 4, Bent 5, Bent 6, and Bent 7, since, in all these cases, the bent types are similar (SL-2) and the length of the piles are the same, but, as can be seen in Figure 42, in Bent 8 the length of the piles not surrounded by the soil is higher than the other three cases so based on the comparison made in 5.3.2.2, Bent 8 has less stiffness that the

others and, considering the results of this, piers for other cases leads to higher safety factors for the problem.

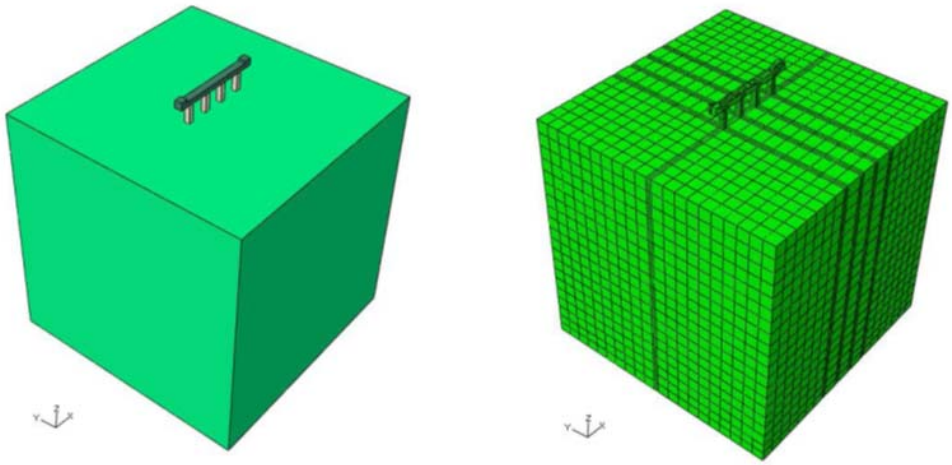

Figure 79
FEM model of bent, piles and soil for pier located at 101+85.00 (bent type: SL2)

The results of finite element analyses of this pier as well as the load displacement curves are shown subsequently.

Load-Displacement Analyses

Figure 80 through 82 show the deformed and undeformed finite element model of the Bent 8 in addition to load-displacement curves for three different directions.

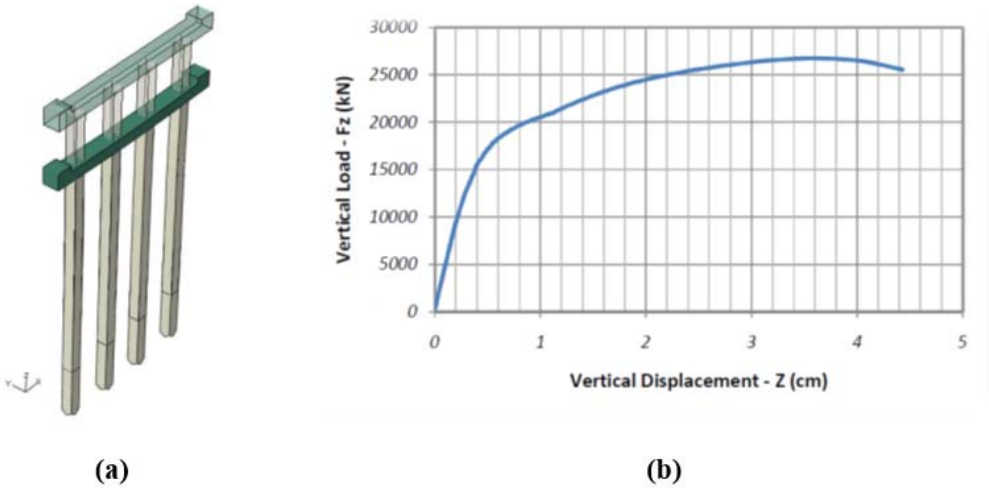

(a) **(b)**

Figure 80
Vertical load (a) deformed and undeformed mesh for half of the model; (b) load-displacement curve

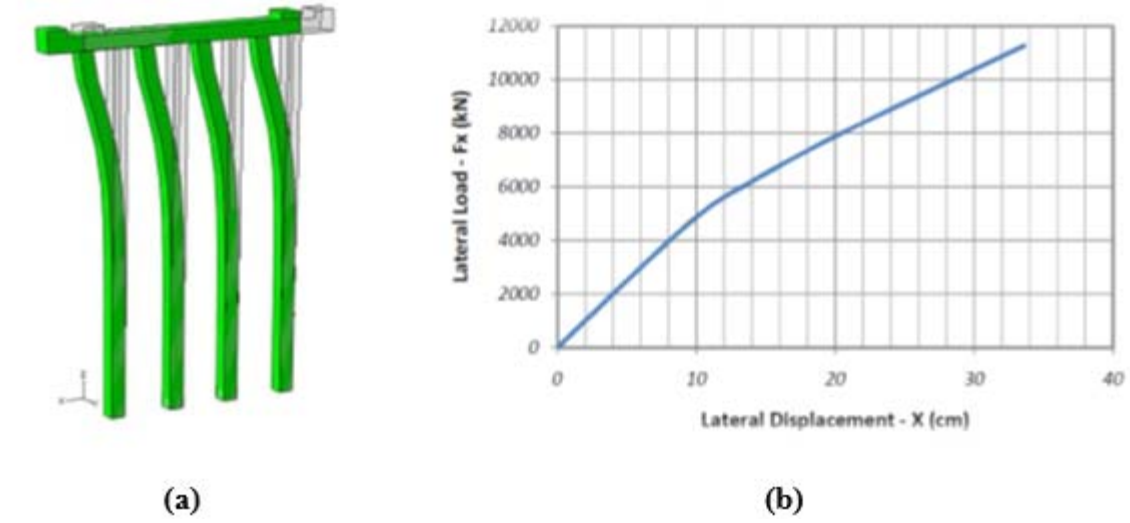

Figure 81
Lateral load in X direction (a) deformed mesh of the pile group; (b) lateral load-displacement curve

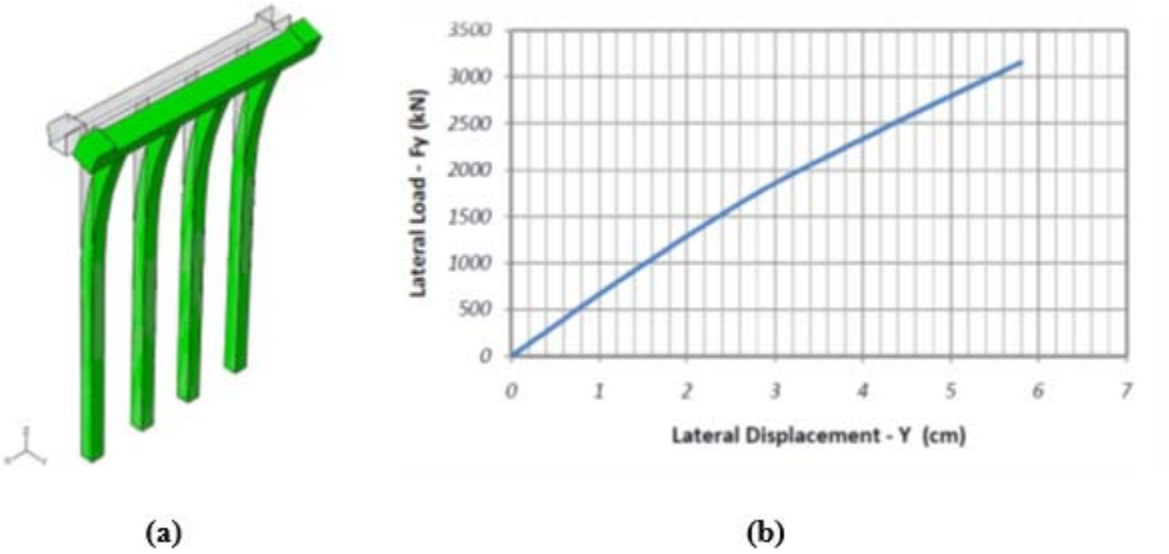

Figure 82
Lateral load applied in Y direction; (a) Deformed mesh of the pile group; (b) Lateral load- displacement curve

Moment – Rotation Curve in the Y Direction

Figures 83 through 85 show the deformed and undeformed finite element model of the Bent 8 in addition to moment-rotation curves for three different directions.

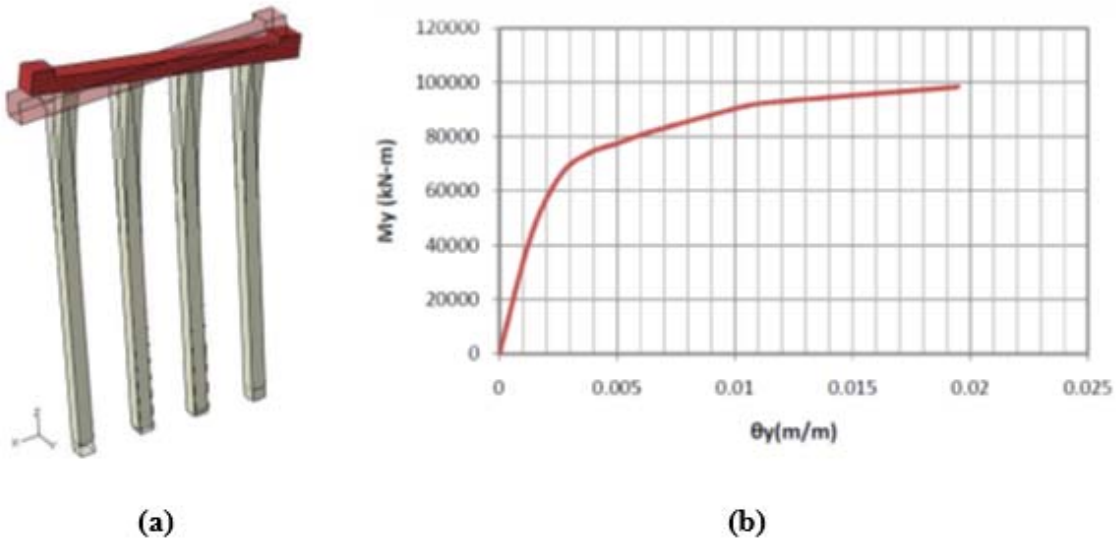

Figure 83
Moment applied around Y direction; (a) deformed and undeformed meshes of the pile group (b) moment-rotation curve

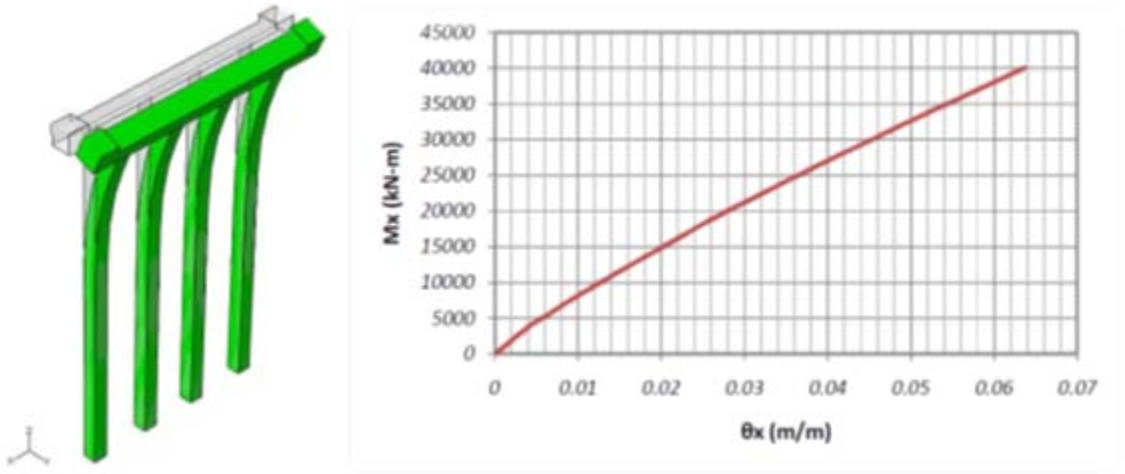

Figure 84
Moment-rotation curve for moment applied around X direction

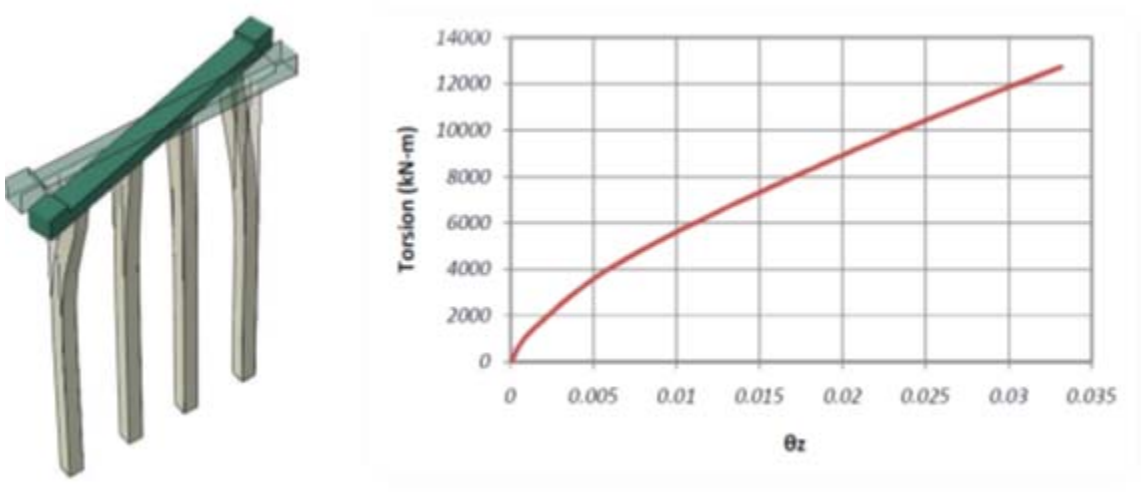

Figure 85
Torsion applied around Z direction; (a) Deformed and undeformed meshes of the pile group; (b) moment-rotation curve

Analyses of Bent 10 (STA 102+45). In the case of Bent 10, the piles are not surrounded entirely by the soil and there is a 14 ft. gap between bent and surface of the soil. The results of this case can be used for Bent 9 since in both cases the bent types are similar (SL-2) and the length of the piles are the same; however, as can be seen in Figure 42, in Bent 10 the length of the pile not surrounded by the soil is slightly higher than Bent 9 so the results in both cases should be identical. The results of finite element analyses of this pier as well as the load displacement curves are shown subsequently.

Load-Displacement Analyses

Figures 86 through 88 show the deformed and undeformed finite element model of Bent 10 in addition to load-displacement curves for three different directions.

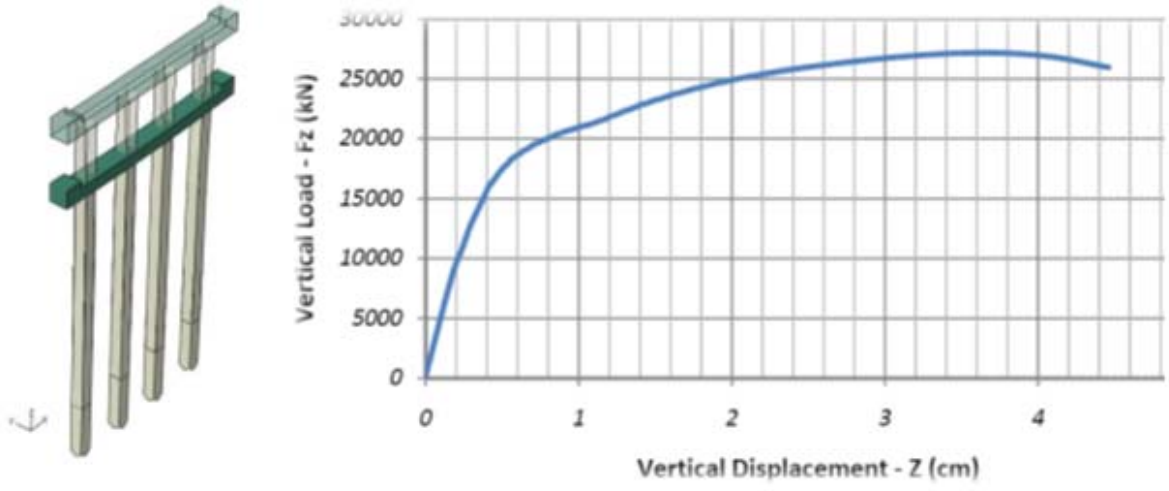

(a) (b)

Figure 86
Vertical load (a) deformed and undeformed model, (b) load-displacement curve

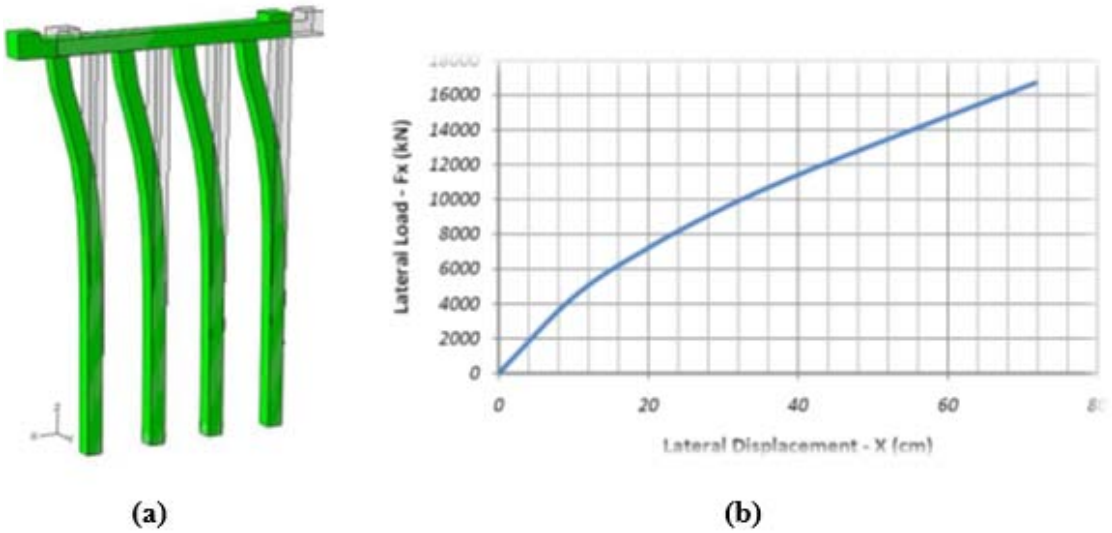

(a) (b)

Figure 87
Lateral load in X direction (a) deformed mesh of the pile group; (b) lateral load-displacement curve

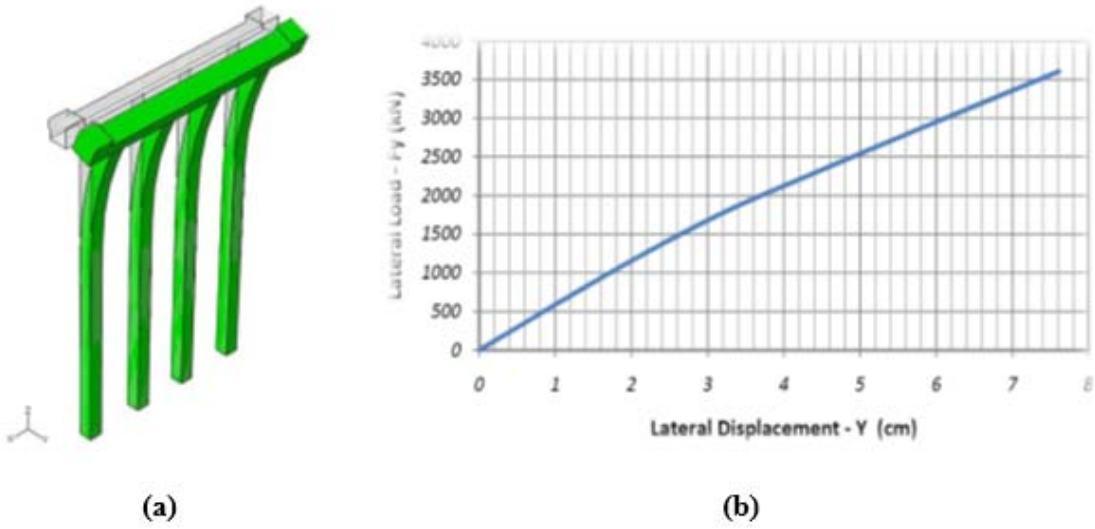

(a) (b)

Figure 88
Lateral load applied in Y direction (a) deformed mesh of the pile group; (b) lateral load- displacement curve

Moment – Rotation Curve around the Y Direction

Figures 89 through 91 show the deformed and undeformed finite element model of Bent 10 in addition to moment-rotation curves for three different directions.

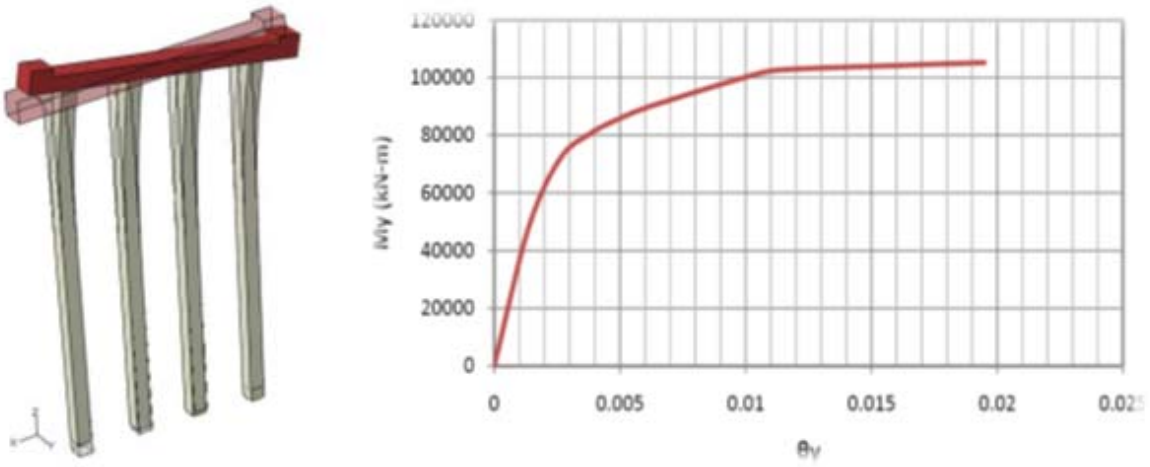

(a) (b)

Figure 89
Moment applied around Y direction (a) deformed and undeformed meshes of the pile group; (b) moment-rotation curve

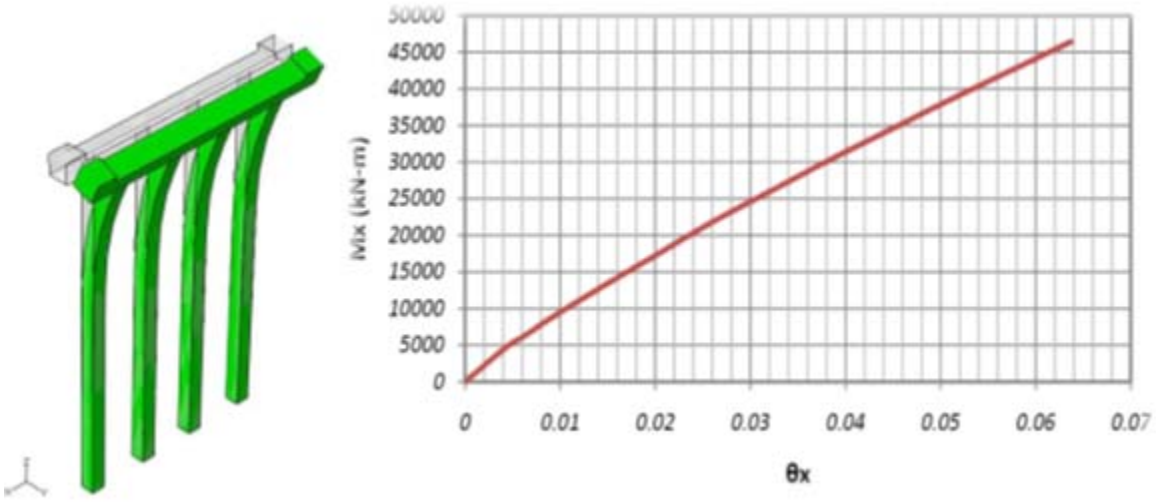

Figure 90
Moment-rotation curve for moment applied around X direction

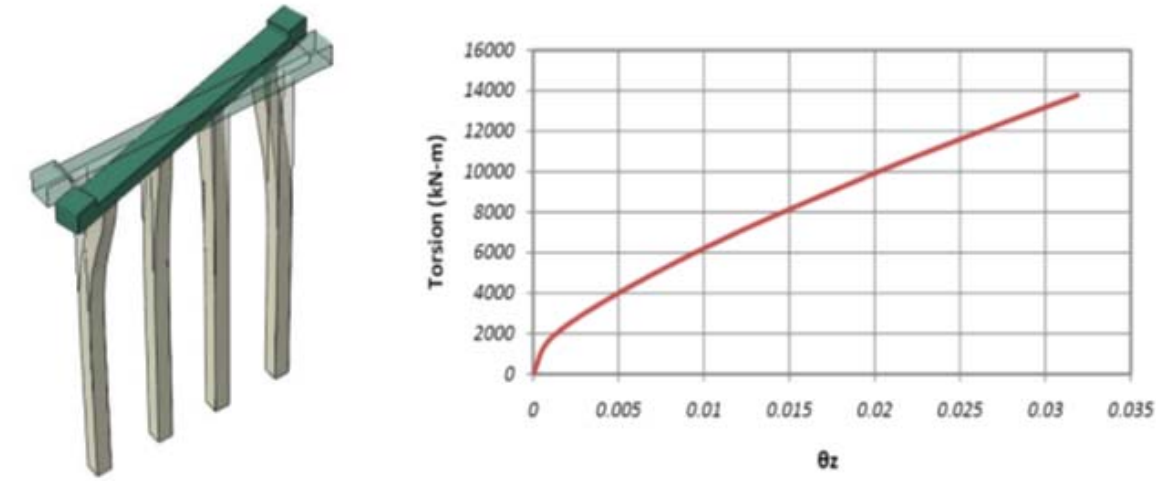

Figure 91
Torsion applied around Z direction (a) deformed and undeformed meshes of the pile group; (b) moment-rotation curve

Analyses of Bent 11 (STA 102+75). At Bent 11, there is a 12-ft. gap between bent and surface of the soil. The results of finite element analyses of this pier as well as the load displacement curves are shown subsequently.

Load-Displacement Analyses

Figures 92 through 94 show the deformed and undeformed finite element model of Bent 11 in addition to load-displacement curves for three different directions.

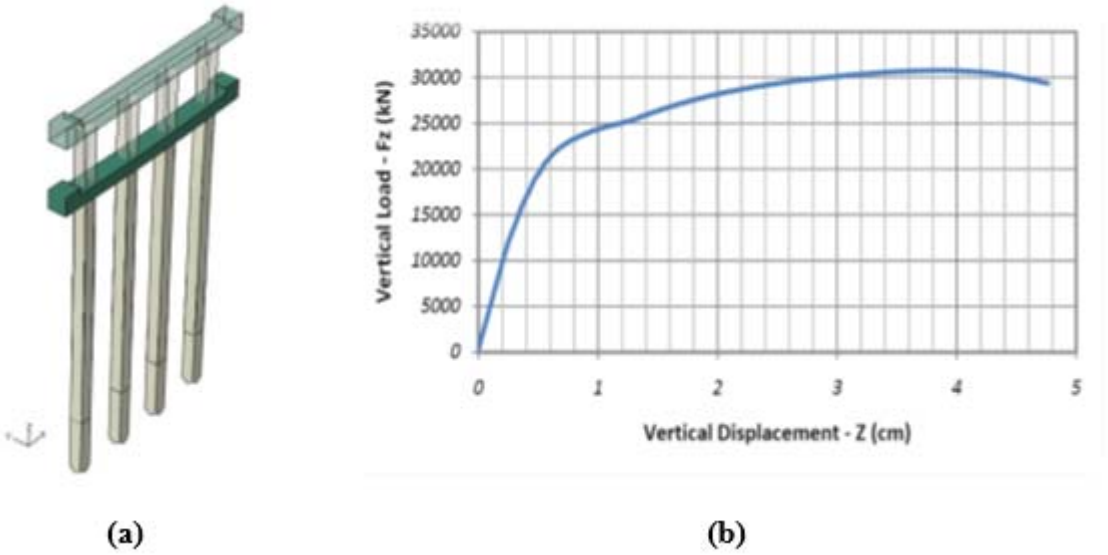

(a) (b)

Figure 92
Vertical load (a) deformed and undeformed model; (b) load-displacement curve

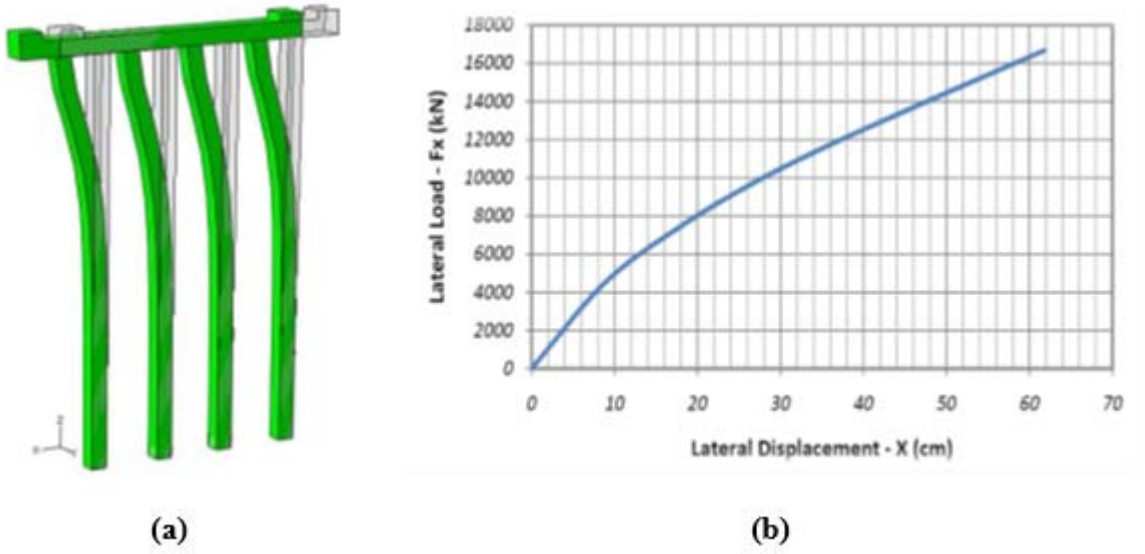

(a) (b)

Figure 93
Lateral load in X direction (a) deformed mesh of the pile group; (b) lateral load-displacement curve

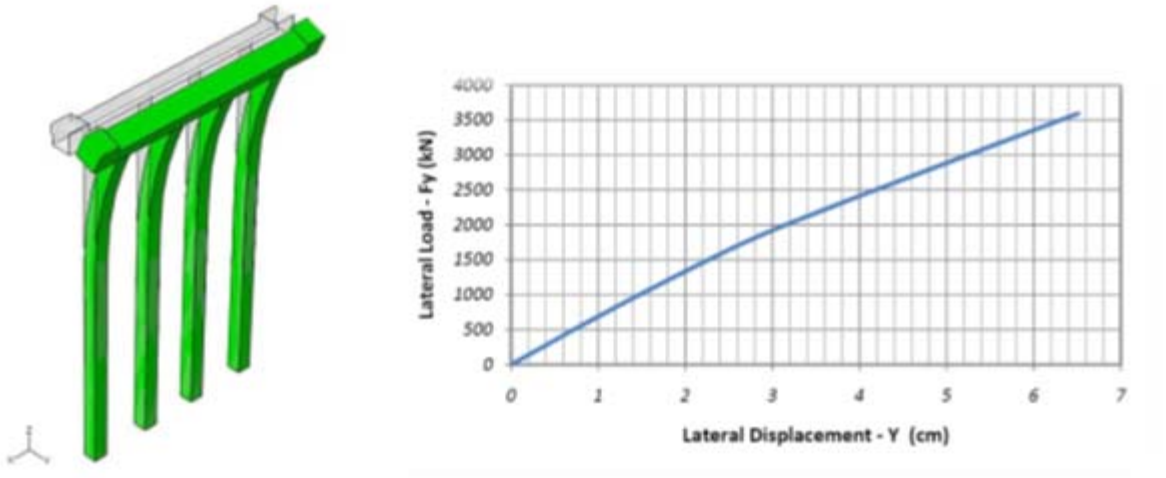

(a) (b)

Figure 94
Lateral load applied in Y direction (a) deformed mesh of the pile group; (b) lateral load- displacement curve

Moment – Rotation Curve in the Y Direction

Figures 95 through 97 show the deformed and undeformed finite element model of Bent 11 in addition to moment-rotation curves for three different directions.

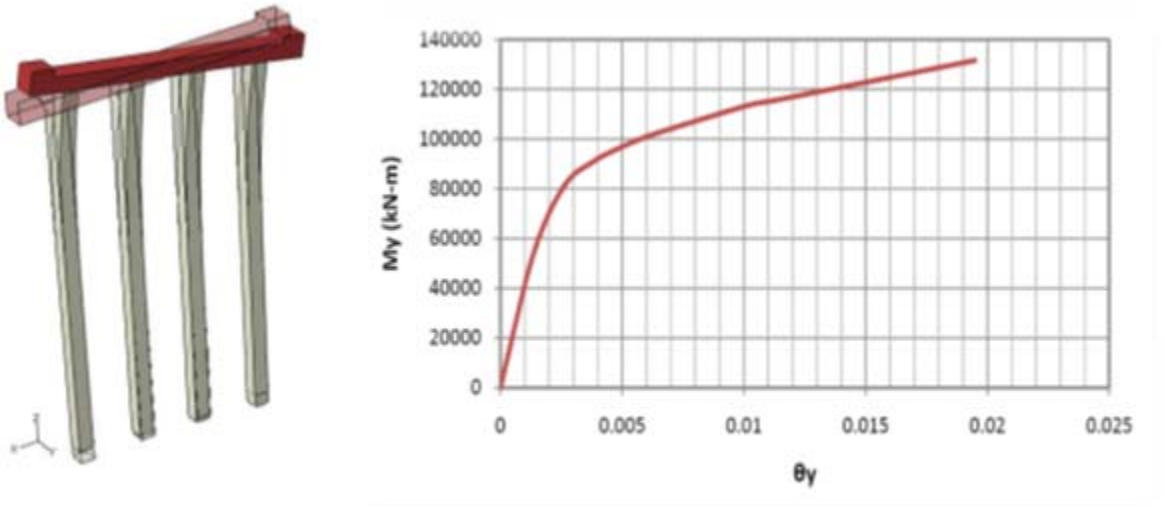

(a) (b)

Figure 95
Moment applied around Y direction (a) deformed and undeformed meshes of the pile group; (b) moment-rotation curve

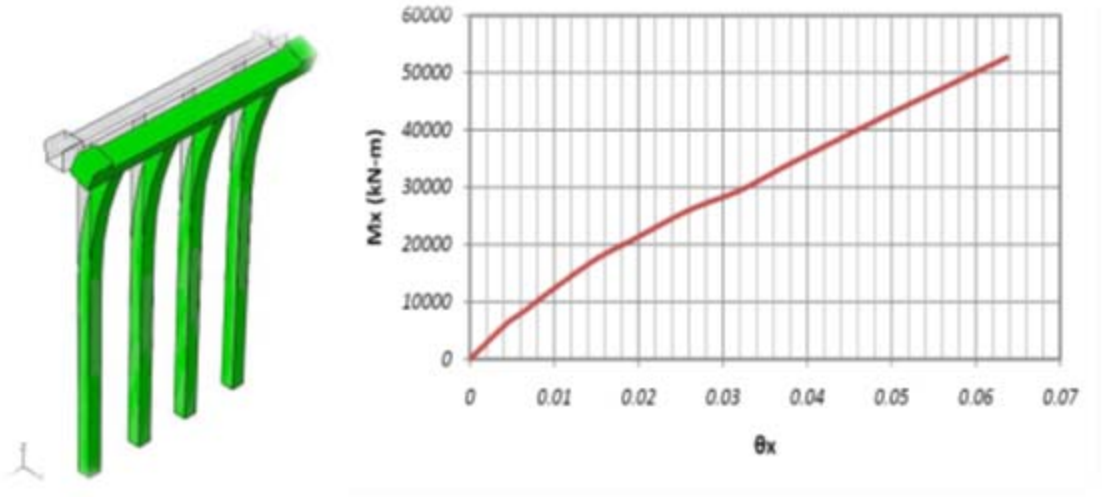

Figure 96
Moment-rotation curve for moment applied around X direction

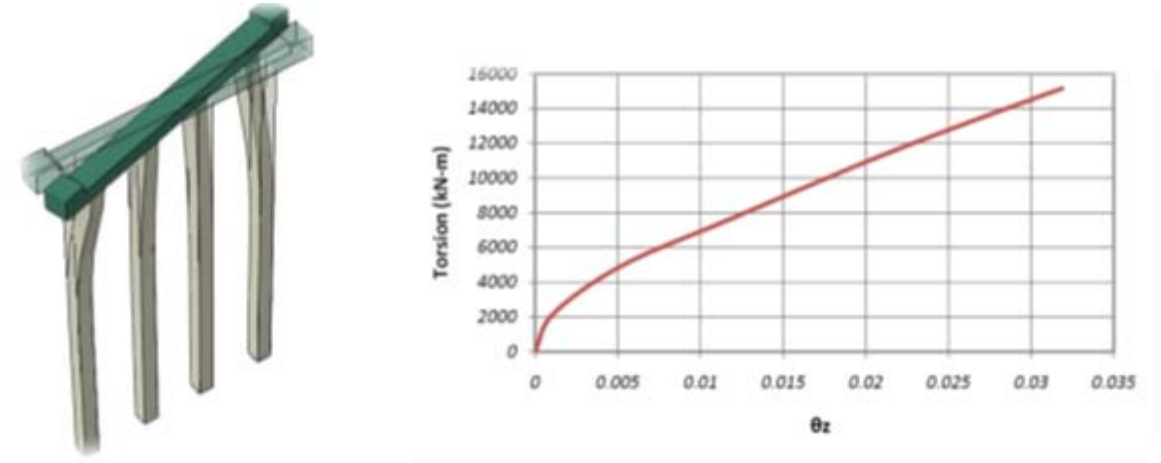

Figure 97
Torsion applied around Z direction (a) deformed and undeformed meshes of the pile group; (b) moment-rotation curve

Bodcau Bayou Bridge

A 3D finite element (FE) model was developed to study the behavior of different parts of the Integral Bridge Abutment under different types of loads similar to the one conducted for the Caminada Bay Bridge. Figure 98 shows the plan of the abutment, namely Bent 1. In this regard, the model parameters of the soil are first determined and then the FE analyses are performed using these parameters.

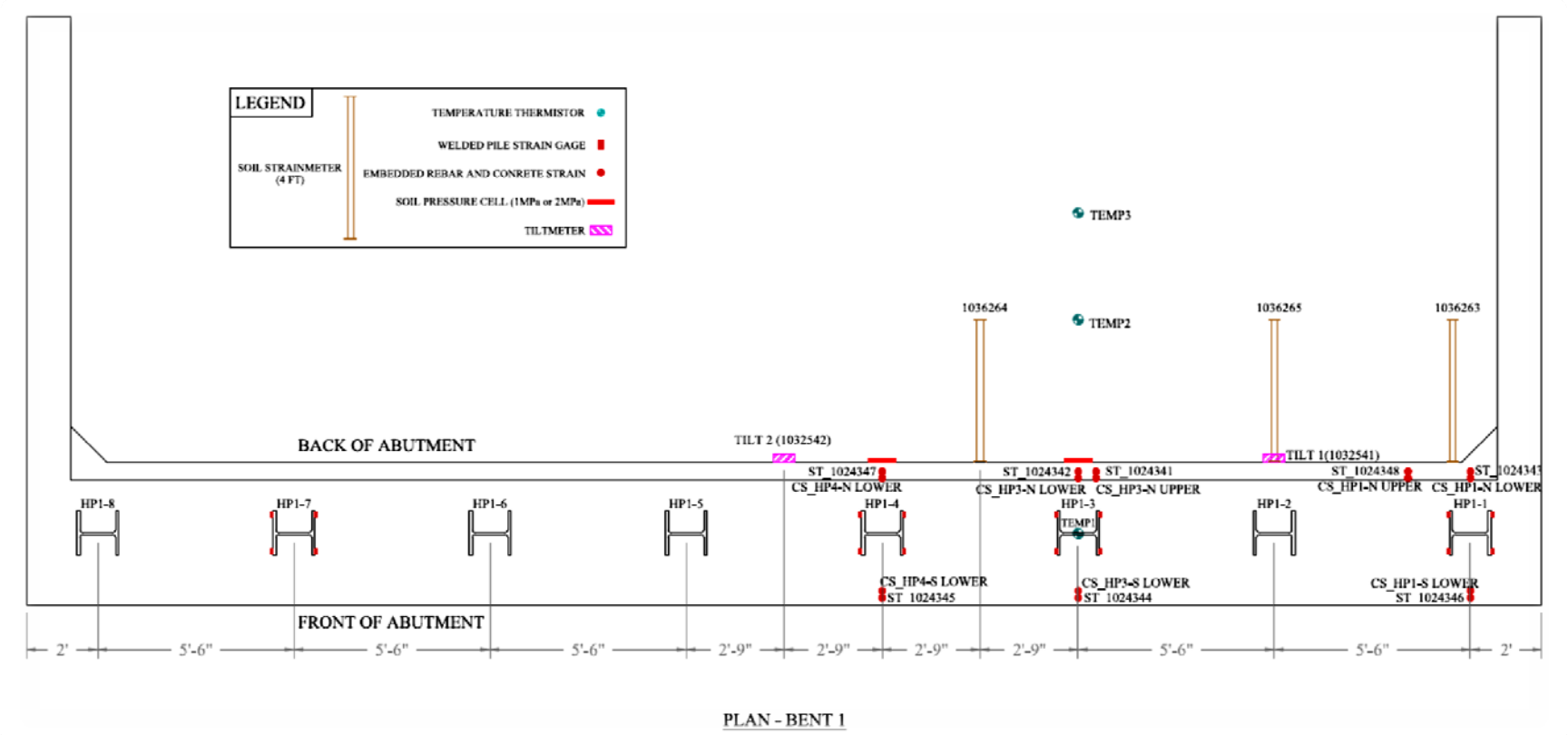

Figure 98
Plan view of Bent 1

Determination of Material Parameters

Before conducting the analysis one needs to obtain the correct material parameters of the soil for the Modified Drucker-Prager constitutive model based on the available data and in-situ measurements. The SPT number is available at STA122+00 which can be used in order to correlate several physical parameters of the soil around Bent 1. The corrected SPT numbers are used to determine the required soil parameters using NovoSPT software. The outcomes of NovoSPT for the variation of Young's modulus, friction angle, and undrained shear strength with the depth are shown in Figure 99 for different estimation approach. From this figure, one can realize that after a depth of 65 ft. (20 m) the soil became stiffer. Therefore, two different soil parameters are considered for the depth between 0-65 ft. (0-20 m) (i.e. Layer I) and >65 ft. (20 m) (Layer II) in the finite element modeling.

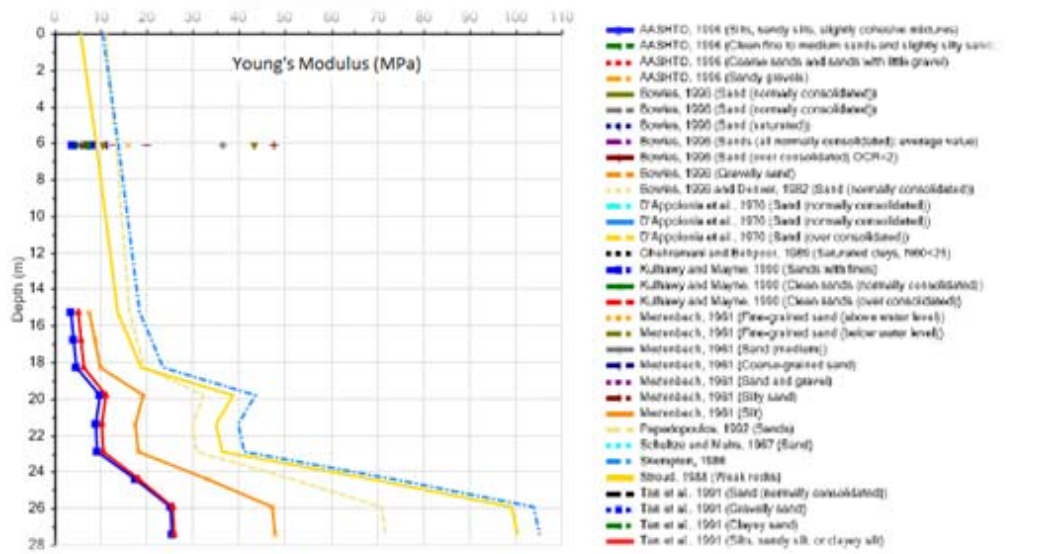

(a)

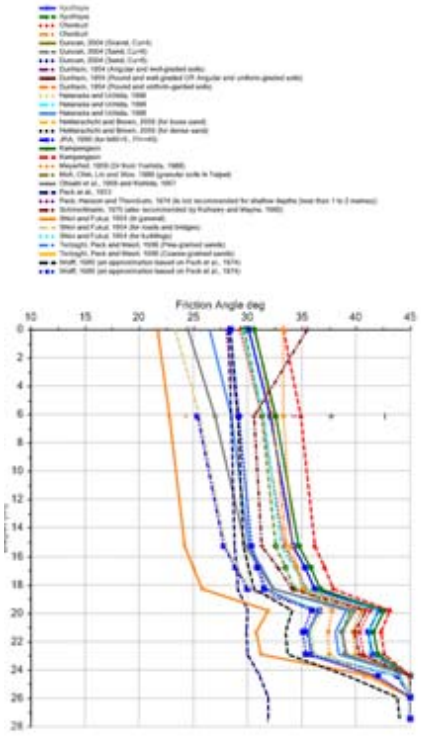

(b)

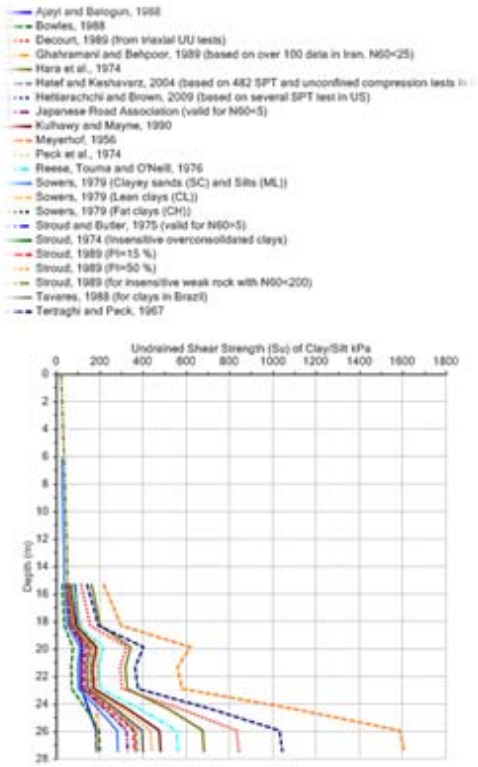

(c)

Figure 99
Soil parameters estimation in various depth of Bent 1 from SPT data at STA122+00; (a) Young's modulus; (b) friction angle; (c) undrained shear strength

Table 15 shows the required soil parameter for analyzing the sub-structure of Bent 1.

Table 15
Soil parameters required for Bent 1, Bodcau Bayou Bridge

Parameter	Layer I (Depth: 0 - 20m)	Layer II (Depth > 20m)
γ_{wet}	19.5 (kN/m^3)	18.6 (kN/m^3)
w	28	32
E	20 (MPa)	60 (MPa)
ν	0.2	0.2
C	0	0
ϕ	30º	40°

Finite Element Model

Figure 100 shows the FE element model of the different parts of the integral abutment of the Bodcau Bayou Bridge. The FE model includes the study of piles, embankment/backfill, abutment, and deck; behavior of the backfill material and surrounding soil under the abutment displacement; and piles and soil interaction using interface elements. This figure shows the HP1 4x89 steel piles with 100 ft. (30 m) length, concrete bent, two layers of surrounding soil (i.e. based on the experimental results of bore holes the modeled soil is divided to two parts: Layer I and Layer II), and the Wing-Wall.

Due to the difference in the stiffness between the soil and piles, the deformation of the pile and surrounding soil was different under the load. In order to simulate such interaction between the pile and soil under different loadings, contact elements were defined at the interface of the soil and pile in the finite element model. By defining a proper value of the coefficient of friction and cohesion (between silt soil and steel), these elements are capable of simulating the interaction between the soil and pile in axial and lateral loadings. The dimensions of the silty soil were chosen in a way that the boundary effect on the pile behavior was minimized.

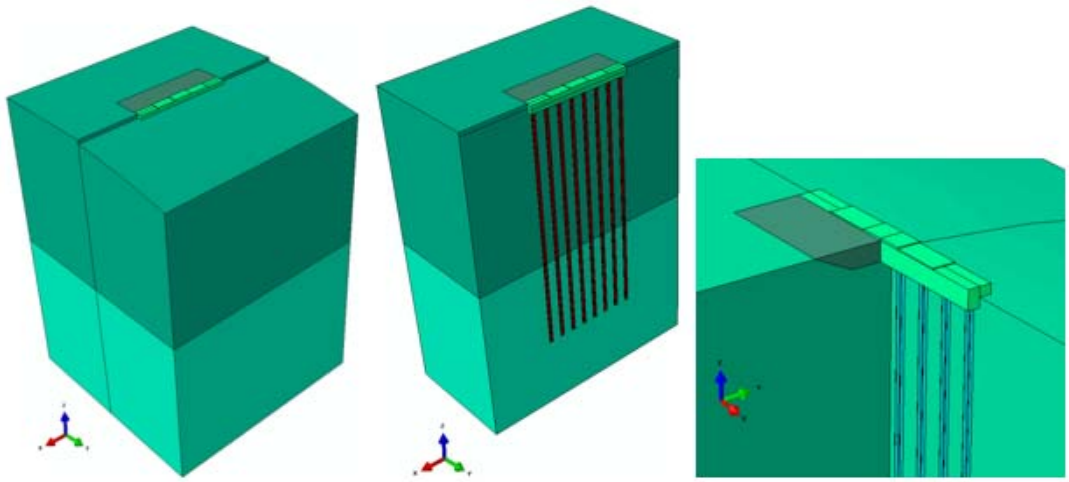

Figure 100
FE model of bent, piles, and soil for Bent 1

Figure 101 shows the finite element mesh of the piles, bent, and soil for the Bent 1. The 10-noded quadratic tetrahedron elements are used for the finite element mesh of the various parts of the model. As it is shown in this figure, a smaller mesh size is considered for the soil near the piles. The overall number of elements used for this model is 83857.

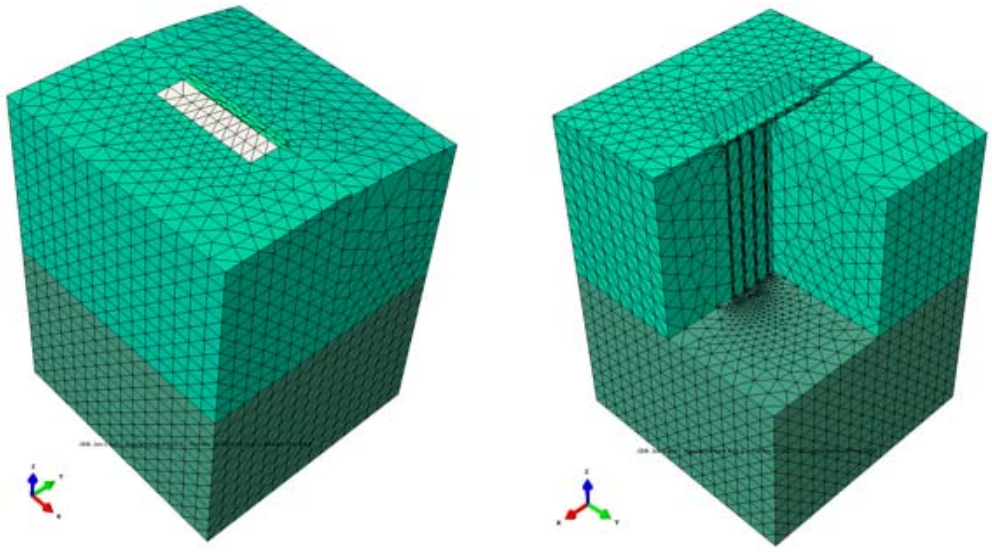

Figure 101
FE mesh of bent, piles, and soil for Bent 1

One of the important parts in the numerical simulation is the proper choice of the constitutive models for the materials used in the analysis. The accuracy of the analysis depends on the correct choice of these models. Materials used in the integral abutment are reinforced

concrete for the bent and Wing-Wall, Steel for the piles along with coarse and fine grain soils. The uncertainty of the soil behavior is more than that of concrete. It is therefore paramount to obtain the proper material model for the soil.

For modeling the behavior of soil, the Modified Drucker-Prager model is taken into account and the Mises type plasticity model with isotropic hardening is used for the concrete and steel *[81]*.

Numerical Analyses Results. After determining the required material parameters, the next step was conducting numerical analyses using the ABAQUS software *[81]*. In these simulations, the piles were assumed to be embedded in perfect contact with the soil before applying the pile loads. The interaction between the pile and the soil was simulated using a penalty-type interface between the steel pile and the silty soil with a friction factor of 0.45. This type of interface is capable of describing the friction between the pile surface and the soil in contact.

The analyses were performed in two steps. The so-called geostatic procedure was used as the first step of the analysis and gravity loads were applied during this step. Ideally, the loads and initial stresses (in-situ stress of the soil) should exactly equilibrate and produce zero deformations. ABAQUS checked for equilibrium during the geostatic procedure and iterate, if needed, to obtain a stress state that equilibrated the prescribed boundary conditions and loads (gravity). This stress state, a modification of the stress field defined by the initial conditions, was then used as the initial stress field in a subsequent analysis.

If the stresses given as initial conditions were far from equilibrium under the geostatic loading and some nonlinearity in the problem definition, the iteration process may fail (for more information, refer to *[81]*).

In the second step, a static, general analysis was invoked and the pile loads and moments were applied at the top surface of the bent in six different directions. In order to capture the load-displacement / moment-rotation response of the pile group, the applied loads / rotations are defined to increase in a linear manner and the average displacement and rotation of the cap are calculated in each case. The results of each type of loading are represented below.

Vertical Load

The pile load versus settlement curve obtained from the finite element analysis is shown in Figure 102 for the applied pressure load on the top surface of the bent. It is noted from the figure that the settlement increases as the load is increased in an approximately linear manner up to about a 5060 kpf (22500 kN) pile load, at which a vertical displacement of about 0.1 in.

(0.27 cm) was encountered. Shortly after that, the pile plunged in a fast downward descent, indicating that the load capacity of the pile had been reached.

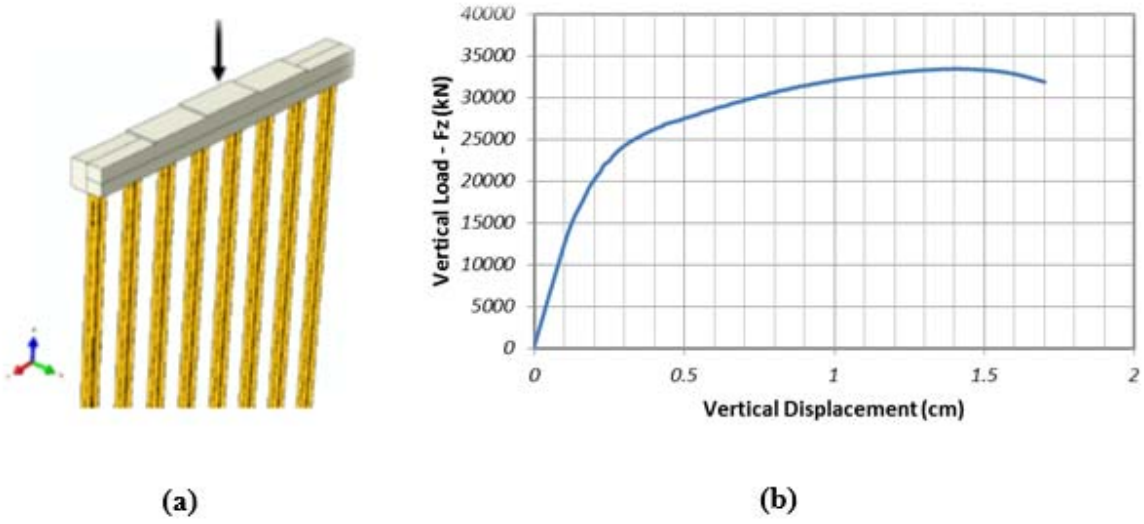

Figure 102
FE results of the Bent 1 (a) vertical load applied to the top of the bent; (b) load-settlement curve.

Lateral Loads in X and Y Directions

Figure 103 indicates the average lateral deformation of the bent versus the applied lateral load in the X direction.

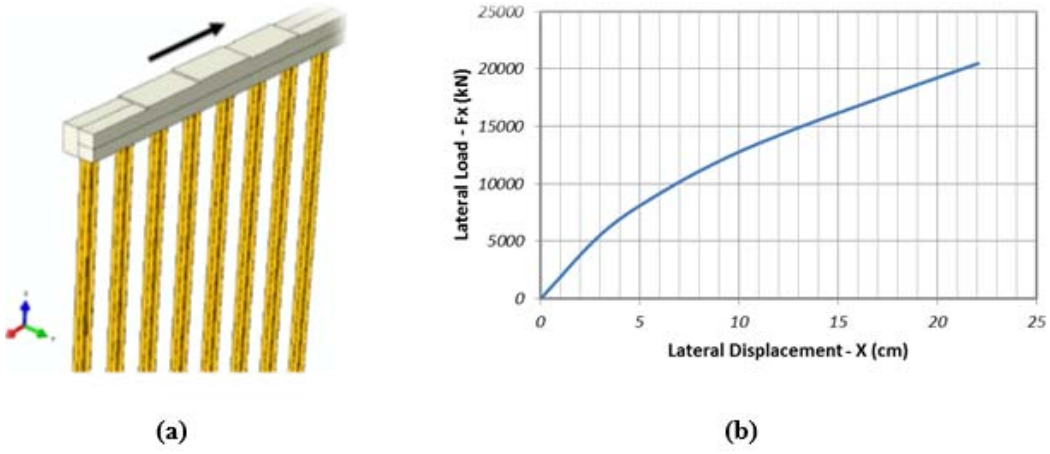

Figure 103
FE results of the Bent 1 (a) lateral load in X direction applied to the top of the bent; (b) load- settlement curve

Figure 104 shows the lateral deflection of one of the piles in the X direction versus the pile length for different amounts of lateral load. It can be seen that for lower amounts of the lateral load, the pile and cap act like a fixed headed pile but when the load is increased a small value of tilt occurs in the cap.

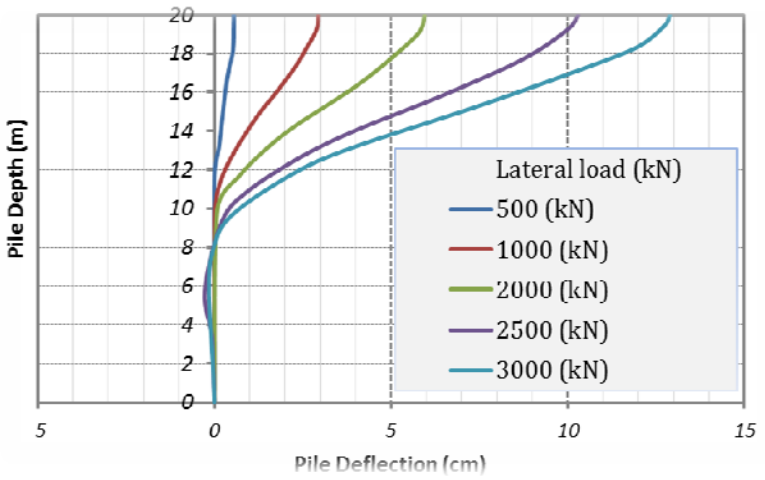

Figure 104
Pile deflection for different lateral loads in the X direction

Figure 105 indicates the average lateral deformation of the bent versus the applied lateral load in the Y direction.

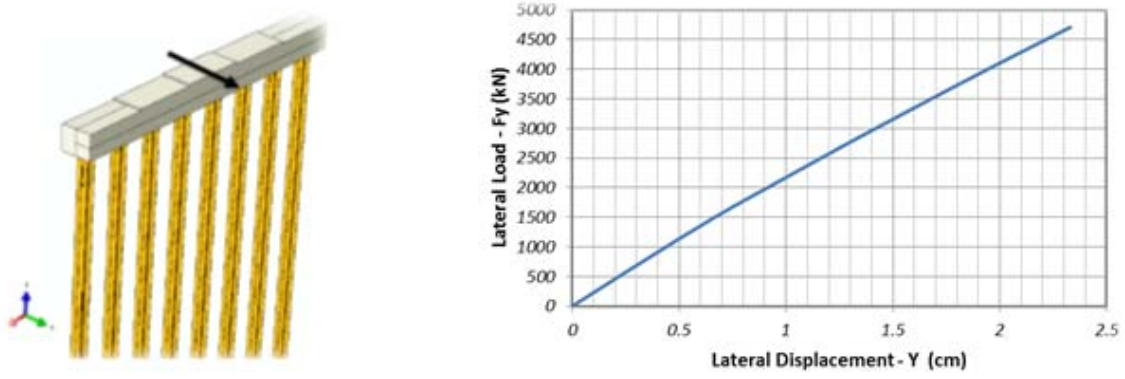

(a) (b)

Figure 105
FE results of Bent 1: (a) lateral load in Y direction applied to the top of the bent; (b) load- settlement curve

Moments around the X and Y Directions

In order to capture the behavior of the pile group under applied moment around the Y direction, linear distributed loads in opposite directions were used on the top of the cap. The resultant coupling between the two distributed loads led to a moment on the cap. The respective rotation was found by measuring the settlement of different positions on one-half of the cap and averaging the results. The deformed mesh and moment-rotation curve of the substructure are shown in Figures 107 and 108 for the applied moment around X and Y directions respectively.

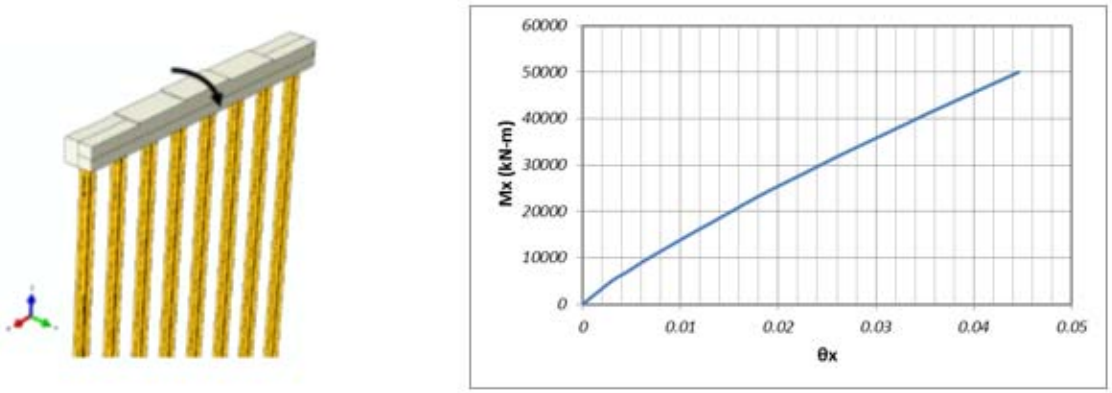

Figure 106
FE results of the Bent 1 (a) moment around X direction applied to the top of the bent; (b) moment-rotation curve

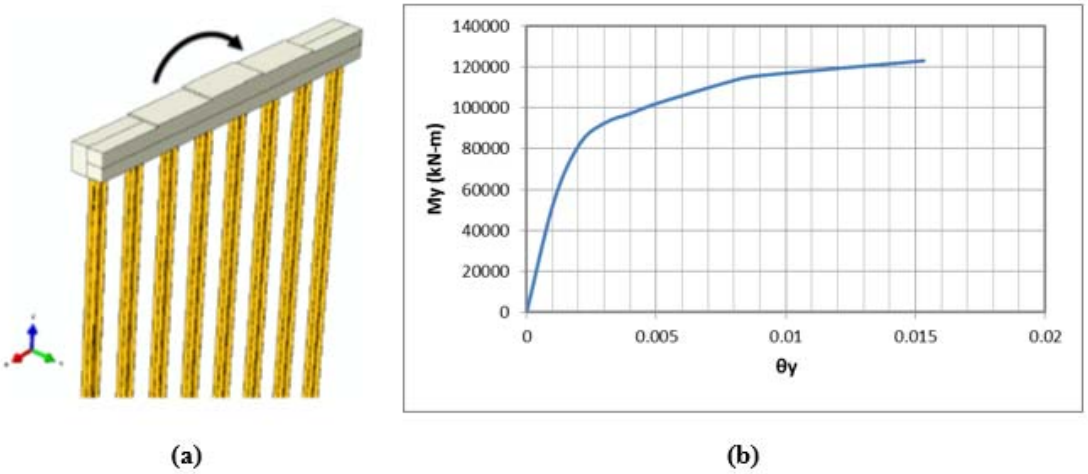

Figure 107
FE results of the Bent 1 (a) moment around Y direction applied to the top of the bent; (b) moment-rotation curve

Torsion around Z Direction

Resultant applied torsion on the cap of Bent 1 is shown in Figure 108 (b). This figure also indicates rotation angle due to different values of torsion.

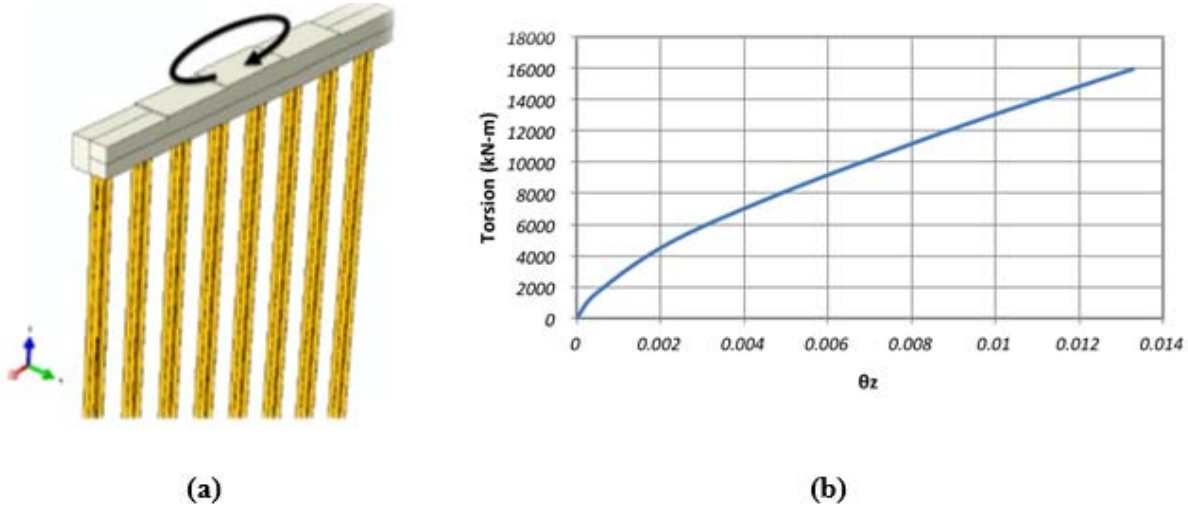

Figure 108
FE results of Bent 1 (a) torsion around Z direction applied to the top of the bent; (b) torsion-rotation curve

Finite Element Analysis Integral Abutment Bridge for Louisiana's Soft Soils–Superstructure

Caminada Bay Bridge

The bridge is located at Grand Isle, LA (29°15'48" N 89°57'24" W), about 100 miles (160 km) south of New Orleans, LA. The total length of the bridge is 3945 ft. (1202 m), while the modeled part is for the first 11 spans, shown in Figures 109 and 110, including a 10 ft. (3 m) sleeper slab, a 40 ft. (12 m) approach slab, a 300 ft. (91 m) continuous concrete slab, and the substructure underneath, such as the abutment, pile, and soil. Each bent is supported by a single row of four precast prestressed concrete (PPC) piles with a square cross section of 36in. In addition, the material properties designed for this bridge are summarized as follows: (a) Class AA (M) concrete, with a strength of 4060 psi (28 MPa), is used for the slabs and bents; (b) Class P (M) high performance concrete, with a minimum compressive strength of 6000 psi at 28days, and an average compressive strength of 10,000 psi at 56 days, is for the PPC piles; (c) Type 316LN stainless steel, with an elastic modulus of 29000 ksi, a tensile strength of 75ksi, and a yield strength of 30 ksi, is for the deformed reinforcing steels in the bents and slabs; (d) Grade 60 black steel, with a 60 ksi yield strength, is for all the other deformed reinforcing steels; (e) Grade 270 steel, with a 270 ksi yield strength, is for the prestressing strands; and (f) the thermal expansion coefficient of the concrete is assumed as 5

με/°F after a synthesized consideration of the specified values 6 με/°F from the AASHTO LRFD (2007), and the lower and upper bounds of 4.7 με/°Fand 6.5 με/°F from the ACI 209 R-92 (2004).

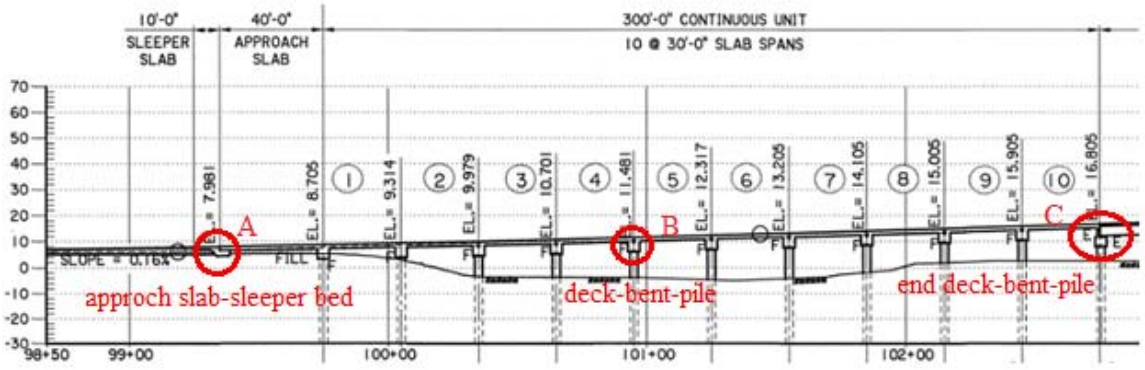

Figure 109
Elevation view of the first 11 spans of Caminada Bay Bridge

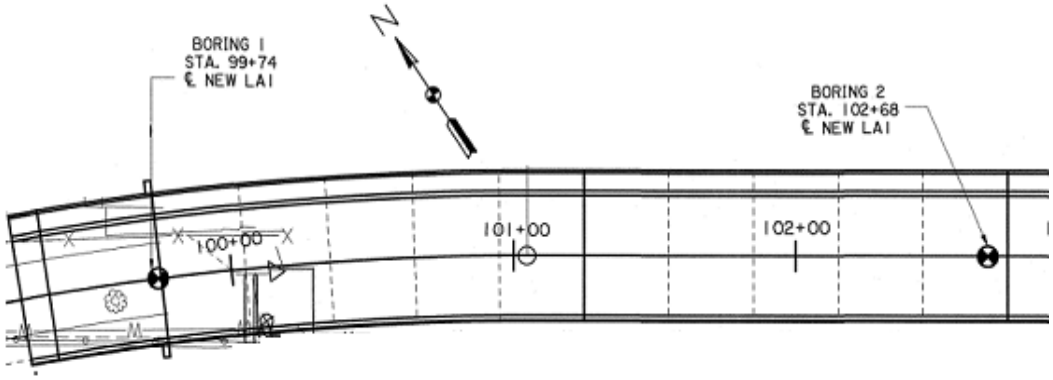

Figure 110
Plan view of the first 11 spans of Caminada Bay Bridge

Model Development

Boundary Conditions. Different from some other commonly designed IABs, where integral joints are primarily constructed at the interfacial locations between the slab-girder-abutment at the two far ends, the bridge discussed in this study has more rigid connecting behaviors throughout the whole length. First, at the left end of the bridge, a 4 in. expansion joint was provided between the sleeper slab and the approach slab; and the approach slab, in turn, is laid on a reinforced rubber pad. Thus, certain friction restraints may exist and obstruct the free movements of the approach slab. Second, for all the interior bents from Bent 1 to Bent 10, tensile steel rebars are constructed both extending from the bents to the slabs, and also from the

pile heads to the bents. Thus, continuous behaviors are expected at these locations. Third, at Bent 11, a strip seal joint is applied between the slab and Bent 11 so that the longitudinal movements and rotations are not fully restrained. Therefore, the boundary conditions for this bridge are assumed and modeled as simple support conditions at the two ends and fixed ones in between. The effects of this assumption on the modeling results will be discussed later.

Soil-Structural Interaction. Two soil boring logs are available from the approach slab to Span 10, and the information obtained at the station 99+74, as shown in Figure 111(a), was adopted to represent the soil condition of the modeled bridge parts. The soil layers that will be used in the numerical model are shown in Figure 111(b), where they can be roughly categorized into three layers: a layer of medium clay for the backfill followed by two layers of medium sand and medium clay below the water table and surrounding the piles, respectively.

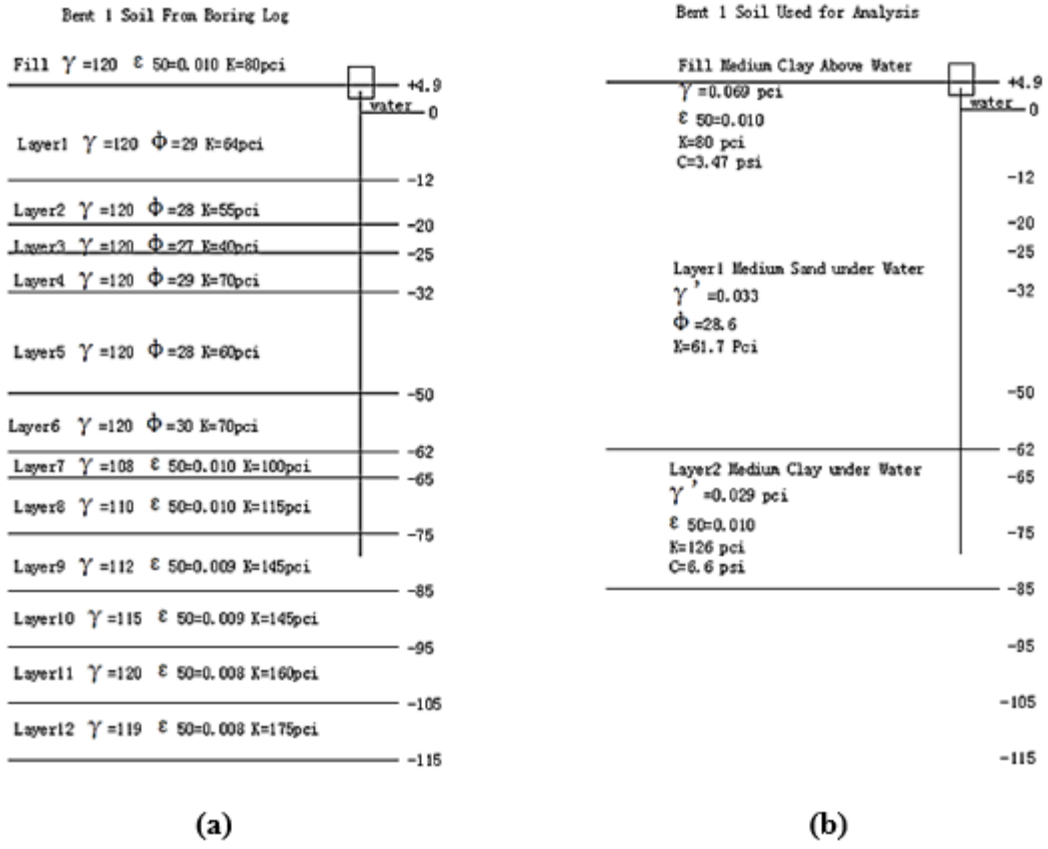

Figure 111
(a) Soil layout from Boring Log 1; (b) soil layers for FEM analysis

Generally speaking, in modeling of the soil-pile interaction behaviors, the p-y curve and elastic continuum methods are commonly proposed in the literature. Specifically, the former one, based

on the Winkler hypothesis, is simple and has been widely applied in the routine design. In this approach, the soil is simplified as a series of discrete elements so that the soil response at one point is independent on the pile deflection elsewhere. The soil-structure interaction behavior is accounted by a series of p-y curves along the pile depths, where the p and y refer to the soil force and pile deflection, respectively. The generations of these p-y curves can be complicated and affected by many parameters, e.g., soil type, shear strength, moisture condition, effective stress, stress history, loading condition, etc.; while they can be more conveniently obtained from some commercial or free software and programs, e.g., COM624P (1991), LPILE, FB-Pier, etc. In this study, the COM624P (1991) program was adopted, where the coded p-y curves in the program are based on the full-scale experiments; thus the continuum effects are explicitly implemented.

In modeling of the backfill-abutment interaction behaviors, several other design curves are provided for sandy soils, e.g., NCHRP (1991), CGS (1992), and Duncan and Mokwa (2001). Among all the curves, the NCHRP (1991) curve, as shown in Figure 112, is commonly adopted in the design. Specifically, the force and displacement relationships between the backfill and abutment are expressed as,

$$F = K\sigma'_v wh \tag{18}$$

where, F = effective soil lateral resistance, K= coefficient of lateral earth pressure for the passive K_p and active K_a conditions, respectively, determined by the ratio of the wall deformation and height (D/H), σ'_v= vertical effective soil stress, equal to the soil density multiplied by the depth of the soil $(\gamma' z)$, wh= width and height dimensions of the tributary area of the abutment backwall.

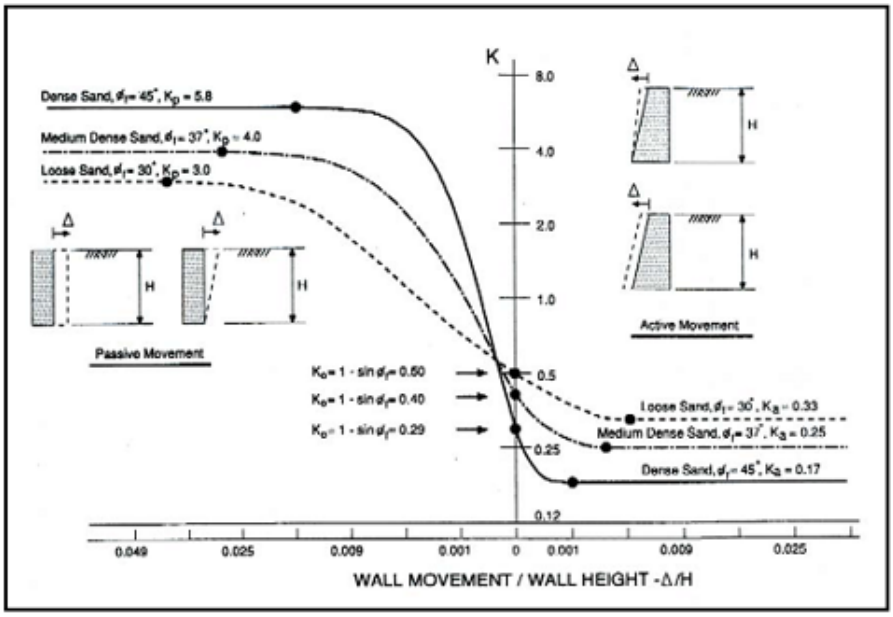

Figure 112
Relationships between wall movements and earth pressures from NCHRP (1991)

Figure 113 (a) and (b) shows the two representative force-displacement (F-D) curves for the loose and dense sand conditions along the three depths behind Bent 1, respectively, and they will be used in the following parametric study. For the cohesive backfill, however, there are no relative design curves available in the codes or reports based on the authors' knowledge. According to CALTRANS (2004), for cohesive soils, the creep effects should be considered in estimating the design earth pressures; while obtaining these soil behaviors are complicated and often require laboratory tests, then the cohesive or other fine-grained soils are often avoided as backfill materials.

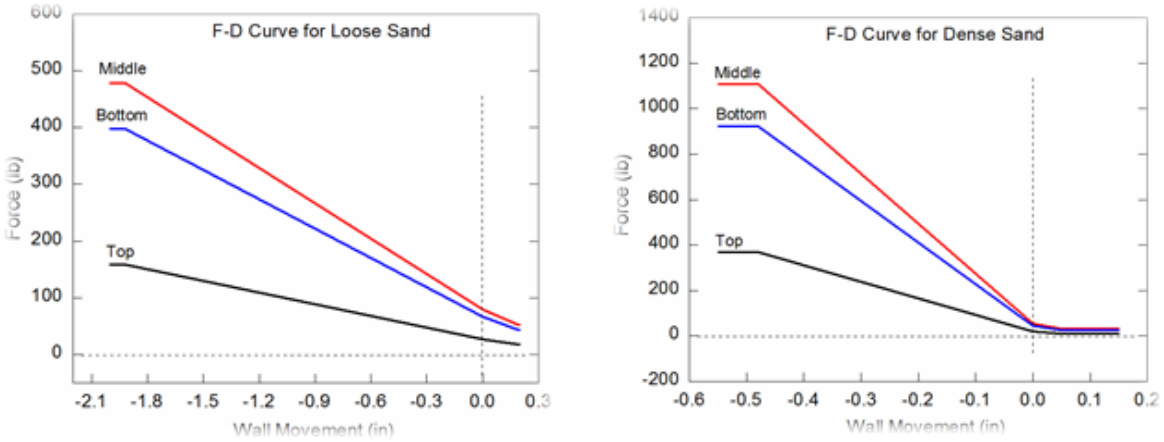

(a) (b)

Figure 113
F-D between Bent 1 and Backfill at three elevations (a) loose sand; (b) dense sand

Numerical Model Development. Based on the above discussions, a 3D finite element model was developed using the commercial software ANSYS 11.0 as shown in Figure 114. Specifically, (1) the 3D Solid45 element, with eight nodes and three degrees of freedom for each node, was adopted for modeling the slabs and bents; and the uniaxial Beam4 element, with six degrees of freedom for each node, for the piles; (2) the unidirectional COMBIN39 spring elements, with the nonlinear force-deflection capability, were adopted for simulating the soil-pile interaction behaviors both in the parallel and perpendicular directions with respect to the bridge traffics; (3) for the backfill-abutment interaction behaviors, they were ignored at this stage considering the complexity to obtain the behaviors of cohesive backfill. This assumption, on one hand, can be justified from the field measurements, in which the observed variations of the pressures for such soil types under the current IAB configurations are negligibly small; on the other hand, the effects of the backfills on this bridge were also proven to be insignificant in the subsequent parametric study; and (4) for the connection behaviors between the piles and bents, the multipoint constraint MPC184 elements were used and the rigid beam connecting option selected.

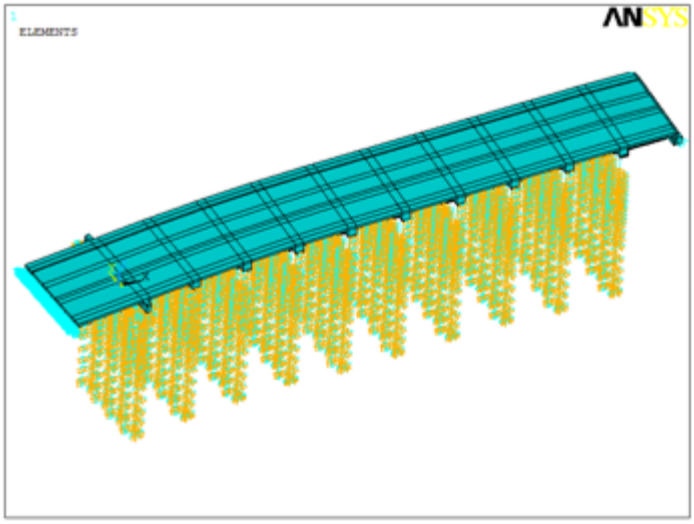

Figure 114
3D FEM of the Caminada Bay Bridge using ANSYS

Besides the structure and soil models, the loading condition is another important aspect. Uniform and gradient variations are two major temperature components considered in bridge thermal analysis. The former, often inducing the expansion and contraction movements, will cause axial forces; and the latter, being further categorized as linear or nonlinear distributions, will induce bending deformations and self-equilibrating thermal stresses. The temperatures within the bridge actually fluctuate differently at various components and locations, while the major temperature variations of this bridge primarily appear at the superstructure based on the field measurements. In the monitoring program, since only the surface temperatures of the slabs are measured, the temperature distribution patterns through the slab depth must be predicted. Hence, using the available temperature predication methods, the bridge temperatures during the approximately two representative hottest and coldest weeks, i.e., 01/01/12 to 01/13/12 and 09/06/11 to 09/16/11 respectively, were simulated. The boundary conditions, i.e., ambient temperatures and wind speeds, are referred to the local weather station (Grand Isle, LA 29.263 N, 89.957 W http://tidesandcurrents.noaa.gov), and the solar radiation was predicted using an algorithm which enables the researcher to consider the relative solar incident angle between the solar and bridge during each hour on different days of the year.

Figure 115 shows the comparisons of the temperatures at surfaces of the bent top and slab bottom locations. The observed good fitting trends between the field measurements and ANSYS predictions during the two selected weeks verify the rationale of the temperature prediction model and the corresponding environmental and material thermal parameters. The

largest temperature gradients during the two modeling periods are plotted in Figure 116 (a), and the normalized results, by subtracting the initial values along the depth of the slabs, are shown in Figure 116 (b). Additionally, the temperature design values for such concrete slabs at the current bridge site, referred to AASHTO LRFD (2007), are also plotted in the corresponding figures. Thus, as can be observed in Figure 117, the temperature differences between the top and bottom slab surfaces during the two periods were less than 11℃ (20°F), which are still within the code specifications. In addition, the temperature distribution through the depth of the slab was in a nonlinear gradient pattern, while the magnitude is not significant. In this case, the temperature gradient through the current slabs could be more approximately and conveniently represented by a simplified linear one using the measured temperatures at the top and bottom surfaces.

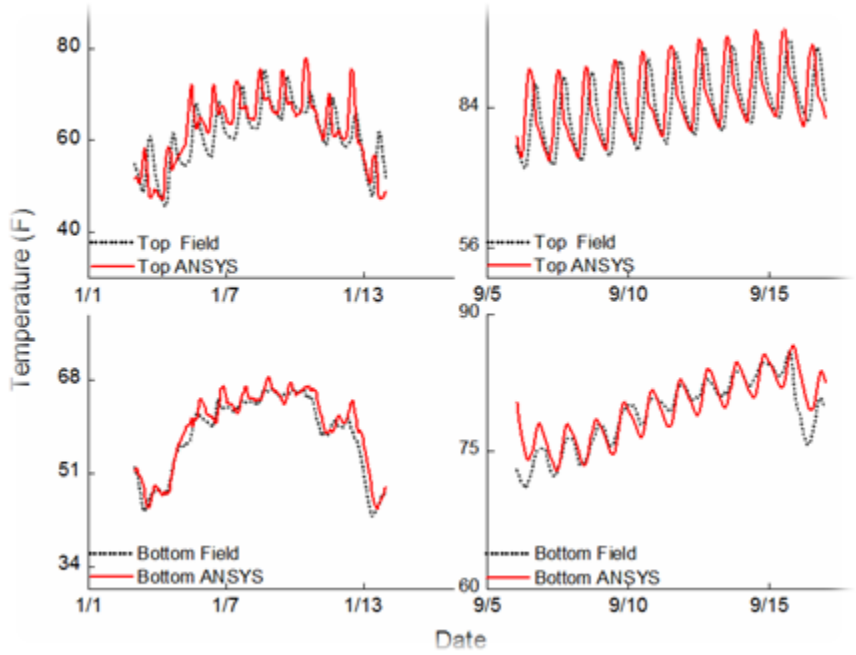

Figure 115
Comparisons of slab temperatures between field measurements and ANSYS predictions 01/01/12 – 01/13/ 12 and 09/06/11 to 09/16/ 2011

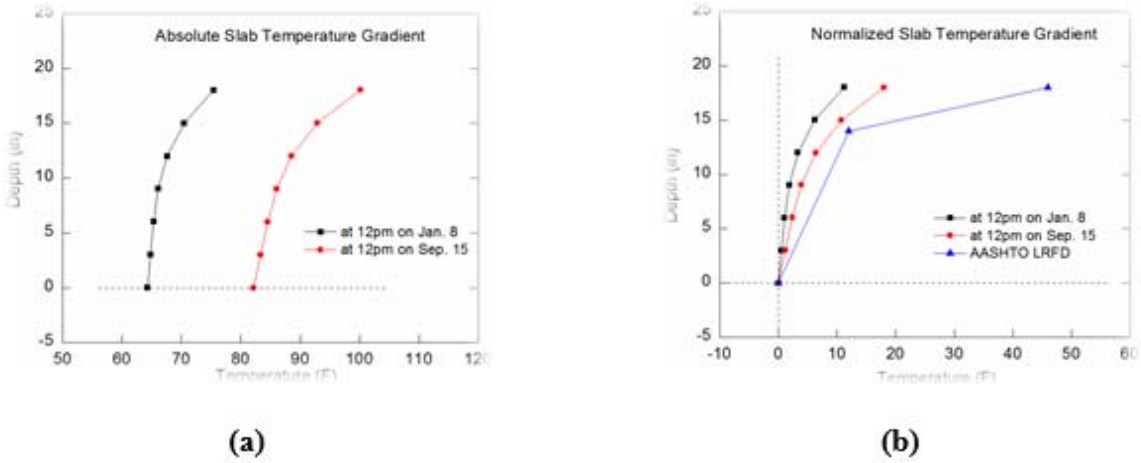

Figure 116
Predicted slab temperature gradients: (a) absolute results (b) normalized results

Numerical Study Results. The thermal behaviors of the bridge within a 24-hour period are simulated and justified with the field measurements at the two representative hot and cold days, i.e., 08/30/11and 02/12/2012, respectively. The measured temperatures at the top and bottom surfaces of the slabs, as shown in Figure 117(a) and (b), are directly applied as node loads in the model, and a linear temperature distribution is assumed through the slab depth. Therefore, the predicted and measured performances, at the locations marked in Figure 118 (a) to (c), are compared in the following aspects, including the top and bottom surface strains, abutment displacements and rotations, slab, and pile bending strains with respect to the x and y axes.

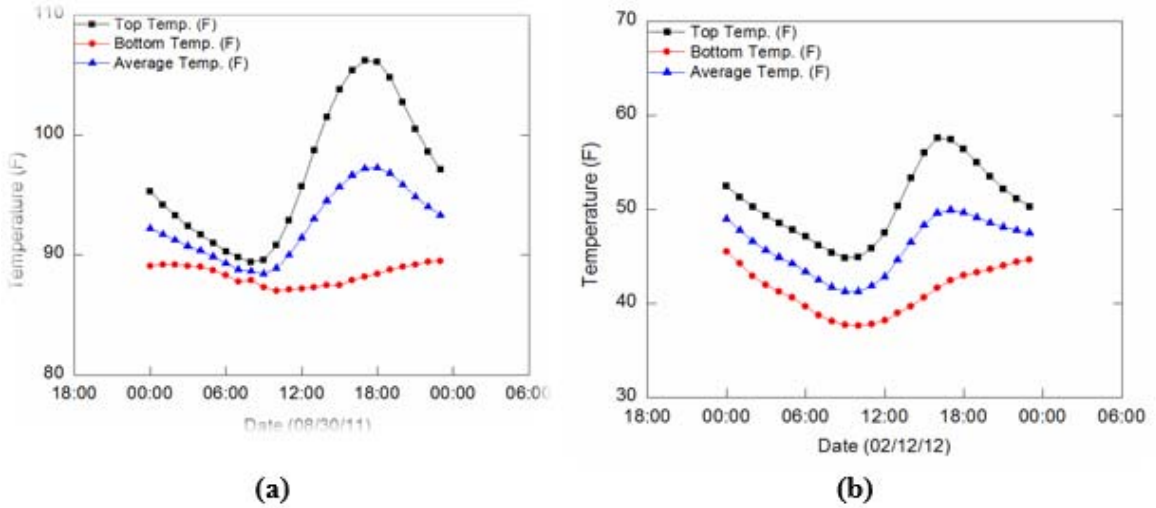

Figure 117
Field measured temperatures of the slabs on (a) 08/30/11and (b) 02/12/12

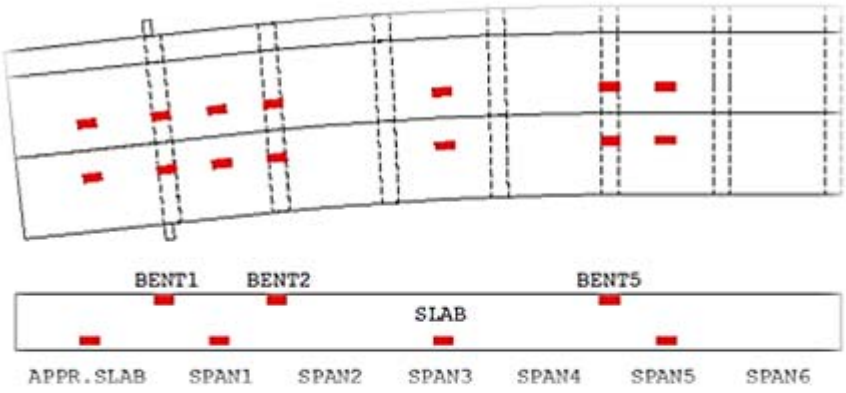

(a)

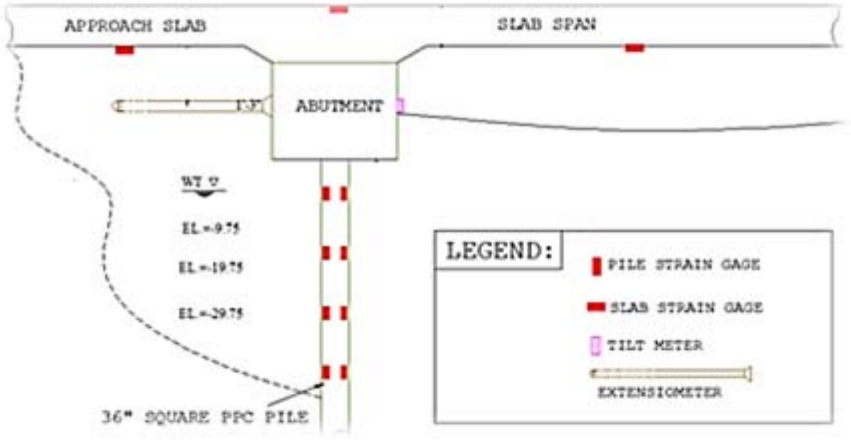

(b)

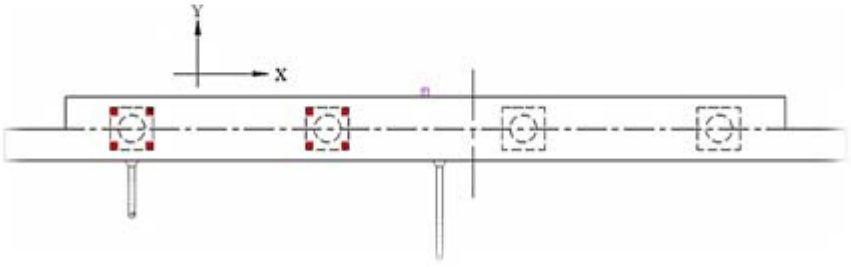

(c)

Figure 118
Instrumentations mounted on Caminada Bay IAB: (a) plan and elevation view of gages on the superstructure; (b) side view of gages on the substructure; (c) plan view of gages on the substructure

The comparisons between the numerical simulations and field measurements are shown from Figure 119 to Figure 124, with all values normalized by subtracting the results at the initial time. It can be observed in these figures that the results generally show similar varying trends between the simulations and measurements for all the items compared, especially for the strains in the slabs and piles. Thus, the proposed numerical model can reasonably represent the bridge and environmental conditions. For the displacements and rotations of Bent 1, however, some discrepancies appeared, but nothing significant. They may be attributed to the following reasons, such as (a) the uncertainty on the soil types and the corresponding compaction degrees behind Bent 1; (b) the modeling error of the support and boundary conditions at the bridge ends; (c) the modeling error of the soil-pile interaction behaviors at Bent 1; and (d) the long term cumulative effects due to the soil plasticity behaviors behind Bent 1. In addition, it should be noted that, during the model calibration process, the responses of the current bridge are extremely sensitive to the loading types (uniform or gradient temperatures), support conditions (free or fixed), flexure rigidities (Young's modulus of piles, soil types surrounding the piles, and pile-bent connections), but quite insensitive to the backfill properties. These features of IABs are further studied in the next parametric study section.

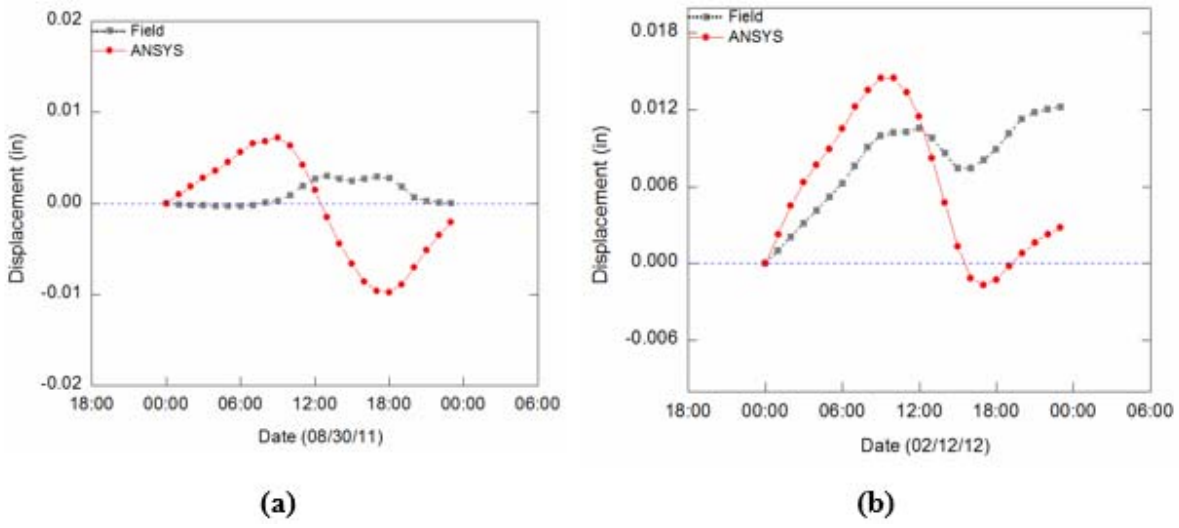

Figure 119
Comparisons of displacements at Bent 1 on (a) 08/30/11 and (b) 02/12/12

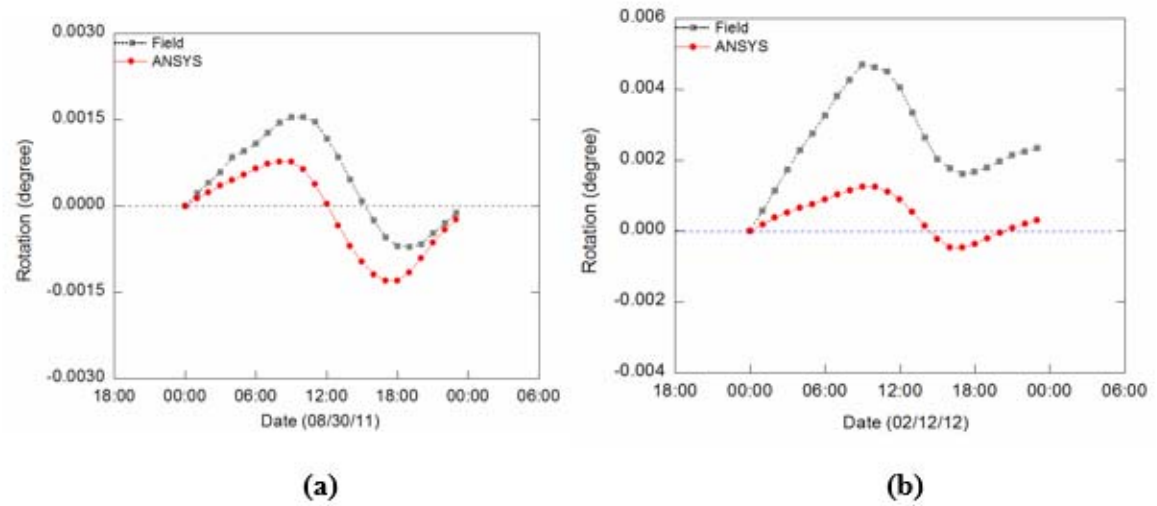

Figure 120
Comparisons of rotations at Bent 1 on (a) 08/30/11 and (b) 02/12/12

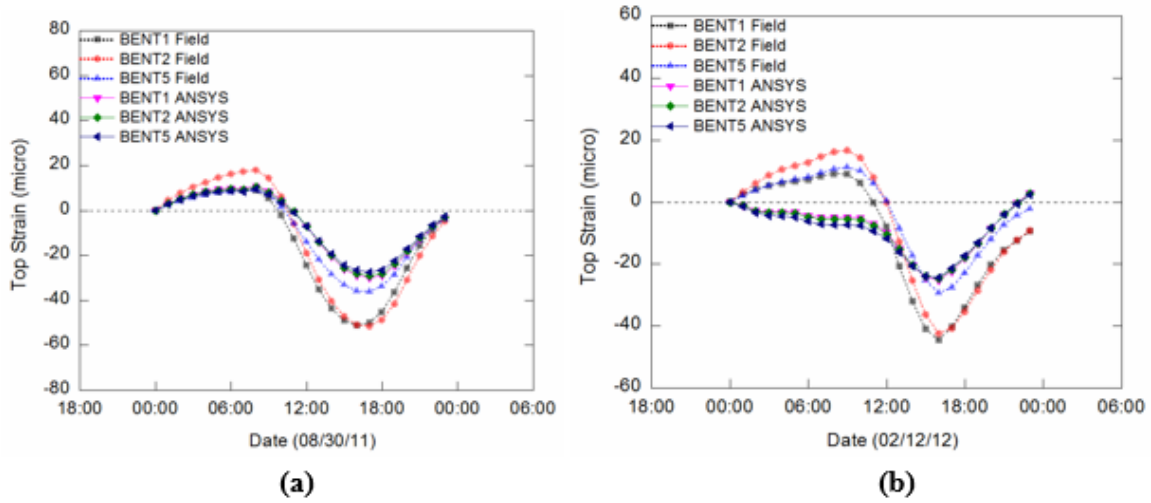

Figure 121
Comparisons of strains at the bent top surfaces on (a) 08/30/11 and (b) 02/12/12

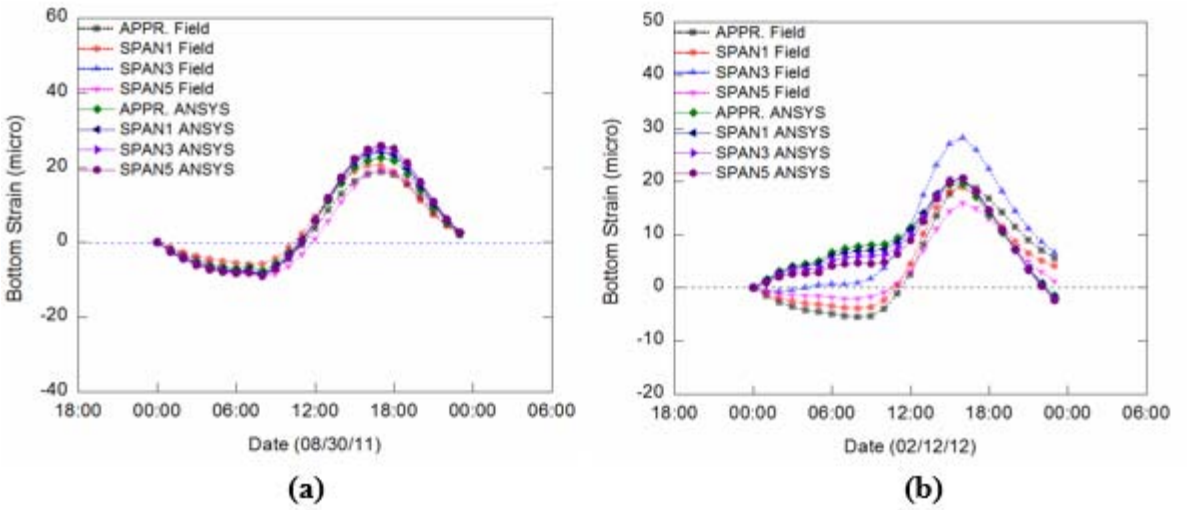

Figure 122
Comparisons of strains at the slab bottom surfaces on (a) 08/30/11 and (b) 02/12/12

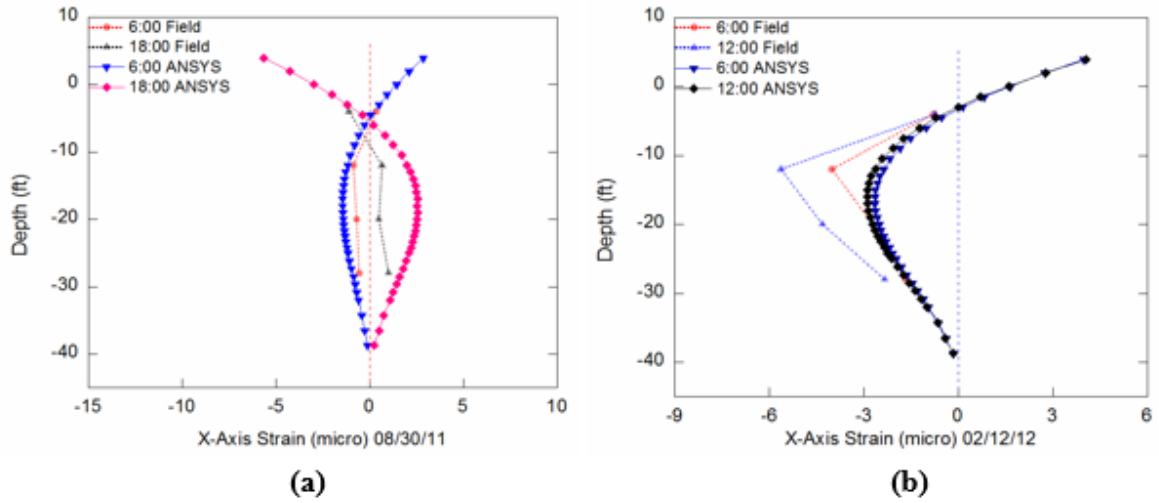

Figure 123
Comparisons of X-Axis bending strains at piles on (a) 08/30/11 and (b) 02/12/12

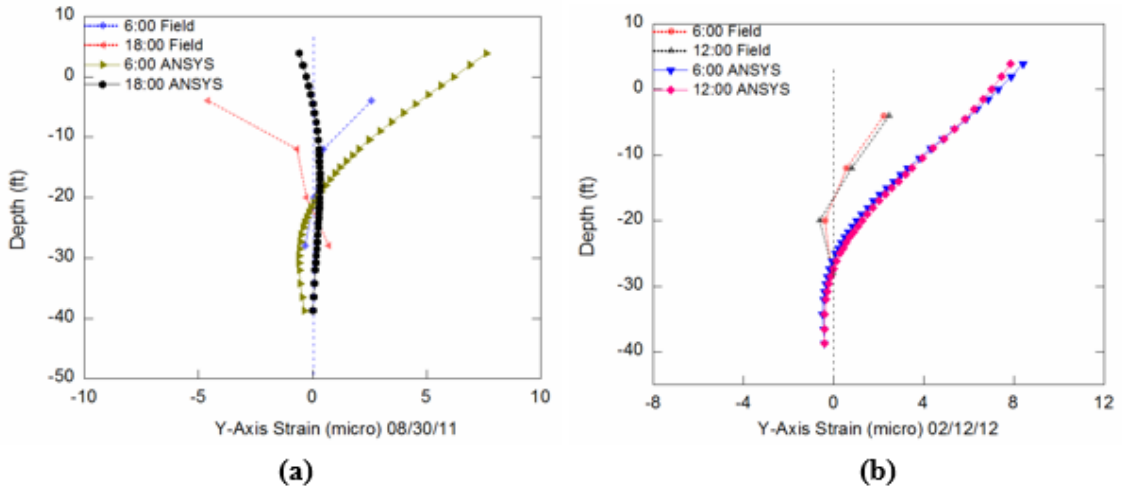

Figure 124
Comparisons of Y-Axis bending strains at piles on (a) 08/30/11 and (b) 02/12/12

Parametric Study. A parametric study was conducted to investigate the behaviors of IABs when applied to other different soil conditions and structure configurations. Generally, many factors may affect the performance of a bridge, while the restraints to the thermal deformations are of significant importance for IABs. These restraints may come from soil resistances, structural rigidities, support conditions, element connecting behaviors, etc. For example, if the restraints are weak, a larger displacement from the superstructure may cause the pile buckling or soil failures; but, if the restraints are strong, the induced thermal forces may be substantial and damage the superstructure elements. The following discussions focus on the bridge responses under the following cases, including (a) the support conditions, i.e., simply and fixed supports at the two ends of the bridge; (b) the soil types behind the abutment and surrounding the piles, i.e., loose sand, dense sand, and stiff clay; and (c) the joint connections at the interfacial locations between the pile and bent, i.e., fully rigid and roller supported.

In addition, only the thermal behaviors due to the temperature variations where both the uniform and gradient temperature variations refer to the temperature design criteria in the AASHTO LRFD (2007) have been considered. Specifically, for the uniform temperature variations, based on the material type and bridge location, an increase of 44.4°C (80°F) was assumed and applied to the concrete slab. For the thermal gradients, considering the bridge location at Zone 2 (one of the four solar radiation zones where the positive and negative temperature distribution patterns being accordingly stipulated), and also the material type, superstructure depth, and wearing surface, the temperatures at top and bottom surfaces of the concrete slab are assigned as 46°F and 0°F, respectively; and a linear gradient distribution is

assumed through the slab depth. Therefore, by varying all these parameters (see Table 16) the performances of the bridge are discussed in the aspects of the displacement of the abutment and pile, the backfill pressures behind the abutment, and the forces in the slab and piles. For the convenience of discussions, the legend for each parametrical studying case is uniformly defined here by its loading conditions and the varying parameters; i.e., U and G refer to the uniform and gradient temperature loadings, respectively. For example, the legend of the G_Fixed Support means the case of the bridge being subject to gradient temperatures and rigidly supported.

Table 16
Parametric study cases

Cases	Effects	Temperatures	Backfills	Soils	Connections	Supports
Case1	Support	U_ 80°F G_ 46°F	Loose Sand	Soft clay	Rigid	Free Fixed
Case2	Backfill	U_ 80°F G_ 46°F	Loose Sand Dense Sand	Soft clay	Rigid	Free
Case3	Soil	U_ 80°F G_ 46°F	Loose Sand	Soft clay Dense Sand	Rigid	Free
Case4	Connection	U_ 80°F G_ 46°F	Loose Sand	Soft clay	Rigid Roller	Free

Effects of Support Conditions. The bridge responses under different support conditions are shown in Figure 125 (a) to (d). Generally, in numerical modeling or routine designs, the support conditions are mostly idealized as either fully free or rigidly fixed, while these extreme assumptions hardly happen in reality. There must be certain possibilities that

either the free deformations are blocked to some degree, or the current manufacture or construction technic cannot developed a perfectly rigid connection. For IABs, the effects of supports on the behaviors of the bridges are supposed to be more obvious than that on traditional jointed ones.

In all parts of this figure, it is reasonable to observe that the case with a free support and uniform temperature variation provides the most significant effects on the bridge performance. For example, it causes comparatively larger displacements, and that, in turn, induce the correspondingly higher backfill pressures on the abutment and greater positive and negative bending moments along the pile depth. For the effects of the support conditions on the slabs, however, they are much more complicated. For example, under the uniform temperature increase condition, the significantly higher compressive strains are generated when the bridge movements are fixed; while under the gradient distribution condition, the maximum positive strains are appearing at the slab surfaces under the free supports condition and that may induce the crack failures of the concrete. In addition, the slab strains distribution along the bridge length show no differences at the locations between the bridge ends and middle parts. This scenario may indicate that the backfills behind Bent1 show negligible effects on the bridge responses compared to the effects from other structural or geotechnical elements, such as the soils surrounding the piles, pile rigidities, or the connections between the piles and bents. Therefore, based on these observations, it is not advisable to allow a large movement at the superstructure for the sake of the substructure safety; however, restraining the thermal movements may also not be beneficial for the behaviors of the superstructure.

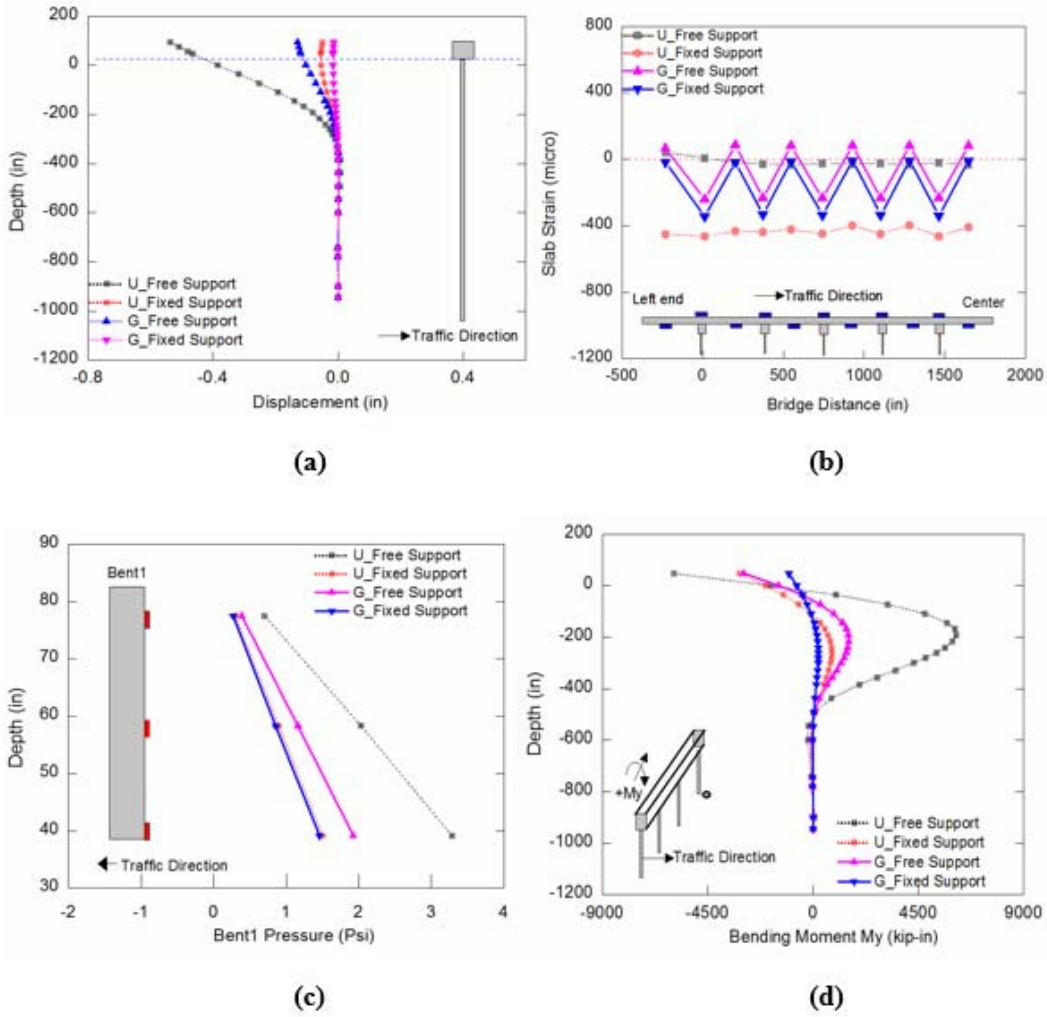

Figure 125
Bridge responses under cases with different support condition

Effects of Backfill behind Abutments. The bridge responses under different backfill material types are show in Figure 126 (a) and (b), where only the behaviors of displacements and backfill pressures are plotted since the variation of the responses at the slabs and piles are negligible. As is shown in these figures, there are almost no discrepancies in terms of the displacements under the different dense and loose sand backfills. This phenomenon again verifies one of the previous arguments; that, for the current structure configurations, the bridge rigidities are largely contributed by the big cross-section PPC piles and rigid pile-bent connections, whereas the shallower depth of the backfill nearly provides no resistances. However, if comparing the performances between the simulated backfill pressures on Bent 1 due to the superstructure movements, the case with the dense sand already reaches its passive critical conditions with the pressures from the top to the bottom as 4 psi, 12 psi, and 20 psi,

respectively; while the pressures through the depth of the loose sand case, with 0.78 psi, 2.3 psi, and 3.7 psi, respectively, are still within its passive critical values of 1.7 psi, 5.2 psi, and 8.6 psi, respectively.

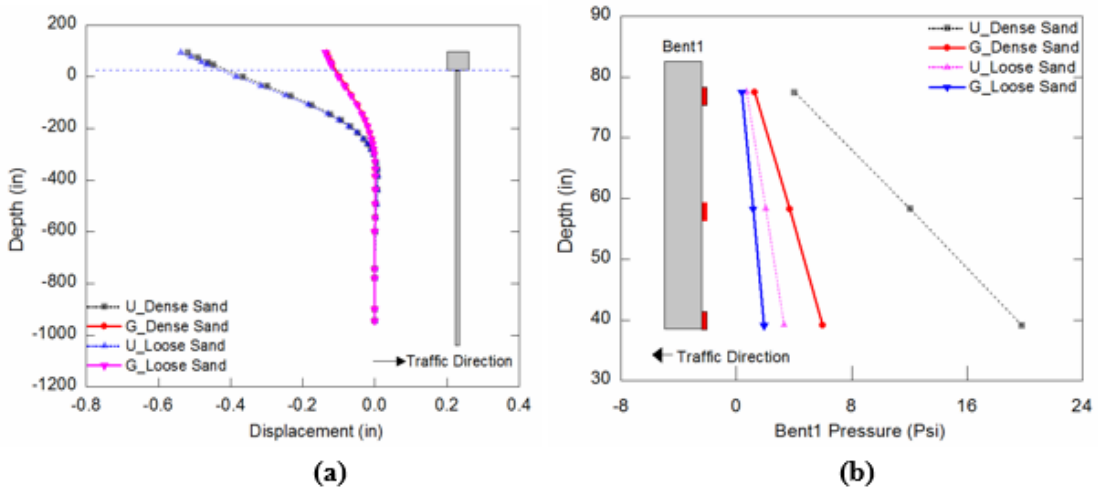

Figure 126
Bridge responses under cases with different backfills behind Bent 1

Effects of Soil Surrounding Piles. Figure 127 (a) to (d) show the bridge responses under conditions with different soil types surrounding the piles. Firstly, apparently different behaviors are generated on the substructure. For example, under the soft clay case, the induced displacement at the slab top surface is almost 1.5 times larger than that under the dense sand condition. In addition, similar to the previous discussions of the support effects, the weak restrains from the soft soils surrounding the piles will also allow a larger pile deformation and that will still induce greater soil pressures behind the abutments and higher bending forces in the piles. Secondly, for the soil effects on the superstructure, the induced strains in the slabs will increase about 48%, if changing the soft clay to the dense sand under the uniform temperature variations. Under gradient temperature distributions, however, it does not show much difference between both soil types. Therefore, the gradient temperature loading is observed to be the critical case which provides much higher positive and negative strains in the slabs than that from the uniform temperature variations.

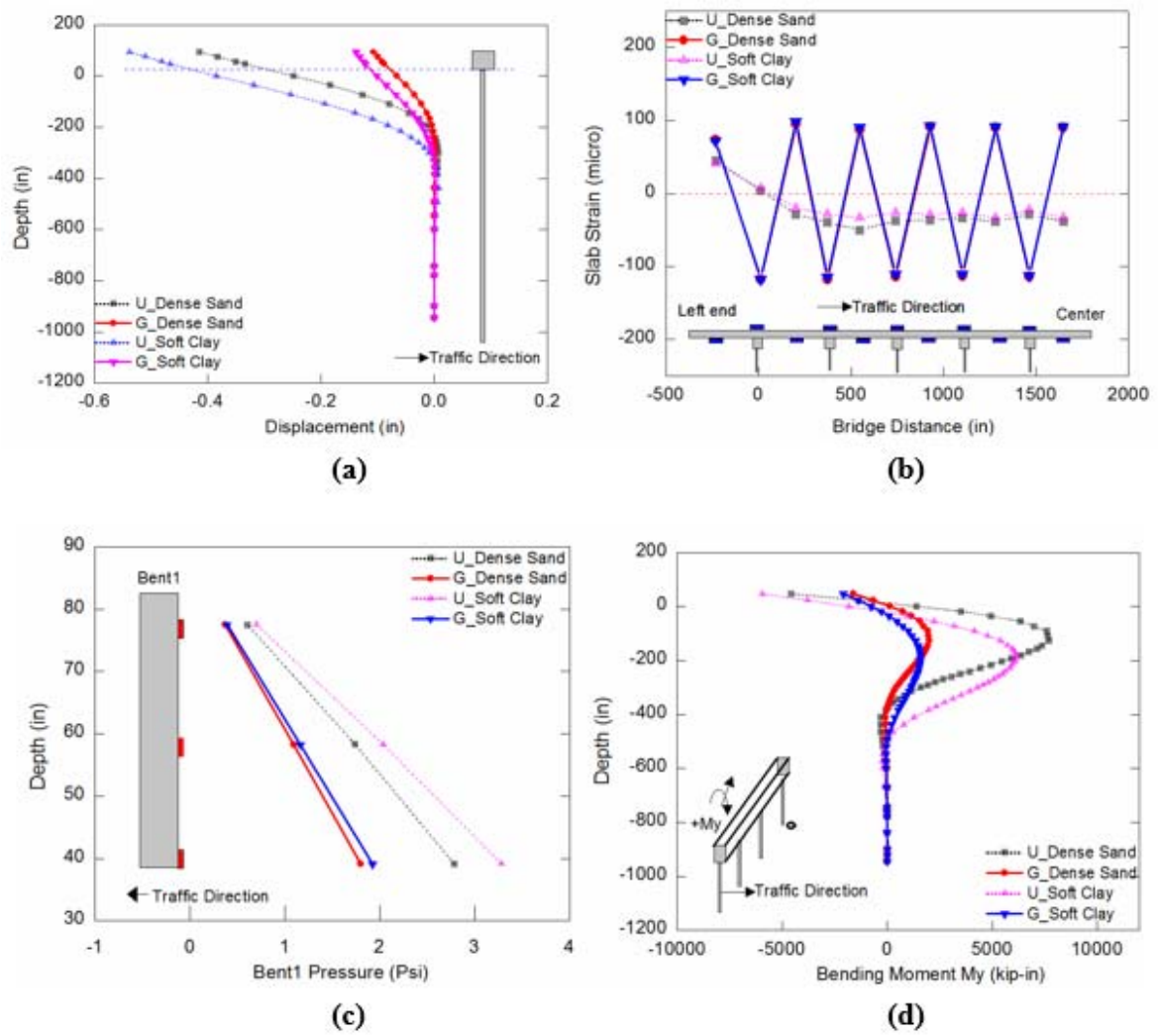

Figure 127
Bridge responses under cases with different soils surrounding the piles

Effects of Slab-Bent Connections. Figure 128 (a) to (d) shows the performances of the bridges with different slab-bent connections. As can be observed, the significant differences, when changing the roller connections to rigid ones, are lying on the induced forces on the piles. Specifically, the rigid connections will induce larger forces at the slab-bent interfacial location; while the forces will be zero for roller cases at the connecting locations, and the maximum values appear approximately at the one-third parts below the pile head. In addition, different abutment rotation behaviors, even though not apparent, are shown in the detailed plots of Figure 128 (a). The rigid connection provides continuous but larger rotations compared to the discontinuous and smaller ones under the roller connections. These differences, to a small degree in the current bridge, will cause relatively larger backfill pressures at the roller connections than at the rigid ones. Finally, the soil effects on the

superstructure, however, are not substantial. Even though the strains under the roller case can be about 40% smaller than that under the rigid connection for uniform temperatures variations, yet the dominant or critical temperature loadings are still from the gradient temperature which shows only 5% differences between the two soil types.

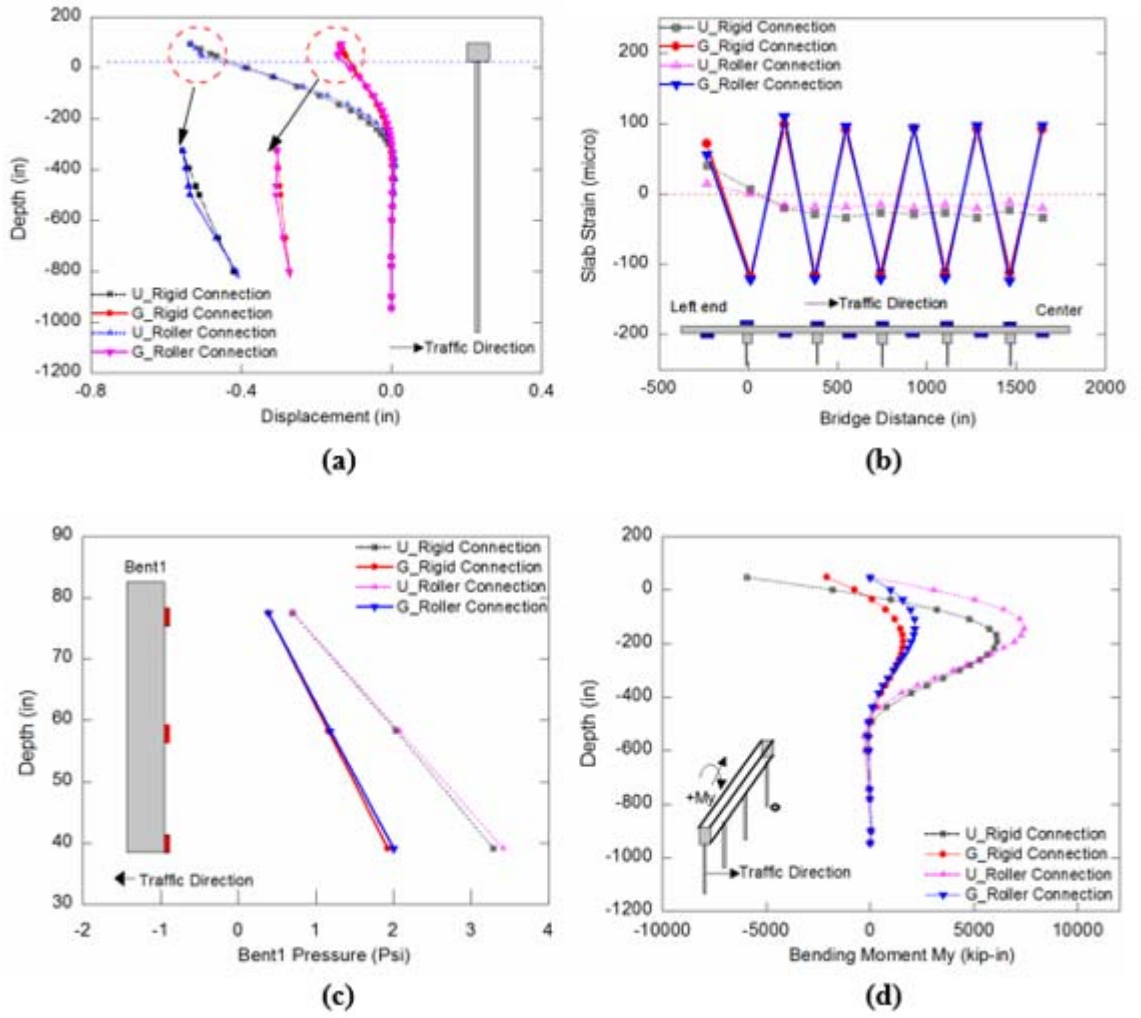

Figure 128
Bridge responses under cases with different connections between slabs and bents

Conclusions

Based on the available information of the bridge, together with the monitoring results over one year, a 3D numerical model is firstly proposed and validated in the study, where the pile-soil and abutment-backfill interaction behaviors are considered. Then, the concerning parameters are varied through a parametric study to further investigate their effects on the bridge thermal performances under the other complicated structural and geotechnical conditions. Some of the conclusions are drawn as follows:

The support conditions in reality may not be completely the same as they were designed for, but they are crucial for integral abutment bridges without expansion joints. For IABs, it is not advisable to allow the fully free support conditions at the superstructure, since the induced movements will cause larger backfill pressures and pile internal forces; whereas, it is also not a good idea to adopt fully fixed supports since they will generate larger internal forces on the superstructure. In this sense, this dilemma may be one of the reasons that restrict the designs of integral constructions on longer span bridges, since the corresponding larger thermal movements, together with other greater thermal effects, have to be appropriately accommodated.

For this specific IAB, the effects from the backfills are negligible. The height of the abutments are shallower compared with the deeper piles with their bigger cross sections. In this sense, the bridge deformations are majorly controlled by the pile rigidities, soil resistances surrounding the piles, and connection behaviors between the pile-bent. For some other general IABs, however, the stiff soils may induce higher internal forces at the superstructure; while the soft soils will provide greater forces at the substructure.

The soils surrounding the piles show the most obvious effects on the bridge responses. Under the current bridge configuration, if changing the soft soils to the stiff ones, it will generate a maximum of 1.5 times smaller bridge displacements and 20% smaller backfill pressures; but at the same time, it will also induce 70% larger pile positive strains and 48% larger slab negative strains. Thus, it seems difficult to design an optimized structure that can benefit both the superstructure and substructure simultaneously.

The connection behaviors between the pile-bent affect the bridge responses in two aspects. On one hand, they switch the locations of the maximum pile internal forces from the interfaces between the pile-bent, i.e., the rigid connection case, to the top third parts below the pile heads, i.e., the roller connection case. On the other hand, they also affect the rotation behaviors of the abutment, and that in turn will slightly affect the backfill pressures and slab strains, even though these changes are not significant due to the small sizes of the abutment in the current bridge.

In summary, for IABs, the thermal movements have to be accommodated by either or both the superstructure and substructure. If the superstructure is allowed to move comparatively free, then the substructure will experience large deformations and internal forces; while if the superstructure is not allowed a larger movement, by adopting fixed boundaries, more stiffer backfills, or other approaches, then the greater internal forces may be induced on the superstructure and that will be beneficial for the substructure. These dilemmas become more

complicated when considering the combinations of different loading conditions, such as the temperature uniform variations, gradient distributions, dead loads, and live loads. In this sense, some of the settling methods for this argument may lie in the attempts of adopting new material types with different physical and mechanical properties.

Field Monitoring Study of Integral Abutment Bridge for Louisiana's Soft and Stiff Soils

Caminada Bay Bridge

The Caminada Bay Bridge, as shown in Figure 129, is located in Grand Isle, LA (29°15'48" N 89°57'24" W), about 100 miles (160 km) to the south of New Orleans, LA. The old jointed bridge was demolished, and a new full IAB was built next to it. The total length of the bridge is 3945 ft. (1202 m), while the monitoring program is conducted on the first 11 spans, as shown in Figure 130, including a 10 ft. (3 m) sleeper slab, a 40 ft. (12 m) approach slab, a 300 ft. (91 m) continuous concrete slab, and the substructure underneath, i.e., abutment, pile, and soil. The width of the bridge is 50.58 ft. including the rails. It consists of two 21 ft. lanes and a 7 ft. sidewalk on the north side. The slabs of the bridge are fully integrated with Bent 1 at the left end, simply supported on Bent 11 at the right end, and rigidly connected with all the other interior bents in between, where each bent is further rigidly supported on a single row of four prestressed precast concrete (PPC) piles. The soil conditions, referred to the boring log information near Bent 1, can be approximately subdivided into two layers, including a medium sandy soil layer under the water level from the ground to the depth of 62 ft. (18.9 m) followed by a medium clay layer through the rest of the piles.

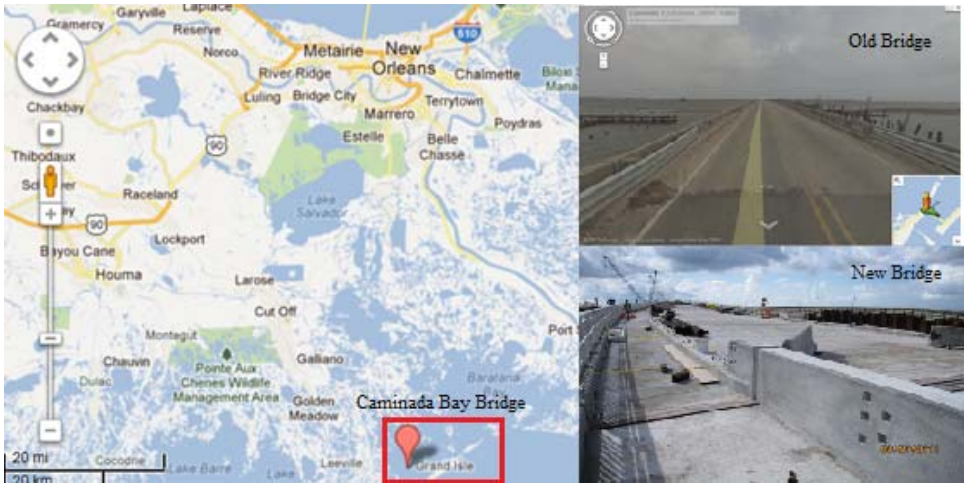

Figure 129
Caminada Bay integral abutment bridge in Louisiana

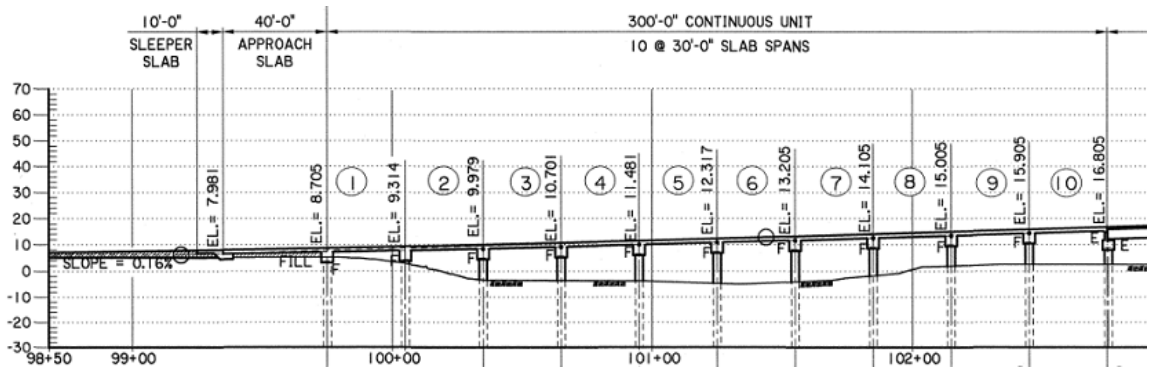

Figure 130
Elevation view of the first 11 spans of Caminada Bay IAB

Data Post-Processing

The data acquisition started from 08/11/11and continued over one year, in which the raw data recorded every 3 minutes 20 seconds. In addition, the raw data have been manipulated by the LoggerNet program and the corresponding average, maximum, and minimum results within each hour were provided. Two post-processing steps were conducted on the raw data before further data analysis. First, the outlier data had to be picked out and removed. Otherwise, they may have affected the results in the subsequent calculations, especially at the conditions when one or several data within one hour was extremely large or small. Secondly, complying with the requirements of the sensor suppliers, a proper temperature correction process should be performed for certain sensor types. That is due to the differences of the thermal expansion coefficients between the steel wire in the sensor gages and that of the measured elements, e.g., the strain gages in concrete slabs and PPC piles.

For the readings from all the 81 instrumentations over one year's monitoring, most of the outliers from the raw data were obvious and appeared within certain time intervals that could be easily filtered and removed by using the Excel tools or by hand; while several others occurred randomly and dispersedly that the aforementioned method was no longer convenient. Hence, a program using the statistical theory was coded in MATLAB (2010) for the data post-processing. Generally, many algorithms have been proposed for the data outlier removal in the statistic field, such as the Standard Deviation Method, Z-score, Modified Z-score, Tukey's, Adjusted Boxplot, MAD, Median Rule, etc. Each method has its own advantages and restrictions, and most of the methods are based on one assumption that the sample data is normally distributed. As shown in Figure 131, about 68%, 95%, and 99.7% of the data will fall within 1, 2, and 3 times the standard deviation from the mean if the data follows a normal distribution. In this sense, if any data existed with a distance, e.g., 2 or 3 times of the standard deviation away from the mean, it can be considered an outlier.

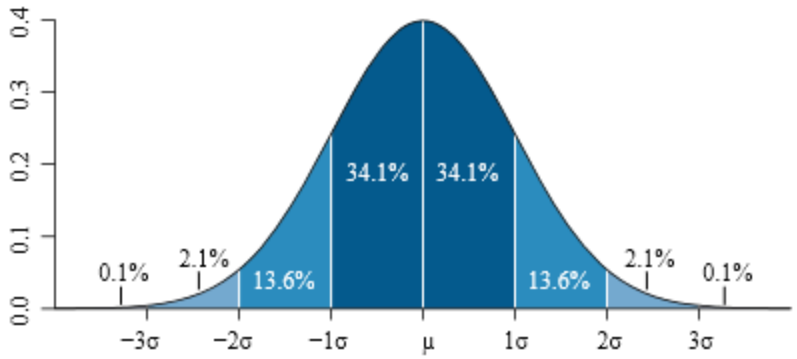

Figure 131
Normal distribution curve

The data from a representative strain gage, i.e., located in the concrete slab of Span 5, is taken out as an example to illustrate the outlier removal algorithm. Four sets of the sample data within one hour, i.e., 08/11 17:00, 09/11 24:00, 10/11 03:00, and 11/11 09:00, are randomly selected from the raw readings, and the normality test is conducted on these data. Figures 132 and Figure 133 show the representative normality test plots of the strain and temperature readings on 08/11 17:00, respectively. All the other calculated results are listed in Table 17, where the conclusion that the distribution is non-normal can be drawn if the P-value is smaller than 0.01 or the A-squared value is larger than the critical values, i.e., 0.787 and 1.072 for 95% and 99%, respectively. Based on the calculations, for most of the strain data within an hour period, they can be considered as normally distributed; while for the temperature results, the data cannot always be considered as normally distributed. For example, the data in the case of 08/11, 17:00 is more uniformly distributed within an hour. Also, for those of other sensors embedded in the soil, e.g., strain gages embedded in the piles under the ground, the temperatures at those locations are almost constant throughout years. Therefore, through a comprehensive comparison between the different outlier methods, together with the consideration of the distribution patterns of the current readings, the SD and Tukey's method are adopted and coded in MATLAB (2010), and the following discussions will be based on the data after the outlier removals and temperature corrections.

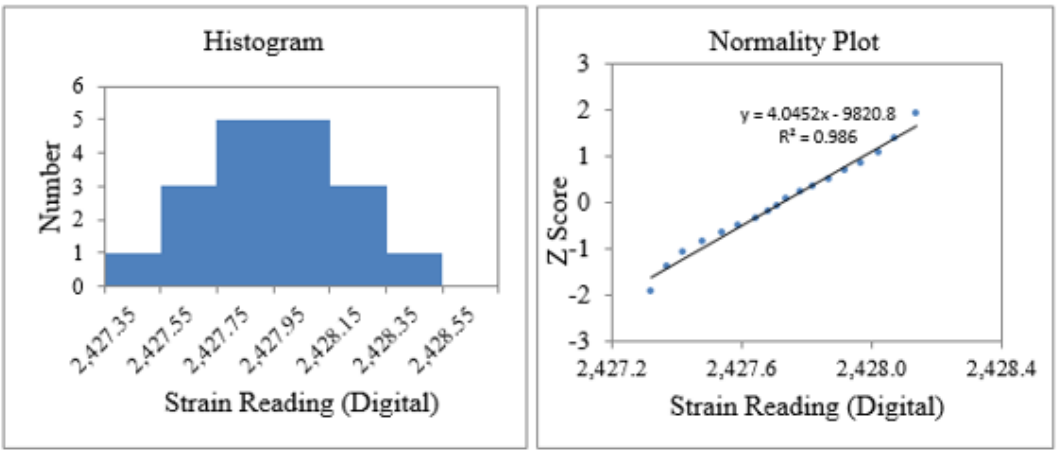

Figure 132
Normality test for the strain data measured at Span 5 on 08/11 17:00

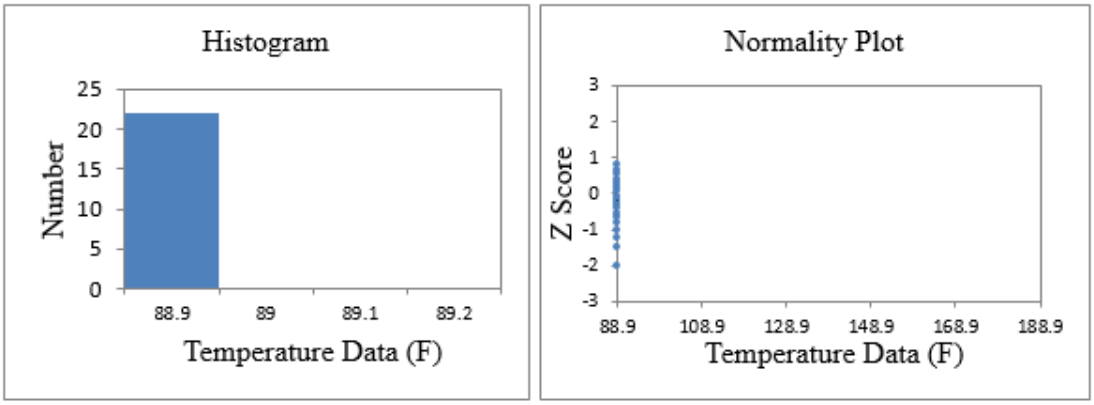

Figure 133
Normality test for the temperature data measured at Span 5 on 08/11 17:00

Table 17
Normality test for the strain and temperature readings of the strain gage at Slab 5

Date	Strain Reading		Temperature Reading	
	A-squared	P value	A-squared	P value
08/11/11 17:00	0.122	0.984	17.627	0
09/11/11 24:00	0.231	0.77	0.714	0.051
10/11/11 03:00	0.213	0.827	0.346	0.442
11/11/11 09:00	0.437	0.264	0.638	0.081

Field Monitoring Results

During the monitoring period from 08/11/11 to 08/11/12, the construction of the bridge had not been completed yet, and no traffic went on the bridge. Thus, the following discussions are mainly about the bridge performance due to the temperature changes. The initial reference condition, or the baseline, for all the instrumentations were set up on 08/11/11, the first day the data is available.

Environmental Conditions. Even though no instrumentation was specifically installed to measure the environmental conditions, e.g., the ambient temperatures and wind speeds, this information is still of great importance to understand the thermal behaviors of IABs. On one hand, the major uncertainties of IABs are largely caused by the temperature changes within the bridges, and those variations in turn are literally determined by the environmental conditions. On the other hand, the current AASHTO LRFD (2007) design temperatures for the traditional jointed bridges, either the uniform or the gradient ones, are all specified based on the local environment conditions at the bridge sites; however, the adaptabilities of these specifications on IABs deserve further investigations and justifications. In this sense, the environmental temperatures and wind speeds, recorded at the bridge site from a nearest weather station located at Grand Isle, LA (http://tidesandcurrents.noaa.gov), are firstly discussed.

Figure 134 shows the measured hourly-varying air temperatures (missing some data due to system being down) and wind speeds at the weather station and Figure 135 shows the detailed daily and monthly average temperatures calculated from the hourly-varying ones. From these two plots, the periodical and cycling trends can be clearly observed, such as the sinusoidal patterns approximately shown from the hourly-varying temperatures. In this sense, the temperatures of the bridge may no longer be uneconomically measured by the thermistors, but rather be more conveniently predicted based on the local environmental conditions. For example, they can be predicted either by fitting a sinusoidal function between the bridge and air temperatures, or by the numerical simulations taking the environments as boundary conditions. In addition, the minimum and maximum ambient temperatures during the monitoring period, as marked in Figure 134, are approximately 4.4℃ (40°F) to 30.0℃ (86°F), respectively, with a difference of 25.6℃ (46°F). Finally, this bridge should be located in the moderate climate region since the number of the freezing days per year is less than 14. Then, the corresponding temperature specifications for the moderate climate region, referred to the AASHTO LRFD (2007) specification, are compared with the field measurements in the following discussions.

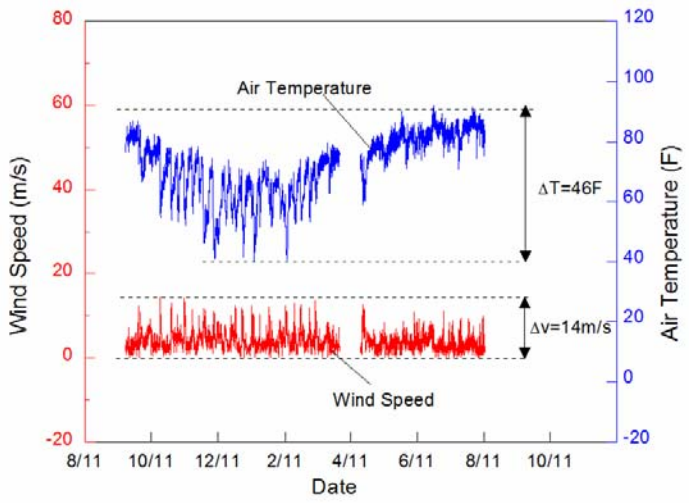

Figure 134
Measured environmental conditions at the weather station

The variations of the wind speeds are also shown in Figure 134. It can be observed that the wind speeds and air temperatures generally do not show high correlating relationships, with a correlation factor of -0.3 in this case. The occurrences of the peak wind speeds, however, are almost in coincidence with the conditions when the temperatures are at sudden drops. In addition, the measured speed values are generally wandering around 16.5 ft/s (5 m/s), with some days larger than 33 ft/s (10 m/s) but smaller than 46 ft/s (14 m/s). According to Elbadry and Ghali (1983), the wind speeds will partly determine the convection coefficients, and those coefficients in turn will affect the heat transfer mechanism at the surfaces of the bridge slabs. For example, in the commercial program FEMMASSE (2000), which is capable of predicting the bridge temperatures, 16.5 ft/s (5 m/s) is a threshold for the calculation of the convection coefficients, and the corresponding values at 33 ft/s (10 m/s) is 2 times larger than that at 16.5 ft/s (5 m/s) (Schlangen 2000). In this sense, under the current air temperatures and wind speeds, the thermal responses at the top surfaces of the slabs should be expected with high variations, which will be proven later

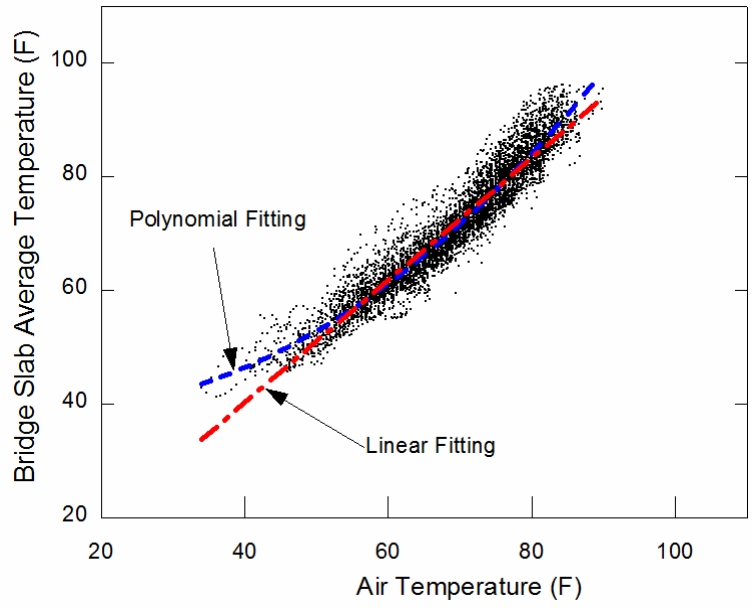

Figure 135
Best fitting of the air temperatures and the bridge slab average temperatures

Slab Strains. For reinforced concrete slabs, the strains in the steel rebar and the surrounding concrete should be the same prior to the cracking of the concrete or yielding of the steel. Generally, since the concrete is weak in tension, about 10% of its limited compressive strength, it may crack at the early stage of loadings; when in compression, however, the concrete can sustain up to 300 microstrains before failure.

Figure 136 shows one representative readings of a strain gage at Bent 5's top rebar locations. The highly-varying strain variations can be observed, and the long term seasonal trends show a negative correlation with the temperature changes. In addition, the calculated thermal stresses during the temperature decrease of 64°F (18°C), if using the maximum 100 microstrain, would be about 360 psi (2.48 MPa). This value is about 9% of the concrete compressive strength. In this sense, the top surface of the bent has a high possibility of cracking due to the temperature variations alone. Similarly, another reading of the representative gage embedded in the bottom parts of the Span 5 slab is shown in Figure 137. The induced compressive thermal stress, if using 40 microstrains, is only about 2% of the compression strength.

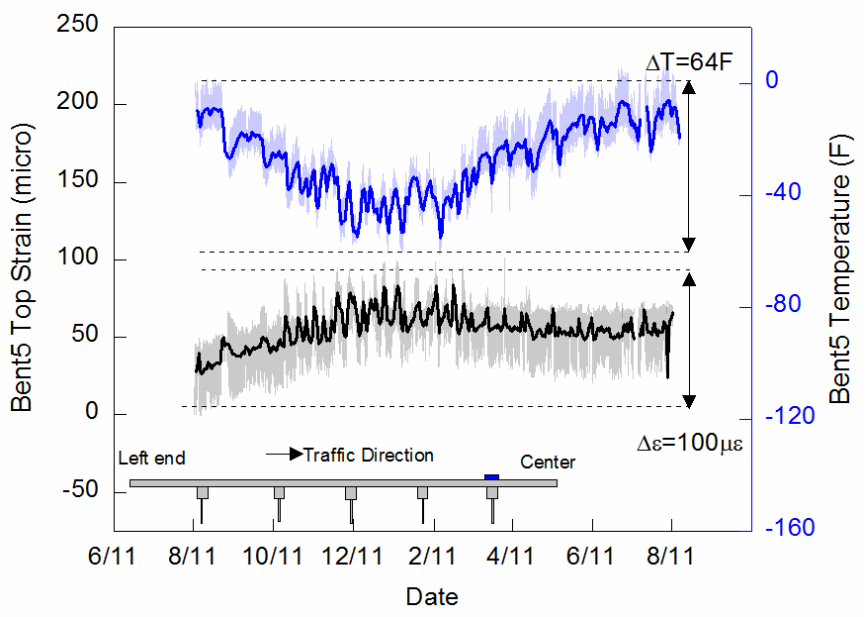

Figure 136
Measured strains and temperatures at the top surface of Bent 5

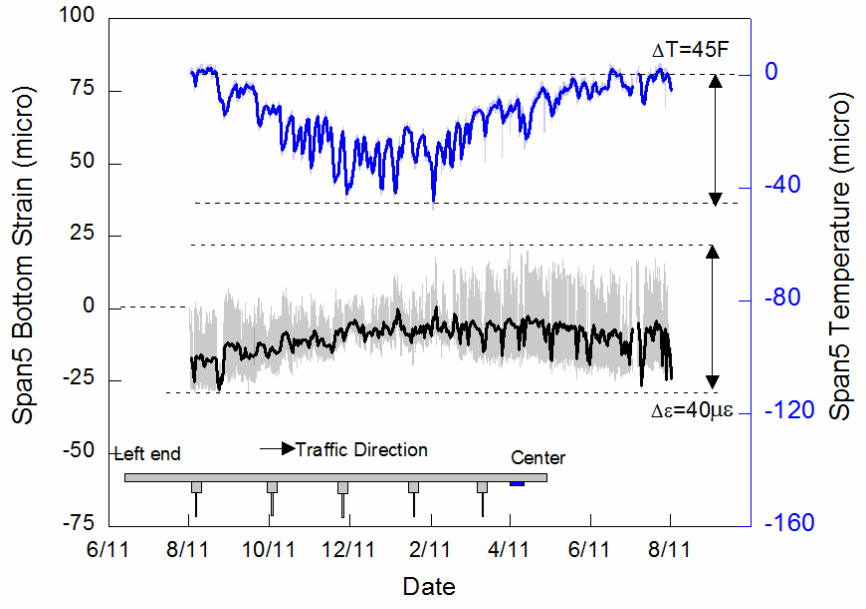

Figure 137
Measured strains and temperatures at the bottom surface of Span 5

Figure 138 shows the comparisons between the strains measured at the top surface of Bent 2 and bottom surfaces of Span 1. A strong negative correlation of behavior is observable between them, which can be attributed to the slab continuity over the bents due to the rigid connections of slab-bent. In addition, Figure 139 shows the strains distributions along the longitudinal direction of the slabs at two representative days, due to the temperature changes

with respect to 08/11/11, i.e., about 9°F (5°C) decrease on 08/14/11and 49°F (27°C) decrease on 01/13/12. It can be observed that no significant strain differences appear at the locations between the bridge ends and middle spans, even though relatively larger strains should have been expected at the bridge ends due to the backfill restraints. This scenario may partly be attributed to one of the following possibilities: (a) the slab strains in this bridge are mostly induced by the temperature gradients rather than the seasonal variations; (b) the restraints from the soft soils at the bridge ends are not significantly strong; or (c) the rigid connecting behaviors between bents and slabs provide more evident structure rigidities than that from the backfills.

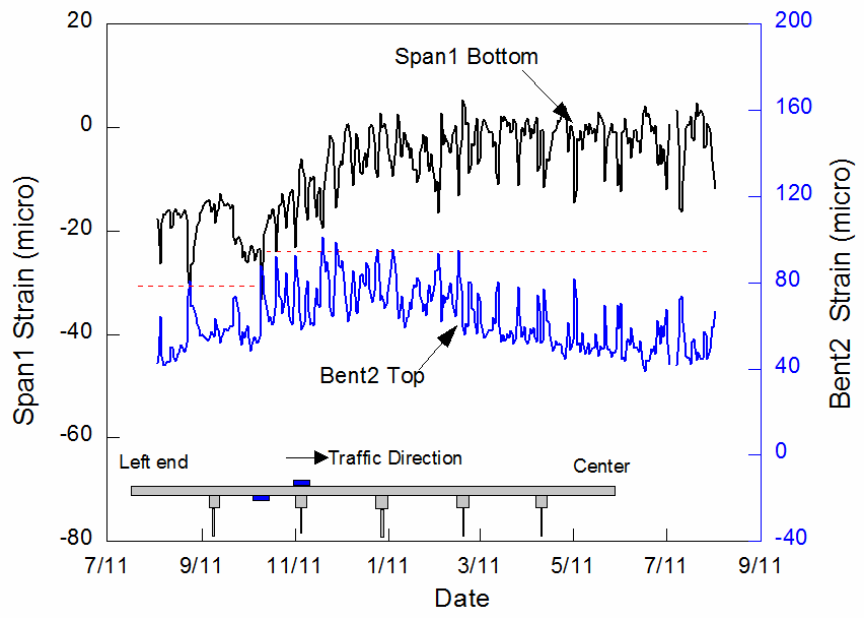

Figure 138
Measured strains at the bottom surface of Span 1 and top surface of Bent 2

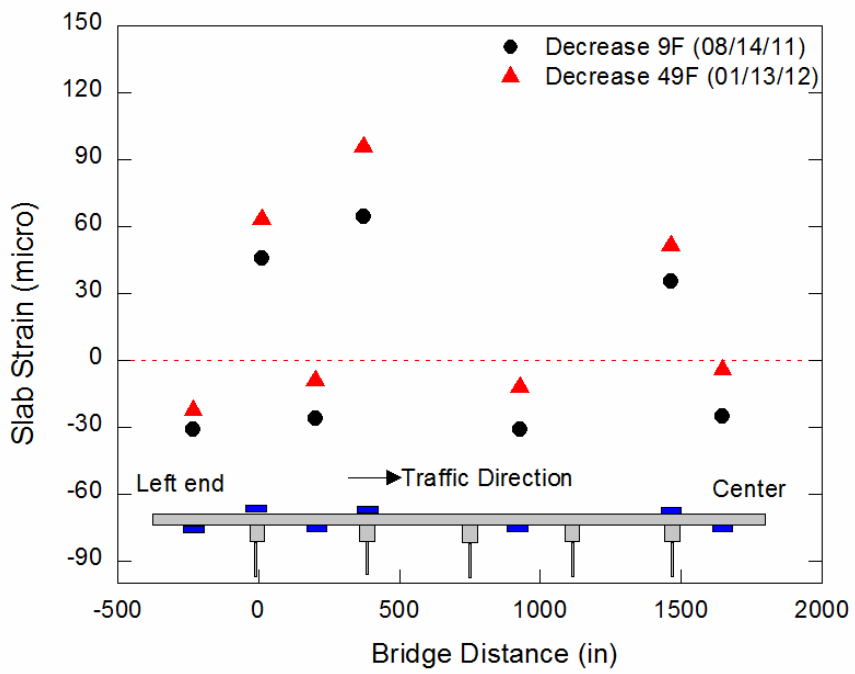

Figure 139
Measured slab strain distributions w.r.t. the temperature variations

Behavior of Piles and Bent-Soil Interaction

The strain meters (Figure 14) measure the displacement of the bent as the bridge expands and contracts. Detailed recordings of the strainmeters are shown in Appendix A. Figure 140 shows a summary of measurements of the strainmeters along with the air temperature. DC49 and DC59 were buried in the soil and were not attached to the bent face, whereas DC52 and DC60 flanges were bolted to the bent face. Overall, a very small displacement (less than ± 0.15 in.) is recorded between August 2011 and September 2012. A zoom-in of the measurements for a few days in January (cold days) and July of 2012 (hot days) are shown in Figures 141 and 142 which clearly show there is negligible movement in DC49 and DC59 and small variation in DC52 and DC60 strainmeters as the temperature changes.

The soil pressure measurements were also recorded using the nine pressure cells that were mounted on the face of the bent (Figure 12). Detailed recordings of the individual pressure cells are shown in Appendix A. Figure 143 shows a summary of the soil pressure measurements. A zoom in of the measurements for a few days in January (cold days) and July of 2012 (hot days) are shown in Figures 144 and 145, respectively. One can notice that the bridge will shrink in cold weather which causes the soil pressure to drop to zero or a small negative value and will expand in hot weather which results in a maximum of 3 psi passive pressure on soil.

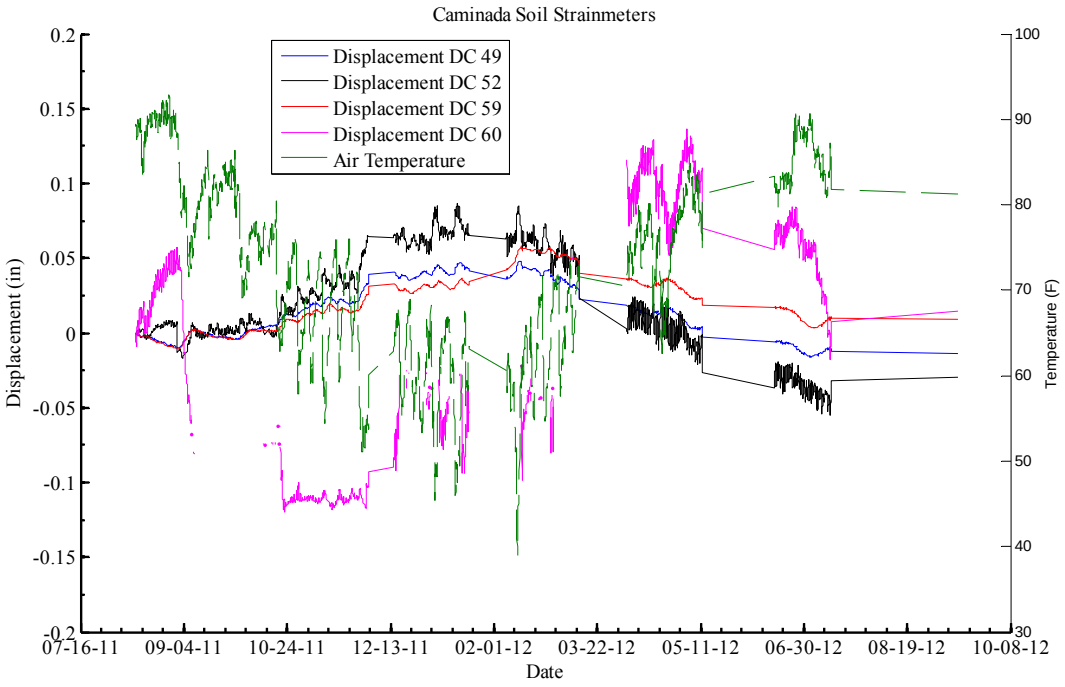

Figure 140
Displacements of Caminada soil strainmeters for entire data set

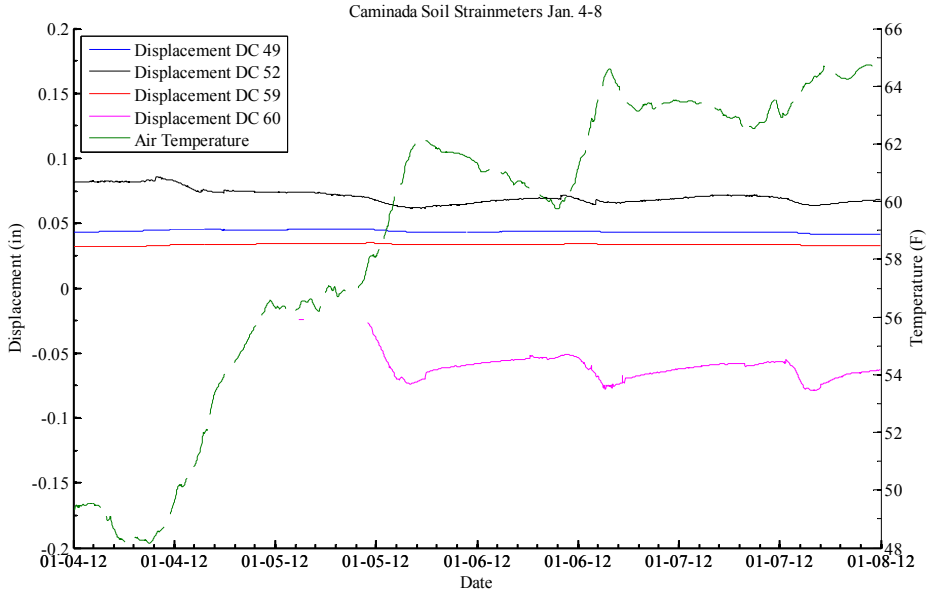

Figure 141
Displacements from Caminada soil strainmeters for 01/04/12 - 01/07/12

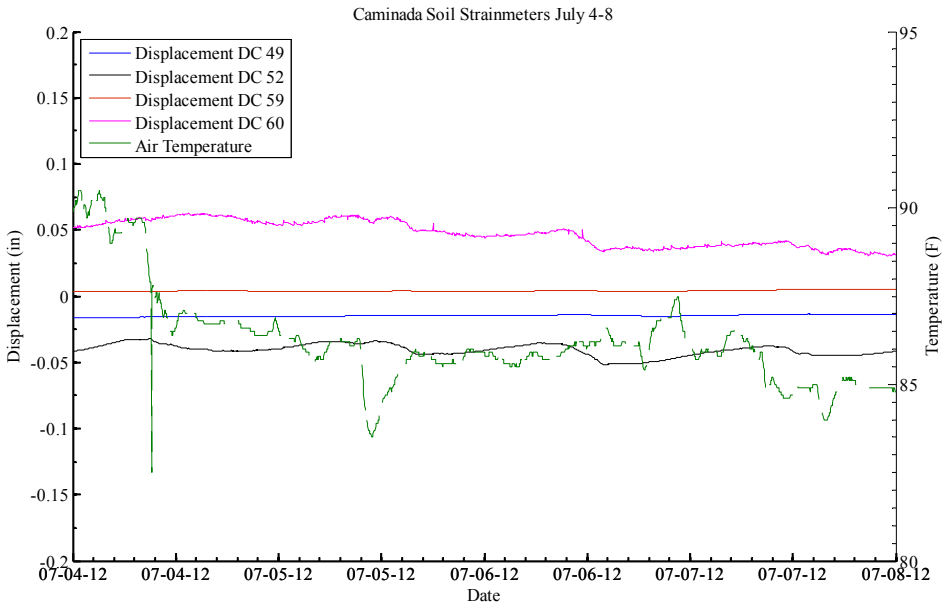

Figure 142
Displacements from Caminada soil strain meters for 07/04/12 - 08/08/12

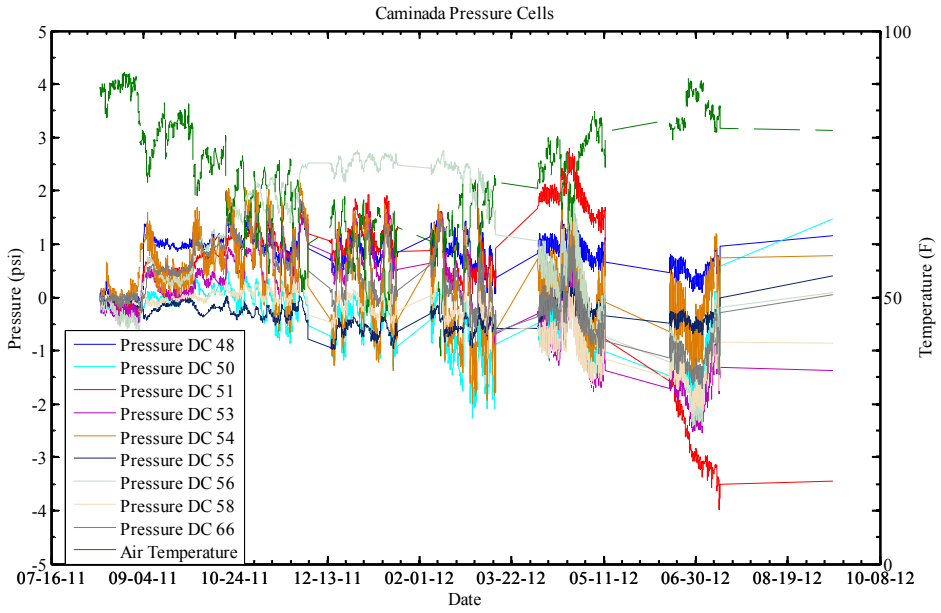

Figure 143
Pressures from all Caminada pressure cells for entire data set

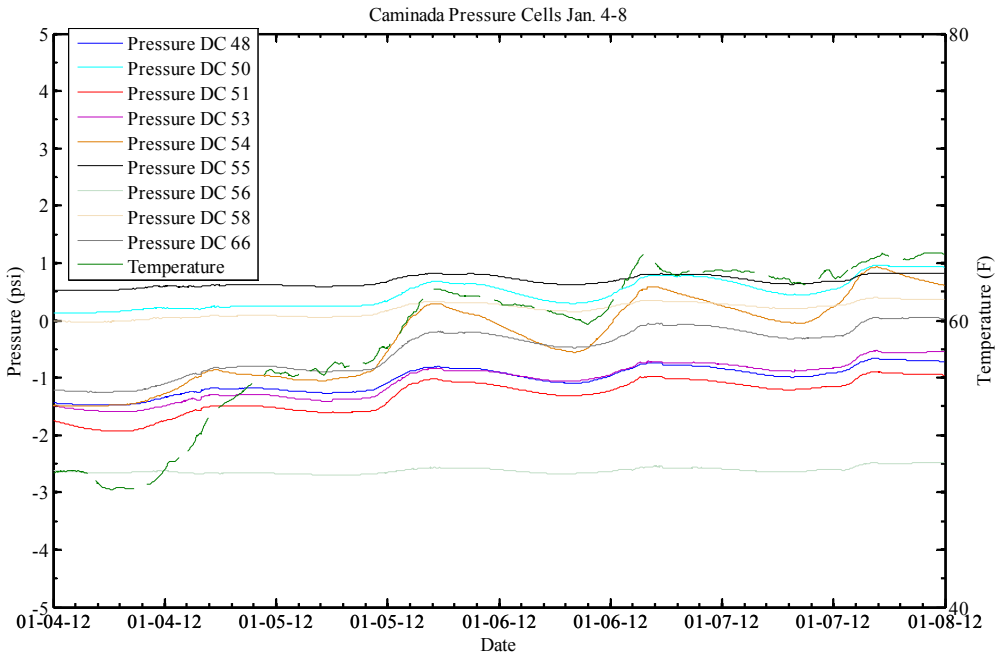

Figure 144
Pressures from all Caminada pressure cells for 01/04/12 – 01/08/12

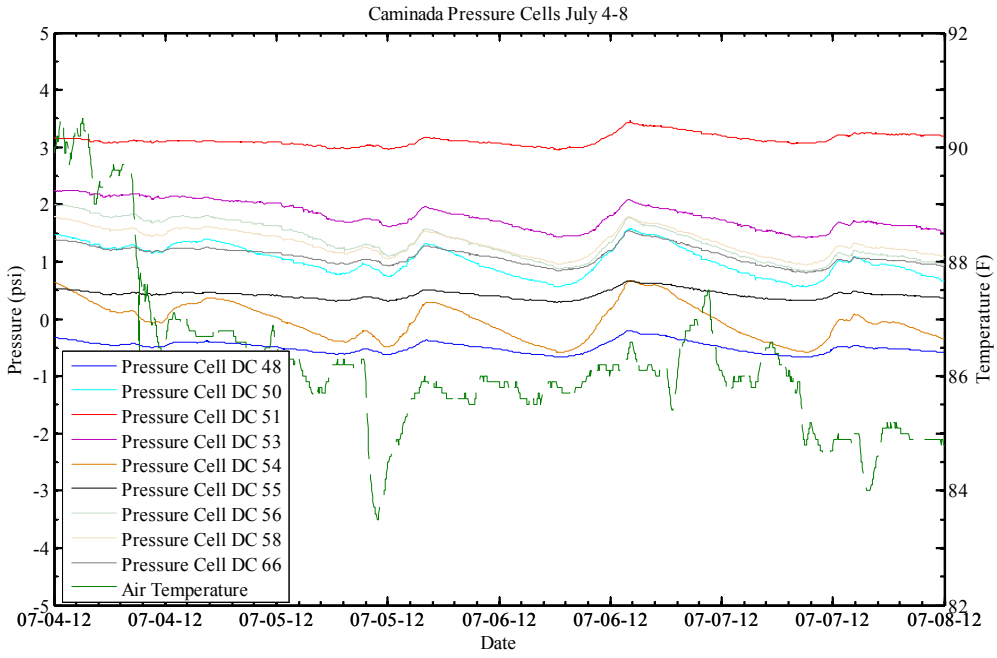

Figure 145
Pressures from all Caminada pressure cells for 07/04/12 – 07/08/12

To calculate bending moments in the piles, the micro-strains for each of the sisterbars were normalized based on the reading collected at the time of installation and were corrected for temperature effects. The transverse, x, and y strains were calculated based on Figure 146 and equations 19-21. The following are the strains that were used to calculate the moments in the respective direction.

$$\varepsilon_t = (\varepsilon_1 - \varepsilon_2 + \varepsilon_3 - \varepsilon_4)/4 \tag{19}$$

$$\varepsilon_x = (\varepsilon_1 + \varepsilon_2 - \varepsilon_3 - \varepsilon_4)/4 \tag{20}$$

$$\varepsilon_y = (-\varepsilon_1 + \varepsilon_2 + \varepsilon_3 - \varepsilon_4)/4 \tag{21}$$

where, ε_1-ε_4 are the measured strains in the four corners of the pile and ε_t, ε_x, and ε_y are the strains in the transverse, x, and y directions, respectively. The moments were calculated as:

$$M = \frac{E \times I \times \varepsilon}{h} \tag{22}$$

where, M is the directional bending moment, E is the modulus of elasticity, I is the mass moment of inertia, ε is the directional strain, and h is the distance between the sensors. The modulus of elasticity for the piles was computed based on:

$$E = 57{,}000\sqrt{f'_c} \tag{23}$$

where, f'_c is the compressive cylinder strength of the concrete after 28 days. The value of f'_c is given as 6000 psi. The mass moment of inertia was calculated based on the gross area of the pile, including the void that has been filled in with concrete.

The moment in each direction was than calculated for each section of pile based on the strain in the representative direction. Moments were calculated for the interior and exterior pile on October 1, 2011, January 1, 2012, April 6, 2012, and July 7, 2012 using the average strain over the particular day. The cracking moment for the pile was calculated assuming no pre-tension. Since concrete cracks in tension, the modulus of rupture was used to determine when the pile will crack. The modulus of rupture, f_r, is equal to 7.5 times the square root of the concrete compressive strength per ACI code. The cracking moment was calculated based on the following equation:

$$M_{cr} = \frac{f_r \times I}{c} \tag{25}$$

where, M_{cr} is the cracking moment, c is the distance of the tensile fibers to the neutral axis (half the pile width = 18 in.), and I is the mass moment of inertia of pile cross section (139,968 in^4).

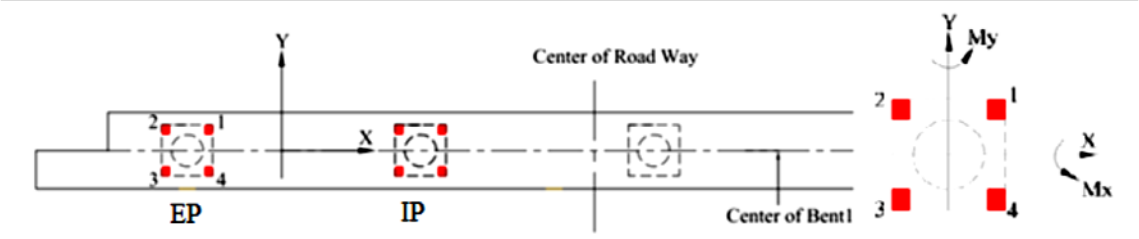

Figure 146
Plan view of pile diagram

The bending moments in the interior and exterior piles are shown in Figure 147 through Figure 150. The effect of thermal stresses is evident from moments in the lateral direction, which change from January, April, July, to October measurements as the moments change from extreme negative values in January to positive values in July as shown in Figure 153 and Figure 154 for both piles. In the direction parallel to traffic, moments show typical trends with value that range from -200 kip-in to 200 kip-in. The concrete cracking of the pile is 4518 kip-in. Clearly, the piles experienced small moments and the design is very conservative.

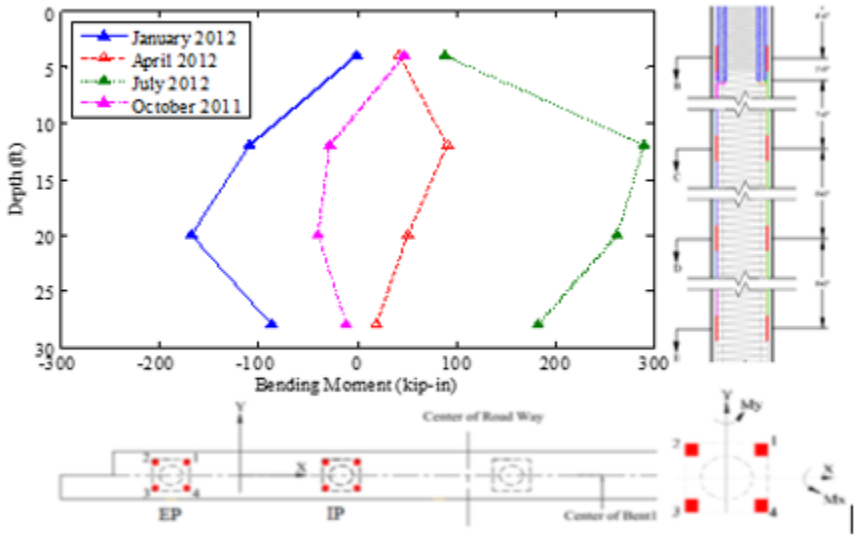

Figure 147
Moment about x-axis, M_x in the interior pile obtained from strain gauge data

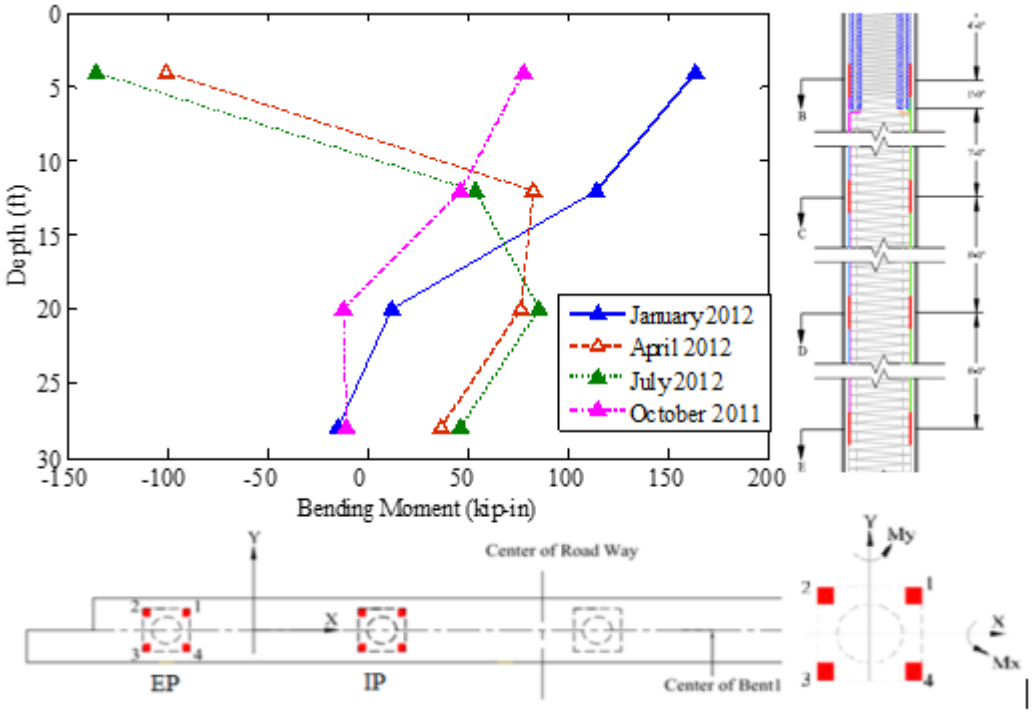

Figure 148
Moment about y-axis, M_y, in interior pile obtained from strain gauge data

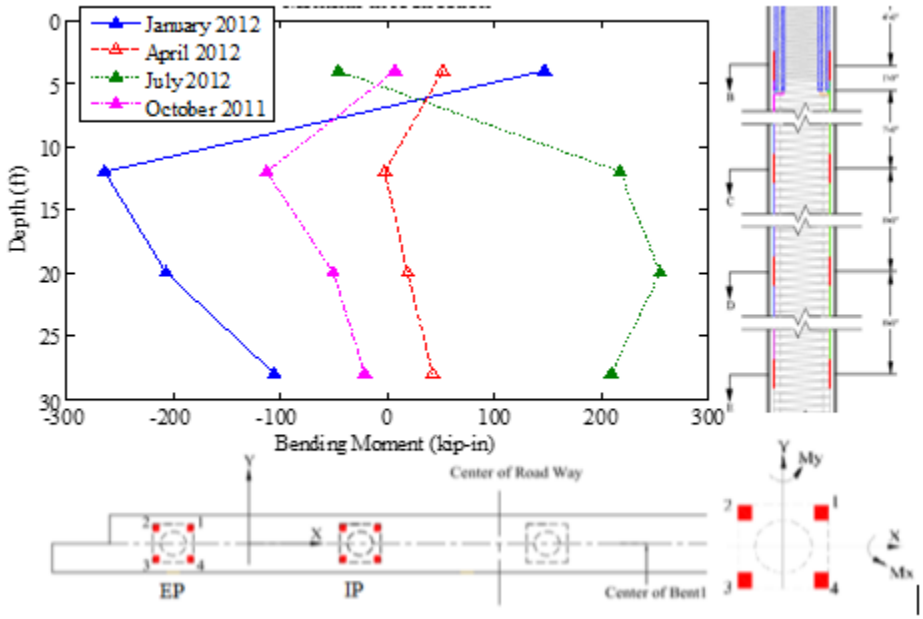

Figure 149
Moment about x-axis, M_x, in the exterior pile obtained from strain gauge data

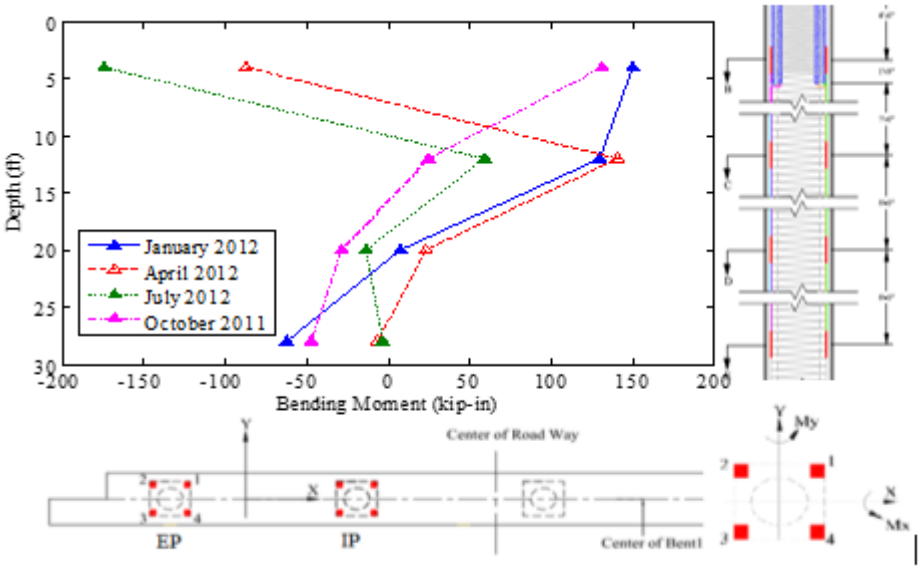

Figure 150
Moment about y-axis, M_y, in exterior pile obtained from strain gauge data

Bodcau Bayou Bridge

Data Post-Processing

The data acquisition system was installed by BDI Company and all pertinent information related to the sensor location and information can be referred to Bodcau Bayou Bridge BDI Structural Monitoring System User's Manual. The important information is illustrated here.

The DataOut table provides the continuous data (vibrating wire measurements and temperatures) for all sensors, which recorded approximately every 3 hours, 45 min. Based on the raw data, the correspondingly hourly-average, hourly-minimum, hourly-maximum, and hourly-delta data were calculated and provided by the LoggerNet program. The following figures describe the hourly-varying responses of superstructure corresponding to the temperature variations.

The data acquisition started from 02/24/12, 16:00. During the monitoring period since then and until now, 11/15/12, the occurrences when the data is missing are listed as follows, and they may be attributed to the mechanical fault of the system.

(1) From 04/05/12, 7:00 to 04/05/12, 12:00 (about 5 hours)

(2) From 05/25/12, 14:00 to 05/25/12, 15:00 (about 1 hour)

Field Monitoring Results

Embedded Sensors in Girders and Decks. All sensors have been have been subject to temperature calibration. Legend is denoted as beam number and sensor location, respectively. For example, I_AT refers to the embedded sensor at Girder A and top surfaces. Figures below show strains measured at the beam top surface, bottom surface, and deck middle sections, respectively (note that beam number is defined as A, B, C, and D in the direction from right to left shown in Figure 27). Sensor location is defined Top (T) and Bottom (B) of girder and middle section of deck (D) shown in Figure 27, as well. The representative results are plotted for measured strains of Beam C at the middle span, as shown in Figure 156.

Based on the observations, all three sensors worked as expected. For sensors at the top and bottom locations, they reasonably vary with temperature variations. The strain variations during the monitoring period are approximately -100 to +100 microstrain.

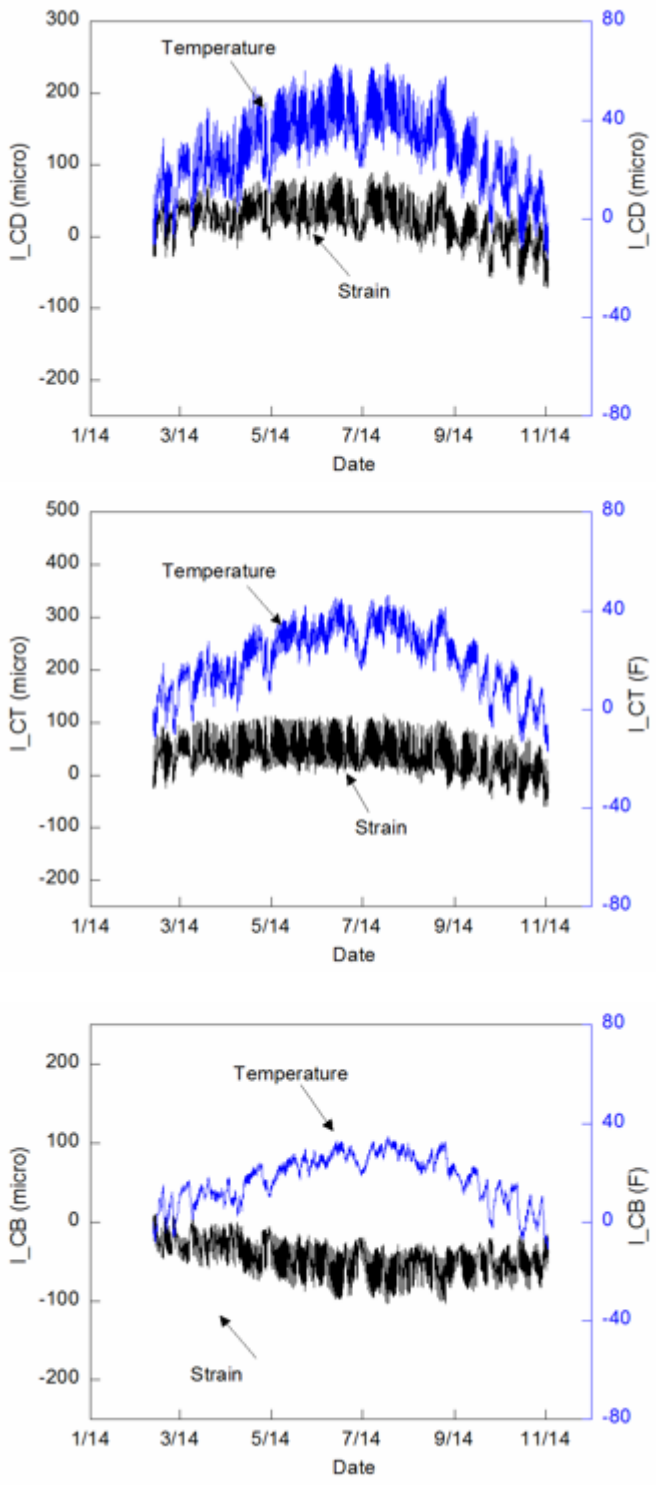

Figure 151
Measured strains and temperatures within in Girder C

Surface Sensors on Girders. All sensors have been have been subject to temperature calibration. Legend is denoted as beam number and sensor location, respectively. For example, O_AT refers to sensor at Girder A and top side surface. Figure 152 shows strains measured at beam top surface, bottom surface, and middle sections. The sensors on the superstructure, i.e., girder and deck, working functionally. The strains reasonably vary with the temperatures. The positive and negative variations of the strains are within the range of ±100 microstrain during the monitoring period.

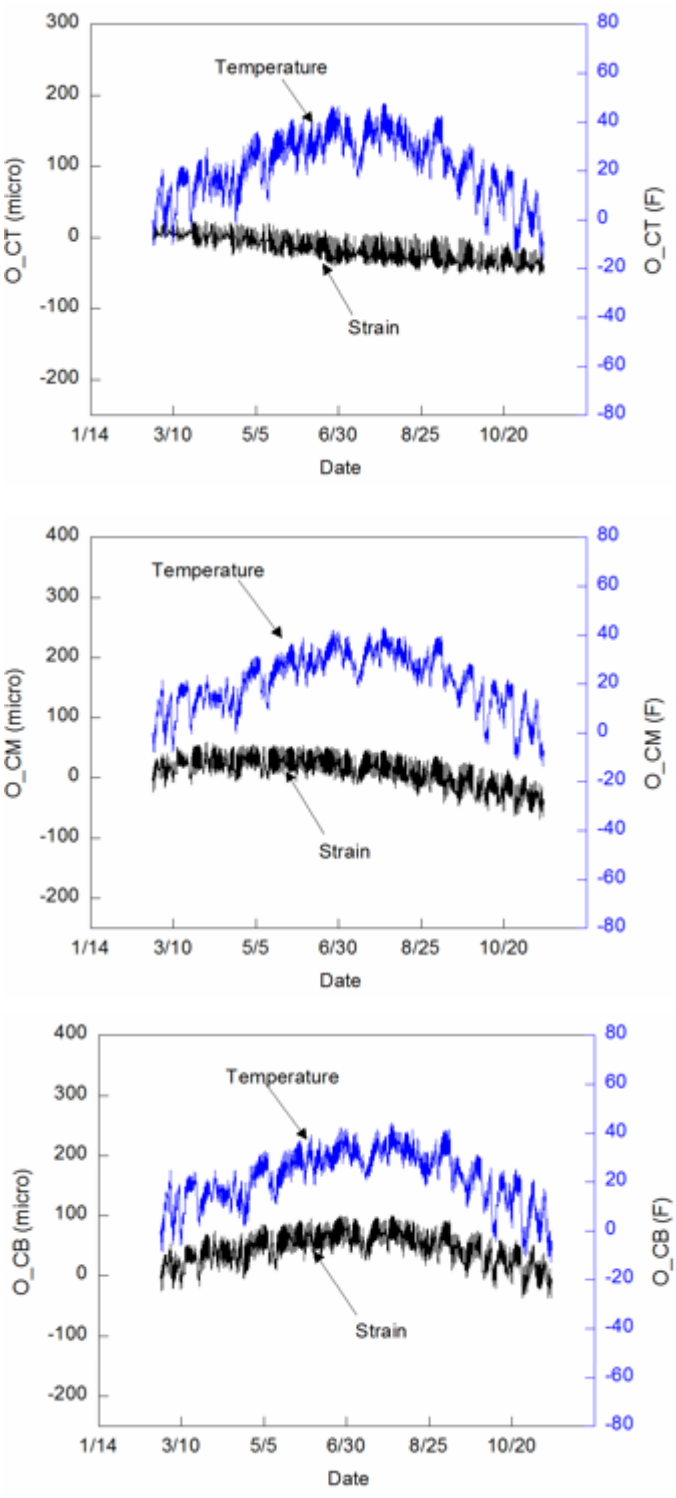

Figure 152
Measured strains and temperatures at outer surfaces of Girder C

Behavior of Piles and Bent-Soil Interaction. Detailed recordings of individual sensors are presented in Appendix B. Referring to the instrumentation plan shown in Figure 21; the four pressure cells show interesting measurements as depicted in Figure 153 where a cyclic variation is evident. A closer look at the measurements for a few days in January (cold days) and July of 2012 (hot days) (shown in Figure 154 and Figure 155) reveals that soil pressure variation coincides with air temperature changes. A small temperature variation resulted in soil pressure changes as shown in Figure 154. Soil pressure ranged between -20 to +20 psi, which is equivalent to a soil passive pressure at a depth of approximately 8 ft.

The three strainmeters (Figure 26) measure the displacement of the bent as the bridge expands and contracts. Figure 156 shows a summary of measurements of the strainmeters along with the air temperature. A small negative displacement (bent moves towards soil) was recorded between 3/12 and 8/12 as a result of thermal expansion followed by an increase at a higher rate as the temperature drops. The displacement ranged from ~0.2 ~ to 0.8 in. A closer look into the data of the strainmeters (Figure 157and Figure 158) show that the bridge expands and contracts daily up to 0.25 in. The Bodcau Bayou Bridge exhibits higher soil-bent interaction and lateral movement of Bent 1 when compared to Caminada Bay Bridge.

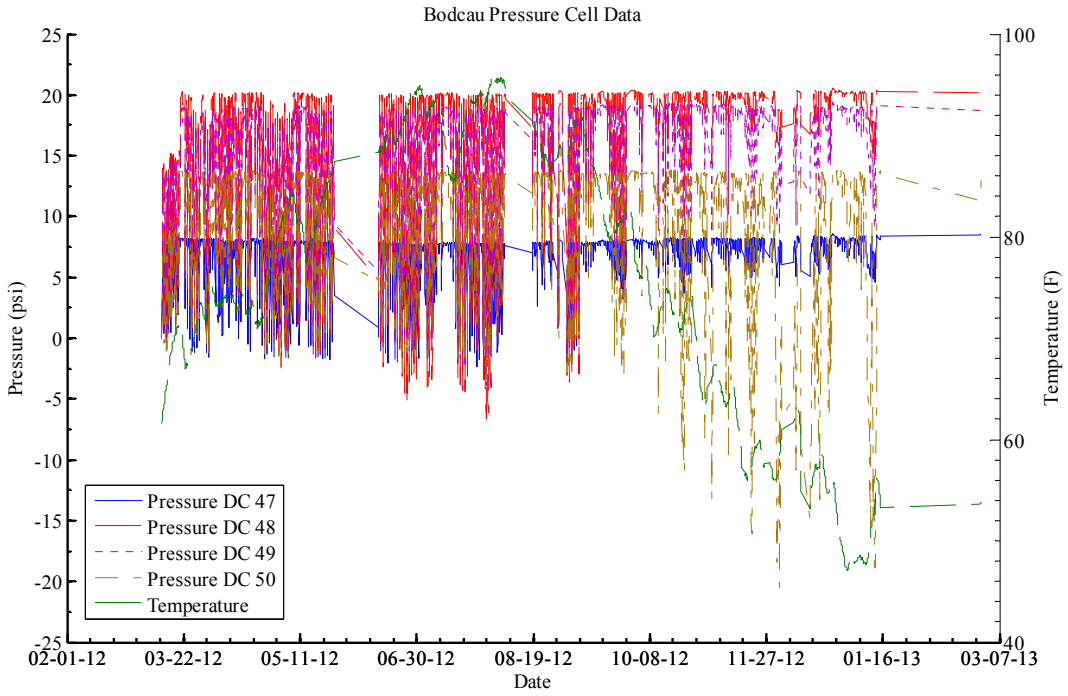

Figure 153
Bodcau Bayou pressure cell data for entire Data Set

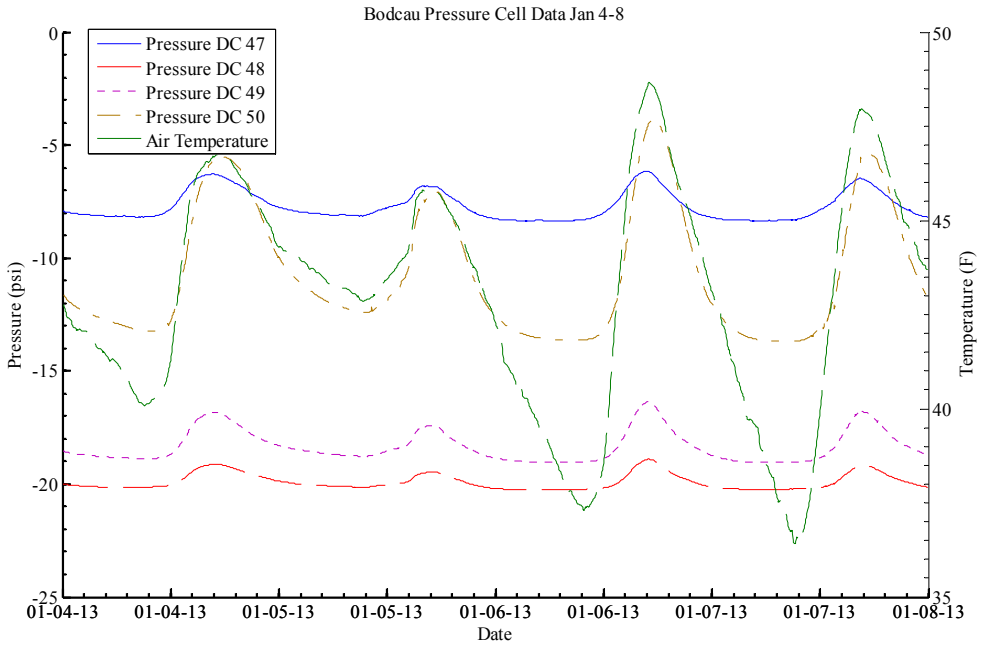

Figure 154
Bodcau Bayou pressure cell data for 01/04/13 – 01/08/13

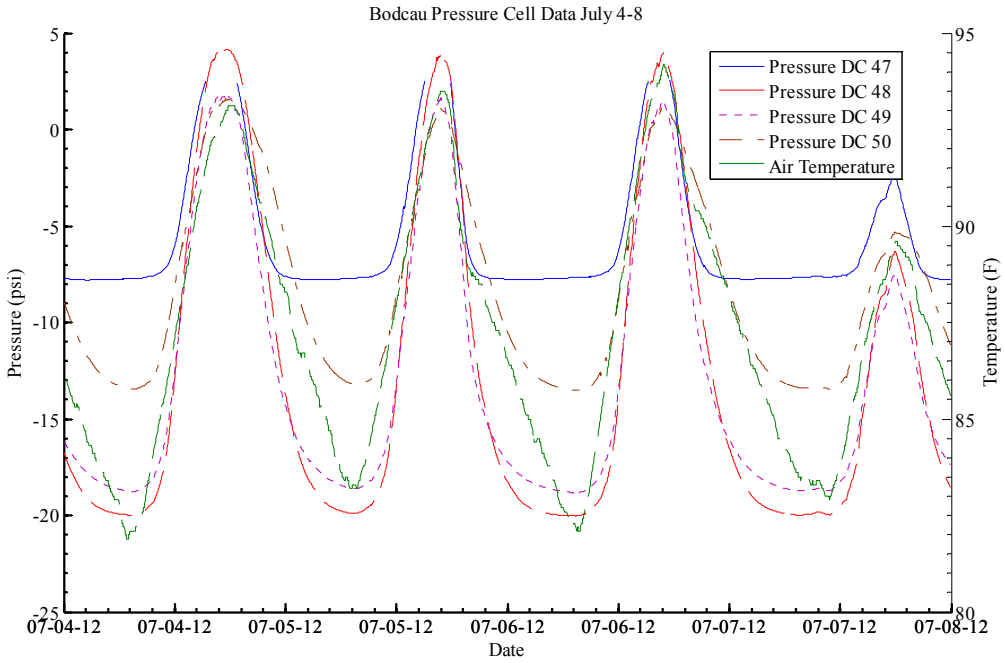

Figure 155
Bodcau Bayou pressure cell data for 07/04/12 – 08/04/12

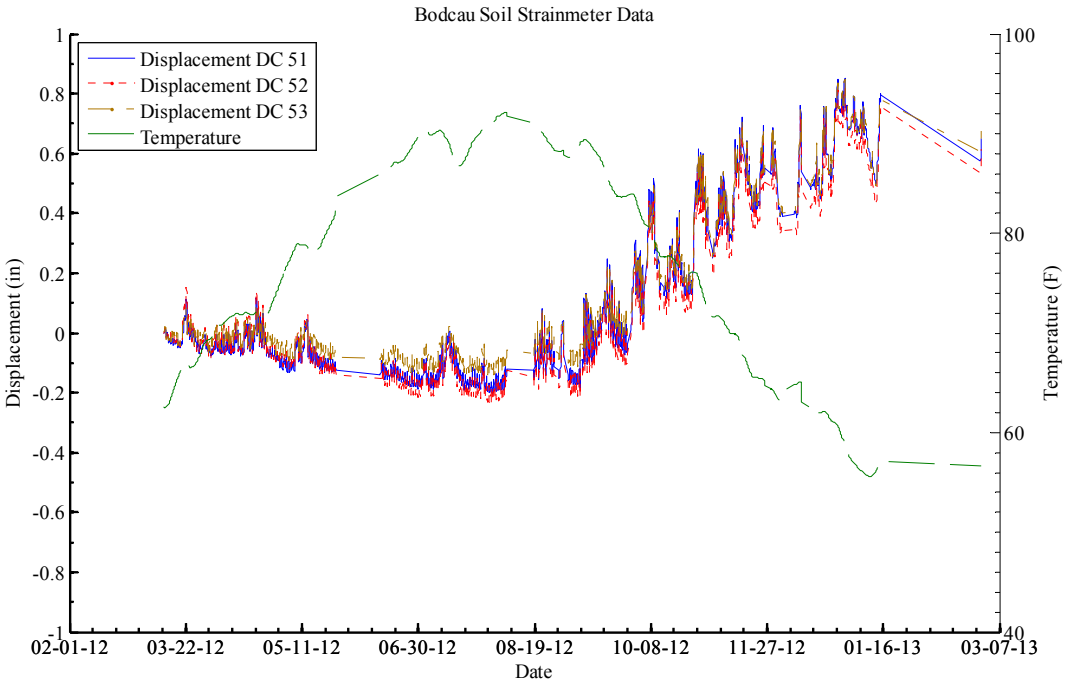

Figure 156
Bodcau Bayou soil strainmeter for entire data set

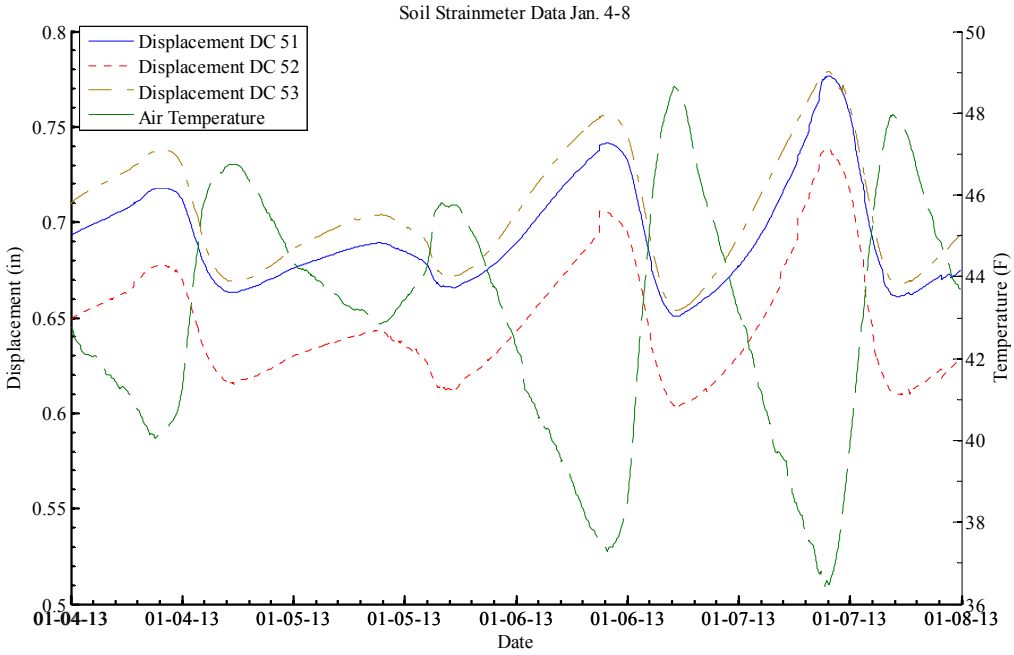

Figure 157
Bodcau Bayou soil strainmeter data for 01/04/13 – 01/08/13

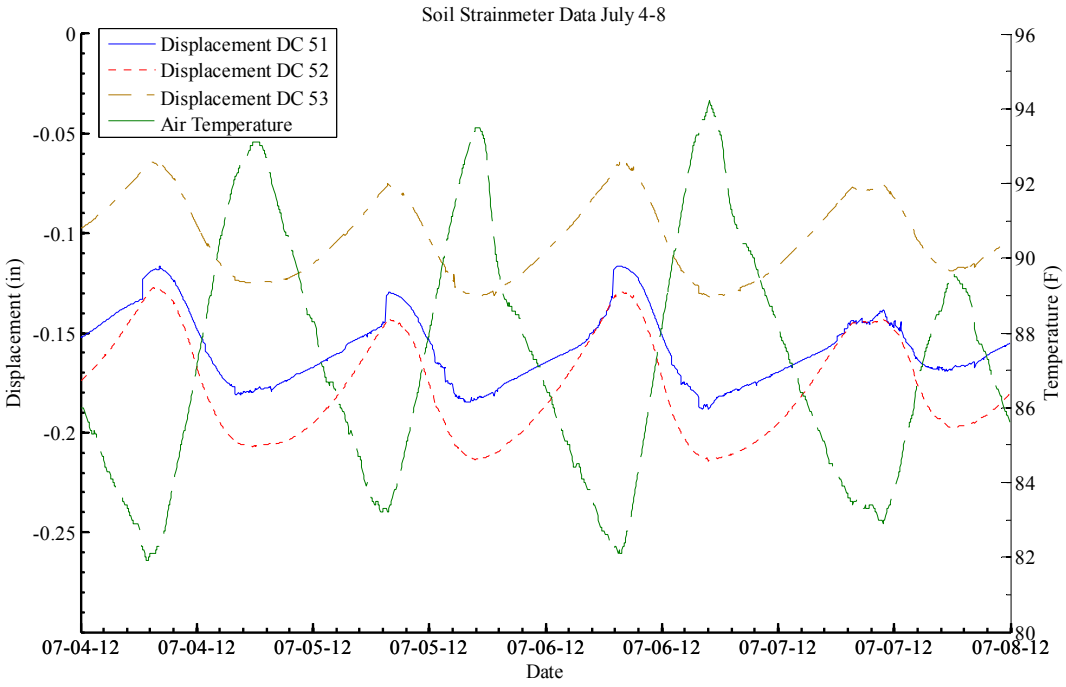

Figure 158
Bodcau Bayou soil strainmeter data for 07/04/12 – 07/08/12

Moment Calculations for Bodcau Bayou Pile Strain Gauges. The change in strain for the Bodcau Bayou strain gauges were normalized to the reading collected at the time of installation and temperature effects were corrected according to the manufacturer guidelines. ASTM A709 Grade 50 steel HP 14×89 piles were installed with the weak axis of the pile cross section parallel to the traffic direction (Figure 159). Strain gauges were welded on the flanges of the piles to measure the strains resulting from bridge expansion/contraction. Four strain gauges (positions A, B, C, and D) were placed on section 1-1 (top section) on all four corners of the piles, while only two (positions A and C) were placed parallel to the centerline on the remaining sections. Many of the sensors on section 1-1 were damaged during data collection.

The cross section and dimensions of an HP 14×89 is shown in Figure 160. The moment of inertia about the weak axis is 326 in^4 and the strong axis moment of inertia is 904 in^4. The expansion and contraction of the bridge will cause bending about the weak axis, therefore only the weak axis moments (parallel to centerline) are considered. The effects of possible torsion and strong axis bending could not be considered because of the amount of damaged sensors in the top section of the piles. Strain gauge sensors were placed at 1.5 in. from the edges of the flange, leaving a total of 11.7 in. between the gauges.

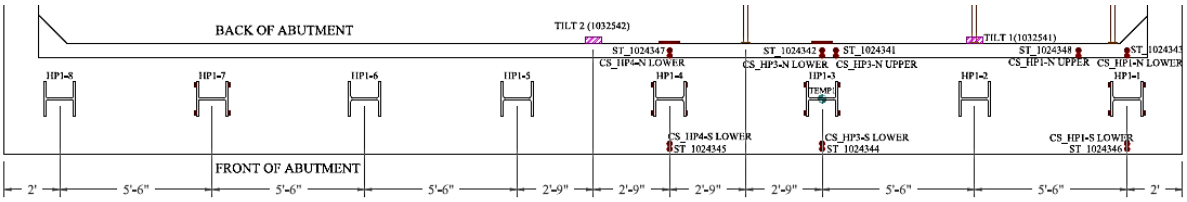

Figure 159
Layout of Bodcau Bayou H-piles in the abutment

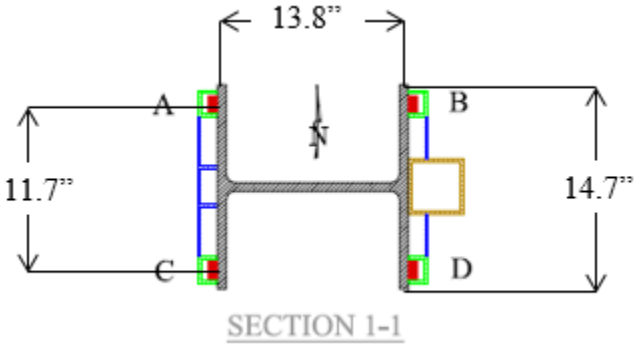

Figure 160
Pile cross section dimensions and sensor spacing

The moment in the pile was calculated based on the strains in the weak axis (i.e. the difference in strain between C and A) as:

$$M = \frac{EI(\varepsilon_{C,D} - \varepsilon_{A,B})}{h} \tag{26}$$

where, M is the moment about the weak axis, E is the modulus of elasticity of the pile (27,900 ksi), I is the moment of inertia about the weak axis (326 in^4), $\varepsilon_{C,D}$ is the measured strain in sensors C or D, ε_c is the measured compression strain in A or B, and h is the distance between the sensors which are equally spaced from the neutral axis. The difference in strain between sensors A and C are approximately opposite in sign and equal in magnitude for all the sections.

The flexural yield moment in the piles is calculated using the following equation:

$$M_y = \frac{If_y}{c} \tag{27}$$

where, M_y is the yield moment, I is the moment of inertia of the weak axis (326 in^4), f_y is the yield strength of the steel (50 ksi), and c is the distance from the neutral axis to the location

of extreme tension or compression (7.35 in). The calculated yield moment of the piles is 2217.7 kip-in.

The bending moments about the weak axis in the instrumented piles are shown in Figure 161 through Figure 164. The effect of thermal stresses is evident from moment change from April-July, to October-January measurements as the moments change from one trend to its mirror image. HP1-7 experienced the highest bending moments (Figure 164) whereas HP1-3 experienced the lowest bending moments (Figure 162). The yield moment is 2217.7 kip-in compared to less than 600 kip-in moment in some piles.

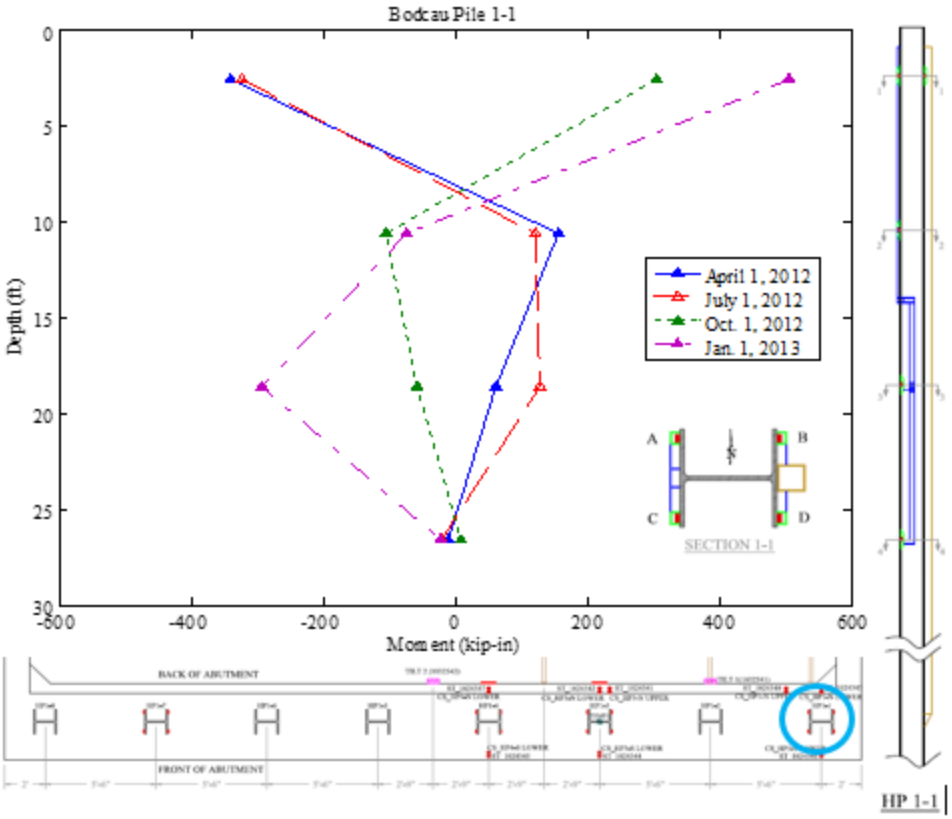

Figure 161
Moments about weak axis in Bodcau Bayou Pile HP1-1

Strain gauges in locations C and D of section 1-1 were damaged and strains of C and D were assumed to be equal magnitude but opposite sign of A and B, respectively. Moments calculated from A and C of section 1-1 was used to simplify graph. Strain gauge A of section 4-4 was damaged and strains were assumed to be the opposite of strains in location C. Yield moment is 2217.7 kip-in.

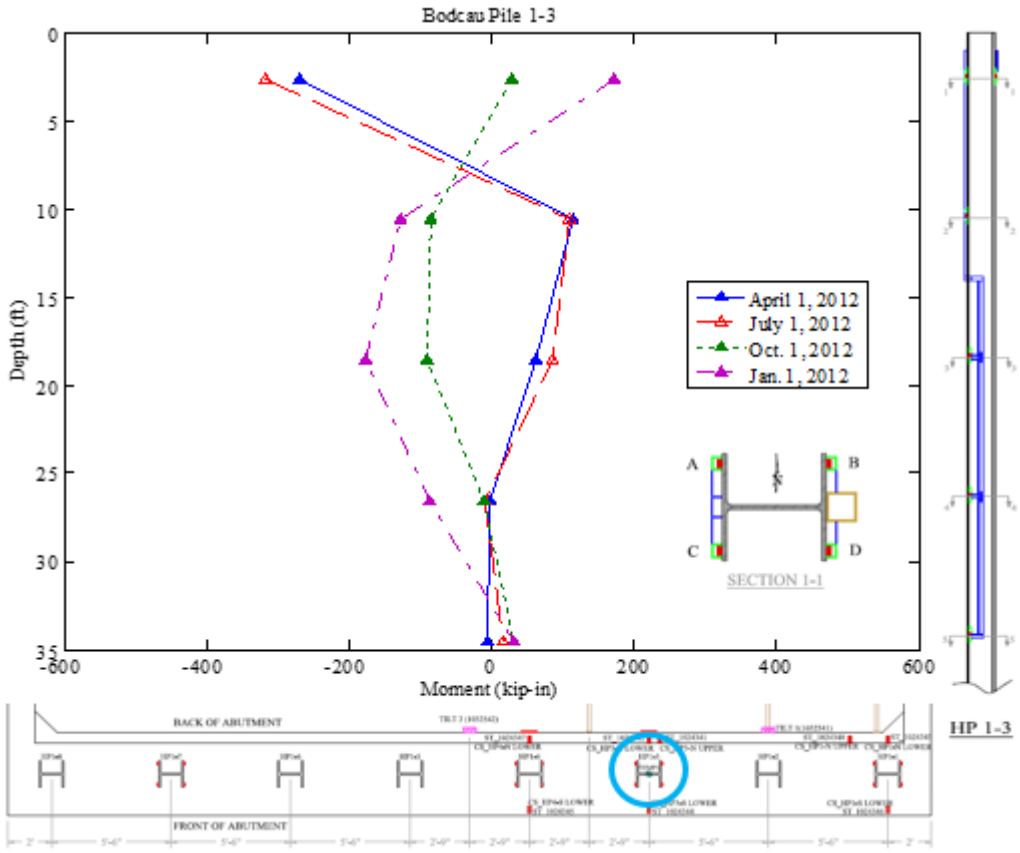

Figure 162
Moment about weak axis in Bodcau Bayou Pile HP1-3. Section 1-1

Strain gauge in location A was damaged in July 2012 and strain gauge in location B was damaged in 06/12. Strains of A and B were assumed to be equal in magnitude but opposite sign of C and D, respectively, for the damaged months. Moments calculated from A and C of section 1-1 were used to simplify graph. Yield moment is 2217.7 kip-in.

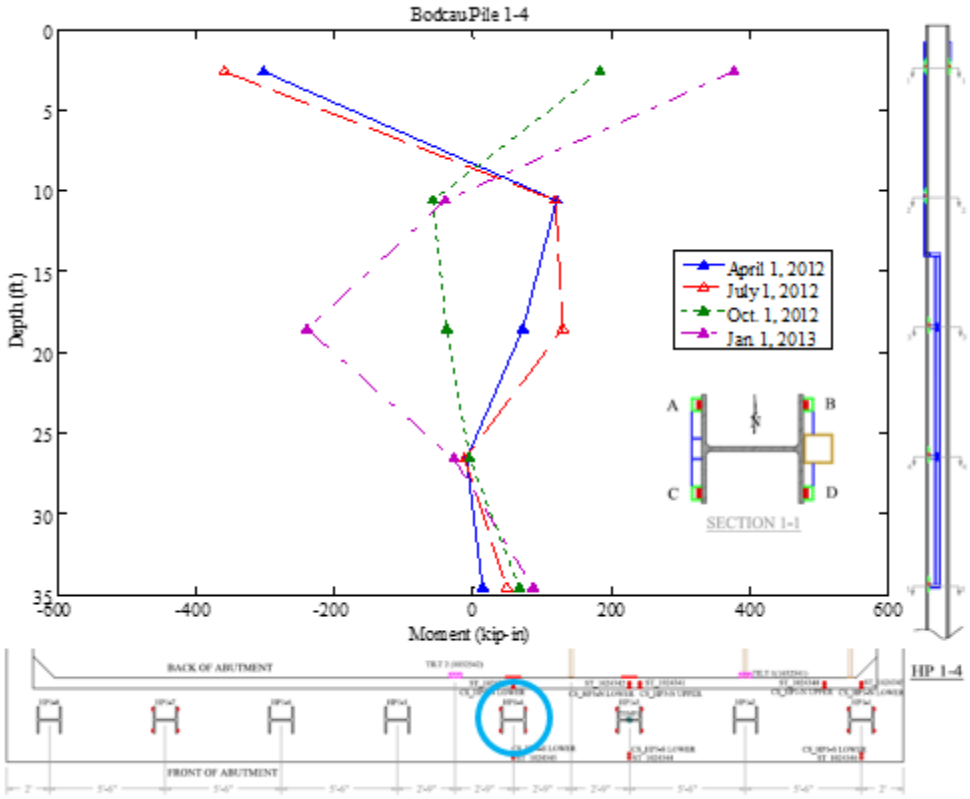

Figure 163
Moment about weak axis in Bodcau Bayou Pile HP1-4. Section 1-1

Strain gauge in location A was damaged in 06/12. Strain of A was assumed to be equal in magnitude but opposite sign of C for the damaged months. Moments calculated from A and C of section 1-1 were used to simplify graph. Yield moment is 2217.7 kip-in.

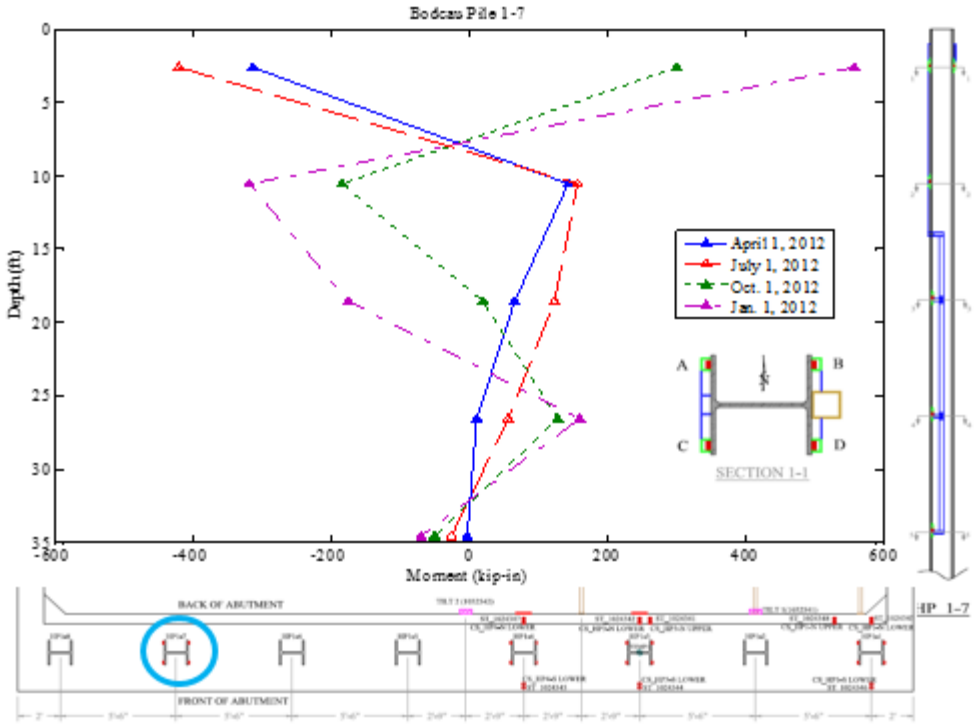

Figure 164
Moment about weak axis in Bodcau Bayou Pile HP1-7. Section 2-2

Strain gauge in location A was damaged in 12/12. Strain of A was assumed to be equal in magnitude but opposite sign of C for January. Moments calculated from A and C of section 1-1 was used to simplify graph. Yield moment is 2217.7 kip-in.

DISCUSSION OF RESULTS

Caminada Bay Bridge

Substructure

A 3D finite element (FE) model was developed to study the behavior of different parts of the substructure of the Caminada Bay Bridge under different types of loads. Particularly the behavior of the piles, embankment/backfill, abutment, and deck along with pile and soil interaction and settlement of soil is addressed through the numerical simulation.

Numerical simulation is performed using ABAQUS/Standard software *[81]*. Based on the medium soil for Caminada Bay Bridge and pile and bents material (reinforced concrete), proper elasto-plastic constitutive models (Modified Drucker-Prager for soil and Mises type plasticity model with isotropic hardening for piles and bents) are adopted in order to model the deformation of the substructure. In order to capture the pile and soil interaction (i.e. friction resistance of pile wall and separation process between pile and soil, when soil is in tension), a surface-to-surface contact algorithm in ABAQUS/Standard is used in the interface of the pile and surrounding soil.

The required material parameters of these models for different soils were determined based on the experimental tests from the boreholes in the site and engineering judgment. For each bent, first the load capacity of the pile group was obtained based on CPT data of field test, which is a reliable approximation of the pile capacity and can be compared with the finite element analyses results after the required material parameter of soil for using in Numerical Analyses were determined. Then the numerical simulation using ABAQUS was conducted.

The strategy for conducting the numerical analyses for substructure was to provide the information regarding the load-deflection responses of the substructure to be used for the superstructure analyses as shown in Figure 170. Therefore the load (and moment) in all six degrees of freedom is applied to the bent-pile-soil system until the soil fails to determine the maximum capacity of the superstructure. The calculation results in terms of the load-deflection (moment-rotation) for each bent were then reported. Eleven bents of the bridge were considered for the numerical analyses.

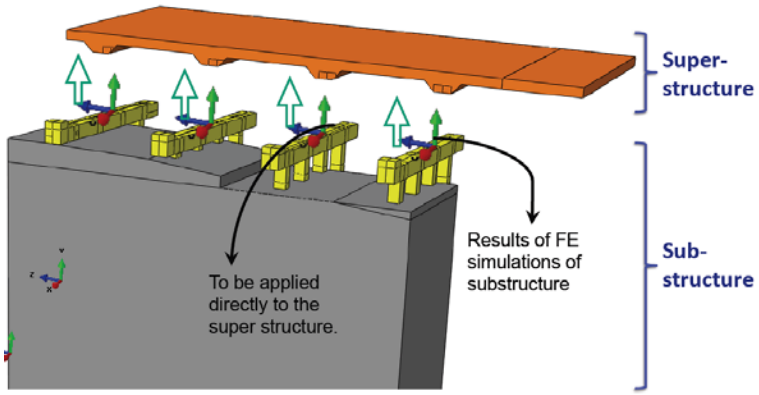

Figure 165
The strategy of conducting the numerical analyses of sub-structure and using the results for super-structure.

All sensors installed in the piles and backfill soil at Caminada Bay Bridge exhibited excellent performance with no anomalies. The large piles (36 in. square prestressed concrete) that were driven in sandy soil deposit offered high lateral support for Bent 1 of the bridge, which resulted in very small lateral movement due to thermal changes in the direction of traffic. Both piles show higher moments in the direction of traffic than in the lateral direction with the exterior pile having slightly higher moments than the interior pile in both directions. In all cases, the highest moment is less than 7% of the concrete cracking moment. The bent and the soil backfill exhibited negligible movements.

Superstructure

Based on the available information of the bridge, together with the monitoring results over one year since 2011, a 3D numerical model was proposed and validated in the study, where the pile-soil and abutment-backfill interaction behaviors are considered. Then, the concerning parameters are varied through a parametric study to further investigate their effects on the bridge thermal performances under the other complicated structural and geotechnical conditions. Some observations and results are discussed below:

Based on numerical simulations, for this specific IAB, the effects from the backfills are negligible. The height of the abutments are shallower compared with the deeper piles with their large cross sections. The bridge deformations are majorly controlled by the piles rigidity, soil resistances surrounding the piles, and connection behaviors between the pile-bent. For some other general IABs, however, the stiff soils may induce higher internal forces on the superstructure, while the soft soils will provide greater forces on the substructure.

Based on numerical simulations, the soils surrounding the piles show the most obvious effects on the bridge responses. Under the current bridge configuration, changing the soft soils to stiff ones will generate a maximum of 1.5 times smaller bridge displacements and 20% smaller backfill pressures; but at the same time, it will also induce 70% larger pile positive strains and 48% larger slab negative strains. Thus, an optimized structure needs to simultaneously benefit both the superstructure and substructure.

Based on numerical simulations, the connection behaviors between the pile-bent affect the bridge responses in two aspects. On one hand, they switch the locations of the maximum pile internal forces from the interfaces between the pile-bent, i.e., the rigid connection case, to the top third parts below the pile heads, i.e., the roller connection case. On the other hand, they also affect the rotation behaviors of the abutment, and that in turn will slightly affect the backfill pressures and slab strains, even though these changes are not significant due to the small sizes of the abutment in the current bridge.

Based on numerical simulations, the soils behind the abutment affect the behaviors of the integral abutments in terms of their displacements and rotations. These effects are complicated, and the soil restraints to the abutment deformations accumulate with time due to the plastic behaviors of the soil. However, at locations far away from the integral abutments or the expansion joints are provided between slab-abutment, these soil restraining effects become negligible.

The measured seasonal temperatures and daily gradients of the slabs, during the monitoring period, either reached or slightly exceeded the design values specified by the AASHTO LRFD (2007).

The strains measured at the surfaces of the top bents and bottom slabs generally showed good correlation with the temperature variations. Based on the measurements during the monitoring period, the maximum tension thermal stresses generated at the top bents may possibly crack the concrete, while the induced compressive stresses are negligible. In addition, under the current soil condition and stiff structure configurations, no evident differences were observed for the thermal strains between the locations at the bridge ends and middle spans.

No appreciable rotations were observed from the approach slab that was integral with the abutment since the rotation on the abutment was small. However, more numerical analysis and field observations are needed to fully understand the approach span performance.

Bodcau Bayou Bridge

Substructure

The similar procedure indicated for the Caminada Bay Bridge was taken into account to develop a 3D finite element (FE) model in order to study the behavior of different parts of substructure of the Bodcau Bayou Bridge under different types of loads. It should be noted that the type of soil is stiff in this case and steel piles are used. The numerical simulation is conducted for one bent (Bent 1).

In spite of welding cover plates for the strain gages for the piles, few strain gages were damaged during pile driving. However, compensation for the lost strain gages was done by assuming a linear strain variation between the tension and compression sides of the pile cross-section. The piles of Bodcau Bayou Bridge are smaller than the ones for Caminada Bay Bridge and offer less bending resistance. This design resulted in less stiffness as the bridge went through thermal changes, which is manifested in more expansion and contraction of the bridge with lateral movement as high as 0.8 in at bent 1. The exterior piles showed higher bending moments than the interior piles. In all cases, the highest moment is less than 27% of the yielding moment of steel.

Superstructure

During the monitoring period, the measured seasonal temperatures and daily gradients of the slabs, either reached or slightly exceeded the design values specified by the AASHTO LRFD (2007).

The strains reasonably varied with the temperatures. The positive and negative variations of the strains were within the range of ±100 microstrain during the monitoring period. Based on the measurements during the monitoring period, the maximum tension thermal stresses generated at the top bents may possibly crack the concrete, while the induced compressive stresses are negligible.

For Caminada Bridge, no evident differences were observed for the thermal strains between the locations at the bridge ends and middle spans. However, such an observation cannot be made for the Bodcau Bayou Bridge since only one section was instrumented.

In summary, no significant issues were observed at this stage and the designs of details for these two monitored bridges seem to be effective in accommodating the thermal effect.

The support conditions in reality may not be completely the same as were designed for, but they are crucial for integral abutment bridges without expansion joints. For IABs, it is not

advisable to allow the fully free support conditions at the superstructure, since the induced movements will cause larger backfill pressures and pile internal forces; whereas, it is also not a good idea to adopt fully fixed supports since they will generate larger internal forces on the superstructure. In this sense, this dilemma may be one of the reasons for restricting the designs of integral constructions on longer span bridges, since the corresponding larger thermal movements, together with other greater thermal effects, have to be appropriately accommodated.

The thermal movements have to be accommodated by either or both the superstructure and substructure. If the superstructure is allowed to move comparatively free, then the substructure will experience large deformations and internal forces; while if the superstructure is not allowed a larger movement, by adopting fixed boundaries, more stiffer backfills, or other approaches, then the greater internal forces may be induced on the superstructure and that will be beneficial for the substructure. These dilemmas will become more complicated when considering the combinations of different loading conditions, such as the temperature uniform variations, gradient distributions, dead loads, and live loads. In this sense, some of the settling methods for this argument may lie in the attempts of adopting new material types with different physical and mechanical properties.

While the monitored period may be sufficiently long enough to make exclusive conclusions on the thermal effect, continued monitoring of the bridge field performance is needed for the combined effect, such as live load and scour effect.

CONCLUSIONS

Recently, the first two full IABs, Caminada Bay Bridge and Bodcau Bayou Bridge, were built on the fine sand/silty sand and lean to fat clay conditions, respectively, in Louisiana. This study reports the monitoring and numerical results for these two bridges. Some of the important observations are concluded as follows:

(1) Based on the observed temperature effects, the design of the piles of Caminada Bay Bridge is very conservative and the piles were driven in a sandy soil deposit. The piles experienced very low bending moments and Bent 1 experienced very small lateral movement which corresponds to very small pressure on the backfill soil. Correspondingly, the rotation of the abutment is small.

(2) The piles that support Bodcau Bayou Bridge are not as stiff as the piles of Caminada Bay Bridge. The bridge expansion and contraction due to thermal changes is evident and correlates well with field measurements of pile lateral movement and bent-soil interaction. The piles experienced relatively larger bending moments than Caminada Bay Bridge did, but still a small moment when compared to the yielding moment.

(3) The measured seasonal temperatures and daily gradients of the slabs, during the monitoring period, are either reaching or slightly exceeding the design values specified by the AASHTO LRFD (2007).

(4) The strains measured at the surfaces of the top bents and bottom slabs generally show good correlations with the temperature variations. Based on the measurements during the monitoring period, the maximum tension thermal stresses generated at the top bents may possibly crack the concrete, while the induced compressive stresses are negligible. In addition, under the current soil condition and stiff structure configurations of the Caminada Bay Bridge, no evident differences are observed for the thermal strains between the locations at the bridge ends and middle spans. Such an observation cannot be made since only one section is instrumented for the Bodcau Bayou Bridge.

(5) Based on numerical simulations on the Caminada Bay Bridge, the soils behind the abutment affect the behaviors of the integral abutments in terms of their displacements and rotations. These effects are complicated, and the soil restraints to the abutment deformations accumulate with time due to the plastic behaviors of the soil. However, at locations far away from the integral abutments or the expansion joints are provided between slab-abutment, these soil-restraining effects become negligible.

(6) Based on numerical simulations on the Caminada Bay Bridge, for this specific IAB, the effects from the backfills are negligible. The height of the abutments are shallower compared with the deeper piles with their large cross sections. The bridge deformations are majorly controlled by the piles rigidity, soil resistances surrounding the piles, and connection behaviors between the pile-bent. For some other general IABs, however, the stiff soils may induce higher internal forces on the superstructure while the soft soils will provide greater forces on the substructure.

(7) Based on numerical simulations on the Caminada Bay Bridge, the soils surrounding the piles show the most obvious effects on the bridge responses. Under the current bridge configuration, changing the soft soils to stiff ones will generate a maximum of 1.5 times smaller bridge displacements and 20% smaller backfill pressures; but at the same time, it will also induce 70% larger pile positive strains and 48% larger slab negative strains. Thus, an optimized structure needs to simultaneously benefit both the superstructure and substructure.

(8) No appreciable rotations are observed from the approach slab that is integral with the abutment since the rotation on the abutment is small. However, more numerical analysis and field observations are needed to fully understand the approach span performance.

(9) No significant issues are observed at this stage and the designs of details for these two monitored bridges seem to be effective in accommodating the thermal effect.

(10) While the monitored period may be sufficiently long enough to make exclusive conclusions on the thermal effect, continued monitoring of the bridge field performance is needed for the combined effect, such as live load and scour effect.

RECOMMENDATIONS

Support conditions in the field may not be completely the same as that were designed for, but they are crucial for integral abutment bridges without expansion joints. For IABs, it is not advisable to allow the fully free support conditions at the superstructure, since the induced movements will cause larger backfill pressures and pile internal forces; whereas, it is also not recommend to adopt fully fixed supports since they will generate larger internal forces on the superstructure. For long span bridges, the corresponding larger thermal movements, together with other greater thermal effects, have to be appropriately accommodated.

For IABs, the thermal movements have to be accommodated by either or both the superstructure and substructure. If the superstructure is allowed to move comparatively freely, then the substructure will experience large deformations and internal forces; while if the superstructure is not allowed a larger movement, by adopting fixed boundaries, more stiffer backfills, or other approaches, then the greater internal forces may be induced on the superstructure and that will be beneficial for the substructure. These problems will become more complicated where considering the combinations of different loading conditions, such as the temperature uniform variations, gradient distributions, dead loads, and live loads. Adopting new material types with different physical and mechanical properties may be a solution.

During the monitoring period, the measured seasonal temperatures and daily gradients of the slabs, either reached or slightly exceeded the design values specified by the AASHTO LRFD (2007). Therefore, it is recommended to re-examine DOTD's specifications for Louisiana bridges in terms of thermal effects.

No significant issues were observed at this stage and the designs of details for these two monitored bridges seem to be effective in accommodating the thermal effect. Therefore, these details can be used for similar bridges. However, more parametric studies using the calibrated model of the current study, considering longer span and longer bridges etc., are recommended to develop more broad applications in Louisiana.

While the monitored period may be sufficiently long enough to make exclusive conclusions on the thermal effect, continued monitoring of the bridge field performance is needed for the combined effect, such as live load and scour effect. Therefore, continued monitoring of the bridge field performance is recommended.

ACRONYMS, ABBREVIATIONS, AND SYMBOLS

AASHTO	American Association of State Highway and Transportation Officials
ABAQUS	Commercial Finite Element Software
ANSYS	Commercial Finite Element Software
ASD	Allowable Stress Design
cm	centimeter(s)
DOTD	Louisiana Department of Transportation and Development
EPS	Extended Polystyrene
FDOT	Florida Department of Transportation
FEM	Finite Element Method
FHWA	Federal Highway Administration
ft.	foot (feet)
IAB	Integral Abutment Bridges
in.	inch(es)
lb.	pound(s)
LFD	Load Factor Design
LLFD	Live Load Factor Design
LRFD	Load and Resistance Factor Design
LSU	Louisiana State University
LTRC	Louisiana Transportation Research Center
m	meter(s)
MSE	Mechanically Stabilized Earth
NYDOT	New York Department of Transportation
TDOT	Tennessee Department of Transportation

REFERENCES

1. Arockiasamy, M., Butrieng, N., and Sivakumar, M. "State-of-the-art of integral abutment bridges: Design and practice." *Journal of Bridge Engineering*, 9(5), 2004, pp.497-506.

2. Kunin, J., and Alampalli, S. ‘‘Integral abutment bridges: Current practice in United States and Canada.’’ *Journal of Performance of Constructed Facilities*, Vol. 14(3), 2000, pp. 104–11.

3. Wolde-Tinsae, A. M., and Greimann, L. F. "General design details for integral abutment bridges." *Civil Engineering Practice*, 3(2), 7-20., 1988, pp. 199-210.

4. Mistry, V. C. (2005) “Integral Abutments and Joinless Bridges,” *Proceedings of the Integral Abutment and Jointless Bridges Conference*, FHWA, Baltimore, 3-11.

5. Burke Jr, M. P. "Design of integral concrete bridges." *Concrete International*, 15(6), 1993, pp.37-42.

6. Maruri, R.F., and Petro, S.H. “Integral Abutments and Jointless Bridge.” *Proceedings of the Integral Abutment and Jointless Bridges Conference*, FHWA, Baltimore, 2005, pp. 12-29.

7. Decleli, M., and Erhan, S. “Effect of Soil and Substructure properties on Live-Load Distribution in Integral Abutment Bridges.” *Journal of Bridge Engineering*, Vol. 13(5), 2008, pp. 527-39.

8. Broms, B. B., and Ingleson, I. “Earth Pressure Against the Abutments of a Rigid Frame Bridge.” *Géotechnique*, Vol. 21, No.1, 1971, pp.15-28.

9. Card, G. B., and D. R. Carder, D.R. "A Literature Review of the Geotechnical Aspects of the Design of Integral Bridge Abutments." *Proj. Rpt. 52*, Trans. Res. Lab., U.K., 1993.

10. Sandford, T. C., and Elgaaly, M. "Skew Effects on Backfill Pressures at Frame Bridge Abutments." *Trans. Res. Rec.* 1415, Natl. Acad. Press,1993, p.1-11.

11. Briaud, J.L., James, R.W., and Hoffman, S.B. "Settlement of Bridge Approaches (the Bump at the End of the Bridge)." *Syn. of Hwy. Prac. 234*, Natl. Acad. Press, 1997.

12. Ng, C. W. W., Springman, S., and Norrish, A.R.M. "Centrifuge Modeling of Spread-Base Integral Bridge Abutments." *Jour. of Geotech. and Geoenv. Engr.*, ASCE, 124 (5), 1998, pp. 376-388.

13. Reid, R. A., Soupir, S.P. and Schaefer, V.R. "Use of Fabric Reinforced Soil Walls for Integral Abutment Bridge End Treatment," *Proc. Sixth Intl. Conf. on Geosyn.*, R. K. Rowe (ed.), Ind. Fabrics Assoc. Intl., 1998, pp. 573-576.

14. Reid, R. A., Soupir, S. P. and Schaefer, V. R. "Mitigation of Void Development under Bridge Approach Slabs Using Rubber Tire Chips." *Recycled Matls. in Geotech. App.*, C. Viupulanandan and D. J. Elton (eds.), ASCE, 1998, p. 37-50.

15. Reeves, J. N., and Filz, G.M. "Earth Force Reduction by a Synthetic Compressible Inclusion," report submitted to GeoTech Systems Corp. and Virginia's Ctr. for Innovative Tech. by Virginia Tech, Dept. of Civil Engr, 2000.

16. Horvath, J. "Integral- Abutment Bridges: Geotechnical Problems and Solutions Using Geosynthetics and Ground Improvement." The 2005 – FHWA CONFERENCE, Integral Abutment and Joint less Bridges (IAJB 2005), 2005.

17. Weakley, K. "VDOT Integral Bridge Design Guidelines." The 2005 – FHWA CONFERENCE, Integral Abutment and Jointless Bridges (IAJB 2005), 2005.

18. Burdette, E.G., Howard, S.C., Ingram, E.E., Deatherage, J.H., and Goodpasture, D.W. "Behavior of Pile Supported Integral Abutments." *Proceedings of the Integral Abutment and Joint less Bridges Conference*, FHWA, Baltimore, 2005, pp. 163-73.

19. Christou, P., Hoit, M., and McVay, M. "Soil Structure Analysis of Integral Abutment Bridges." *Proceedings of the Integral Abutment and Jointless Bridges Conference*, FHWA, Baltimore, 2005.

20. Dicleli, M., Albhaisi S.M. "Estimation of Length Limits for Integral abutment bridges." *Journal of Bridge Engineering*, 2004.

21. Oesterle, R., and Volz, J. "Effective Temperature and Longitudinal Movement in Integral Abutment Bridges." *The 2005 – FHWA CONFERENCE, Integral Abutment and Jointless Bridges* (IAJB nics, Vol. 31(4), 2005, pp.339-55.

22. Russell, H. G. and Gerken, L. J. (1994). "Jointless bridges - the knowns and the unknowns." *Concrete International*, 16(4), 44-48.

23. Hoppe, E. " Field Study of Integral Back wall with Elastic Inclusion." The 2005 – FHWA CONFERENCE, Integral Abutment and Joint less Bridges (IAJB 2005), 2005.

24. Horvath, J. "Integral- Abutment Bridges: Geotechnical Problems and Solutions Using Geosynthetics and Ground Improvement." The 2005 – FHWA CONFERENCE, Integral Abutment and Joint less Bridges (IAJB 2005), 2005.

25. Yannotti, P. A., White, H.L. "New York State Department of Transportation's Experience with Integral Abutment Bridge." The 2005 – FHWA CONFERENCE, Integral Abutment and Jointless Bridges(IAJB 2005), 2005.

26. Conboy, D.W., Stoothoff, E.J. "Integral Abutment Design and Construction: The New England Experience." The 2005 – FHWA CONFERENCE, Integral Abutment and Jointless Transportation, ISU, 2005.

27. Huckabee, P. "Plastic Design of Steel HP-Piles for Integral Abutment Bridges." *Proceedings of the Integral Abutment and Jointless Bridges Conference*, FHWA, Baltimore, pp. 270-80. *Analytical Methods in Geomechnicics*, Vol. 29(6), 2005, pp. 597-25.

28. Husain, I., Huh, B., Low, J., and McCormick, M. "Moose Creek Bridge- Case Study of a prefabricated Integral Abutment Bridge in Canada." The 2005 – FHWA CONFERENCE, Integral Abutment. 130(11), 2005, pp. 1140-1151.

29. Bonczar, C., Berena, S., Civjan, S., DeJong, J., Crellin, B., and Crovo, D. "Field Data and FEM Modeling of the Orange- Wendell Bridge." The 2005 – FHWA CONFERENCE, Integral Abutment and Jointless Bridges (IAJB 2005), 2005.

30. Elbadry, M., Elzaroug, O. "Control of cracking due to temperature in structural concrete reinforced with CFRP bars." *Composite Structure Journal*, Volume 64, Issue 1, April 2004, pp. 37-45.

31. Potgieter, I. C., and Gamble, W. L. (1989). "Nonlinear temperature distributions in bridges at different locations in the United States." *PCI Journal*, Precast/Prestressed Concrete Institute, July-Aug 1983, pp. 80-103.

32. Girton, D. D., Hawkinson, T. R., and Greimann, L. F. "Validation of design recommendations for integral abutment piles." Final Rep.HR-272, Iowa State Univ., Ames, Iowa, 1989.

33. Thippeswamy, H. K., and GangaRao, H. V. S. "Analysis of in-service jointless bridges." *Transportation Research Record* (1476), 1995, pp. 162-170.

34. Arsoy, S. “Experimental and Analytical Investigations of Piles and Abutments of Integral abutment bridges,” Ph.D. Dissertation, Virginia Polytechnic Institute and State University, 2000.

35. Faraji, S., Ting, J. M., Crovo, D. S., and Ernst, H. "Nonlinear analysis of integral abutment bridges: Finite-element model." *Journal of Geotechnical and Geoenvironmental Engineering*, 127(5), 2001, pp. 454-461.

36. Lehane, B. M, Keogh D. L. and O’Brien, E. J. “Simplified elastic model for restraining effects of backfill soil on integral abutment bridges.” *Computers & Structures,* Volume 73, Issues 1-5, 12 Oct 1999, pp. 303-313.

37. Steward, D.P., Jewell, R.J. and Randolph, M.F. (1994) “Design of piled bridge abutment on soft clay for loading from lateral soil movements.” *Geotechnique*, Vol. 44, 1994, pp. 277-96.

38. Abendroth, R.E., Greimann, L.F., and Ebner, P.B. “Abutment pile design for joint less bridges.” *Journal of Structural Engineering*. Vol. 115(11), 1989, pp. 2914-2929.

39. Greimann, L. and Wolde-Tinsae, A.M. “Design model for piles in jointless bridges.” *Journal of Structural Engineering*. Vol. 114(6). 1988, pp. 1355-1369.

40. Wang, S.T., and Reese, L.C. “COM624P – Laterally Loaded Pile Analysis Program for the Microcomputer, Version 2.0.” Washington, D.C. United States Department of Transportation, 1993.

41. Greimann, L.F., Abendroth, R.E., Johnson, D.E., and Ebner, P.B. “Pile design and tests for integral abutment bridges.” College of Engineering, Iowa State University." *Integral Abutment and Jointless Bridges* (IAJB 2005), 1987.

42. Springman, S.M. “Lateral loading on piles due to embankment construction.” MPhil Thesis, Cambridge University. 1984.

43. Steward, D. P. “Lateral loading of piled bridge abutments due to embankment construction.” Dissertation, Perth University of Western Australia, 1992.

44. Greimann, L.F., Yang, P., and Wolde-Tinsae, A.M. “Nonlinear analysis of integral abutment bridges.” *Journal of Structural Engineering*. Vol. 112, No. 10. 1986, pp. 2263-2280.

45. Ellis, E.A., and Springman, S.M. “Modeling of soil-structure interaction for a piled bridge abutment in plane strain FEM analyses.” *Computers and Geotechnics*, Vol. 28(2), 2001, pp. 79-98.

46. Faraji, S., Ting, J.M., Crovo, D.S., and Ernst, H. “Nonlinear Analysis Of Integral abutment bridges: Finite-Element Model.” *Journal of Geotechnical and Geoenvironmental Engineering* (ASCE), 2001, 127(5), 454-461.

47. Hara, T., Yu, Y.Z., and Ugai, K. “Behaviour of piled bridge abutments on soft ground: A design method proposal on 2D elasto-plastic-consolidation coupled FEM.” *Computers and Geotech*, 2004.

48. Steward, D.P., Jewell, R.J., and Randolph, M. F. “Numerical modelling of piled bridge abutments on soft ground.” *Computers and Geotechnics*, 1993,pp. 21–46.

49. Roscoe, K. H. and Burland, J. B. “On the generalized behaviour of ‘wet’ clay.” *Engineering Plasticity*. Cambridge University Press, 535-609, 1968, pp. 41-51.

50. Wakai, A., Ugai, K., Matsuda, T., and Gose, S. “Analysis of lateral displacement of a pile supported abutment constructed in soft subsoil profile.” *Journal of the Japanese Geotechnique* 1997.

51. Erhan S., and Dicleli M. “ Live load distribution equations for integral bridge substructures.” *Engineering Structures*, 31, 2009, pp. 1250-1264.

52. Khodair, Y.A. and Hassiotis, S.“Analysis of soil-pile interaction in integral abutment” *Computers and Geotechnics*, Vol32(3), pp. 201-09.

53. Frosch, R., Wenning, V., and Chovichien, V. “The In-service behavior of Integral Abutment Bridge: Abutment-Pile Response” *Proceedings of the Integral Abutment and Jointless Bridges Conference*, FHWA, Baltimore, 2005.

54. Kerokoski, O., and Laaksonen, A. “Soil-structure Interaction of Jointless Bridge.” *Proceedings of the Integral Abutment and Jointless Bridges Conference*, FHWA, Baltimore, 2005, pp. 323-36.

55. Duncan, J.M. and Arsoy, S. “Effect of bridge-soil interaction on behavior of piles supporting integral abutment bridges.” *Transportation Research Record*, No. 1849. 2003, pp. 91-97.

56. Greimann, L., Phares, B., Faris, A., and Bigelow, J. “Integral Bridge Abutment-to-Approach Slab Connection.” Final Report, Iowa DOT Project No. TR-530 & TR-539, 2008.

57. White, H. “Integral abutment bridge: comparison of current practice between European countries and the United States of America,” Special report-transportation research and development bureau, 2134, 2008.

58. Hassiotis, S. “Data gathering and desing of an integral abutment bridge.” 18th Engineering Mechanics Division Conference (EMD2007).Development bureau, NY., 2007.

59. Dicleli, M., and Albhaisi S.M. “Maximum length of integral abutment bridges supported on steel h-piles driven in sand.” *Engineering Structures*, 25(11), 2003, pp.1491_504.

60. Dicleli, M. “Integral Abutment-Backfill Behavior on Sand Soil—Pushover Analysis Approach” *Journal of Bridge Engineering*, 2005.

61. Brena, S.F., Bonczar, C., Civjan S.A., Dejong, J., and Crovo D.S. “Evaluation of seasonal and yearly behavior of integral abutment bridge.” *Journal Bridge Engineering*, 12(3), 2007, pp. 296-305.

62. Civjan, S.A., Bonczar, C., Brena, S.F., Dejong, J., and Crovo, D.S. “Integral abutment bridge behavior: Parametric analysis of a Massachusetts bridge.” *Journal Bridge Engineering*, 12(1), 2007, pp.64-71.

63. Karantzikis, M., and Spyrakos, C.C. “Seismic analysis of bridges including soil–abutment interaction.” Proceedings of the12th World Congress on Earthquake Engineering. Paper No. 2471, 2000.

64. Spyrakos, C.C., and Loannidis, G. “Seismic behavior of a post-tensioned integral bridge including soil–structure interaction (SSI).” *Soil Dynamics and Earthquake Engineering*, 2003, pp.23-53.

65. Dunker, K.F., and Liu, D.J. “Foundation for integral abutment.” Practice Periodical on *Structural Design and Construction*, Vol. 12(1), 2007, pp. 22-30., New Zealand.

66. Comodromos, E.M. and Pitilakis, K.D. “Response evaluation for horizontally loaded fixed-head pile groups using 3D non-linear analysis.” *International Journal for Numerical and Analytical Methods in Geomechanics*, Vol. 29, 2005, pp. 597-625, 2005.

67. Ooi, Ph.S.K., Chang, B.K.F., and Wang S.H. “Simplified Lateral Load Analyses of Fixed-Head piles and pile Group.” *Journal of Geotechnical and Geoenvironmental Engineering* (ASCE), 2004.

68. Abendroth, R.E., Greimann, L.F., and Laviolette, M.N. “An Integral Abutment Bridge with Precast Concrete Piles,” PROJECT REPORT-CTRE-99-48, IHRB –TR-438, 2007.

69. Burdette, E.G., Wasserman, E.P., Goodpasture, D.W., and Deatherage, J.H. “Field performance of integral abutment bridges in Tennessee.” *Transportation Research Record*, No. 00404. 1999.

70. Elchelman, A.W. “The Effect of Integrated Exposed Strands on Behavior of Prestressed Concrete Piles in Integral Abutments,” Thesis submitted in Partial Fulfillment of the Requirements, 2002.

71. Mistry, V. C . “Integral Abutments and Jointless Bridges (IAJB) 2004 Survey Summary.” *Proceedings of the Integral Abutment and Jointless Bridges Conference*, FHWA, Baltimore (IAJB 2005), 2005, pp. 3-11.

72. Arsoy, S., Duncan, J.M., and Barker, R.M. “Performance of Piles Supporting Integral abutment bridges.” Transportation Research Record 1808, TRB, National Research Council, Washington, D.C., 2002.

73. Hartt, S.L., Standford, T.C., and Davids, W.G. “Monitoring a Pile - Supported Integral Abutment Bridge at a Site with Shallow Bedrock Phase II.” Technical Report, Maine Department, 2006.

74. Jorgenson, J.L. “Behavior of abutment piles in an integral abutment in response to bridge movements.” *Transportation Research Record*, No. 903, 1983, pp. 72-79.

75. Lawver, A., French, C., and Shield, C.K. "Field performance of integral abutment bridges." *Transportation Research Record*, No. 1740, 2000, pp. 107-117.

76. Hassiotis, S., Lopez, J.R., and Bermudez. R., "Full- Scale Testing of an Integral Abutment Bridge." The 2005 – FHWA CONFERENCE, Integral Abutment and Jointless Bridges (IAJB 2005), 2005.

77. Civjan, S., Brena, S., Butler, D.A., and Crovo, D.S. "Field Monitoring of Integral Abutment Bridges." *Transportation Research Record*. No. 1892, 2004, pp. 160-69.

78. Liu, D., Magliola, R., Dunker. K. "Integral Abutment Bridges- Iowa and Colorado Experience." The 2005 – FHWA CONFERENCE, Integral Abutment and Jointless Bridges (IAJB 2005), 2005.

79. AASHTO. "Standard Specifications for Highway Bridges." Washington, D.C. American Association of State Highway and Transportation Officials. 16th Edition, 1998.

80. Maruri, R.F. and Petro, S.H. "Integral Abutments and Jointless Bridge." *Proceedings of the Integral Abutment and Jointless Bridges Conference*, FHWA, Baltimore, 2005, pp. 12-29.

81. Hibbitt, D., Karlsson, B., Sorensen P. "ABAQUS 6.8-3, User Manuals." Dassault Systèmes Simulia Corp., Providence, RI., 2008.

82. Ellis, E. A. and Springman, S. M. "Modeling of Soil-structure interaction for a piled bridge abutment in plane strain FEM analyses." *Computer and Geotechnics* VOL 28, 2000, pp. 79-98.

83. Khodair, Y. A. and Hassiotis, S. "Analysis of soil-pile interaction in integral bridge," *Computers and Geotechnics* 32(3): 201–209, 2005.

84. Kulhawy, F.H., and Mayne, P.W. "Manual on estimating soil properties for foundation design," Cornell university, Ithaca, New York, 1990.

85. Bowles, J. E. "Foundation analysis and design (5th edition)" McGraw-Hill Higher Education, 1996.

86. Terzaghi, K., Peck, R. B., Mesri, G. "Soil mechanics in engineering practice." John Wiley, 1996.

87. Hatanaka, M. and Uchida, A. "Empirical correlation between penetration resistance and internal friction angle of sandy soils." *Journal of the Japanese Geotechnical Society*, 1996.

88. NovoSPT 1.8 software "SPT correlation software," Novo Tech Software Ltd, 2009.

89. Helwany, S. "Applied Soil Mechanics, With ABAQUS Applications." John Wiley and Sons, Inc., New York, 2007.

90. Bustamante, M., and Gianeeselli, L. "Pile Bearing Capacity Predictions by Means of Static Penetrometer CPT." *Proceedings of the 2nd European Symposium on Penetration Testing,* ESOPT-II, Amsterdam, Vol. 2, pp. 493-500, 1982.

91. Schmertmann, J.H. "Guidelines for Cone Penetration Test, Performance and Design." U.S. Department of Transportation, Report No. FHWA-TS-78-209, Washington, D.C., p. 145, 1978.

92. De Ruiter, J., and Beringen, F. L.''Pile foundations for large North Sea structures.'' *Mar. Geotech.,* Vol 3 (3), 267–314, 1979.

93. Zhang, Z., and Tumay, M.T., "Statistical to Fuzzy Approach Toward CPT Soil Classification" *Journal of Geotechnical and Geoenvironmental Engineering,* ASCE, Vol. 125, No. 3, pp. 179-186, 1999.

94. Titi, H. H. and Abu-Farsakh, M. Y. "Evaluation of Bearing Capacity of Piles from Cone Penetration Test Data". Report No. FHWA/LA.99/334. Louisiana Transportation Research Center, Baton Rouge, Report No. FHWA-TS-78-209, Baton Rouge, LA, pp. 96, 2000.

95. Das, B. M. "Principles of Geotechnical Engineering" fifth edition, BROOKS/COLE

96. Skempton, A. W. "Standard Penetration Test Procedures and the Effect in Sands of Overburden Pressure, Relative Density, Particle Size, Aging and Overconsolidation," *Geotechnique*, Vol. 36, No. 3, 425 – 447, 1986.

This public document is published at a total cost of $250
42 copies of this public document were published in this first printing at a cost of $250. The total cost of all printings of this document including reprints is $250. This document was published by Louisiana Transportation Research Center to report and publish research findings as required in R.S. 48:105. This material was duplicated in accordance with standards for printing by state agencies established pursuant to R.S. 43:31. Printing of this material was purchased in accordance with the provisions of Title 43 of the Louisiana Revised Statutes.